RETROFITTING THE PRECAST RC WALL PANELS USING EXTERNALLY BONDED CFRP LAMINATES

Teză destinată obținerii
titlului științific de doctor inginer
la
Universitatea Politehnica Timișoara
în domeniul INGINERIE CIVILĂ ŞI INSTALAŢII
de către

Ing. Mihai Fofiu

Conducător ştiinţific:	prof.univ.dr.ing. Valeriu Stoian
Referenţi ştiinţifici:	prof.univ.dr.ing. Nicolae Ţăranu
	prof.univ.dr.ing. Daniela Lucia Manea
	prof.univ.dr.ing. Daniel Dan

Ziua susţinerii tezei: 03.11.2017

Seriile Teze de doctorat ale UPT sunt:

1. Automatică
2. Chimie
3. Energetică
4. Ingineria Chimică
5. Inginerie Civilă
6. Inginerie Electrică
7. Inginerie Electronică şi Telecomunicaţii
8. Inginerie Industrială
9. Inginerie Mecanică
10. Ştiinţa Calculatoarelor
11. Ştiinţa şi Ingineria Materialelor
12. Ingineria sistemelor
13. Inginerie energetică
14. Calculatoare şi tehnologia informaţiei
15. Ingineria materialelor
16. Inginerie şi Management

Universitatea Politehnica Timişoara a iniţiat seriile de mai sus în scopul diseminării expertizei, cunoştinţelor şi rezultatelor cercetărilor întreprinse în cadrul Şcolii doctorale a universităţii. Seriile conţin, potrivit H.B.Ex.S Nr. 14 / 14.07.2006, tezele de doctorat susţinute în universitate începând cu 1 octombrie 2006.

România, 300159 Timişoara, Bd. Republicii 9,
Tel./fax 0256 403823
e-mail: editura@edipol.upt.ro

Preface

The preliminary works for this thesis initiated in October 2012, when the author enrolled to the Department of Civil and Industrial Buildings, Faculty of Civil Engineering, Politehnica University of Timișoara, Romania as PhD Student under the supervision of Prof. Valeriu Stoian. I received the task to continue the extensive research project that was already running on the behaviour of precast reinforced concrete wall panels under seismic loads. The studies were started by Dr. István Demeter and continued by Dr. Carla Toduț.

During the first year of doctoral studies I started the experimental testing being acquainted with the experimental procedures in the Laboratory of Reinforced Concrete Structures by Dr. Carla Toduț, Dr. István Demeter, Dr. Nagy-György, Mr. Nicolae Albu during the master studies. The first experimental test was performed in April 2013 and the last one in July 2015. All along this time I was for the most part involved physically in every operation from the construction of the specimens to the retrofitting procedure and laboratory testing. Manager of SC Mirocom SRL, Eng. Fofiu was helpful in the technical and logistic aspects of the specimen construction. The experimental tests were performed in collaboration with PhD Student Andrei Bîndean and other colleagues and students from the Department. Technical staff member Mr. Nicolae Albu was the workmanship fellow of the author during the construction, set-up and strengthening of the specimens. The test rig and the hydraulic equipments were installed Mr. Nicolae Albu while MAPEI Corporation Romania provided the strengthening materials and lend a helping hand in their application.

After the completion of the tests it followed roughly two years of data processing, further literature survey and the elaboration of the thesis followed. During this time I received valuable guiding from Prof. Tamás Nagy-György, Assoc. Prof. Sorin Dan, and Assoc. Prof. Ștefan Iosip-Moț under the careful oversee from Prof. Valeriu Stoian. The final draft of the thesis was reviewed by Prof. Nicoale Țăranu from Technical University "Gheorghe Asachi" Iasi, Prof. Daniela Lucia Manea from Technical University of Cluj-Napoca, Prof. Daniel Dan and Prof. Stoian Valeriu from Politehnica University Timisoara.

I am deeply grateful to my supervisors, Prof. Valeriu Stoian, for the encouragement, generous support and enlightening guidance in carrying out this research and in producing this thesis.

I would like to thank Dr. Carla Todut, Dr. Demeter Istvan, Prof. Tamás Nagy-György, their expert guidance and support in conducting the experiments. I am also very grateful for the assistance and cooperation from Andrei Bîndean.

I would also like thank the friends, and my colleagues in the Politehnica University Timisoara for their help and support.

Special thanks got o Mapei Corporation Romania, Eng. Cristian Cartaș and his team who sponsored my research with strengthening materials and also helped in their application.

I deeply thank my parents for their love, care and support during these years, they have been a constant source of love and comfort for me, and I would not be where I am today without them. I am much indebted to them.

Finally, I thank with love Renata, my wife, for her love, patience, and understanding, she allowed me to spend most of the time on this thesis.

Timişoara, October 2017 Mihai Fofiu

” This paper is partially supported by the Sectoral Operational Programme Human Resources Development (SOP HRD), ID134378 financed from the European Social Fund and by the Romanian Government”.

“This paper was partially supported by MAPEI Company by representative Mr. Cristi Cartas”

“This paper was partially supported by MIROCOM SRL Company by representative Mr. Mihai Fofiu”

FOFIU, Mihai

Retrofitting the precast RC wall panels using externally bonded CFRP laminates

Teze de doctorat ale UPT, Seria 18, Nr. 4, Editura Politehnica, 2017, 192 pagini, 132 figuri, 10 tabele.

ISSN: 2393-4816
ISBN: 978-606-35-0186-9

Cuvinte cheie: CFRP, Laminates, seismic actions, retrofitting, ciclyc test, wall, reinforced concrete, precast, openings.

Rezumat: This work is relevant to the field of earthquake engineering and addresses the seismic behaviour of the reinforced concrete walls. The objectives of the thesis are to investigate the seismic performance of the precast reinforced concrete walls and reveal the effects of the seismic retrofit by externally bonded carbon fibre reinforced polymers laminates. The experimental program consisted of ten quasi-static cyclic tests on near-full scale precast reinforced concrete wall specimens. The experimental variables referred to the opening type and the strengthening condition. The influence of the cut-out opening size on the shear strength, stiffness and ductility was considerable. The retrofitting technique by means of CFRP-EBR laminates improved the behaviour characteristics, primarily in terms of maximum load bearing capcity and maximum displacement; however, certain limitations were identified on the use of this strengthening system in reversed cyclic applications.

Table of Contents

Table of Contents 5
Symbols and abbreviations 7
List of Figures 10
List of tables 14
1. INTRODUCTION 15
1.1. Framework 15
1.2. Motivation and objectives 16
1.3. Overview of the thesis 16
2. LITERATURE REVIEW 19
2.1. Seismic zones in Romania 19
2.2. Precast reinforced concrete large panel buildings in Romania 22
2.3. RC walls seismic laboratory test 30
2.4. Retrofitting procedures using FRP for RC 34
2.1. Retrofitted RC walls seismic laboratory test 39
3. EXPERIMENTAL PROGRAM 43
3.1. Introduction 43
3.2. Test Specimens characteristics 44
3.3. Material properties 57
3.3.1. Concrete 57
3.3.2. Reinforcement 59
3.3.3. Strengthening Materials 60
3.4. Repair and Strengthening 63
3.4.1. Strengthening using EBR-CFRP combined with NSM-CFRP 63
3.4.2. Strengthening using EBR-CFRP laminates 67
3.5. Experimental test set-up 70
3.6. Loading protocol 74
3.7. Boundary conditions 76
3.8. Instrumentation 76
4. RESULTS 79
4.1. Failure details and behaviour of the reference specimens 79
4.2. Failure details and behaviour of the FRP strengthened specimens 87
4.3. Force-drift ratio data analysis 94
4.3.1. Hysteresis loops 94
4.3.2. Cyclic envelops 97
4.3.3. Monotonic Envelopes 100
4.3.4. Backbone envelopes 103
4.4. Energy dissipation analysis 108
4.5. Strength and ductility analysis 122
4.6. Displacement analysis 124
4.7. Stiffness analysis 126
4.8. Theoretical study using Eurocode and CNR provisions 129
4.9. Cracking Pattern 136
5. CONCLUSIONS AND PERSONAL CONTRIBUTIONS 141
5.1. Conclusions 141
5.2. Personal contributions 143

5.3. Published papers and acknowledgements 144
6. FURTHER RESEARCH RECOMMENDATIONS 147
Bibliography 149
APPENDIX A - Force-drift ratio analysis comparison between similar specimens 161
Hysteresis loops comparison 162
Cyclic envelope M2 166
Cyclic envelope M1 169
Backbone envelopes 172
APPENDIX B – Test logs 174
Specimen 13 S-E3-RT 175
Specimen 14 S-EL2-T 177
Specimen 15 EL2-TR..... 179
Specimen 16 L1-E1-T 180
Specimen 16 L1-E1-TR..... 182
Specimen 17 L3-T 183
Specimen 17 L3-TR 185
Specimen 18 -L3-E3-T 187
Specimen 18 -L3-E3-TR 188

Symbols and abbreviations

Symbols

Φ	diameter of reinforcing bar
A	in-plane area
A_c	cross section area of concrete
A_o	in -plane area of the opening
A_s	cross section area of reinforcement
A_{sw}	cross-sectional area of the shear reinforcement
A_w	in-plane area of the web-panel
b_w	thickness of the web
C	class of concrete
CD_j	Cumulative Drift corresponding to a point "j" on the response
CED_j	Cumulative Energy Dissipated corresponding to a point "j" on the response
CED_{max}	Maximum Cumulative Energy which could be theoretically Dissipated during the response
CR_j	Cumulative Drift corresponding to a point "j" on the response
ED_{max}	Maximum Energy which could be theoretically Dissipated during the response
Es	modulus of elasticity of steel reinforcement
f_{ck}	diameter of reinforcing bar
f_{cm}	mean value of concrete cylinder compressive strength
$f_{cm,cube}$	mean concrete compressive cube strength
f_t	tensile strength of steel reinforcement
f_y	yield strength of steel reinforcement
f_{ywd}	design yield strength of the shear reinforcement
j	is a point on the load displacement curve=a data line in the data file
l_w	wall length
N	axial load
N1, N2	axial loads acting above pier#1 and pier#2

R	drift ratio
s	spacing of stirrups
V	lateral load; shear force
$V_{exp,max}$	maximum experimental shear force
V_j	lateral load value corresponding to a point "j" on the load displacement curve
$V_{rd,c}$	design shear resistance of the member without shear reinforcement
$V_{Rd,max}$	design value of the maximum shear force, which can be sustains by the member, limited by crushing of the compression struts
$V_{rd,s}$	design shear resistance of the yielding of shear reinforcement
z	level arm of internal forces
α_{cw}	coefficient taking account of the state of the stress in the compression chord
α_s	aspect ratio
δ	displacement
δ_j	is the drift level corresponding to a point "j" on the load displacement curve
θ	inclination angle of concrete strut to the vertical direction
μ	ductility factor
$\mu_{0,85}$	ductility measured from at 0,85 pre- and post-peak shear strength

Abbreviations

13,14,15,16,17,18	Number of specimens
A	Type A test set-up
AFRP	Aramid fibre reinforced polymer
BFRP	Basalt fibre reinforced polymer
C	Cycle
C2, C2	first and second load displacement cycle
CD	Cumulative drift
CED	Cumulative energy dissipated
CF	Carbon fibre
CFRP	Carbon fibre reinforced polymers

CR	Cumulative drift ratio
D	Displacement transducer
DCM	Medium ductility class
E1	Narrow door opening
E36-7	Exterior wall (Project type 770-81)
EBR	Externally bonded reinforcement
EC2	Eurocode 2
ED	Energy dissipated
EL2	Door and window opening
FRP	Fibre reinforced polymers
G	Strain gauge
GFRP	Glass fibre reinforced polymers
I54-2a	Interior wall (Project type 770-81)
L1-E1	Small window enlarged to door opening
L3	Wide window opening
L3-E3	Wide window opening enlarged to wide door opening
M1	Monotonic envelope
M2	Average cyclic envelope
NSM	Near surface mounted
OB	Romanian smooth reinforcing bar
P	Pressure transducer
PC	Romanian ribbed reinforcing bar
pcs	Pieces
PRCLP	Precast reinforced concrete large panel
PRCWP	Precast reinforced concrete wall panel
RC	Reinforced concrete
RT	Prior to damage strengthening (retrofitted and tested)
S	Solid
STNB	Romanian smooth wire reinforcement
T	Test
TR	Post-damage strengthening (tested and retrofitted)
TRM	Tensile reinforced mortar
xp	Reinforcement bar

List of Figures

Figure 2-1 – SHARE European Seismic Hazard Map 2013 [3] 19
Figure 2-2 – SHARE map and P100-1 2013, peak ground accelerations for Romania overlay. 20
Figure 2-3 – Building 23
Figure 2-4 – Residential buildings distribution based on the type of building 23
Figure 2-5 – Apartment buildings distribution based on the construction materials 24
Figure 2-6 – Dwellings distribution based on construction materials 24
Figure 2-7 – Population distribution based on buildings 25
Figure 2-8 – Front view of Project Type 770-81 building [50] 25
Figure 2-9 – Ground floor plan for 770-81 project type [50] 26
Figure 2-10 – P+10 Precast building without and with thermal rehabilitation 27
Figure 2-11 – P+4 project type 770-81 precast building, original and with attic added later 27
Figure 2-12 – P+4 project type 770-81 precast building, original and with attic added later 28
Figure 2-13 – P+4 typical precast apartment buildings 28
Figure 2-14 – Panoramic view of precast buildings neighbourhood 28
Figure 2-15 – Precast buildings neighbourhood in Bucharest [53] 29
Figure 2-16 – Precast buildings neighbourhood in Cluj Napoca and Brașov [54, 55] 29
Figure 2-17 – Precast buildings neighbourhood in Galați and Timișoara [56, 57] ... 29
Figure 2-18 – Aramid reinforcement bars [81, 82] 34
Figure 2-19 – Aramid fibre sheets [87, 88] 35
Figure 2-20 – BFRP rebars and fabric [93, 94] 35
Figure 2-21 – GFRP reinforcement [105, 106] 36
Figure 2-22 – GFRP mesh [116] 37
Figure 2-23 – CFRP laminates and mesh [119, 120] 37
Figure 2-24 – EBR system for mesh and laminates [137, 138] 38
Figure 2-25 – NSM system for CFRP laminates [139] 38
Figure 3-1 – Testing timeline 43
Figure 3-2 – Construction of the specimens (Timisoara) 45
Figure 3-3 – Construction of the specimens (Stei) 47
Figure 3-4 – Opening cut-out procedure 48
Figure 3-5 – Tested specimens 49
Figure 3-6 – Reinforcement details for PRCWP 13 S-E3 and 14 S-EL2 50
Figure 3-7 – Reinforcement details for PRCWP 15-EL2 51
Figure 3-8 – Reinforcement details for PRCWP 16-L1-E1 52
Figure 3-9 – Reinforcement details for PRCWP 17-L3 53
Figure 3-10 – Reinforcement details for PRCWP 18-L3-E3 54
Figure 3-11 – General view of experimental specimens, designation of wall specimen's components and opening dimensions 57
Figure 3-12 – Recipe used for concrete manufacturing 58
Figure 3-13 – Concrete testing: (a) testing machine; (b) compression test on cube 59
Figure 3-14 – FRP reinforcement used 61
Figure 3-15 – Strengthening strategy using NSM-CFRP combined with ERB CFRP .. 64
Figure 3-16 – NSM-CFRP combined with EBR-CFRP strengthening process 67

Figure 3-17 – The position of the EBR CFRP laminates for PRCWP 15 and PRCWP 16 68
Figure 3-18 – The position of the EBR CFRP laminates for PRCWP 17 and PRCWP 18 69
Figure 3-19 – Anchorages for the EBR CFRP system 70
Figure 3-20 – Loading beams detail [49] 71
Figure 3-21 – Casted loading beams 71
Figure 3-22 – Hydraulic jacks and pumps 72
Figure 3-23 – Experimental test set-up 73
Figure 3-24 – Lateral and vertical reaction frames 73
Figure 3-25 – Lateral loading procedure 74
Figure 3-26 – Positive and negative direction of loading 75
Figure 3-27 – Axial loading 76
Figure 3-28 – Data acquisition system 77
Figure 3-29 – Displacement transducer position 77
Figure 3-30 – Piezo-resistive pressure transducer and pressure gauge 78
Figure 4-1 – Failure details of PRCWP 14-S-EL2-T 80
Figure 4-2 – Failure details of PRCWP 15 82
Figure 4-3 – Failure details of PRCWP 16-L1-E1-T 84
Figure 4-4 – Failure details of PRCWP 17-L3-T 85
Figure 4-5 – Failure details of PRCWP 18-L3-E3-T 86
Figure 4-6 – Failure details of PRCWP 13-S-E3-RT 87
Figure 4-7 – Failure details of PRCWP 16-L1-E1-TR 89
Figure 4-8 – Failure details of PRCWP 17-L3-TR 92
Figure 4-9 – Failure details of PRCWP 18-L3-E3-TR 93
Figure 4-10 – Cycles' loading points and subsections 94
Figure 4-11 – Hysteresis loops for the reference specimens 95
Figure 4-12 – Hysteresis loops for the retrofitted specimens 96
Figure 4-13 – Comparison between hysteresis loops 97
Figure 4-14 – Construction of cyclic envelopes M2 97
Figure 4-15 – Cyclic envelopes M2 for the reference specimens 98
Figure 4-16 – Cyclic envelopes M2 for the strengthen specimens 99
Figure 4-17 – Cyclic envelopes M2 comparison 100
Figure 4-18 – Construction of monotonic envelopes M1 100
Figure 4-19 – Monotonic envelopes M1 for the reference specimens 101
Figure 4-20 – Monotonic envelopes M1 for the strengthen specimens 102
Figure 4-21 – Cyclic envelopes M1 comparison 102
Figure 4-22 – Backbone Envelope (Type 1) for the reference specimens 103
Figure 4-23 – Backbone Envelope (Type 1) for the strengthen specimens 104
Figure 4-24 – Backbone Envelope (Type 2) for the reference specimens 105
Figure 4-25 – Backbone Envelope (Type 2) for the strengthen specimens 106
Figure 4-26 – Backbone Envelope comparison: (left) Type 1; (right) Type 2 107
Figure 4-27 – Construction of energy dissipation curves 109
Figure 4-28 – Cumulative energy dissipated vs drift ratio for the reference specimens 110
Figure 4-29 – Cumulative energy dissipated vs drift ratio for the strengthen specimens 111
Figure 4-30 – Cumulative energy dissipated vs cumulative drift for the reference specimens 112
Figure 4-31 – Cumulative energy dissipated vs cumulative drift for the reference specimens 113

Figure 4-32 – Cumulative energy dissipated per half cycle for the reference specimens 114
Figure 4-33 – Cumulative energy dissipated per half cycle for the strengthen specimens 115
Figure 4-34 – Cumulative energy dissipated per cycle for the reference specimens 116
Figure 4-35 – Cumulative energy dissipated per cycle for the strengthen specimens 118
Figure 4-36 – Energy dissipated per cycle for the reference specimens 119
Figure 4-37 – Energy dissipated per cycle for the reference specimens 121
Figure 4-38 – The shear strength for the reference specimens 122
Figure 4-39 – The shear strength for the strengthen specimens 122
Figure 4-40 – The shear strength for the tested specimens 123
Figure 4-41 – Shear strength ratios..... 123
Figure 4-42 – Ductility Coefficient 124
Figure 4-43 –Drift ratio for the reference specimens 124
Figure 4-44 – Drift ratio for the strengthen specimens 125
Figure 4-45 – Drift ratio for all tested specimens 125
Figure 4-46 – Stiffness degradation for reference specimens..... 126
Figure 4-47 – Stiffness degradation for strengthen specimens..... 127
Figure 4-48 – Stiffness degradation comparison 128
Figure 4-49 Initial Stiffness of the tested specimens 128
Figure 4-50 – Shear resistance of reference specimens comparison 133
Figure 4-51 – Shear resistance retrofitted specimens comparison..... 134
Figure 4-52 – Shear resistance with angle θ=45° comparison 134
Figure 4-53 – Shear resistance comparison between computed elemenets 135
Figure 4-54 The cracking pattern of the tested elements 139
Figure A- 1 – PRCWP 14-S-EL2-T, 17-EL2-T hysteresis comparison 162
Figure A- 2 – PRCWP 17-S-L3-T, 18-L3-E3-T hysteresis comparison 163
Figure A- 3 – PRCWP 17-S-L3-TR, 18-L3-E3-TR hysteresis comparison 163
Figure A- 4 – PRCWP 17-S-L3-T, 18-L3-E3-T, 17-S-L3-TR, 18-L3-E3-TR hysteresis comparison..... 164
Figure A- 5 – PRCWP 13-S-E3-RT, 14-S-EL2-T hysteresis comparison 164
Figure A- 6 – PRCWP 17-S-L3-T, 17-S-L3-TR, 15-EL2-TR hysteresis comparison . 165
Figure A- 7 – All specimens hysteresis comparison 165
Figure A- 8 – PRCWP 13-S-E3-RT, 18-L3-E3-T and 18-L3-E3-RT M2 Envelope comparison..... 166
Figure A- 9 – PRCWP 14-S-EL2-T, 17-EL2-T M2 envelope comparison 166
Figure A- 10 – PRCWP 17-S-L3-T, 18-L3-E3-T, 17-S-L3-TR, 18-L3-E3-TR M2 envelope comparison..... 167
Figure A- 11 – PRCWP 13-S-E3-RT, 14-S-EL2-T M2 envelope comparison..... 167
Figure A- 12 – PRCWP 17-S-L3-T, 17-S-L3-TR, 15-EL2-TR M2 envelope comparison 168
Figure A- 13 – All specimens M2 envelope comparison 168
Figure A- 14 – PRCWP 13-S-E3-RT, 18-L3-E3-T and 18-L3-E3-RT M1 Envelope comparison..... 169
Figure A- 15 – PRCWP 14-S-EL2-T, 17-EL2-T M1 envelope comparison 169
Figure A- 16 – PRCWP 17-S-L3-T, 18-L3-E3-T, 17-S-L3-TR, 18-L3-E3-TR M1 envelope comparison..... 170
Figure A- 17 – PRCWP 13-S-E3-RT, 14-S-EL2-T M1 envelope comparison..... 170

Figure A- 18 – PRCWP 17-S-L3-T, 17-S-L3-TR, 15-EL2-TR M1 envelope comparison 171
Figure A- 19 – All specimens M1 envelope comparison 171
Figure A- 20 – Backbone Type 1 envelope comparisons 172
Figure A- 21 – All specimens Backbone Type 1 comparison 172
Figure A- 22 – Backbone Type 2 envelope comparisons 173
Figure A- 23 – All specimens Backbone Type 2 comparison 173

List of tables

Table 3-1 – Overview of the experimental program 44
Table 3-2 – Variables of the experimental program 57
Table 3-3 – Properties of the concrete 59
Table 3-4 – Properties of steel reinforcement (measured) 60
Table 3-5 – Properties of steel reinforcement (typical) 60
Table 3-6 – Properties of CF materials and epoxy resins 62
Table 3-7 – Properties of the repair mortars 62
Table 3-8 – Cycle drift magnitudes 74
Table 3-9 – Transducers type and characteristics 78
Table 4-1 – Shear resistance evaluated using Eurocode provisions 132

1. INTRODUCTION

1.1. Framework

This paper addresses the seismic response of precast reinforced concrete walls and the possibility to retrofit them. The seismic risk on Romania is one of the highest in Europe and seismic hazard for almost half of the territory of Romania is determined by the Vrancea seismic region, which is situated beneath the southern Carpathian Arc. This region has intermediate-depth earthquakes at depth from 70 to 160 km and in following years a large earthquake is expected to occur. Aside from this region several other zones of shallow seismicity activity located both within and outside Romanian borders are considered dangerous.

In the communist era of Romania there was a high demand for new housings for the citizen in the urban area, thus the need for buildings with good seismic response and fast development was needed. The answer came in form of the typical Eastern Europe apartment buildings made with wall structural systems made either of precast reinforced concrete large panels (PRCLP) or monolithic. Romania is no exception with tens of thousands of mid-rise apartment buildings build during the 1960 up until 1990, the most common ones are the 5-storey(P+4) ones with 4 apartments on each level, staircase and no elevator shaft.

Although the seismic response of these building proved to be adequate, the use of reinforced concrete large panels as structural system diminished due to several factors like space requirements and the antipathy of the people for everything that was communist after the revolution in 1989. Since these buildings are several decades old now, a large majority of them were tested during their lifetime by several major earthquakes (1977, 1986 and 1990) but some of them are showing their age and present "scares" in form of large cracks in the panels.

In terms of functionality this apartment buildings are not up to today's living standards and the owners of such apartments are in search for solution to improve the comfort of their homes by modifying the existing floor plan. However, this proves to be quite difficult as the reinforced concrete wall structural system is not modular, forcing the occupants to create new openings in the existing walls or to increase the existing openings by cut-outs. One typical example of such instance is at the ground floor apartments where many owners decided to change the occupancy from residential to commercial, so they need more open space and larger windows, but by creating such facilities they damage the integrity of the structural system and endanger the performance of the walls.

In the past few decades, there have been considerable advancements in the design procedures of reinforced concrete (RC) shear walls for new construction, such as the new performance-based seismic design and capacity design principles. Alongside these advances for new buildings research has begun in the field of retrofitting of these buildings with reinforced concrete walls as structural system, nonetheless the fact that there are so many opening possibilities, different design of the panels during the years and distinct retrofitting strategies, the search continues for the most effective retrofitting procedure and the understanding on of the cut-outs on the seismic behaviour.

1.2. Motivation and objectives

In order to experimentally evaluate the seismic performance of precast reinforced concrete large panel buildings, special equipment and tools are needed, therefore, similar research in this area is limited. Given the large number of existing buildings that use this structural system it is necessary to evaluate their behaviour and their seismic load bearing capacity. In Romania, these buildings are residential buildings and is common practice for the owners to have openings cut-out in the RC walls. This behaviour leads to the redistribution of efforts in the elements and potentially putting the building at risk of collapse, making the research of the influence of the different types of openings on the performance of the element imperative.

Research regarding the retrofitting of Reinforced Concrete (RC) elements using different procedures with FRP materials exist in the literature, most of these research programmes involve theoretical studies. Experimental programmes are present, however, most of these are focused on RC elements subjected to bending. In regards to shear elements literature experimental test are scares and are focused on small scale elements. In Romania, most of these buildings are of significant age (more than 30 years old) and were subjected to seismic actions during their lifetime so the search for effective retrofitting procedures using new technologies has begun.

The above-mentioned arguments establish the motivation for the development of the experimental programme presented by the author in this thesis. The practical applications of the research are wide in range and of significance influence.

The research theme is focused on experimental studies on the behaviour of precast reinforced concrete large panels subjected to reversed cyclic loading, simulating the seismic action. The objectives of this thesis are to provide further understanding and improve the knowledge on several key discussions.

- How does the precast reinforced concrete wall panels perform and fail when subjected to in-plane reversed cyclic loading?
- Can the ERB-CFRP strips retrofitting technique restore the walls initial load bearing capacity?
- How does the retrofitting procedure influence the failure modes of the elements?
- Does the size and type of opening or weakening influence the structural behaviour and capacity at limit states?
- What is the energy dissipation capacity of the shear walls with different openings and how does it compare to the retrofitted counterparts?
- Are design code provisions for estimating the shear strength accurate?
- How does the results obtained compare to others found in literature?

1.3. Overview of the thesis

The thesis is composed of six chapters and two appendices totalising more than 180 pages. The thesis focuses on ten quasi-static cyclic tests on near-full scale precast wall panels.

In the first chapter, the framework of the thesis is introduced, the motivation and objectives that lead to the research are given and an overview of the thesis is presented.

Chapter 2 offers a general presentation of the seismic zones in Romania and the ways scientist try to predict the earthquakes. Additionally, the distribution of the

most popular and widely used construction system for apartment buildings in Romania is given, with the presentation of the prototype used for the experimental campaign. Afterwards, a review of the literature on RC wall tests is presented, followed by a description of retrofitting strategies and materials and an extensive review on retrofitted RC wall tests.

In Chapter 3 a detailed description of the experimental program is given. The chapter commences with the timeline of the tests alongside the description of the experimental specimens in terms of concrete outlines, steel reinforcing details. Subsequently, the properties of the three structural material types are presented. Special attention was paid to the description of the retrofitting strategies employed in the research and the technique used to apply them. In the followings the test set-up, the loading protocol and boundary conditions are detailed. The experimental program is concluded by the instrumentation of the specimens.

In the 4th Chapter the results obtained by the ten cyclic wall tests are rendered in two ways, namely primary results and detailed test logs. The primary results consist in the load-displacement response, the loading and displacement histories, the final cracking pattern, a brief description of the observed behaviour and failure mode, and a limited number of photographs on failure details. Another extensive part of the chapter is the analysis of the results. In accordance to the general seismic performance characteristics of the lateral load resisting members the following analysis types were undertaken: strength and ductility analysis, displacement analysis, stiffness analysis, theoretical study and energy dissipation analysis. In addition to the measured response analyses, the observed behaviour aspects peculiar to concrete members were also addressed through cracking analysis.

In Chapter 5 the conclusions are drawn with respect to the retrofitting effect of the FRP-EBR system on the cyclic response of the precast reinforced concrete wall panels. The chapter is concluded by an account of the author's publications and his personal contribution to this work.

In the last chapter, an outlook is provided for future research directions.

The Appendices contain supplementary descriptive information consisting in charts which would have been disruptive if presented in the main body of the thesis. In Appendix A a comparison between similar specimens in regards to their force-drift ratio analysis is made and in Appendix B the detailed test logs for all specimens are given

2. LITERATURE REVIEW

2.1. Seismic zones in Romania

Romania is situated in the southeaster part of Central Europe and is the twelfth country of Europe, considering its area of 238391 km^2 [1]. In the southern part, Romania borders Serbia and Bulgaria, part of this border being the Danube (1075 km). Other borders are with Hungary, Ukraine, Moldova and the Black Sea. The country is crossed by the Carpathian Mountains which are a subdivision of the larger Alps-Himalayan System part of the Alpide belt. According to USGS [2] the Alpide belt is the second most seismically active region worldwide accounting for 17% of the largest earthquakes.

By looking at the SHARE earthquake hazard map of Europe [3] Figure 2.1, one can see that Europe has zones with high seismic hazard, the map was evaluated with a time-independent, probabilistic approach. Although the southern part of Europe has the largest risk in terms of seismic actions with peak ground accelerations exceeding 0.5g, the central-eastern part is dominated by a confined region high ground acceleration, the region in question is the Vrancea region, the most dangerous seismic zone in Romania.

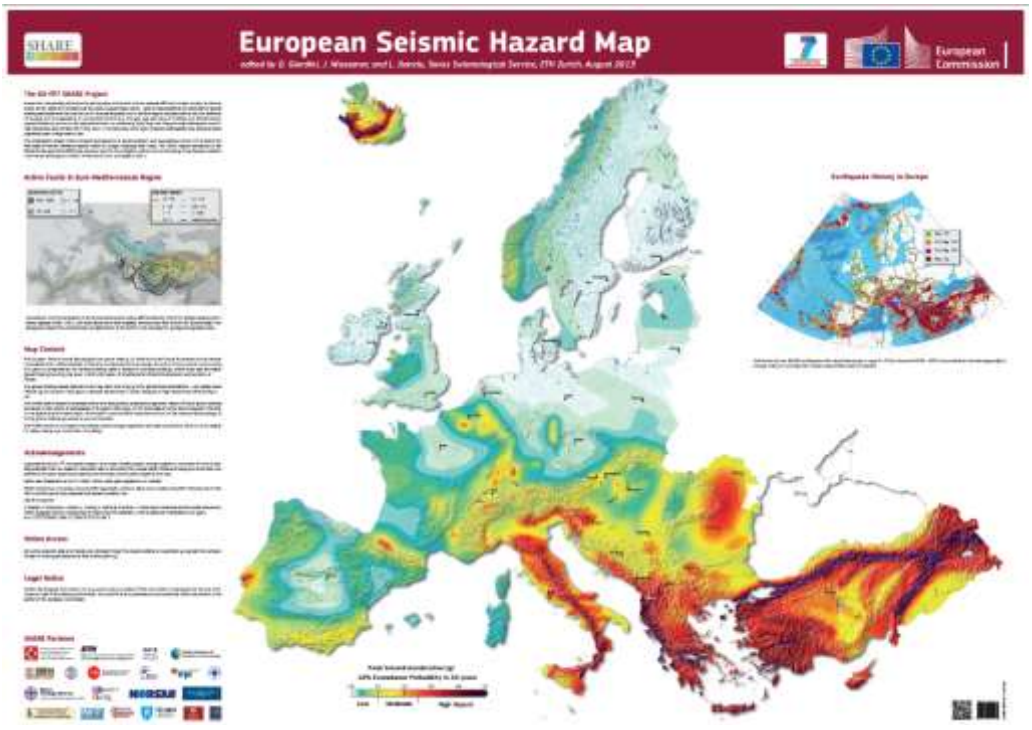

Figure 2-1 – SHARE European Seismic Hazard Map 2013 [3]

Located in the subcrustal lithosphere in the beginning of the Eastern Carpathians Vrancea is characterized by earthquakes of intermediate-depth. Several other zones with intermediate-depth seismicity exist worldwide, the Hindu Kush region (e.g. [4, 5, 6]), Bucaramanga in Columbia (e.g. [7, 8]), Tonga-Kermadec region (e.g. [9, 10]). However, this is not the only active seismic zone in the country, according to Radulian et al. [11] several other seismic areas of hazard exist: East Vrancea Zone, Bârlad Depression, Predobrogean Depression, Intramoesian Fault, Făgăraş – Câmpulung zone, Danubian zone, Banat and Crişana – Maramureş zones, Transylvanian Depression. By overlaying the Romania norm peak ground accelerations map [12] over the SHARE earthquake hazard map Figure 2.2, one can see that the Vrancea region is the most hazardous zone and the two maps coincide in terms of hazard areas, with peak ground accelerations of 0.4g according to the Romanian norm and in the range of 0.3-0.4 according to SHARE map.

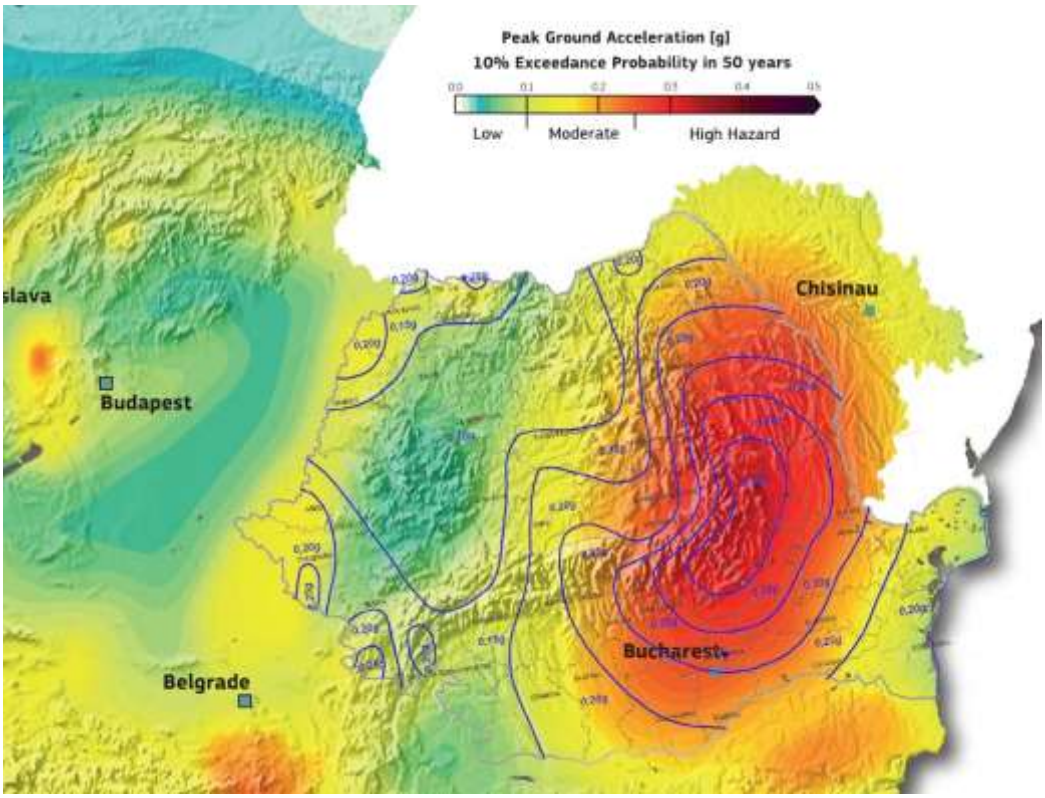

Figure 2-2 – SHARE map and P100-1 2013, peak ground accelerations for Romania overlay.

"Seismic hazard describes a natural phenomenon associated with an earthquake and can be quantified by a level of severity (e.g., peak ground acceleration, macro-seismic intensity), its occurrence frequency and location" [13]. The seismic hazard of the region was intensely researched using neo-deterministic methods (e.g. [14, 15, 16, 17]), and probabilistic (e.g. [18, 19, 20]), for this the accelerograms of the large 1977, 1987 and 1990 earthquakes were used. The source spectra and site amplification functions from S-waves in the frequency range of 05 to

20 Hz derived by Oth et al. [21] from 55 intermediate-depth Vrancea can be used as a basis for stochastic simulations of ground motions resulting from scenario earthquakes. Besides the seismic hazard assessment, another very important aspect is when, where and how strong will the next big earthquake be. For the intermediate depth earthquake of Vrancea the question of when and how strong will the next earthquake be being very critical. Several studies were performed in order to assess the magnitude of the next earthquake.

A comparison with the SHARE research projects results for Romania was made by F. Pavel et al. [22] who made a probabilistic seismic hazard analysis based on the Cornell-McGuire approach within the BIGSEES ("Bridging the gap between seismology and earthquake engineering: from the seismicity of Romania towards a refined implementation of Seismic Action EN1998-1 in earthquake resistant design of buildings" [23] national research project for the Eurocode 8 requirements. They obtained several differences and concluded that further studies are need for obtaining a map that reflects precisely the seismic hazard of Romania.

B. M. Sørensen et al. [24] derived an intensity prediction equation for Vrancea region, applicable for three different distance measures with comparable levels of uncertainty, and are valid in the magnitude range Mw=6.4–7.7, the region 20.5–30.7°E; 41.7–48.4°N in the depth range h=73–181 km and in the distance range R=0–520 km. The derived ground motion prediction equations (GMPE) are not valid for shallow, crustal earthquakes but these earthquakes should not be neglected when making a seismic hazard analysis. Although the authors of the paper acknowledge the uncertainties with the input data like the earthquake source parameters (can be neglected [25]) and the intensity data, the results have an uncertainty of ca. 0.6 intensity units. The activity in the Region has been recently analysed by A. Craiu et al. [26], investigating over 1600 earthquakes with magnitudes between 1.8 and 5.5.

Seismic hazard prediction is very intricate and arduous because of the specificity of each regions characteristics and classic seismic hazard analysis is not relevant ever to strong and deep earthquakes in Vrancea. [27].

For predicting the next large earthquake and design early warning systems various approaches are used by researchers in the literature.

O. V. Novikova et al. [28] used the medium-term prediction CN algorithm [29] based on the quantitative analysis of premonitory phenomena, to successfully predict four large earthquakes with magnitude of 7 or above since 1932, however the 1945 earthquake with magnitude of 6.4 was a failure to predict. All predicted earthquakes have TIPs (Time of Increased Probability) going ahead of the main shock. The 1977 earthquake is preceded by alarm 2.1 months in advance, the 1986 12 months in advance and the 1990 has an alarm 9 month early. For the more recent period of 1194-2003 C.L. Moldoveanu et al. [30] continued to monitor the activity using CN algorithm, however, in the aforementioned period no strong earthquakes with magnitude over 6.0 occurred, only one false alarm of 18 months was recorded.

Another method used for predicting earthquakes is by using the M8 algorithm [31], L.L. Romashkova and V.G. Kossobokov [32] concludet that the original version of the M8, algorithm is not suitable for Vrancea region due to the low number of earthquakes with magnitude larger than 4.0. However, staring with 2007 the M8 algorithm is being used to predict earthquakes [33]. A comprehensive evolution and predictions using M8 algorithm is presented by V. G. Kossobokov [34, 35].

M. Böse et al. [36] revised scaling relation for earthquake early warning in Romania proposed by Wenzel et al. [37] and although the shortcomings of the EEW system that relies on the information of the single station [38] apply to the on-site warning system present in Romania [39], the specifics of Vrancea region with the

earthquakes epicentres basically in one location make this system far more acceptable and trustworthy than other systems. By applying their proposed revised scaling relation to the October 27, 2007, (M_W=6.0) Vrancea earthquake they managed to predict quite accurate the ground motion, with all predictions giving adequate results.

A comprehensive state of the art in regards to geodynamics and intermediate-depth seismicity in the area was done by Zadeh et al. [13], proposing further perspective studies to improve several key aspects like which kind of studies should be conducted in the region to explain the unresolved problems, the better understanding of the lithosphere and the mantle beneath Vrancea and how to better the earthquake forecast and develop reliable seismic models.

E. S. Georgescu strived to investigate the consequences of the two major earthquakes from Romania in 1940 and 1977. The study showed that in 1977 the death toll was larger in many cases due to existing pre-1940 buildings that were damaged and buildings built in the period 1950-1976, as seen by the collapse of Block OD16 and Block 30. [40]. The general populations perception of earthquake hazard was investigated by I. Armaș who made a seismic risk perception in Bucharest. The central conclusion was that the population is not prepared to manage the consequences of a major earthquake. There is still a difference in the way people perceive seismic risk based on gender. [41]. When it comes to recent simulations of risk assessment for Bucharest, the economic loss would be in the range of 5-13 bill. € and the number of affected people between 3000 and 38000, with a resulting debris of 2.5-11.0 mill. Tones. As the earthquake magnitude increases the degree of uncertainty decreases and the number of operators necessary for intervention is approximately one third of the number of people in need of assistance. [42]

2.2. Precast reinforced concrete large panel buildings in Romania

In Romania one of the most widely spread construction type of apartment buildings are the ones with precast reinforced concrete walls. The popularity of these structural system gained momentum in the post second world war era, when a large number of apartments were needed in the urban areas. According to [43] in the urban population living in apartment blocks in 1966 was 17.4% and it has increased to over 42% by 1977 reaching a staggering 71.4% by the early nineties. The mass construction of apartment buildings made out of reinforced concrete, precast or cast in place, started in the 1945, peaked in the 1980's and stared to die down in the early nineteens after the revolution. During the period of 1946-2000, over 65 000 reinforced concrete apartment building were built, out of these over 30 000 were made out of precast concrete [44]. The number of buildings constructed during 1945-2010 is presented in Figure 2.3, it can be seen that the peak period is from 1970-1990, after that the rate of constructing these apartment buildings declined severely.

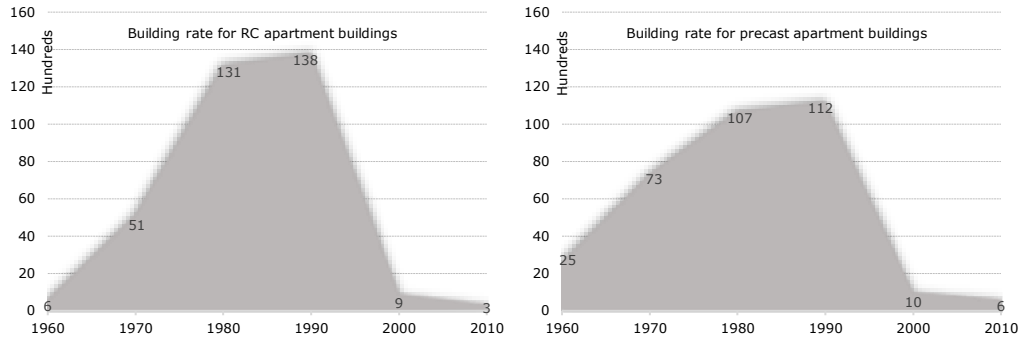

Figure 2-3 – Building

Looking at building distribution in Romania from 1945-1990 and nowadays presented in Figure 2.4, [44] we can see than the proportion remained the same, only 2 percent of the total residential buildings are apartment buildings. These would indicate that the vast majority of the population lives in individual homes or duplex buildings, still one should keep in mind that in each apartment building is composed of several dwellings. Out of these 2% of building the reinforced concrete building structure and precast ones are preponderant.

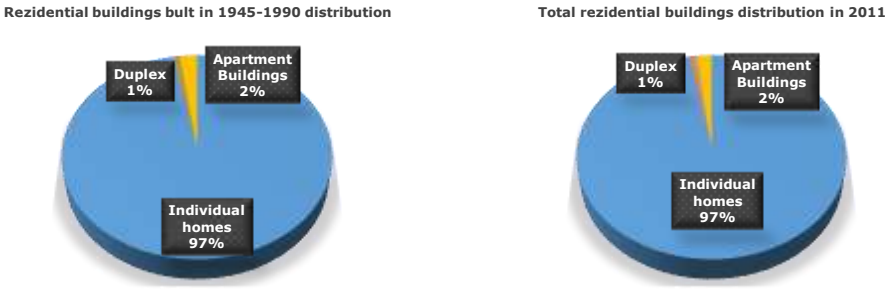

Figure 2-4 – Residential buildings distribution based on the type of building

In Figure 2.5 the distribution based on the construction type of the apartment buildings is presented for the 1945-1990 period and nowadays. [44] It can be seen that the proportions are similar, with the masonry buildings being more popular nowadays than reinforced concrete ones due to the height restrictions in rural areas near the large cities, where a considerable number of new apartment buildings with 3 to 4 levels were build.

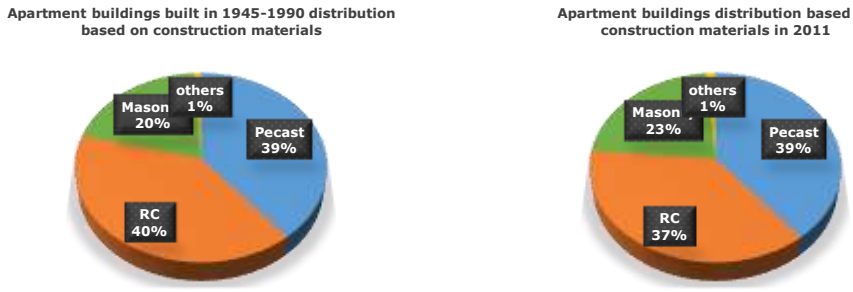

Figure 2-5 – Apartment buildings distribution based on the construction materials

As previously stated in one apartment building there are more than one dwellings, in 11 levels buildings existing up to 66 dwellings, thus the necessity of a chart representing the distribution of dwellings based on construction material arises. In Figure 2.6 the distribution of dwellings based on their construction material [44] is presented and analysing the chart one can see that most of them are precast dwellings and reinforce concrete ones with a combined share close to 50%. A short examination of the large-panel structures was published by Demeter et al. [45]

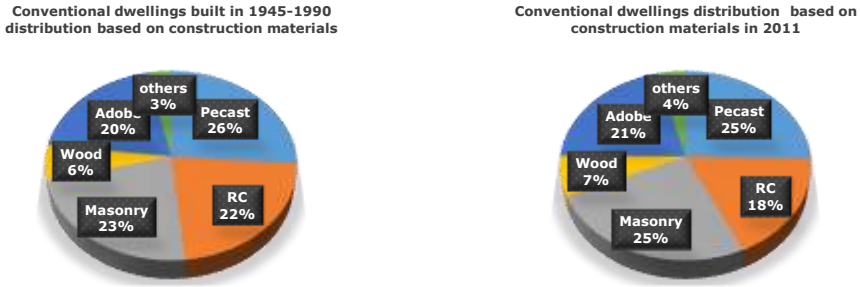

Figure 2-6 – Dwellings distribution based on construction materials

Romania has a population of approximately 20 million people [46], the highest number for population was measured in 1992 with over 22 million people living in the country. Although the trend of stable population is descending, Romania is the 7th largest country in European Union by population [47] and the 58th worldwide [48]. When it comes to where Romanians live, 35%, of the population lives in apartment buildings, as presented in Figure 2.7, meaning close to 7 0000 000 people [44]. Out of these by extrapolating to the chart presented in Figure 2.5 we can say that 2.75 million people live in precast apartment buildings and over 2.50 million live in reinforced concrete apartment buildings. As the peak construction period for these buildings was over 30 years ago, most of the people living in apartment building have an old dwelling constructed in the socialist era.

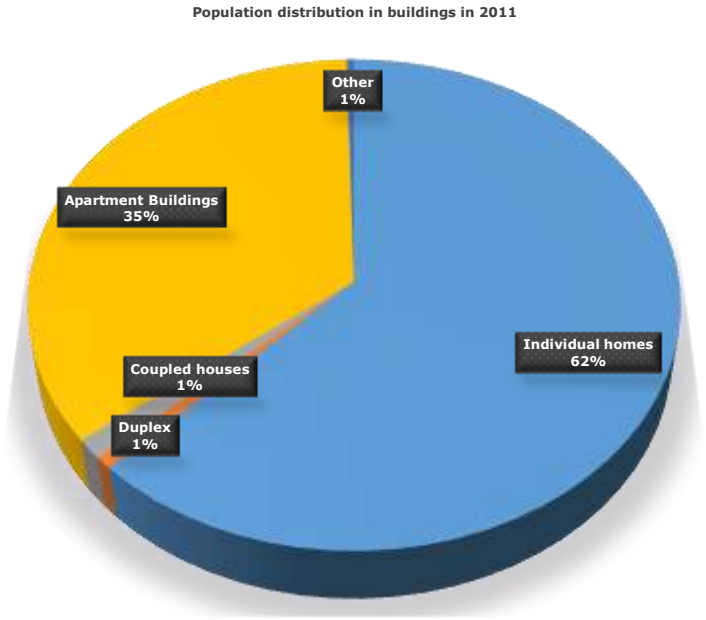

Figure 2-7 – Population distribution based on buildings

For the current thesis, a typical large panel building was chosen, the Romanian Project Type 770-81 built after the 1977 earthquake in 1982, the same one used in previous work related to seismically performance of sheer precast walls, done by D. Istvan [49] and C. Todut [50] within this experimental program. The ground floor plan of the building is presented in Figure 2.9.

Figure 2-8 – Front view of Project Type 770-81 building [50]

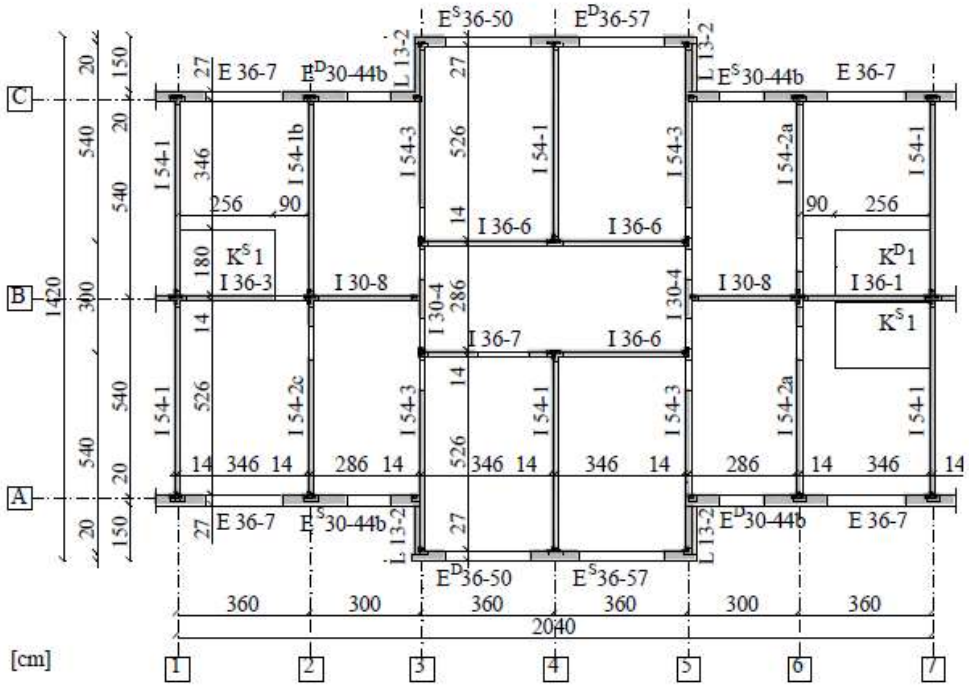

Figure 2-9 – Ground floor plan for 770-81 project type [50]

The shear walls of the building are connected vertically to adjoining walls while the horizontal ones are connecting the walls to the floor panels slabs. Details regarding the connections were previously presented. [50]. For this thesis, besides the existing two shear walls from previous works, 4 new shear walls were cast. All details regarding the materials and reinforcement placement and properties are presented in Chapter 3.2. The material properties of the shear walls build in that era were in the preceding works [49]. The specimens tested in this thesis are build according to the P100 regulations from 1981, the revised regulation after the 1977 earthquake. The first official seismic design specification was the Decision no. 84351 from 1941, a short 9 page provisions that was updated in 1945. This norm was operating until 1963 when the first P.13 was published. Although, during this period a more comprehensive norm STAS 2923-58 from 1958 was developed having 2 volumes with over 200 pages combined [51]. In 1970 the P13 was updated. After the large 1977 earthquake from Vrancea the first P100 was approved in 1978 and updated in 1981, in which the precast reinforced concrete panel buildings were discussed. After a decade, a revised P100 was released in 1991 that was very shortly afterwards updated in 1992. In 1996 an addendum was introduced to the existing P100. After the EUROCODE 8 was introduce in 2003, Romania adopted the P100-1 from 2006, which was lately with some modifications became the P100-1 from 2013, the most recent norm to date. A detailed history of the Romanian codes and their differences was published by F. Z. Gobesz [52].

Figure 2-10 – P+10 Precast building without and with thermal rehabilitation

Figure 2-11 – P+4 project type 770-81 precast building, original and with attic added later

Figure 2-12 – P+4 project type 770-81 precast building, original and with attic added later

Figure 2-13 – P+4 typical precast apartment buildings

Figure 2-14 – Panoramic view of precast buildings neighbourhood

Figure 2-15 – Precast buildings neighbourhood in Bucharest [53]

Figure 2-16 – Precast buildings neighbourhood in Cluj Napoca and Brașov [54, 55]

Figure 2-17 – Precast buildings neighbourhood in Galați and Timișoara [56, 57]

2.3. RC walls seismic laboratory test

Precast reinforced concrete shear walls have been in use in buildings for many years and had positive behaviours during major earthquake occurrence throughout the history. Several major studies were developed in order to investigate the seismic response of these panels when subjected to in plane loading.

I. Demeter [49] investigated the shear behaviour of precast large reinforced concrete panel, in the thesis the author investigated 3 panel with different characteristics, one solid panel PRCWP 1-S-T, one with a door opening cut-out from the solid panel PRCWP 3-S/E1-T and one with a large door opening cut-out from the solid one PRCWP 5-S/E3. The specimens were subjected to in plane reversed cyclic loading, to assess the influence of the cut-out opening on the seismic behaviour. The test set-up used was designed to simulate the shear behaviour and not the flexural one. During the test the author reported that the primary failure mode was ruled by diagonal compression. The effect of the cut-outs on the energy dissipation, stiffness and shear strength are significant.

C. Todut [50] made a similar research in which the author tested five near full-scale elements with different original openings and cut-outs. The program included two specimens with initial door opening PRCWP 7-E1-T, PRCWP 12-E1-T, one with an initial large door opening PRCWP 8-E3-T, one with large widow opening cut-out from small widow opening PRCWP 10-L1/L3-T and one with small widow opening PRCWP 11-L1-T. The author reported that specimens with small opening have a higher capacity to dissipate energy compared to the ones with large openings, also important stiffness reduction was observed for the ones with large openings. The author also investigated the prediction of shear behaviour using ATENA 2D software for numerical analysis, obtaining similar results and concluding that for the prediction of maximum displacement and lateral loads there is no need for sophisticated models.

R. Taleb [58] examined 4 Reinforced concrete single span shear walls with different opening types and locations. The specimens were scaled down to 40% and were designed to represent the lower three stories from a typical 6-storied building and subjected to lateral reversed cyclic loading. The author concluded that the shear strength was different depending on the direction of loading due to the openings different locations.

T. Holden et al [59] constructed and tested two identical half-scaled precast cantilever wall specimens and subjected them to in-plane reversed cyclic loading. The difference between the two was the design approach for each. One was a classic code compliant reinforced specimen, design to emulate the ductile behaviour of a cast-in-place reinforced concrete with development of plastic hinges at the base, whilst the other was a hybrid system. Its features included carbon fibre prestressed tendons, steel fibre reinforcement for improving the crack control and tapered energy dissipating bars. The conclusions of the experimental tests were that "classic" first specimen managed to dissipate more energy, however the energy dissipated resulted in permanent damage in the base pasting hinge region, whereas for the "innovative" secondary specimen the energy is dissipated using the specially designed energy dissipaters. Another advantage of the prestressed system is that it self-centres after each loading cycle, meaning that it has far less residual deformation and cracks upon unloading.

K. Beyer et al [60] studied the shear deformations for displacement demands in inelastic range using the results from 34 quasi-static cyclic test available in literature. The paper showed that the assumption of constant shear stiffness and

shear deformations thorough the loading process of slender RC walls controlled by flexure modelled by beam elements is not true.

The behaviour of RC cantilever walls under cyclic loading was explored by K. Pilakoutas and A. Elnashai in [61, 62] where the authors tested 6 specimens referred to as SW4-SW9. The elements were monolithically cast in place in the horizontal direction in three pairs each having the same flexural reinforcement only different shear reinforcement. Different types of failure were observed depending on the shear reinforcement distribution, however the characteristics of strength and deformations were not notable affected by the shear reinforcement placed in excess of the amount required to resist maximum load. The failure happened when yielding of link reinforcement, that enables shear stresses to be resisted in concrete, and when shear resistance of compressed concrete was exceeded. In the second part of the study the stiffness, yield levels, vertical deformations and energy dissipation capacity are discussed. The conclusions were that in the analysis of structures subjected to extreme forces in inelastic state should take into account a reduced cracked section stiffness. The main part of the energy dissipated by the specimens is due to flexure, although shear deformations are significant compared to the total, when it comes to overall energy dissipated it cannot be considered to contribute. The strain I longitudinal reinforcement near the tip was higher than analytically expected and shear reinforcement location, detailing and strength is critical for the shear capacity of the section.

Composite steel-concrete shear walls with vertical steel encased profiles were investigated by D. Dan et al [63] in a theoretical and experimental study. The specimens tested were 6 1:3 scale CSRCW elements denominated CSRCW1-CSRCW6 and subjected to quasi-static reversed cyclic horizontal loads, with a constant vertical load. The particularities of the specimens consist in the embedded steel profiles position and cross section, all having the same reinforcement distribution. The authors reported a bending failure mode, with crushing of the compressed concrete and yielding of the reinforcement bars at the extremities of the element. It is recommended to place these walls in zones with high seismic activities, since they dissipate more energy than traditionally reinforced elements. Shear failure can be avoided from the design process by designing the elements at bending moment and shear force associated to the capable bending moment. The authors recommend using a high class of concrete for a more dissipative behaviour and connectors between steel profiles and reinforced concrete at the ends.

T. A. Tran [64] in his thesis investigated five large-scale cantilever structural wall specimens (RW-A20-P10-S38, RW-A20-P10-S63, RW-A15-P10-S51, RW-A15-P10-S78 and RW-A15-P2.5-S64), in order to simulate the seismic behaviour, they were subjected to combined constant axial load and reversed cyclic lateral loading. The variables included the wall shear stress level, axial load level and shear-span ratio. The failure modes observed were different for the specimens, the deformations capacities for all specimens were very similar reaching approximately 3% drift ratio with the first yielding of reinforcement between 0.5-0.7% drift. Significant stress loss is impacted by the axial loads level, wall shear stress level and aspect ratio. The contribution of shear to total displacement broadly increased slightly from the beginning to the end of the test for the walls with high shear stress level, whilst the opposite trend was observed with decreasing contribution of shear deformation with increasing lateral drift ratio. For 2.0 aspect ratio walls extension deformations and slip of longitudinal boundary reinforcement accounted for approximately 10 to 25% of the top flexural displacements, whilst for 1.5 aspect ratio walls tended to be higher, from about 10 to 40%. The slip and extension deformations reached their local maximum

simultaneously with the appearance of the horizontal crack along the wall-foundation block interface at 0.75-1% drift ratio.

A. Athanasopoulou in his thesis [65] designed an experimental program comprising 9 walls, 2 of which were tested in a previous campaign. Four of the specimens were constructed with regular reinforced concrete according to 2005 ACI Code seismic provisions and the other three were constructed using HPFRC material. The specimens were all subjected to the same reversed cyclic displacement and the HPFRC ones were tested under approximately the same shear stress level. Two shear span-to-length ratios were evaluated, 1.2 and 1.5. The author compared the behaviour of the RC walls and the HPFRC ones and observed that both had stable hysteresis loops with the later ones having a larger drift capacities and secant stiffness. Both exhibited horizontal sliding at the wall base along the cold joint during the later stages of the test, with this aspect being critical for HPFRC walls, thus the author recommends dowel reinforcement to be used to strengthen the cold joint.

Precast reinforced concrete wall panels were studied by S. J. Bristowe [66], Four precast reinforced concrete wall panels design according to the 1990 NBCC and CSA, 1984 were subjected to reverse cyclic loading in order to assess their response. During the tests the author realized that the specimens were sliding horizontally along the ground-wall interface, thus the control of this phenomena was need. In order to avoid a brittle failure, the author concluded that shear reinforcement is necessary when increasing the participation of the wall by limiting the horizontals sliding. The joint rotation, horizontal wall panel sliding and wall panel deformations were used to evaluate the seismic behaviour of the walls. The author deduced the fact that precast wall panels can serve as the main seismic lateral load bearing elements when design and detailed properly.

The influence of concrete strength on the deflection, shear capacity, displacement ductility, cumulative energy dissipation and overall response on shear walls was investigated by H. Liu [67] who evaluated the revered cyclic loading response of two reinforced concrete ductile flexural shear walls. The walls had identical dimensions, layout and reinforcement except the shear reinforcement transverse distributed. For the concrete two types of ready-mix concrete were used, one with 35 Mpa compressive strength and one with 70 Mpa compressive strength. The specimens were tested and having a constant 600±5 kN axial load using load control up until yielding and deflection controlled afterwards. For the curvature ductility, an increase of 117% was noted by doubling the compressive strength of the concrete, whilst for the displacement ductility a 17% increase was found. The initial stiffness is higher as the concrete strength increases and the cracks develop faster at higher loads but have smaller crack widths. The energy dissipated was increased by 4 % for the higher strength concrete element, so the overall capabilities are increased by the stronger concrete.

M. Edgrado in his thesis "Experimental cyclic behaviour of reinforced concrete wall houses loaded in their weak direction" [68] published the experimental results of six full scale houses loaded in their weak direction, perpendicular to the shear walls. By comparing the wall slab frame, which developed plastic hinges at the top and bottom of the reinforced concrete walls, and the infield frame with masonry and RC it was observed that the lateral strength was increased by 5.12 times for the masonry wall and 7 times for the concrete one, whilst the lateral stiffness was increased 106 times for the masonry infilling and 177 times for the concrete one.

Reinforced concrete walls subjected to reversed cyclic loading were also investigated by Palermo D. in his PhD Thesis [69], a series of two large scale structural walls DP1 and DP2 were investigates to complete the literature data in regards to

shear failure, at the time the investigations were mostly concentrated on the flexural behaviour of the walls. The walls were constructed with two stiff top slab to transmit the forces and bottom slab to simulate a rigid foundation. The walls were subjected to lateral cyclic loads, with DP1 specimen having a constant axial load imposed of 940 kN from the actuators and another 260 kN from the self-weight of the top slab. The DP2 specimen had the top axial force removed. For each displacement level two repetitions were imposed, the displacement control was 1mm. The author concluded that the imposed axial loads significantly influence the ultimate strength and failure mods of the walls, squat walls dissipate fewer energy compared to the slender walls.

Low aspect ratio reinforced concrete walls were tested on a large scale by J. F. Rocks [70], whom conducted the tests on phase one of the research programme in which he tested four SW1-SW4 of the seven specimens large-sized reinforced concrete shear squat walls. When designing the specimens five peak shear strength equations, FEA software and VecTor 2 were considered. The key findings of the author were that the peak shear resistance decreases with repeated cycling greater than that associated with peak shear strength at lateral displacements. The stiffens predicted by VecTor 2 and the one computed by ASCE 43-05 and ASCE 41-06 recommendations are different from the ones measured for each wall. An inexplicable phenomenon occurred during testing in which all specimens had peak shear force resistance larger in the positive direction.

C. Greifenhagen and P. Lestuzzi [71] investigated the deformation capacity of squat shear walls not designed for seismic actions. Four lightly RC walls in 1:3 scale simulating the existing building in Switzerland were investigated. The variances between the specimens were the axial force ratio, concrete quality and horizontal reinforcement, all specimens were compared with other existing studies from the literature. The study obtained drift capacity greater than 1% shear walls designed for gravity loads only. Vertical reinforcement arrangement, axial force ratio, and degree of restraining at the top of the wall govern the drift capacity of squat shear walls. Brittle failure occurs for cantilever walls with rotation restraints, as opposed to the ones without fixed top end. Crack patterns differentiate with concrete compressive strength and of the axial force ratio.

Seismic performance of shear walls was also analysed by Nasr, A. M. in his PhD Thesis [72], five wall specimens were tested in the research with two of them being retrofitted using CFRP laminates. The RC walls were had different openings, one was a solid wall (C-S), one with a window opening (C-WO) and one with a door opening near the edge (C-DO). The test specimens were subjected to standard in-plane cyclic loading protocol, with a constant axial load appreciated as 10% of the walls compressive strength. The structural capacity of the walls with openings was lower compared to the solid one with roughly 13%. The ductility of RC walls is influenced by opening size, geometry and location as confirmed by the study conducted by the author. All specimens failed in shear, for the solid one concrete crushing at the base was observed with flexural and shear cracks appearing during the test. The specimens with openings had different behaviours in the left and right piers, for the window opening both piers failing in shear whilst the door opening right narrow pier failed in flexure by crushing of concrete.

2.4. Retrofitting procedures using FRP for RC

Several different retrofitting procedures for reinforced concrete structures exist in the literature. Based on the elements characteristics and purpose the appropriate retrofitting procedure can be chosen. An introduction into FRP, properties, process and concepts are presented by M. A. Masuelli [73] who outlines the large functionality that these products (Aramids, Composites, Glass-FRP, and Carbon FRP) have. Several different recent retrofitting procedures using FRP are presented in this chapter.

Fibres of aromatic polyamide in which 85% of the amide linkages are attached directly to two aromatic rings are called "aramid". These are one of the first polymers used in retrofitting existing structures. Aramid Fibre Reinforced Polymer (AFRP) can replace the classic reinforcement since they are not prone to corrosion, accelerated aging tests on aramid fibre reinforcement was done by Soroushian et al. [74]. When using FRP rebar the bond between the bars and the concrete is a critical issue, studies regarding the bond of aramid reinforcement were done using the pull-out test giving an average bond of FRP rebar of 40% to 100% of steel reinforcement [75, 76, 77]. In Figure 2.18 aramid reinforcement bars are presented, these can be used to replace the reinforcement [78, 79, 80]

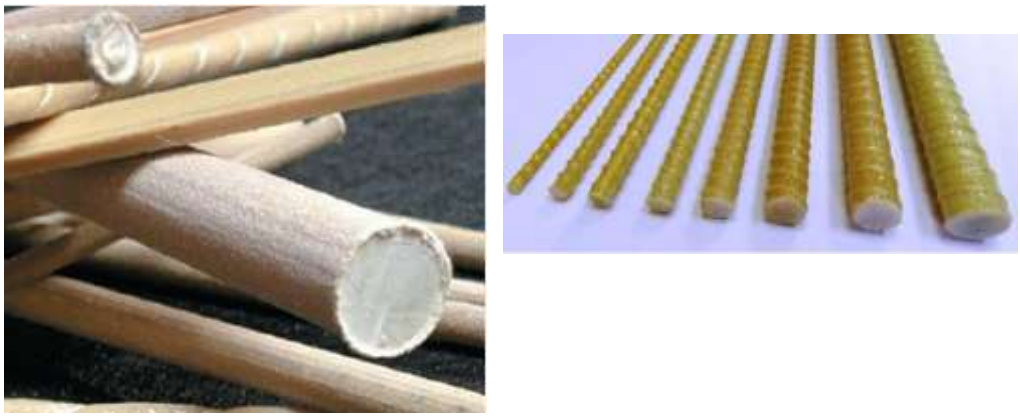

Figure 2-18 – Aramid reinforcement bars [81, 82]

Other ways of using aramid fibres are as sheets and laminates as presented in Figure 2.19. The sheets are usually applied as externally bonded system (EBR) for confining the concrete elements [83, 84], where good results were obtained, with increasing the ductility, strength and energy dissipation capacity of the elements. Also, exposure to freeze-thaw cycles and wet-dry ones showed no reduction in strength. The laminates can be used as EBR or as NSM systems [85, 86], with both methods having good results increasing the load bearing capacity, with the NSM system being slightly better but also dependent on the texture of the material, the more textured the material the better the bond and behaviour. However, the aramid fibres are not so popular for retrofitting reinforced concrete elements because other newer materials with better properties exist.

Figure 2-19 – Aramid fibre sheets [87, 88]

Another material that is not very commonly used in retrofitting procedure is the basalt fibre reinforced polymers (BFRP). These fibres were first developed by the Moscow Research Institute of Glass and Plastic in the 1950s by melting basalt rocks. A review of these basalt fibres and their composites was made by V. Fiore et al. [89]. The first concern with this material was the safety, since it presents similar composition to asbestos. However, studied showed that it poses no threat to humans and can be safely used. [90, 91]. The mechanical properties of these fibres are similar to those of glass fibre when it comes to tensile strength, but the Elastic modulus of these fibres is higher [92]. These FRP materials can come in different forms, either as reinforcement or fabric as presented in Figure 2.20.

Figure 2-20 – BFRP rebars and fabric [93, 94]

Studies have been made on the possibility of replace classic steel reinforcement bars with basalt fibres ones using an automate wet lay-up process [95, 96]. BFRP sheets and bars were also used in order to strengthen beam [97, 98] with good results. A review of BFRP and their application in structural engineering was made by L. J. Ouyang et al. [99]. These polymers are being studied in all aspects of structural retrofitting, including columns jacketing, shear walls strengthening, increasing flexural capacities of concrete slabs etc.

Glass Fibre Reinforced Polymers (GFRP) as the name implies is a composite made out of glass fibres contained with a polymer matrix. The GFRP is more widely spread in retrofitting of old, existing constructions and new ones than the aramid ones. One of the main advantages is that the GFRP is easier to produced and it is being used in different domains successfully for a long period of time. As in the case of AFRP the GFRP comes in several forms.

GFRP is not prone to corrosion so it comes as rebar for replacing the classic steel ones as presented in Figure 2.21. The behaviour of reinforced structures with GFRP bars has been studied by [100, 101, 102, 103] and many others, with the specimens having a good behaviour when subjected to external loads, with beams failing in either shear or flexure. The behaviour of shear walls reinforced with GFRP was studied by N. A. A. R. Mohamed [104] who tested four large scale shear walls specimens, one with steel reinforcement as reference and the others with GFRP bars. The results obtained were promising, with GFRP reinforced walls having larger drift capacities, no premature shear, sliding, anchorage or bond failure. The main advantage of GFRP reinforcement is the fact that no permanent deformation is reached up until 80% of ultimate capacity, however, this behaviour comes with its own drawback, which is the main disadvantage of GFRP reinforcement, the energy dissipated is smaller compared to the steel reinforced specimens.

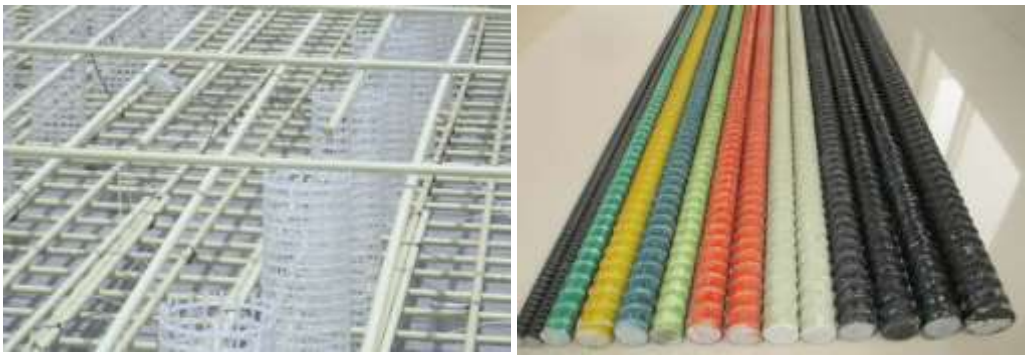

Figure 2-21 – GFRP reinforcement [105, 106]

Another way of using GFRP is by means of externally bonding the material to the existing structure. The GFRP can come in form of a mesh as presented in Figure 2.22 or bars. The mesh is generally used for confinement of concrete [107, 108] of columns and beams, with good results reported in the literature. The mesh can be made into a laminate using resin and mounted using EBR system [109], whilst the bars can be NSM [110, 111, 112, 113]. Another way of using GFRP is by creating a tensile reinforced mortar (TRM) system. This is based on a GFRP mesh imbedded in high strength mortar. The amount of research based on this system is not so vast compared to the others, however, there are several papers discussing this procedure and system [114, 115]

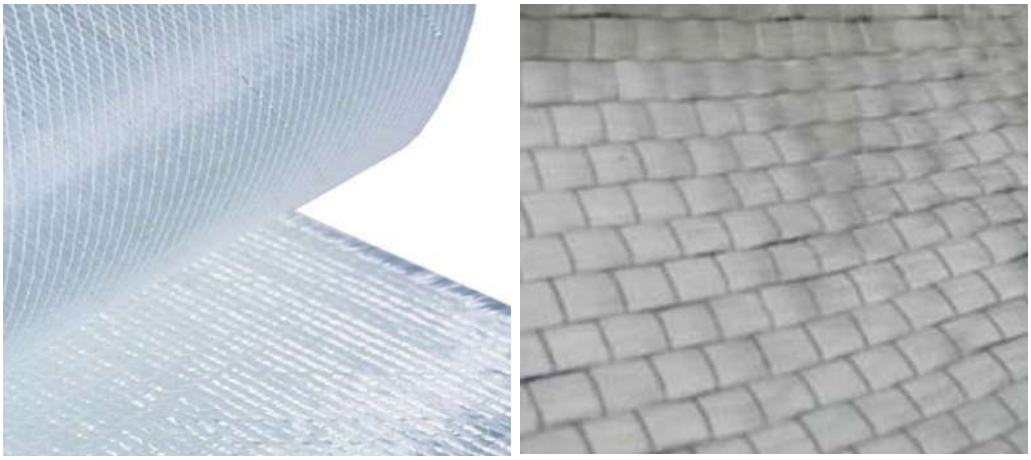

Figure 2-22 – GFRP mesh [116]

Another very important aspect of the GFRP system is the durability and the behaviour during long exposure to aggressive environments, although all GFRPs has the same common material (glass), the properties and behaviour during sustained aging and environmental tests are different [117]. The strength of GFRP rods were reduced after 300 days in environmental chamber slightly different for different types of rods. Compared to steel reinforcement the GFRP lost more tensile properties in 300 days but in the first 200 days the rate of steel degradation is much higher than that of GFRP, meaning not sufficient reinforcement corrosion was developed in 300 days. [118].

The most popular way of retrofitting existing RC structures is by using Carbon Fibre Reinforced Polymers (CFRP). Compared to the other presented FRP systems the carbon has the highest elasticity modulus and the largest tensile strength. The only downside of CFRP is cost, since it is significantly more expensive than other FRP systems. Many studies have been made in regards to the use of CFRP for structural rehabilitation of reinforced concrete structures, in terms of shear strengthening, flexural strengthening, confinement of concrete etc. The mode of use is different depending in the type of CFRP, woven fabrics or laminates as presented in Figure 2.23.

Figure 2-23 – CFRP laminates and mesh [119, 120]

The CFRP woven fabric can be used for confining RC columns [121, 122] and improving the ductility factor, lateral displacement and energy dissipation capacity of the elements. The sheets are also used widely for increasing the flexural resistance of beams [123, 124, 125]. The beams flexural capacity was increased with 20%-50% making this a successful rehabilitation solution. Another way of using CFRP is by bonding laminates to the surface of the element EBR Figure 2.24. [126, 127, 128] with good results. The technique involves preparing the surface in order to apply the retrofitting material, after the surface is prepped the epoxy resin which ensures the bond between the two materials is applied. Before the resin can harden the CFRP laminates is applied to the element. However, in terms of flexural and shear retrofitting the near surface mounted (NSM) system is preferred (Figure 2.25), because it ensures a better bond between the FRP and the concrete. The system was investigated [129, 130, 131, 132] with excellent results in terms of increasing the flexural and shear capacity of the elements. The procedure is more complicated and time consuming compared to the EBR system which makes it impossible in certain circumstance. On the surface of the element a groove has to be cut in order to insert the laminate for retrofitting. Within the groove a primer is applied and afterward the CFRP laminate is inserted ensuring the bind with the concrete on both sides of the laminate. With CFRP a very important aspect is the bond between the concrete and the retrofitting material, the bond is usually ensured by epoxy resins [133] so the behaviour of the bond in extreme conditions is important [134, 135, 136].

Figure 2-24 – EBR system for mesh and laminates [137, 138]

Figure 2-25 – NSM system for CFRP laminates [139]

2.1. Retrofitted RC walls seismic laboratory test

In the literature, there are several researchers whose experimental test regarding the retrofitting procedure for shear walls have improved the knowledge on the behaviour and capacities of these elements. Elnady [140] studied the behaviour of nine specimens designed according to 1970's practice under cyclic and pseudo dynamic test. Two specimens were refence specimens and tested without using any rehabilitation in order to have a base observation and measurements. The other seven specimens were rehabilitated using CFRP sheets in order to prevent brittle failure and to increase the shear strength. By adopting this solution, the author managed to eliminate the brittle shear failure, achieving a more ductile behaviour with more energy dissipation capacities. Steel laminates were used as anchoring system for the CFRP wrapping in the bottom edge which prevented deboning and localized the damage in the bottom end zones. The CFRP in the web increased significantly the crack control of the specimen and reduced the pinching in the hysteretic loops, giving the specimens the ability to dissipate more energy.

Four shear wall specimens were tested by J. Lombard et al. [141], one refence wall, a repaired one and two walls were strengthen using externally bonded carbon fibre tow sheets. In-plane quasi-static cyclic loads were applied as force controlled up to the yield point and displacement control with controlled steps until failure. The objective was to determine the feasibility of using CFRP tow sheets for repair and strengthening of shear walls. The author concluded that this system can be used as repair method for damaged walls in order to recover the initial elastic stiffness, whilst as strengthening system it managed to increase the ultimate capacity of the specimen, the yield load and the cracking load.

Similar tests to the one presented in this thesis were done within the same experimental research programme in previous phases by I. Demeter [49] in phase one, whom tested four specimens that were retrofitted using EBR CFRP sheets. Two of them were strengthened, meaning the CFRP system was applied prior to damage and two specimens were retrofitted post damage. The specimens were all with openings cut-out from solid ones, two had door openings denoted E1 and two had large door opening denoted E3 (see chapter 3.2). Although none of the specimens with openings managed to match the solid refence one load bearing capacity, in both cases for the retrofitted specimens the initial load bearing capacity was increased, whilst for the specimens with door opening strengthened the increase was more than 50% of the unstrengthen specimen. For the large door opening specimen the strengthen one had only a small increase in the load bearing capacity due to different concrete qualities. The tests were continued by C. Todut [50], who tested six elements with different opening types and different retrofitting or strengthening procedures. Two specimens were retrofitted post damage using EBR-CFRP sheets system, one specimen was strengthened using EBR-CFRP sheets combined with NSM-CFRP laminates, two other specimens were retrofitted using textile reinforced mortar (TRM) and the last was retrofitted using NSM-CFRP laminates combined with EBR-CFRP sheets. In almost all cases the retrofitting procedure proved to be successful, managing to restore the initial load bearing capacity of the specimens and increase the displacement failure. In terms of energy dissipation, no definitive conclusion could be drawn from the experimental tests since close to half of elements dissipated more energy compared to the reference one, whilst the other half dissipated less energy.

D. Dan studied the behaviour of two steel-concrete shear walls with encased steel profiles retrofitted using FRP composites [142, 143]. From a series of test on several specimens with encased steel profiles, two were selected to be retrofitted using CFRP

composites strips and laminates. The aim was to restore or even possibly improve the initial load bearing capacity and behaviour of the specimens, affected by seismic actions. The specimens cracked and crushed concrete was removed and replaced with high strength repair mortar before being retrofitted. The retrofitting strategy was chosen based on the careful analysis of the behaviour and failure mode of the reference specimens, with three main aspects to be resolved: restore the shear capacity of the walls, restore the flexural capacity along the edges and provide local confinement. For this vertical and horizontal CFRP composites strips and laminates were used symmetrically on both faces of the specimens. Using this technique, the author managed to restore the initial load bearing capacity of the elements, however, the dissipated energy was lightly smaller and the initial stiffness was up to 80% of the initial element but decreased faster.

Partial bonding of the CFRP to the concrete wall was studied by S. Qazi et. al. [144], whose study consists of two reinforced concrete shear walls under-reinforced in terms of shear reinforcement subjected to quasi static monotonic lateral loads. One of the specimens was strengthened using partially bonded CFRP polymer strips to the wall. The objective was to reach reasonable drift and strength capacities for the strengthened element without deteriorating the walls energy dissipation capacity. The strengthening was applied to the wall edges to simulate the conditions on the field where the wall edges are not reachable since they are usually connected to columns. CFRP mesh was used on both directions, horizontally and vertically. The findings of the research support the use of CFRP polymers EBR for concrete shear walls, with the strengthened specimen showing improvements in terms of lateral load bearing capacity and deformations. The cracks propagation was also limited by the strengthening procedure, with cracks appearing only in the lower half of the specimen despite the higher drift level. The overall capacity of the specimens to dissipate energy was not damaged by the strengthening procedure, with CFRP being externally bonded it allowed for the concrete to crack and dissipate energy.

A retrofitting system for reinforced concrete shear walls using a new composite called "CarboFlex" was investigated by Zhou H. et. al. [145]. The initial specimen was tested using quasi-static loading procedure in displacement control, with 3 mm displacement control, until the specimen had only 40% of its initial maximum load bearing capacity. Afterwards the specimen was repaired and strengthened using a new carbon fibre based polymeric composite wrap "CarboFlex" [146]. The retrofitted element had a maximum load bearing capacity of 80% of the initial specimen with the backbone curve showing ductility and significant strength sustainability of the retrofitted wall. By confining the walls base and top parts using CarboFlex system, a "bubble" appeared at the base part of the specimen during the combined axial and lateral loads application, but did not fail. This proves the ability of the system to dissipate energy that may have ruptured the fibres, enabling the bond to retain its strength after the concrete was severely crushed.

Four specimens categorized as low-rise and medium rise walls were tested and retrofitted using a combined system of GFRP and CFRP by B. Li and C.L. Lim [147]. The specimens were subjected to in-plane cyclic loading with displacement control with two cycles for each drift ratio, additionally two vertical forces were applied to the specimens, these forces were computed based on the concrete compressive strength. The retrofitting system was chosen based on engineering judgement and intuition, with the FRP strips being applied using the EBR procedure. The aim of the retrofitting scheme was to shift the failure mode of the wall towards a more ductile one. By comparing the results of the original specimens and the repaired ones, the author concludes that the FRP can be used as repair and strengthening material for RC walls

damaged by seismic actions, with their main advantage being the ease of installation and minimal intervention to the existing structure. The flexural strength and stiffness was increased by the FRP sheets, with the CFRP ones proving to be more effective than the GFRP ones. The shear strength was increased by the FRP jackets, with the addition of the GFRP sheets to confine the jackets, and shear cracking was controlled by much reduced shear displacement. While some anchorages underwent premature failure at the base of the wall, they only failed after the specimen reached its initial load bearing capacity.

J. E. Woods et al. [148] studied nonductile reinforced concrete shear walls subjected to in plane seismic loading strengthened using EBR sheets. The specimens had typical structural deficiencies found in structures build during the 1960s and 1970s, these deficiencies included insufficient shear reinforcement, low concrete quality and lack of boundary elements. The authors evaluated the effectiveness of EBR vertically and horizontally CFRP sheets to repair and strengthen the walls. The results showed that the ductility, energy dissipation capacity and flexural strength were significantly increased, with the procedure restoring the initial strength and stiffness of the damaged elements.

An innovative way of applying the FRPs for seismic strengthening of reinforced concrete walls was proposed by K. Kobayashi [149], in which the author installs the aramid fibres in a zigzag sewing path, on predrilled holes on the surface of the wall. One of the main advantages of this technique is that the anchorage for the FRP band is secured so that the material can take the full tension force. Other advantages are the possibility to reduce the amount of FRP used to obtain the necessary capacity and the concrete wall surface does not have to specially prepared, by smoothing and applying epoxy-primer. The proposed strengthening procedure proved to be a success both mechanically and economically. The shear capacity of the walls was increased in proportion with the number of strands in the sewing band. This method is also suitable to be used for infill-brick walls, when there is the need for them to carry horizontal forces, and this system also prevents the out of plane collapse.

A. A. Khalil in his thesis [150] investigated the rehabilitation of two specimens using unidirectional and bidirectional CFRP sheets. The unidirectional sheets were used for confining the end columns elements of the walls, to improve the ductility of the specimen, whilst the bidirectional ones, with the fibres aligned at 45 degrees, were attached to the web of the wall in two layers to increase the shear resistance. Both rehabilitated walls reached a higher lateral displacement, compared to the refence one, by 42% and 60% respectively. The energy dissipated was higher than the one of the refence wall due to additional strength and ductility. Both walls had increased failure loads and ductility improvements making the retrofitting strategy a success.

Basalt FRP used for strengthening concrete shear walls were investigated by D. Shen et al. [151], whom tested six specimens with aspect ratio of 1.6, characterized as medium-rise, subjected to quasi-static cyclic loads. The control was based on force up until 150 kN and then it was displacement controlled with 4 mm increments starting at 16mm. One specimen was tested as-build and represented the control specimens, the other five specimens were strengthen using different BFRP strips configurations. Three specimens (SHW1-SHW3) were strengthened with the intent to increase their shear capacities by using X-shaped 200 mm wide BFRP sheets anchored with fan type anchors made also from BFRP. Two of the specimens SHW4 and SHW5 aimed to increase both the flexural and shear capacities, for this the boundary of the walls were strengthened with BFRP sheets. The use of BFRP for strengthening RC walls is an effective technique, with the specimens having improved the seismic

performance under cyclic loading. In all cases the secant initial and final stiffness was larger compared to the reference specimen, the ultimate displacement increased and also the energy dissipation capacities were significantly higher.

The use of FRP composites to strengthen RC walls with post-construction openings, like doors and windows, was investigated by A. S. Mosallam & A. Nasr [152]. A total of five large-scale shear wall were tested in order to demonstrate the difference in behaviour between solid elements and the ones with openings. One solid wall was evaluated and taken as reference and in two specimens, with the exact same dimensions, two opening types were created, one window opening and door opening. The specimens with openings were retrofitted using CFRP wet layup laminates, horizontally to increase the shear resistance and vertically to improve the flexural capacity of the specimens. All walls were subjected to in-plane full-reversal cyclic loading protocol with a constant axial load of 10% of the maximum compressive strength at 28 days. The results were positive with both strengthened walls achieving higher peak loads compared to the unstrengthen ones, which was expected, but was also higher than the control solid wall. Another important aspect of the study was the influence of the opening type, size and position to the overall strength and ductility. Additionally, the retrofitting system location and size is crucial, with the specimen with door opening having a smaller ductility compared to the unstrengthen counterpart, this was attributed to the presence of localized interfacial shear stresses at the CFRP/concrete interface that led to local debonding of the composite laminates.

S. J. Hwang et al. tested six reinforced concrete walls subjected to in-plane quasi-static cyclic loading, with two cycles for each drift ratio [153]. One element was a structural wall, one was a partition wall and the rest four walls were retrofitted partition walls. The objective of the paper was to enhance the seismic behaviour of frame structures with partition walls by retrofitting them using CFRP. The author concluded that the application of CFRP sheets without any anchorage system is meaningless, nevertheless, if anchored properly this system is effective in enhancing the diagonal compression strength. For low-rise shear walls the use of vertical CFRP is more effective than the horizontal ones and the diagonal compression strength can be rationally predicted using the softened strut-and-tie model with the CFRP sheets treated as shear reinforcement.

B., S. Mohammed studied one way RC wall panels with openings strengthened using CFRP [154]. A total of sixteen specimens were tested in groups of four. So, there were four groups, the first two series were tested without CFRP layout and the third and fourth series were the ones with the CFRP strengthening system. The CFRP sheets were positioned around the openings. The RC walls with openings strengthened with CFRP had better load bearing capacity compared to the unstrengthen ones. This was due to the fact that the principal stresses acting on the upper corners of the openings were reduced. The more effective way of retrofitting is with CFRP pattern with 45 to the corners.

3. EXPERIMENTAL PROGRAM

3.1. Introduction

The research objective is to simulate the behaviour of RC structural walls subjected to seismic actions. The experimental program involved testing scaled models of PRCLP designed and constructed according to the code provisions that were in effect in the 1980's. The overview of the experimental program is presented in Table 3.1, the experimental test was conducted in the Reinforced Concrete Structures Laboratory of Civil Engineering Department, Construction Faculty, Politehnica University Timisoara, Romania. The presented research is a continuation of a larger investigation regarding PRCLP started by I. Demeter [49] and continued by C. Todut [50]. Demeter tested five specimens known as PRCWP [1,3,4,5,6], comprising of solid walls with and without door opening cut-outs. Several of these walls were repaired and post-damage retrofitted with EBR-CFRP or prior-to-damage strengthened using EBR-CFRP. Todut continued the research and investigated six more specimens known as PRCWP [7-12], comprising of walls having initial small window openings, small and large door opening, as well as large window and large door opening cut-outs. Todut adopted several different retrofitting strategies, for the post-damage and prior-to damage strengthening procedures, using EBR-CFRP, EBR-CFRP combined with NSM-CFRP and TRM.

Ten experimental tests were carried out on six different specimens known as PRCWP [13-18], two existing ones from the previous stage tests and four new build one, starting April 2013 until July 2015, as presented in Figure 3.1. The tested specimens had different opening types and cut-outs. Several specimens were retrofitted prior-to-damage or post-damage using EBR-CFRP strips or EBR-CFRP combined with NSM. The tests were performed by fixing the specimens to the floor through a foundation beam and loading them using a loading beam (see chapter 3.5)

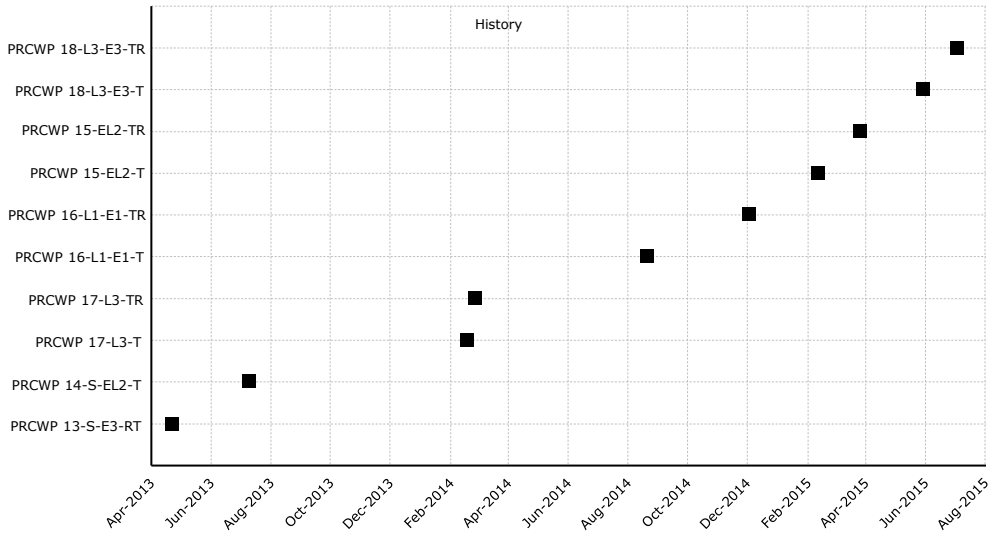

Figure 3-1 – Testing timeline

Table 3-1 – Overview of the experimental program

Program ID	Laboratory	Reinforced Concrete Structures
		Civil Engineering Department
		Construction Faculty
		Politehnica University Timisoara
	Country	Romania
	Year	2013-2015
Specimen	Designation	PRCWP
	Construction Type	civil
	Specimen Type	wall element
	Concrete technology	precast
	Opening	large door cut-out: door and window cut-out; dorr and window; door cut-out; large window; large door cut-out
	Strengthening	non; EBR-CFRP strips; NSM-CFRP
	no. of specimens	6
	Scale	0,83
Boundary conditions	Set-up	A-type
	Loading	quasi-static cyclic
	Boundary Condition	restrained rotation

3.2. Test Specimens characteristics

The experimental wall specimens were constructed and designed according to the 1980 Romanian large panel manufacturing practice. In this thesis, the prototype wall specimens were chosen to be the interior wall denoted I54-2a and the exterior longitudinal panel denoted E 36-7, see Chapter 2.2. This wall types can be considered representative for the post 1977 large panel building and can be found in several different plans of the 770-series. The dimensions of the prototypes were as follows:

- I54-2a: Length: 5100 mm
  Height: 2580 mm
  Thickness: 140 mm

- E 36-7: Length: 3580 mm
  Height: 2830 mm
  Thickness: 140 mm

Considering the limitations imposed by the testing facility and the lifting capabilities of the bridge crane available in the laboratory, all the tested elements are scaled down with a reduction factor of 0,83, corresponding to 1:1.2 model. Each experimental test specimen can be referred to as a wall because it represents one storey, one bay and one plane member. In order to simulate the connection joints towards the adjacent panels of the as-build conditions, all tested units have T-shaped

boundary elements which also prevent the out-of-plane displacement during the in-plane lateral loading. These elements are referred to as wings.

The specimens tested in this thesis were fabricated on two different sites. Two of the six specimens, namely 13 and 14, were manufactured in Timisoara in 2007 with the reinforcement and concrete provided by the construction firm. As reported by Demeter [49] the experimental walls were cast in horizontal position as the original large panels. The concrete was poured in the modular wood formwork in two phases, first in the web-panel and after several days of curing, the timber formwork was removed and the wing elements were poured. The other four specimens were manufactured in Stei, county Bihor, at a concrete station within a construction firm. These specimens were also cast in horizontal position and vibrated in the formwork, but the T-shaped boundary elements were cast simultaneously with the web-element. After the manufacturing, the first two specimens were stacked horizontally one on top of the other in laboratory, while the other four transported 200 km stacked horizontally in the truck and then stored in vertical position in the laboratory yard.

In Figure 3.2 the manufacturing of the elements made in Timisoara is presented, and in Figure 3.3 the ones made in Stei.

Figure 3-2 – Construction of the specimens (Timisoara)






Figure 3-3 – Construction of the specimens (Stei)

As the two specimens manufactured in Timisoara were solid elements and in this thesis the author wanted two specimens with openings cut-outs, two opening were designed and cut-out from the specimens in the laboratory, by removing a door-shaped portion from a solid wall the rectangular outline of the web-panel changes and it becomes a frame-like element composed of two piers and a spandrel beam at the sides and above the opening, respectively. The first element (13) had a door opening cut-out while the second one (14) a door and window opening cut out. The specimens with cut-out made in Stei had the cut-out simulated from the manufacturing process so the physical cutting of the opening was not necessary, in order to ease the fabrication process. All the reinforcement details were manufactured and cast as if the element had an opening cut-out. In Figure 3.4 the process of cutting the openings in the solid walls is presented. First the outline of the opening was created using paint, then by using a mixt asphalt/concrete cutting machine the opening cut be cut out by tracing the outline previously made. The walls were placed in horizontal position in order to simplify the cutting procedure. Special measures had to be enforced in order for the wall not to crack under its own weight, due to the fact that it was standing only on the wing elements, so wooden supports were placed under the web element.

Figure 3-4 – Opening cut-out procedure

For the experimental program the author had to test the specimens as unstrengthen first and afterwards, repair and strengthen them, in order to be able to retest them. Thus, the specimens were named using distinguishing notations by adding at the end of the tested specimens name the suffix T, TR or RT. T stands for element unstrengthen tested prior to damage, TR for element tested, retrofitted post damage then rested and RT stand for elements retrofitted prior to damage and tested.

In Figure 3.5 all the possible combinations of initial opening and cut-outs are presented. The green circles are for the first specimens tested in this experimental program by Demeter [49], the purple circles are for the second series of test performed by Todut [50], while the orange circles depict the specimens tested by the author in this thesis. Also from Figure 3.5 one can see the labels of the elements with respect to their opening type. The complete name of the specimens starts with the number assigned to it in the investigation of PRCWP, then the type of opening and then the strengthening condition.

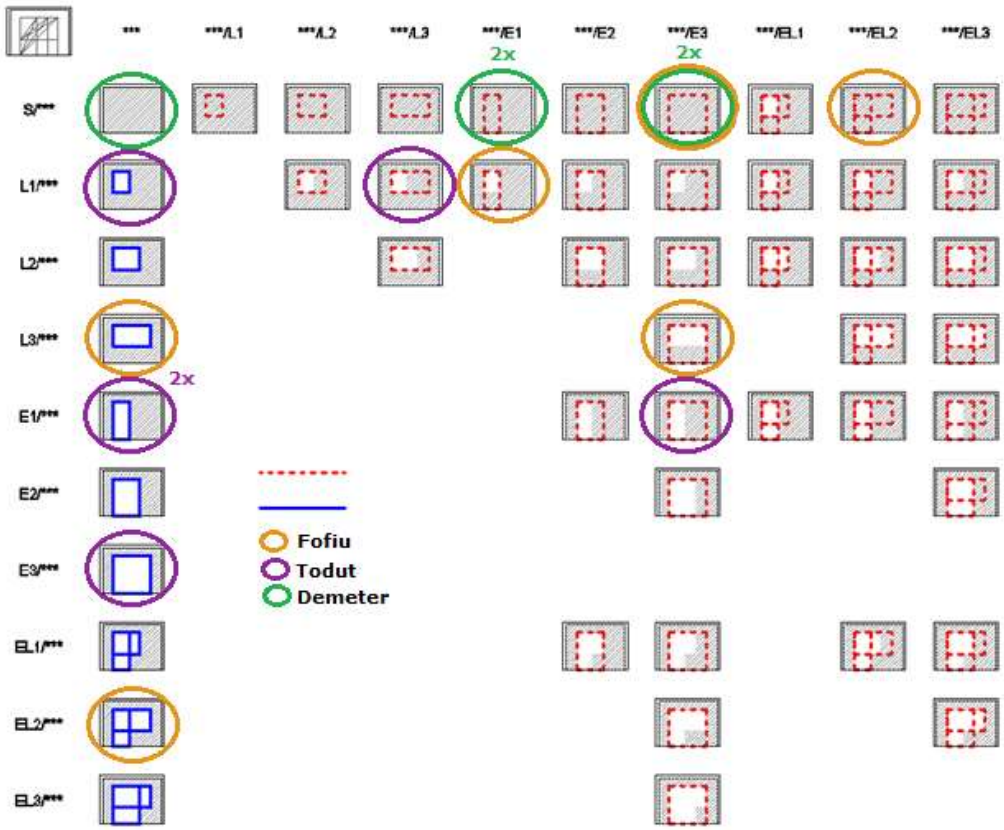

Figure 3-5 – Tested specimens

The steel reinforcement details for the solid specimens manufactured in Timisoara are given in Figure 3.5. The web panel element was reinforced with single curtain composed welded wire mesh of Φ3 diameter cold drawn wires at 100 mm centres, horizontal rebar of Φ 10 diameter at 265 mm pacing and in two vertical continuity bars of Φ14. The T-shaped boundary elements were reinforced by spatial cage consisting of 4 Φ14 mm diameter, a Φ16 mm diameter vertical continuity bar and Φ8 mm plain stirrups at 85 mm pace.

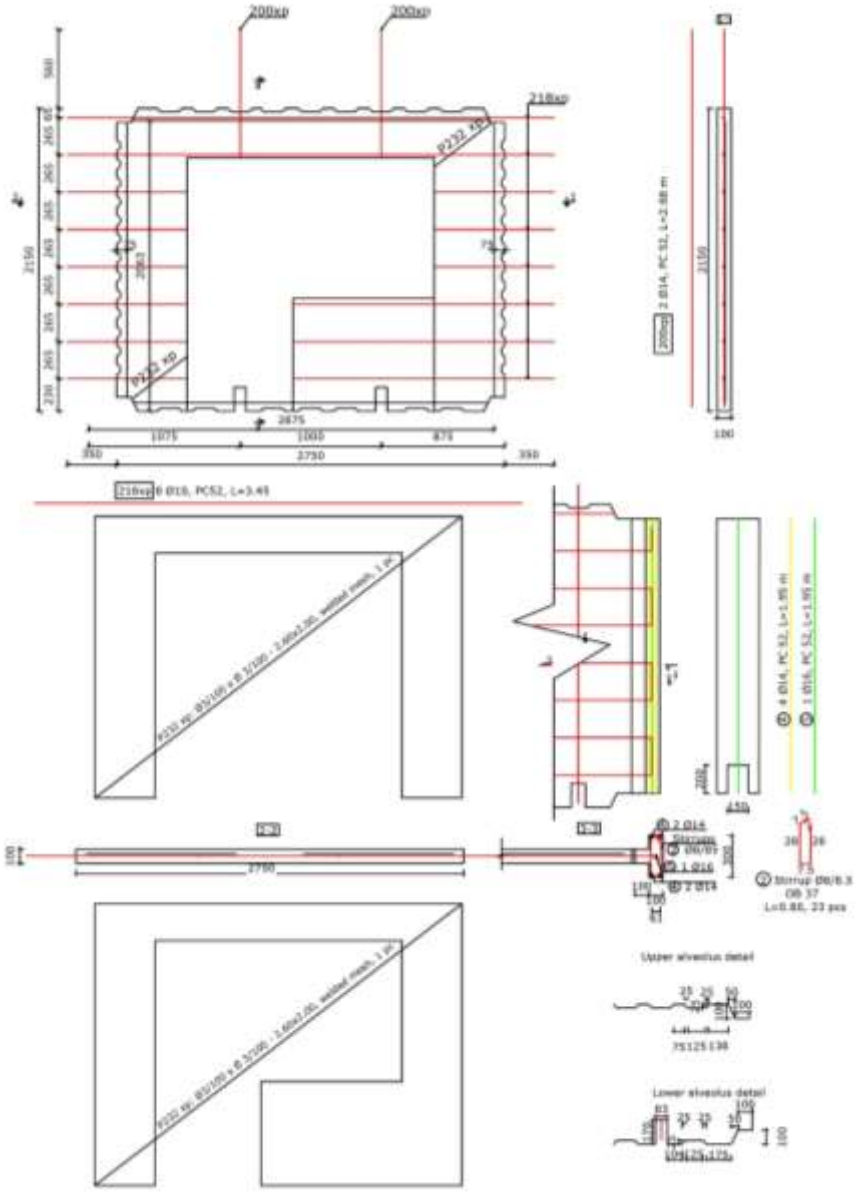

Figure 3-6 – Reinforcement details for PRCWP 13 S-E3 and 14 S-EL2

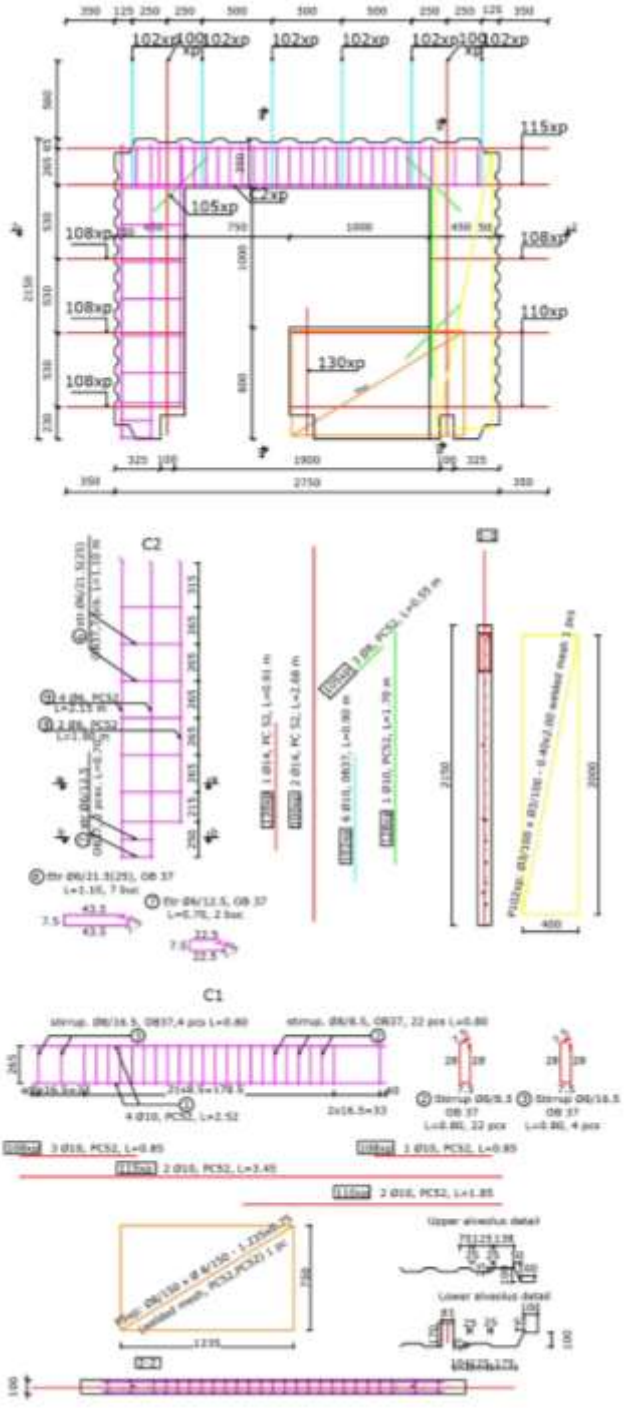

Figure 3-7 – Reinforcement details for PRCWP 15-EL2

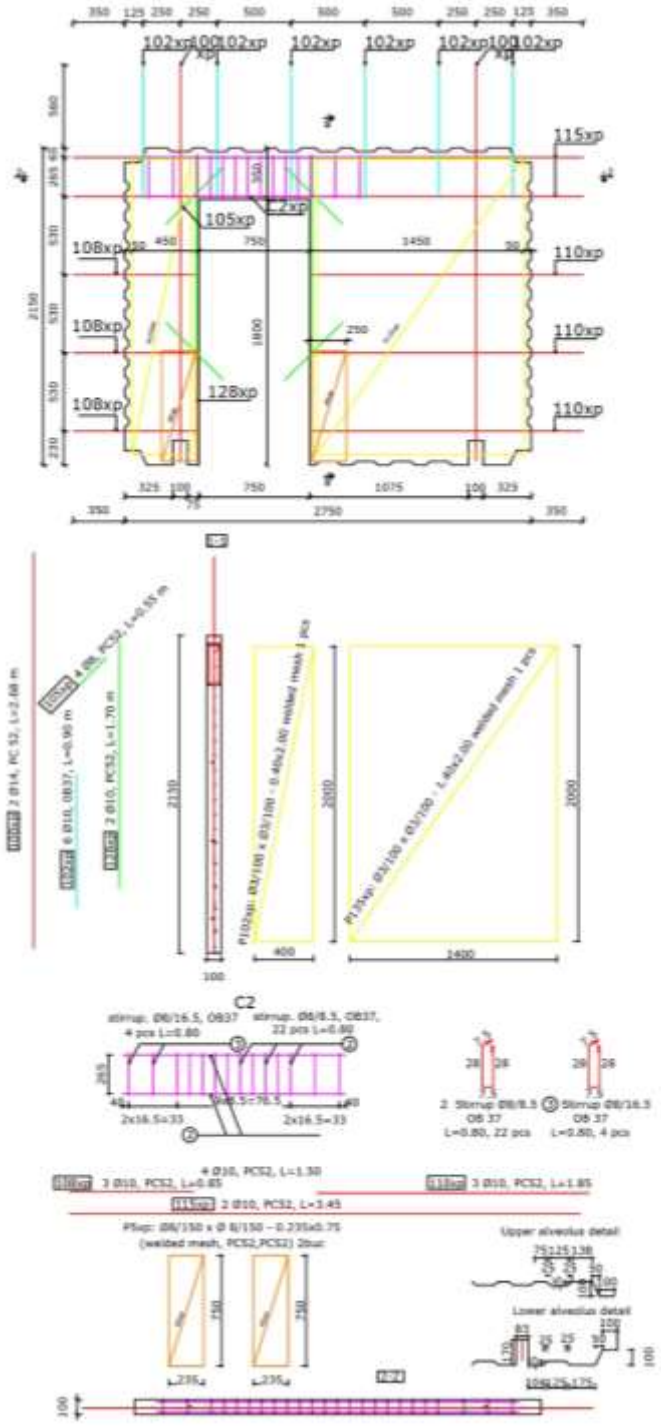

Figure 3-8 – Reinforcement details for PRCWP 16-L1-E1

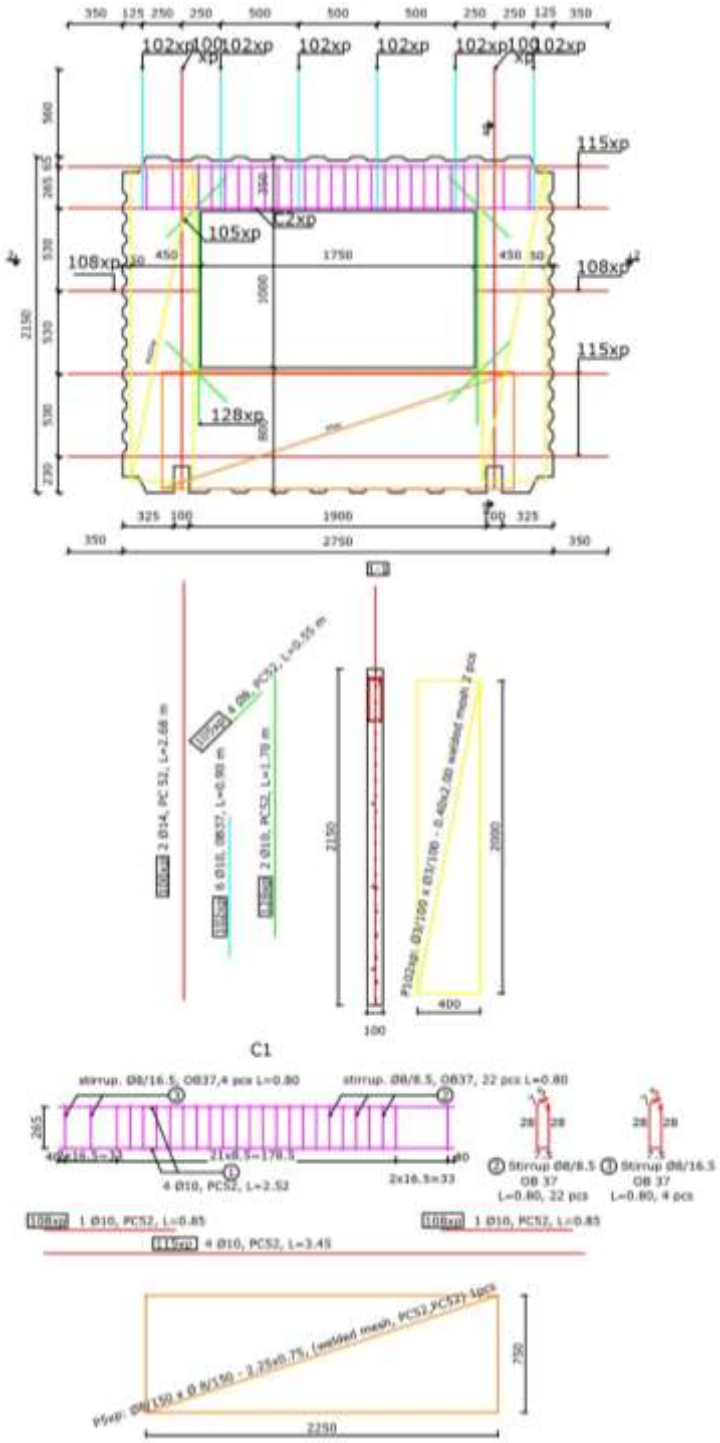

Figure 3-9 – Reinforcement details for PRCWP 17-L3

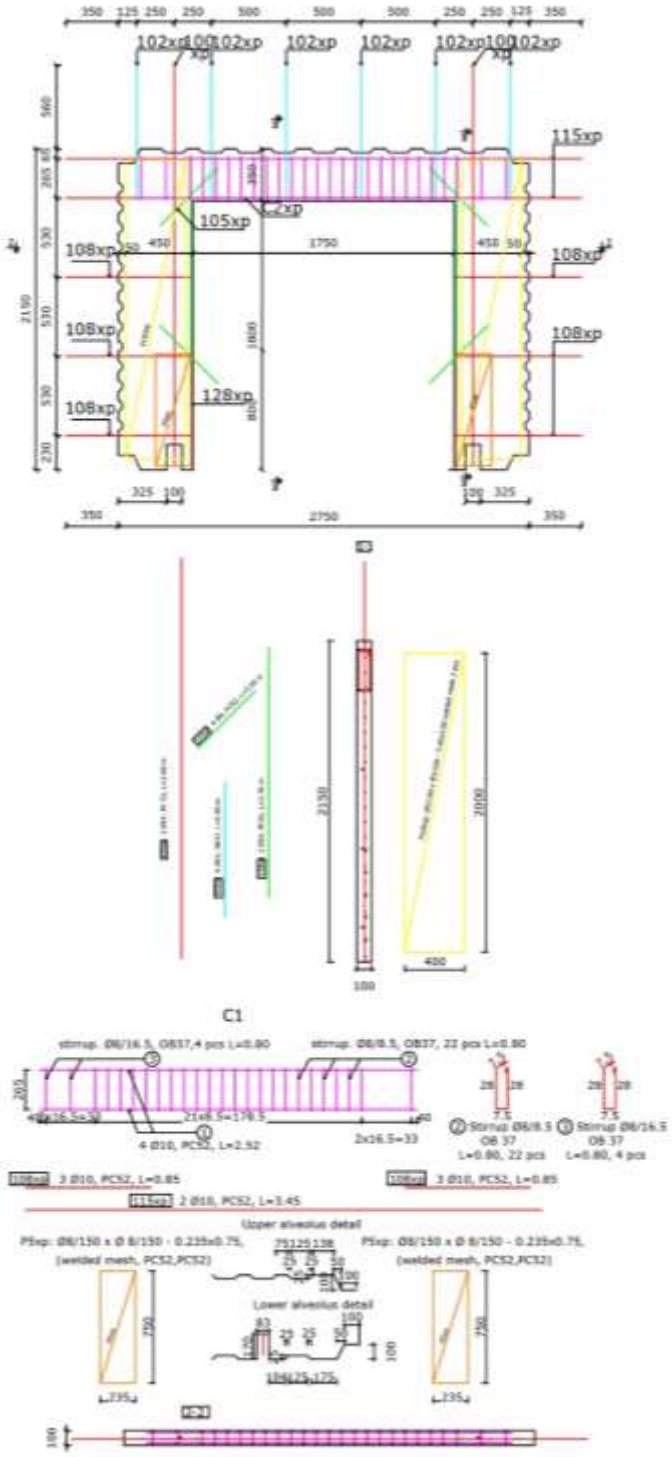

Figure 3-10 – Reinforcement details for PRCWP 18-L3-E3

The reinforcement details for the specimens manufactured in Stei, PRCWP 15-EL2, PRCWP 16-L1-E1, PRCWP 17-L3, PRCWP 18-L3-E3 are presented in Figure 3.7, Figure 3.8, Figure 3.9 and Figure 3.10, respectively. All specimens had some kind of initial opening and the reinforcement is in accordance with the opening type. In the coupling beam above each opening there is a spatial steel reinforced cage comprised of 4 Φ10 mm diameter bars with Φ8 mm stirrups. The spatial cage length of the narrow door or window opening differs from the one of the large door or window opening. The PRCWP 15-EL2 specimen had a vertical spatial steel reinforcement cage on the entire height of the left pier, the cage comprised of 6 Φ6 mm diameter bars and Φ6 mm stirrups. In all specimen piers that were not reinforced with spatial cages vertical and horizontal steel bars and welded mesh was provided. In the parapet of all specimens welded mesh of Φ8 mm diameters cold drawn wires and 150 mm centres was present. It can be seen for the specimens having opening cut-outs how the reinforcement was placed in order to simulate the opening cutting through the bars and the welded mesh.

The specimens analysed in this program and their specific opening dimensions are presented in Figure 3.10 alongside the designation of wall panel elements (piers, spandrel and parapet).

The dimensions of the opening are:

EL2: Door: Length: 750 mm
Height: 1800 mm
Window: Length: 1000 mm
Height: 1000 mm

E1: Door: Length: 750 mm
Height: 1800 mm

E3: Door: Length: 1750 mm
Height: 1800 mm

L3: Window: Length: 1750 mm
Height: 1000 mm

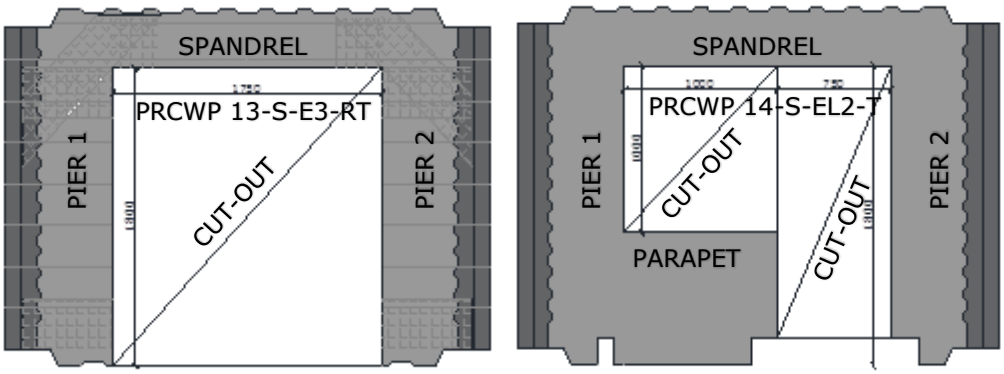

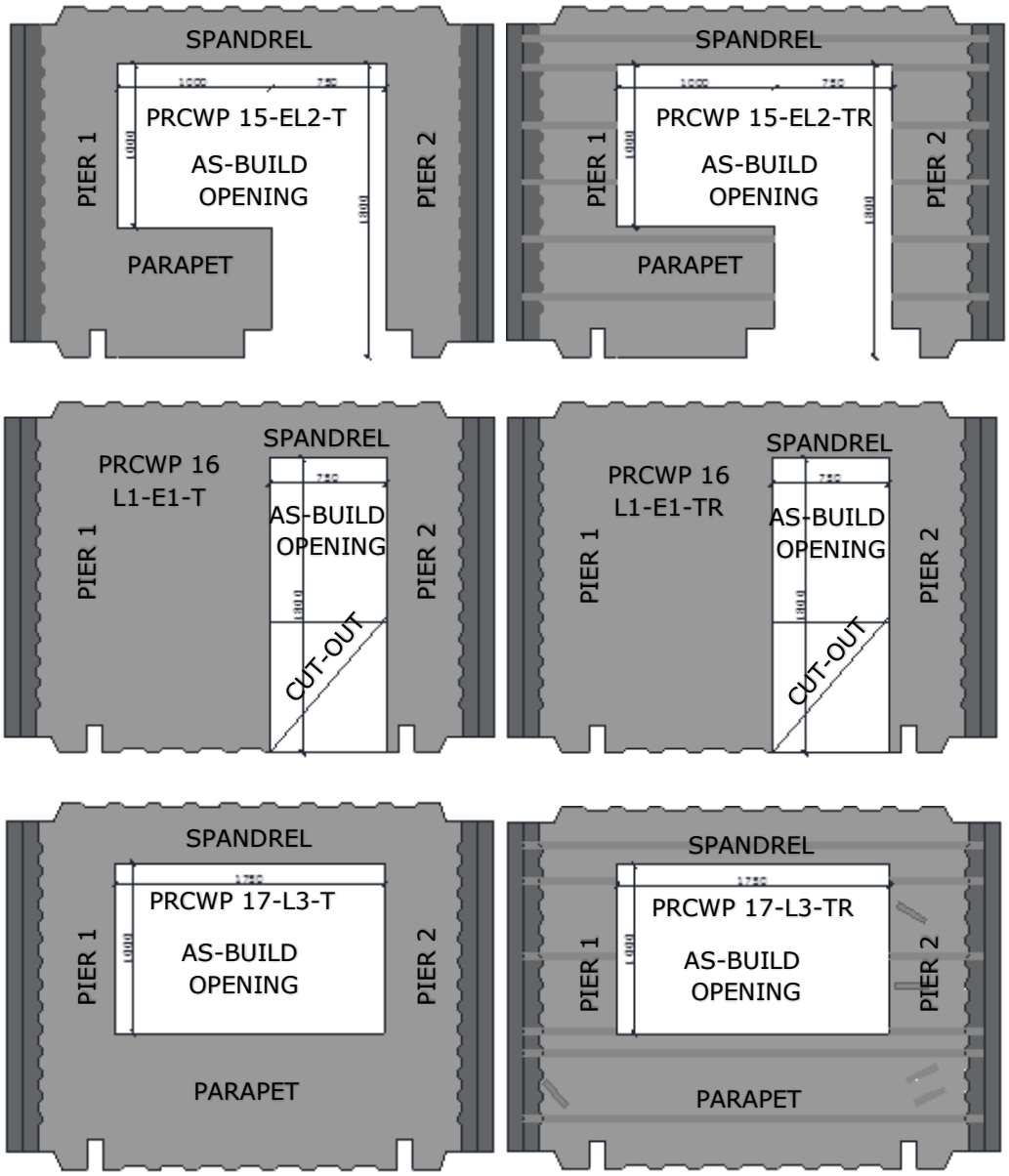
SPANDREL
PRCWP 15-EL2-T
AS-BUILD
OPENING
PIER 1
PIER 2
PARAPET
SPANDREL
PRCWP 15-EL2-TR
AS-BUILD
OPENING
PIER 1
PIER 2
PARAPET
PRCWP 16
L1-E1-T
SPANDREL
AS-BUILD
OPENING
CUT-OUT
PIER 1
PIER 2
PRCWP 16
L1-E1-TR
SPANDREL
AS-BUILD
OPENING
CUT-OUT
PIER 1
PIER 2
SPANDREL
PRCWP 17-L3-T
AS-BUILD
OPENING
PIER 1
PIER 2
PARAPET
SPANDREL
PRCWP 17-L3-TR
AS-BUILD
OPENING
PIER 1
PIER 2
PARAPET

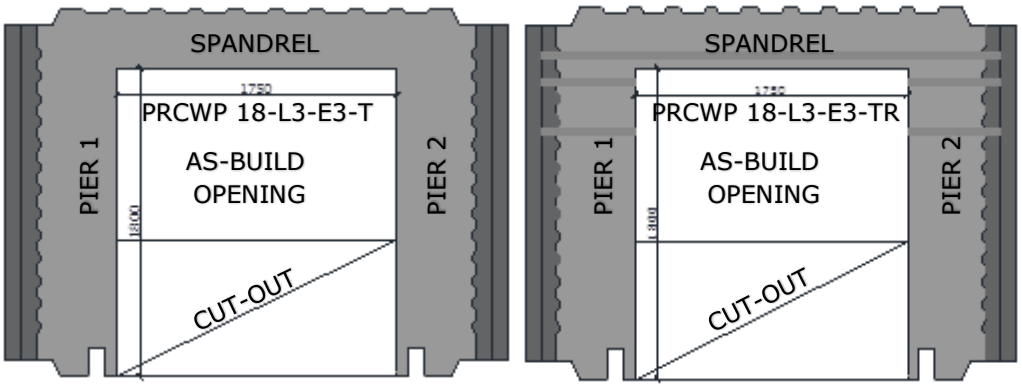

Figure 3-11 – General view of experimental specimens, designation of wall specimen's components and opening dimensions

Table 3-2 – Variables of the experimental program

Element label	As-build/cut-out opening type	Strengthening condition
PRCWP 13 S-E3-RT	solid/large door (S/E3)	Prior-to-damage strengthened (RT)
PRCWP 14 S-EL2-T	solid/narrow door and window (S/EL2)	Unstrengthen (T)
PRCWP 15 EL2-T	door and window (EL2)	Unstrengthen (T)
PRCWP 15 EL2-TR		Post-damage strengthened (TR)
PRCWP 16 L1-E1-T	small window/narrow door (L1/E1)	Unstrengthen (T)
PRCWP 16 L1-E1-TR		Post-damage strengthened (TR)
PRCWP 17 L3-T	wide window (L3)	Unstrengthen (T)
PRCWP 17 L3-TR		Post-damage strengthened (TR)
PRCWP 18 L3-E3-T	wide window/wide door	Unstrengthen (T)
PRCWP 18 L3-E3-TR		Post-damage strengthened (TR)

3.3. Material properties

Materials used in the wall test consisted of concrete, steel reinforcement, CFRP reinforcement and repair mortar. Tests, in accordance to [155], were carried out on the concrete from all walls, while for the walls manufactured in Timisoara, material test were also carried out, by Demeter [49], on the steel in compliance with [156, 157].

3.3.1. Concrete

For the PRCWP 13-S-E3 and PRCWP 14-S-EL2 manufactured in Timisoara, tests on the concrete were performed by Demeter [49]. In Table 3.3 the results for the concrete strength of the elements manufactured in Stei are presented. The

concrete was provided by the concrete station were the walls were constructed, and was prepared in accordance to the concrete recipe for C16/20 concrete class presented in Figure 3.12. From each specimen six 150 mm edge cube samples were obtained, after the concrete had settled and hardened for one or two days the samples were removed from the moulds and were placed into water basin and maintained there during strength development.

The tests on the compressive strength of the cubes were carried out at the Laboratory of Civil Engineering Department, Construction Faculty, Politehnica University Timisoara, Romania, using the Universal testing machine of 2000 kN, as presented in Figure 3.13, the samples were tested after a hardening time of minimum 39 days and maximum 66 days, so the coefficient $\beta_{cc}(t)$, given in Eurocode 2 [158], for the concrete strength variation in time was not considered necessary. The results of the compression test obtained are similar for all samples, indicating a good and constant concrete quality, however, it can be seen that the concrete compressive strength indicated, for PRCWP 17-L3, a class that is superior to the desired C16/20.

					Recipe nr. 1							Date:	25.06.2013			
												Type:	C16/20 -XC1+XC2			
Concrete type	Concrete Class	Cement		Additive A_{d1}		Additive A_{d2}		Additive A_{d3}		D max	Granulocyte Zone	T	A/C	ϱ_b Kg/m^3	Supplementary conditions	
		Type	Dosage	Type	Dosage	Type	Dosage	Type	Dosage							
	1	2	3	4	5	6	7	8	9	10	11	12	13	14	15	
	20	II IALL 42,5R	320	SIKA PLAST-10	0,70%	-	-	-	-	16	Conf SR 13510	S2	0,52	2380	P4	

Granulocyte / Type	Humidity %	Passes through the squared sieve												
		-	0.125	0.25	0.5	1	2	4	8	16	###	###	63	-
1; (0-4) mm			2	6	23	49	77	99	100	100				
2; (4-8) mm			-	-	-	-	0,33	6,33	97,3	100				
3; (8-16) mm			-	-	-	-	0,08	0,15	2,69	93,7				
4; (-) mm														
42 % of type 1			0,8	2,52	9,66	20,58	32,34	41,6	42	42				
20 % of type 2			-	-	-	-	0,07	1,26	19,5	20				
38 % of type 3			-	-	-	-	0,03	0,06	1,78	35,6				
0 % of type 4														
TOTAL (mixture)			0,8	2,52	9,66	20,6	32,4	42,9	63,3	97,6				

Quantities for one m^3 of concrete			
Water (kg)	Additive		Dried aggregate (total in kg)
A=Cx a/c = 166	A_{d1}=C.PAD/100= SIKAPLAST10=2,25 kg	A_{d2}=C.PAD/100= -	A_{d3}=C.PAD/100= -	Ag=ϱ_b-(C+A+A_{d1}+A_{d2}+A_{d3})= 1894

Quantities for one m^3 of concrete						Quantities/one batch of _____m^3	
Type	Dried		Aggregate Humidity		Wet Aggregate	Wet Aggregate	Tolerances kg
	%	kg	%	kg	kg	kg	
1: (0-4)	42	795	5	40	835		
2: (4-8)	20	379	3	11	390		
3: (8-16)	38	720	1	7	727		
4: (-)							
	Σ	1894	Σ	58	1952		
			Cement		320		
			A-(Ag-Ad)		105,76		
			A_{d1} (Additive)		2,24	SIKAPLAST-10	
			A_{d2} (Additive)		-		
			A_{d3} (Additive)		-		
			TOTAL		2380		

Figure 3-12 – Recipe used for concrete manufacturing

This can be attributed to the recipe used that was made in order to ensure each time a minimum quality of C16/20. It can be seen from Table 3.3 that the compressive strength of samples from PRCWP 18-L3-E3 is extremely low for the reason that the samples had frozen in the moulds before placing them in water. Fortunately, during the transportation and the test it was observed that the specimen did not have the same low compressive strength so a similar strength to the other ones was assumed. In order to compute the concrete class the measured cube strength $f_{cm,cube}$ was transformed into cylinder values f_{cm}, by assuming a reduction for cylinder strength of 18 % as specified by [159] and then the mean to characteristic transformation was performed by using the formula [160]:

$$f_{ck} = (1 - 1{,}64 \times 0{,}15) \times f_{cm}$$

Where:

f_{ck} is characteristic concrete compressive strength
f_{cm} mean concrete compressive strength for cylinders

Table 3-3 – Properties of the concrete

Element	**$f_{cm,cube}$ (N/mm²)**	**f_{cm} (N/mm²)**	**f_{ck} (N/mm²)**	**Class**
PRCWP 15-EL2	27,35	22,43	16,91	C16/20
PRCWP 16-L1-E1	29,03	23,80	17,95	C16/20
PRCWP 17-L3	34,1	27,96	21,08	C20/25
PRCWP 18-L3-E3	10,25	8,41	6,34	C6/7,5

Figure 3-13 – Concrete testing: (a) testing machine; (b) compression test on cube

3.3.2. Reinforcement

For the specimens manufactured in Timisoara, tensile tests were performed using the Universal Testing Machine of the Steel Structures Laboratory from Politehnica University Timisoara, for each type of reinforcement used, namely: smooth (OB37), ribbed (PC52) hot-rolled bars and cold-drawn ribbed welded mesh (STNB). These tests were done by Demeter [49] and the results are presented in table 3.4. For the specimens manufactured in Stei the properties of the reinforcement are considered to be the typical Romanian reinforcements characteristics presented in Table 3.5.

Table 3-4 – Properties of steel reinforcement (measured)

Re-bar type	**Production/Surface**	**φ (mm)**	**f_y (Mpa)**	**f_t (Mpa)**	**f_t/f_y**
OB	Hot-rolled/smooth bar	6	400	550	1,38
		8	425	507	1,19
PC	Hot-rolled/ribbed bar	10	450	564	1,25
		14	395	584	1,48
		16	385	613	1,59
STNB	cold-drawn/ribbed wire	4	618	667	1,08

Table 3-5 – Properties of steel reinforcement (typical)

Type	**Grade**	**ϕ (mm)**	**f_{yk} (Mpa)**	**f_{tk} (Mpa)**	**f_t/f_y**
OB37	S255	6-12	255	360	1,41
PC52	S355	6-14	355	510	1,44
PC60	S420	6-12	420	590	1,40
STNB	S490	3-4	490	590	1,20

3.3.3. Strengthening Materials

For the repair of the concrete that was very damaged, high strength mortar was used form Mapei. Two types of mortar were used, one was the Mapegrout Rapido which has the property of fast setting time between 50-60 minutes [161], the other mortar used was the Mapegrout Easy Flow GF, which is a pre-blended, one-component thixotropic cementitious mortar, made from sulphate-resistant hydraulic binders, polyacrylonitrile synthetic fibres, inorganic, fibres, organic corrosion inhibitors, special admixtures and selected aggregates [162]. The products technical data sheets are presented in Table 3.7. In two cases, for the PRCWP 15-EL2-TR and 17-L3-TR, the cracks were injected with fluid epoxy resin. This procedure was carried out where the cracks were large enough and facilitated the epoxy resin free flow in order to completely fill the cracks.

Three types of FRP composites were used in this thesis, carbon fibre laminates from Mapei for the main strengthening system, unidirectional carbon fibre fabric used for the anchors, carbon fibre grid used as confinement. The properties of the experimental CF-products and resin matrix are taken from data sheets provided by the producer. The characteristics are presented in Table 3.6, while the CF-products are presented in Figure 3.14.

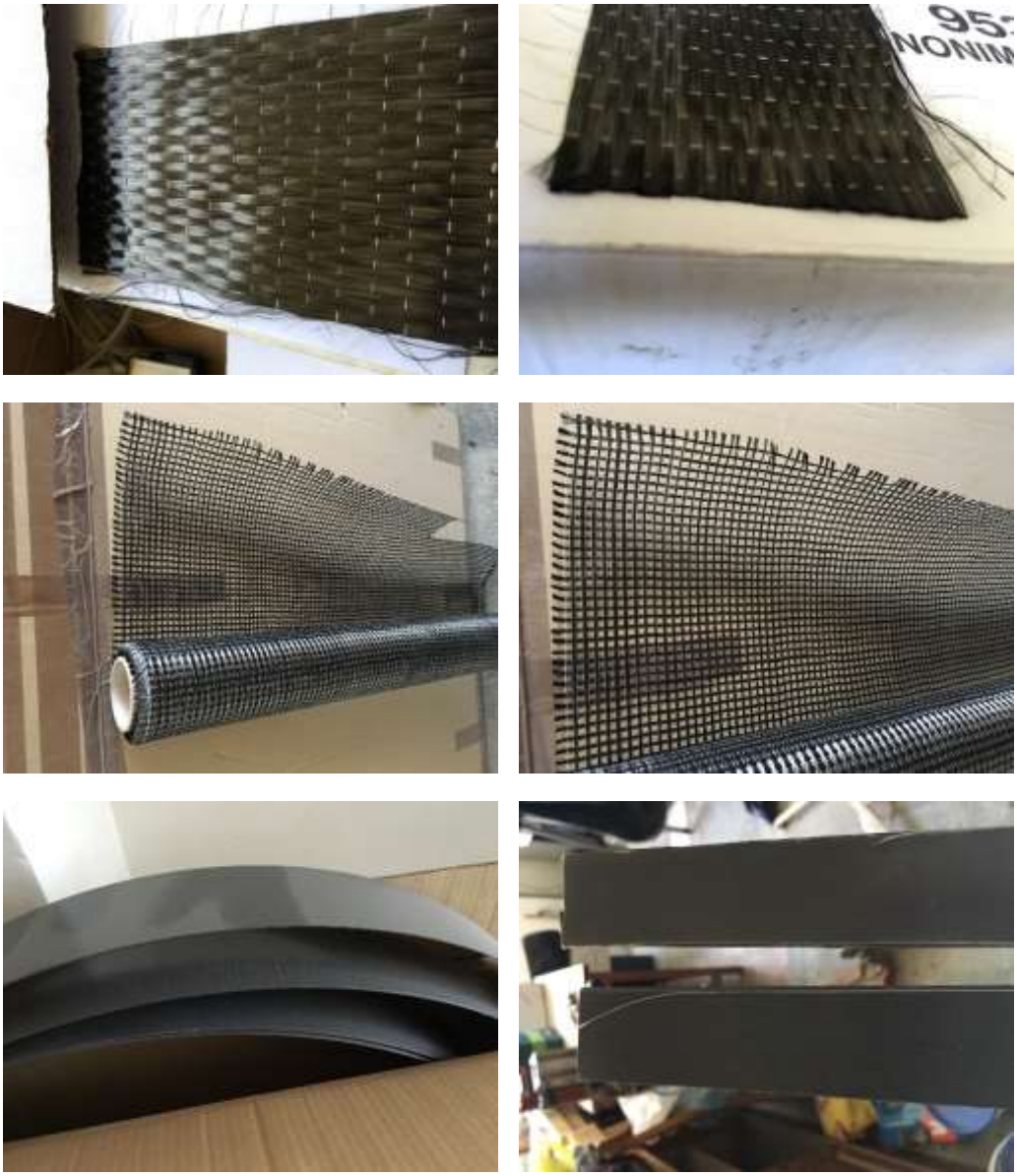

Figure 3-14 – FRP reinforcement used

Table 3-6 – Properties of CF materials and epoxy resins

Product	Carboplate E170/100/1.4	Mapewrap C UNI-AX 300/40	Mapegrid C170	Mapewrap 12	Mapewrap 31	Mapewrap primer 1	Adesilex PG2
Type	Carbon fibre plate	Carbon fibre fabric	Carbon fibre grid	Epoxy resin	Epoxy resin	primer	Epoxy resin
Thickness (mm)	1,4	0,767	n/a	n/a	n/a	n/a	n/a
Weight	225 g/ml	300 g/m^2	170 g/m^2	1,7 kg/l	1,05 kg/l	1,12 kg/l	1,72 kg/l
Tensile strength (MPa)	3100	4830	4800	n/a	40	n/a	n/a
Tensile modulus (Gpa)	170	230	230	n/a	n/a	n/a	n/a
Elongation at break (%)	2,0	2,0	2,0	n/a	n/a	n/a	n/a
Application temperature range	n/a	n/a	n/a	from+5°C to+30°C	from+10°C to+35°C	from+10°C to+30°C	from+10° C to+30°C
Hardening time	n/a	n/a	n/a	7 days	7 days	7 days	7 days

Table 3-7 – Properties of the repair mortars

Product	Mapegroud Rapido	Mapegrout Easy Flow GF
Compressive strength at 28 days [N/mm^2]	>28	>60
Modulus of elasticity	24	27
Specific consumption [kg/m^2] for 1 cm thickness	18	18,5
Thermal compatibility to freeze-thaw [MPa]	>1,5	>2
Density of mix [kg/m^3]	2150	2200
Maximum aggregate size [mm]	1	2,5
Application temperature range	From +5°C to 35°C	From +5°C to 35°C
Pot life of mix	approx. 15 min	approx. 1 hour
Setting time	≤30 minutes	n/a
Waiting between layers	approx. 15 minutes	maximum 1-2 hours
Flexural strength at 28 days [MPa]	>8	>11
Bond strength to concrete after 28 days [MPa]	>1,5	>2
Reaction to fire	A1	A1

3.4. Repair and Strengthening

The author of this thesis adopted two strengthening strategies for the experimental specimens, one using Near Surface Mounted (NSM) Carbon Fibre Reinforced Polymers (CFRP) combined with Externally Bonded Reinforcement (EBR) Carbon Fibre Reinforced Polymers (CFRP) and the other using Externally Bonded Reinforcement (EBR) Carbon Fibre Reinforced Polymers (CFRP) laminates. Before the strengthening material could be applied to the specimen, the damages created by the unstrengthen test needed to be addressed. In order to do this the crushed concrete was replaced with high strength repair mortar and the observed cracks were cleaned, and superficially filled with epoxy resin. In case of two specimens, namely PRCWP 15-EL2-TR and 17-L3-TR, the main diagonal crack was large enough to allow the injection of epoxy resin inside, in order to seal it and weld together the two concrete parts divided by the crack. The main objective of the retrofitting strategies was to restore or increase the specimens initial lateral load bearing capacity.

The strengthening strategies are adopted according to the observed behaviour and failure mode of the unstrengthen (reference) specimens, with focus on the critical zones. Each specimen has its own unique strengthening strategy based on what was observed during the unstrengthen tests. The general characteristics of the behaviour of the reference specimens were as follows: shear cracking of the piers was the main reason for failure, concrete crushing of the spandrel-pier connection joint, concrete crushing of the bottom extremities of the piers. Hence, the main objective was to increase the shear capacity of the piers, to provide confinement effect at the opening corners and at the end of the wing wall. These strengthening strategies were partially presented in [163, 164, 165]. After the first specimen had been strengthened prior-to-damage trying to improve all of the above-mentioned aspects of the specimen, the costs of the strengthening procedure were analysed and proposed for the retrofitting of one 5 storey high building. After discussions with several companies the author concluded that this strengthening strategy is to expensive, time consuming and messy for the general beneficiary to accept. Therefore, only one specimen was retrofitted using these strategy, the rest of the specimens the focused was also on the costs of the strategy.

3.4.1. Strengthening using EBR-CFRP combined with NSM-CFRP

The first retrofitting strategy was adopted for the prior to damage strengthened specimens 13 S-E3-RT, the only specimen that was not tested initially as unstrengthen. Considering the reinforcement of the specimen, which is specific to a solid element (see Figure 3.6), and the opening type of a large door (E3), the specimen had two symmetrically reinforced piers connected by the spandrel. The author of this paper presents the retrofitting strategy only for one side of the specimen, however one should keep in mind that both sides of the specimen were symmetrically retrofitted.

The strengthening strategy is presented in Figure 3.15, it can be seen that for each side of the piers, six NSM-CFRP laminates were used. Each plate had was 12 mm wide and 1.4 mm thick, the distance between the laminates was 250 mm. For the spandrel, two NSM-CFRP laminates were installed having the same dimensions as the ones placed in the piers. For the confinement of concrete in the critical areas, EBR-CFRP mesh was used at the spandrel-to-pier connection and at the bottom parts of the pier.

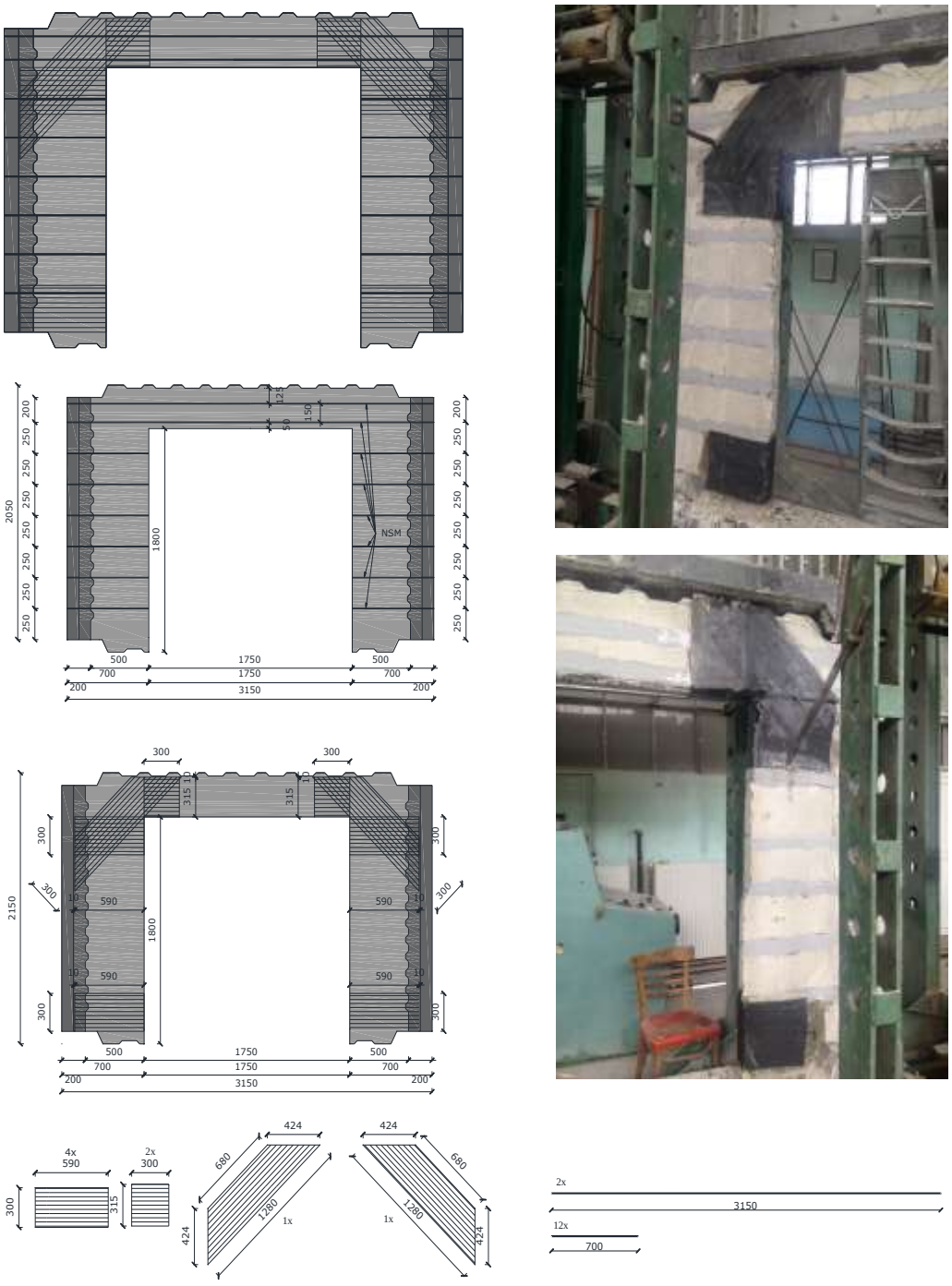

Figure 3-15 – Strengthening strategy using NSM-CFRP combined with ERB CFRP

The process of strengthening is presented in Figure 3.16. The first step was to cut the channels for the near surface mounted reinforcement strips, this was done by using a double disk grinding machine, the thickness of the channels was 6 mm while the depth was designed to be 13 mm. Due to the fact that it is very difficult to obtain constant depth thorough the entire channel's length, it was accepted that in some case the depth was larger than 13 mm, however, a minimum depth of 12 mm was needed in order for the reinforcement to be fully imbedded in the concrete. After the channel were made, the holes for the anchorages were drilled in the wing element. Each reinforcement plate was anchored in the wing element using epoxy resin. The holes for the anchorages had Φ12 diameter. The next step was to clean the entire channels and holes using a vacuum cleaner and to check the depth before the reinforcement with the epoxy resin was inserted. The first resin used was the primer, it was applied using a small brush, and left to cure for 3 hours. After the primer has set, the NSM reinforcement was introduced in the channels alongside the epoxy resin need to create the bond between the concrete and the reinforcement. The resin was left to cure for one day before we prepared the specimen for the application of the confinement CFRP sheets.

The surface of the element, were the confinement reinforcement will be placed, was polished using a special grinding machine, in order to achieve a fully smooth surface for the CF mesh. The concrete edges of the specimen were the sheets would wrap around the element were rounded at a radius of about 20 mm, for the effectiveness of the confining solution. Local Φ10 mm holes were drilled for the anchorages of the system. After the surface preparation, the entire specimen was cleaned and the epoxy resin was prepared. The first step was applying the primer, after the appropriate time for setting passed, the epoxy resin for the anchorages was prepared. In case of the anchorages the same resin was used as for the NSM laminates, this had a more viscous consistency and was better at filing the holes of the anchorages. The anchorages were made from the same CF sheets as the ones used for the confinement. The resin used for the CF sheets had a much more liquid consistency compared with the one used for the NSM laminates, this helped the bond between the CF sheets and the concrete by impregnating itself between the CF weave.






Figure 3-16 – NSM-CFRP combined with EBR-CFRP strengthening process

3.4.2. Strengthening using EBR-CFRP laminates

All specimens manufactured in Stei were retrofitted using externally bonded (EBR) Carbon Fibre Reinforced Polymers (CFRP) laminates, and the retrofitting strategy was applied post-damage. Each of the tested specimens had slightly different distribution of the strengthening materials on their surface depending on the behaviour of the unstrengthen specimen and on the cracks pattern distribution. All the details regarding the retrofitting strategy for each specimen are presented in Figure. 3.17 and Figure 3.18. Similarly, to the previous retrofitting strategy, in the thesis only one side of the element is presented, however both sides were symmetrically reinforced.

The dimensions of the CFRP laminates were the same for all the specimens, they were 3,2 cm wide and 1.4 mm thick and anchored using either CFRP mesh or CFRP grid. Given the fact that all walls had some type of opening, the spandrel had one CFRP plate running alongside the opening for all the specimens, however, the position of the plate differs as it can be seen in Figure 3.17.

The surface of the element, were the EBR CFRP will be placed, was polished using a special grinding machine, in order to achieve a fully smooth surface. Local Φ10 mm holes were drilled for the anchorages of the system. After the surface preparation, the entire specimen was cleaned and the epoxy resin was prepared. The first step was applying the primer, after the appropriate time for setting passed, the epoxy resin for the anchorages was prepared. In this retrofitting procedure, the epoxy resin used for the anchorages was the same one used for the EBR CFRP laminates, this ensured a good bond between the anchorages and the CF laminates. The resin used was the Mapewrap 12, its properties are presented in Table 3.6. Special attention was granted to the amount of resin used for the anchorages in order not to create a protruding part on the element surface, over which the EBR CFRP would not be able to pass without bending. The anchorages were made from the same CF sheets as the ones used for the confinement presented in 3.4.1. The next step was to place the laminates on the surface of the wall, for these a more viscous resin was used, this ensured a better bond between the retrofitting system and the concrete surface on which it had been placed and since the CF laminates are solid, the resin could not impregnate the them so a liquid resin was not recommended.

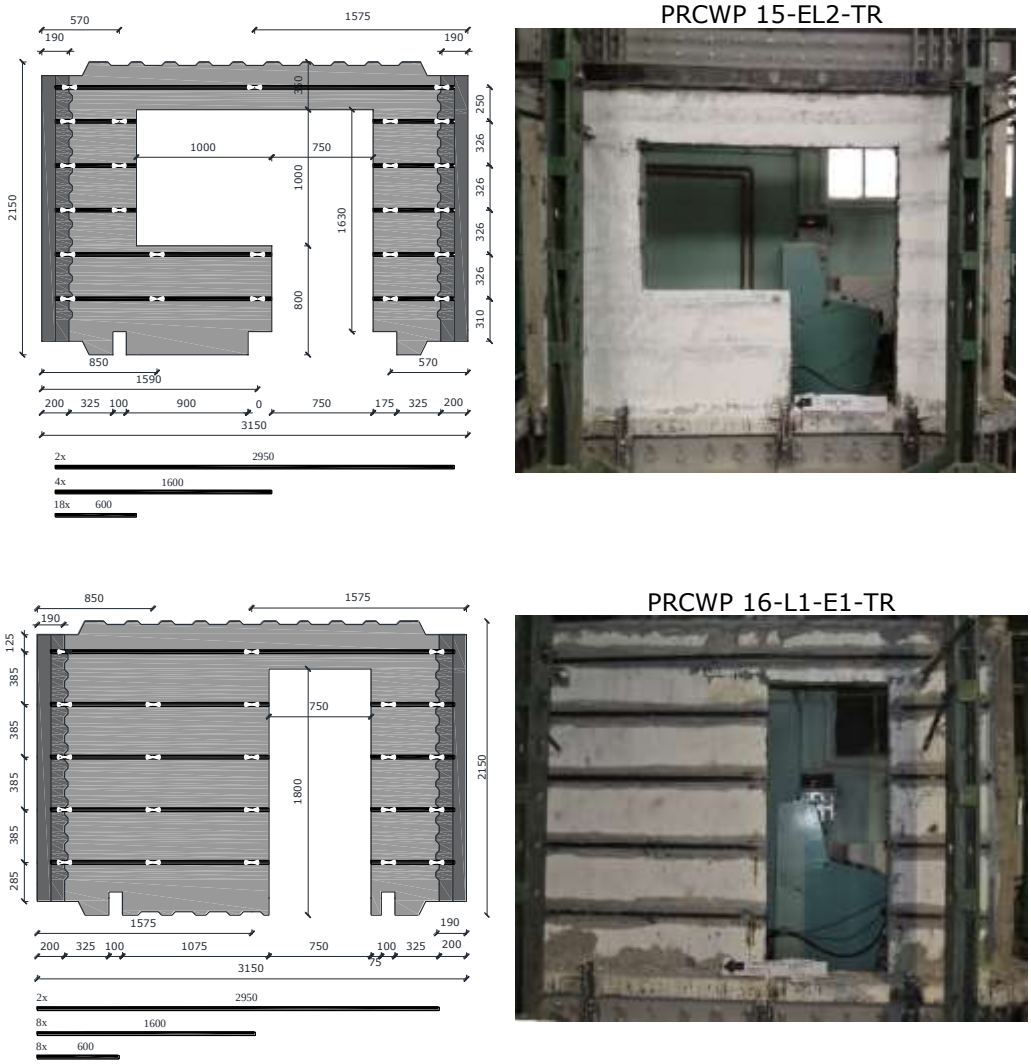

Figure 3-17 – The position of the EBR CFRP laminates for PRCWP 15 and PRCWP 16

The PRCWP 15-EL2-TR was retrofitted on each side using one plate with 2950 mm length for the spandrel, five laminates having 600 mm length for the right pier, for the left pier three 600 mm length laminates and two 1600 mm laminates for the parapet were used. For the anchorages CFRP mesh was used and a total of 25 anchorages were necessary.

For each side of the PRCWP 16-L1-E1-TR the following reinforcement was needed, one plate with 2950 mm length for the spandrel, four laminates having 600 mm length for the right pier and for the left four three 1600 mm length laminates used. For the anchorages CFRP mesh was used and a total of 23 anchorages were necessary.

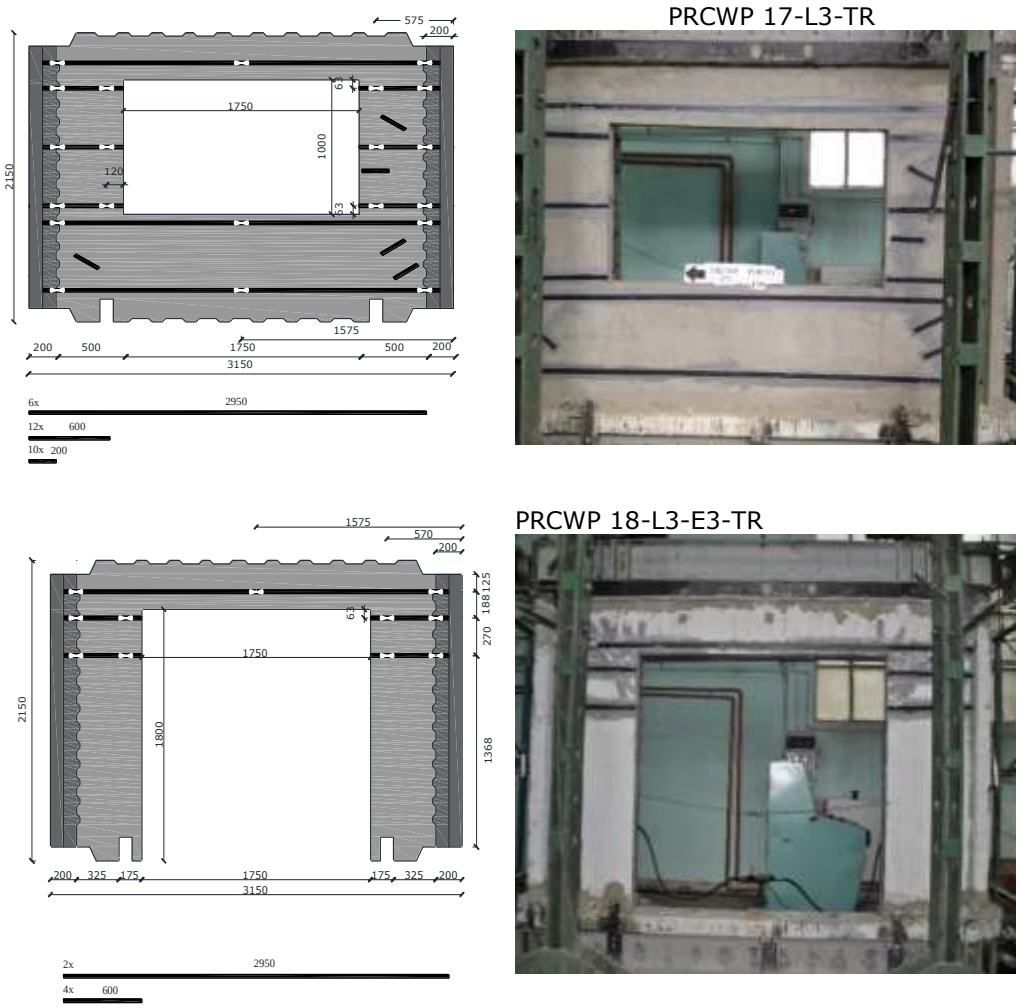

Figure 3-18 – The position of the EBR CFRP laminates for PRCWP 17 and PRCWP 18

The PRCWP 17-L3-TR was retrofitted on each side using one plate with 2950 mm length for the spandrel, three laminates having 600 mm length for the right pier and for the left pier three 600 mm length laminates were used, for the parapet two 2950 mm laminates were used. For this specimen also stitching reinforcement was used, so five 200 mm length laminates were placed on the large cracks in the left and right pier. For the anchorages CFRP mesh was used and a total of 21 anchorages were necessary.

For each side of the PRCWP 18-L3-E3-TR the following reinforcement was needed, one plate with 2950 mm length for the spandrel, two laminates having 600 mm length for the right pier and similarly for the left one two 600 mm length laminates were used. This specimen had the simplest approach to its retrofitting strategy since there were no noticeable cracks in the piers. For the anchorages CFRP grid was used and a total of 11 anchorages were necessary.

Figure 3-19 – Anchorages for the EBR CFRP system

3.5. Experimental test set-up

The entire test set-up was used before by Demeter [49] and Todut [50] in their thesis and since this work is a continuation of the experimental programs investigated and reported by my colleagues very few modifications were performed on the set-up for the current specimens. The test set-up configuration comprises of four vertically steel reaction frames (Figure 3.24b) of 1000 kN capacity, anchored on the existing steel anchorage point in the Reinforced Concrete Structures Laboratory, two truss type steel lateral reaction frames of 1000 kN capacity (Figure 3.24a), the hydraulic loading device, electric pump, hand pumps, a series of hydraulic jacks, cylinders and hoses of 375 bar working pressure (Figure 3.23). For transmitting the forces to the specimen two loading beams were used, one placed at the top of the element named cap beam and one at the bottom of the element named base beam. These beams were designed by Demeter [49] to be used in all the experimental test that followed, hence the high steel percentage in the beam and the high concrete class of the beams. The loading beams details for the concrete outline and the arrangement of reinforcement are presented in Figure 3.20 [49], they consist of two U300 steel channels and a reinforced concrete T beam, these were connected using Φ20 mm threaded rods. For the top panel, horizontal edges shear keys were formed and at the beam end shear steps were provided as seen in Figure 3.20. In order to connect the beams to the reaction frames, special connection details were provided. For the base beam Φ70 mm steel bolt hinges and for the cap beam ball bearings at the end. For the experimental wall anchorage to the base beam Demeter designed a lap-welding of 4-5 vertical continuity steel rebar, depending on the opening type of the specimen, however Todut in her experimental program improved the system by also lap-welding them steel rebar from the specimen to the steel L channels which were fixed to the base beam. In all the test presented in this thesis the improved version of the anchorage was used. The space between the two beams and the wall specimen was filled with high strength repair mortar, the same one used to repair the crushed concrete in the strengthened tests with the material properties being presented in Table 3.7.

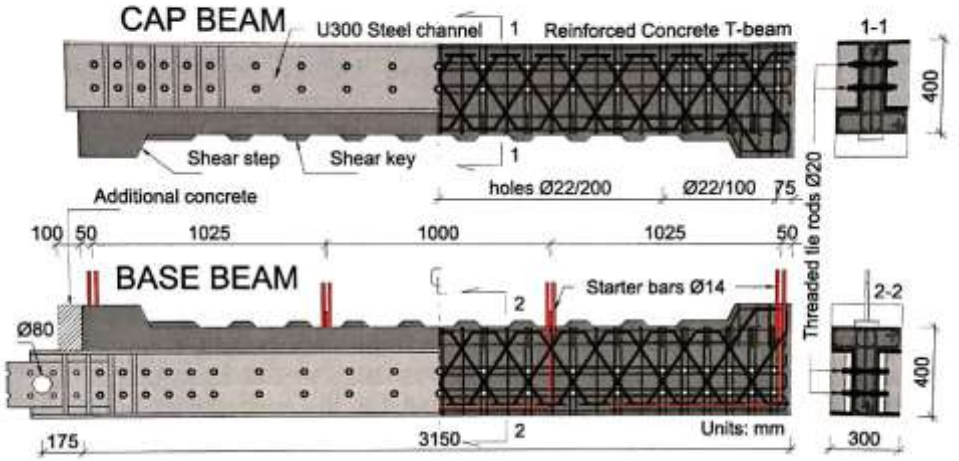

Figure 3-20 – Loading beams detail [49]

Figure 3-21 – Casted loading beams

For imposing the loads onto the tested specimen, four hydraulic jacks were used. Two for imposing the lateral loads acting at the ends of the top beam, whilst the other two were used to impose de vertical (axial) loads. The jacks were actuated by hydraulic pumps, for the lateral loads a single electric pump was used since the specimen was loaded only one side at the time (see paragraph 3.6). For the vertical loads manual or electric pumps were used, based on the conditions in the laboratory and on the availability of the pumps. For each test three pumps were used in total, as the vertical loads were composed of an alternating part and a constant one (see paragraph 3.6) It need to be mentioned that the same configuration for the test set-up was used throughout the entire experimental program for all the investigated wall test specimens.

Figure 3-22 – Hydraulic jacks and pumps

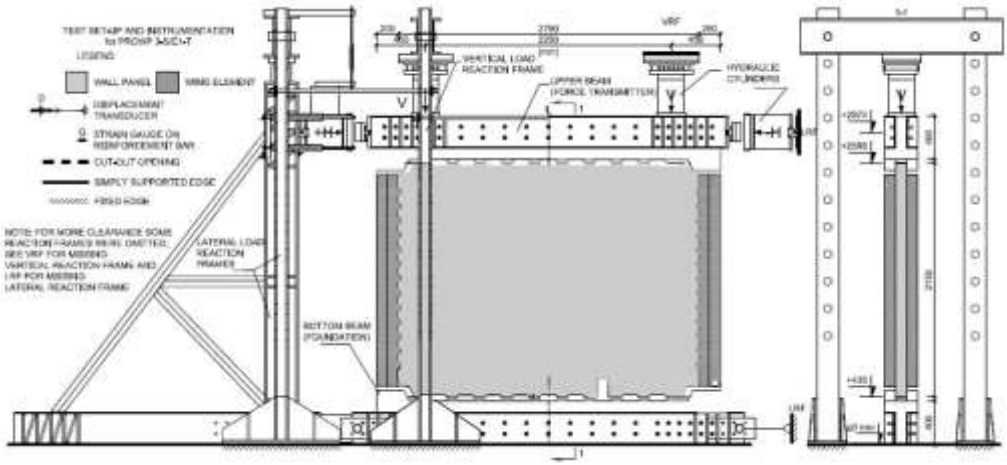

Figure 3-23 – Experimental test set-up

Figure 3-24 – Lateral and vertical reaction frames

3.6. Loading protocol

The test specimens were subjected to quasi-static in-plane reversed cyclic seismic loads and alternating gravitational loads. The protocol is the same one used in previous research programs and it is based on literature inspection published by Demeter et al. in [166, 167]. For the seismic (lateral) loads a reversed cyclic, displacement controlled increasing displacement amplitude was adopted (Figure 3.25), two hydraulic cylinders were used at the end of the top beam to impose the shear forces. The displacement control was taken as the horizontal drift computed as the difference between the horizontal displacement measured at the top of the specimen and the horizontal displacement measured at the bottom of the specimen. This distance is approximately equal to 2150 mm so the 1% drift ratio corresponds to 21,5 mm, computed with the formula:

$$R\% = \frac{drift}{height} * 100$$

The positive and negative loading directions can be also seen in Figure 3.25, the displacement amplitudes were multiplies of the base value computed above, thus the increment (ΔR%) of 0.1% was applied. The subsequent displacement levels for these conditions were as follows: 0.1%, 0.2%, 0.3%, 0.4%, etc. ass seen in table 3.8, corresponding in terms of drift to 2.15 mm, 4.3 mm, 6.45 mm, 8.6 mm etc. For each drift ration a number of two (n=2) cycles were performed, in order to have a comprehensive observation on the behaviour of the specimens, furthermore, for the small displacement up to 1 mm, increments of load control were imposed, for a better assessment of the behaviour under more gentle loading conditions. The load control was in increments of 50 kN, namely 50 kN, 100 kN, 150 Kn, etc. until 1 mm drift ration was obtained.

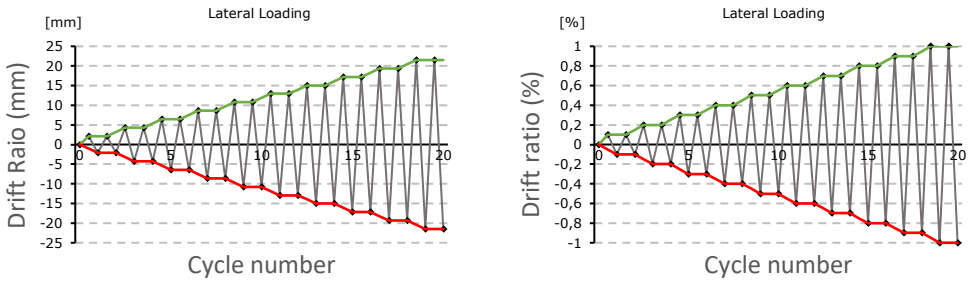

Figure 3-25 – Lateral loading procedure

Table 3-8 – Cycle drift magnitudes

Cycle	1;2	3;4	5;6	7;8	9;10	11;12	etc
Drift (mm)	2,15	4,30	6,45	8,60	10,75	12,90	+2,15
Drift ratio (%)	0.1	0.2	0.3	0.4	0.5	0.6	+0.1

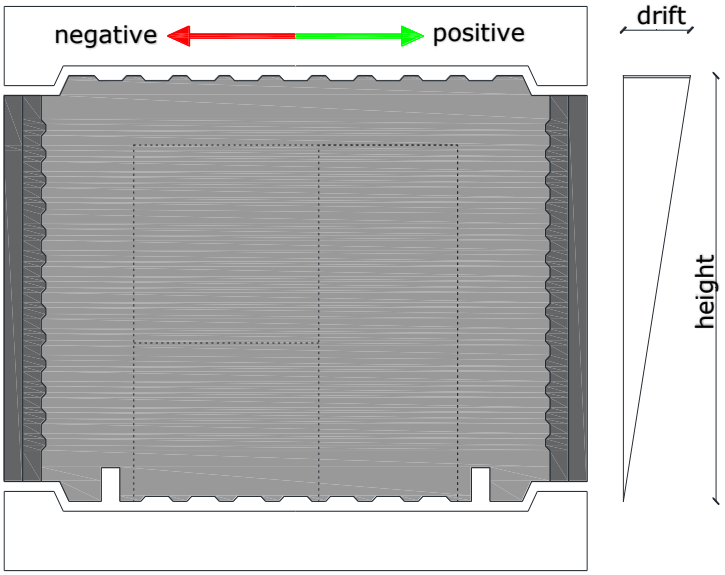

Figure 3-26 – Positive and negative direction of loading

To replicate the real behaviour of the specimens, two hydraulic jacks were used at the top of the loading beam, in order to simulate the gravity loading conditions at the base of a five-storey building. These axial loads were comprised of a constant part and an alternating one. This was necessary to restrain the rocking rotation of the loaded specimens, this was required due to the fact that the base beam was not fixed to the strong floor, thus having no vertical tension reaction forces. The only forces opposing the overturning moment generated by the lateral loads were brought by the axial loads. If these loads were kept constant the walls would rock at a lateral load corresponding to an overturning moment, so we would not be simulating the shear behaviour of the specimens. The value of the constant axial load was considered 100 kN, whilst the increase of the alternating load was controlled by the elevations of the ends of the specimens, measured using vertically oriented displacement transducers D7 and D8, see section 3.8. So, for each 1mm of displacement noticed at the ends the corresponding vertical (axial) load was increased by 100 kN, giving us an increment of 100 kN/mm. As presented in Figure 3.27, the loads were labelled as N1 and N2, the vertical loads which were closest to the loaded end of the top beam were increased, so the N1 load was increased for the positive lateral loading direction, and N2 was increased for the negative lateral loading direction as seen in Figure 3.27.

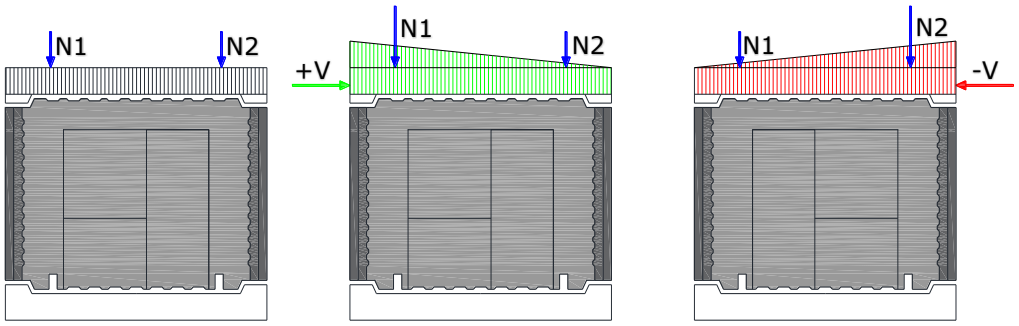

Figure 3-27 – Axial loading

3.7. Boundary conditions

As previously mentioned in this thesis, the experimental program is a continuation of a larger investigation regarding PRCLP buildings, the boundary conditions are the same one used by Todut [50] and Demeter [49] before me. Namely the experimental program exhibits a restrained rotation type of boundary condition for all the wall specimens. By adopting this boundary condition, we were able to stimulate the shear behaviour combating the flexural one, by reducing the shear spam. The test set-up is featuring an almost zero overall base moment through the hinged end connections. However, in case of specimens with openings, like the ones presented in this thesis, it is possible for some interior moments to develop. These moments are limited by the increasing axial loads presented in These moments are limited by the increasing axial loads presented in Chapter 3.6, which act against the vertical tensile forces.

The diagonal tension shear transfer mechanism was eliminated by the absence of any vertical reinforcement attachment to the loading beam, and by the use of constant and variable compression axial loads, meanwhile the sliding-dowel collapse mode was eliminated by considering the shear keys. Therefore, the only mechanism allowed is the diagonal compression shear transfer.

3.8. Instrumentation

The performance of the tested specimens was assessed by measuring two quantities, namely the displacements and the forces. For each specimen, a total of 10 displacements and three pressures were measured. For data acquisition, the Almemo 5990-0 system was used with 35 possible inputs, for the experimental program we used a maximum of 13 inputs, the system is presented in Figure 3.28, while the full specifications can be found in [ahl5990].

The displacements were measured using linear potentiometers, they were fixed either to an independent steel frame or directly on the specimen. The position of the displacement transducers is presented in Figure 3.29. All transducers were connected to the measuring points using steel wires with a very low elasticity, so the measuring error from the elongation of the wire to be minimal.

Figure 3-28 – Data acquisition system

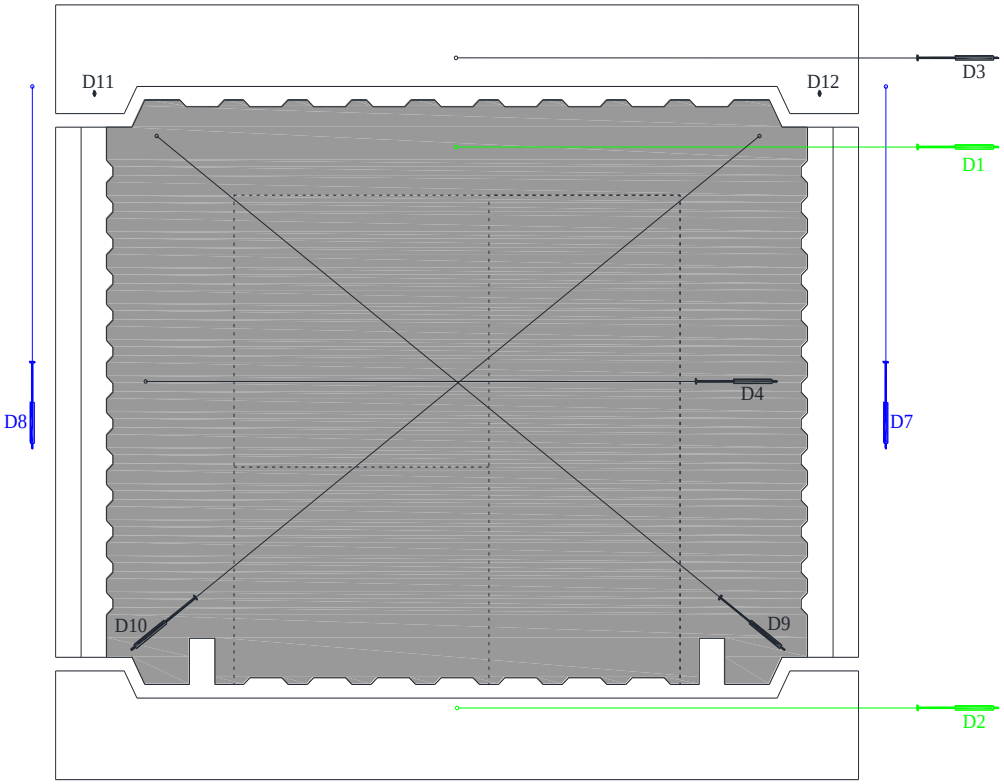

Figure 3-29 – Displacement transducer position

The displacements used to control the loading are highlighted in Figure 3.29 with green and blue. There were four displacements that controlled the loading, two horizontal ones for the drift (D1, D2) and two vertical ones (D7, D8) for the axial loads, described in Chapter 3.6. For the top displacements, were the largest

measurements were expected, the Almemo FA150T transducers were used with a measuring range of 150 mm, these were the longest transducers available in the laboratory. For the smallest displacements expected, in the out of plane region the smallest transducers were used, the Almemo FWA025TR with a measuring range of 25mm. For the rest of the displacements the Almemo FWA100TR were used with a measuring range of 100 mm. In Table 3.9 the type of transducer for each displacement is presented and its characteristics.

Table 3-9 – Transducers type and characteristics

Displacement	Transducer type	Range (mm)	Resolution (mm)	Independent linearity (%)
D1	FWA150T	150	0.01	0.075
D2	FWA100TR	100	0,01	0.075
D3	FWA150T	150	0.01	0.075
D4	FWA100TR	100	0,01	0.075
D7	FWA100TR	100	0,01	0.075
D8	FWA100TR	100	0,01	0.075
D9	FWA100TR	100	0,01	0.075
D10	FWA100TR	100	0,01	0.075
D11	FWA025TR	25	0.001	0.2
D12	FWA025TR	25	0.001	0.2

For the pressure measurement, piezo-resistive transducers were mounted on the hydraulic hoses. A total of three measurements were needed, one for the lateral loads and two for the axial loads. The force was computed by multiplying the pressure measured by the gage with the piston area of the hydraulic cylinder. For the 16-L1-E1-TR, 15-EL2-T/TR and 18-L3-E3-T/TR specimens, only two pressure transducers were used due to the fact that one transducer broke down during the 16-L1-T test. In this cases for one of the vertical loads a pressure gauge (manometer0 was used in order to measure the force. The pressure transducers were Almemo FD8214 21U with a range of 0-600 bar and a resolution of 0.1 bar. In Figure 3.30 the pressure monitoring equipment is presented.

Figure 3-30 – Piezo-resistive pressure transducer and pressure gauge

4. RESULTS

In the next pages the results obtained by the nine cyclic wall tests are presented. All the recorded data was subjected to an intense screening and removing of any data acquisition "bugs", by eliminating all unsuccessful cycle attempts, removing all duplicated values, and by reassigning the correct sign to the force when changing of the loading direction. Basically, this smoothing operation was carried out by eliminating several data lines from the recorded data file, in order to have fluent and readable graphs and diagrams. After the analysis of the data we have obtained the following important aspects: the general observed behaviour and failure modes of the walls during the experimental tests, the force-drift ratio analysis, the dissipation of energy, the ductility of the elements, the stiffness degradation, weakening assessment, and computation of the final cracking pattern.

4.1. Failure details and behaviour of the reference specimens

The general behaviour aspects that were observed during the test of the reference, unstrengthen specimens, consists of a significant number of cracks, appearing in all regions of the element, concrete crushing at the base and corners of the openings and reinforcement yielding. Detailed data of the failure mode is presented below.

PRCWP 14-S-EL2-T presented cracks in the left and right pier, in spandrel, parapet, spandrel-pier connection, parapet-pier connection, and wings, the first crack appeared in the spandrel right pier connection at 0.3% drift ratio (6.45 mm) in the first cycle loaded from right. The concrete was crushed at the spandrel- right pier connection, at the parapet-left pier connection and at the wings. In Figure 4.1 the failure details are presented

Figure 4-1 – Failure details of PRCWP 14-S-EL2-T

For PRCWP 15-EL1-T the failure details are presented in Figure 4.2 and it presented large diagonal cracks in the left pier. The right pier displayed little cracks while in the spandrel a moderate number of cracks appeared. The first crack appeared at 0,3 % (6,45 mm) drift level. Concrete crushing was observed at the left corners of the widow opening and in the intersection of the two large diagonal cracks.

Figure 4-2 – Failure details of PRCWP 15

PRCWP 16-L1-E1-T displayed a very atypical behaviour with severe concrete crushing at the base of the element including the wings. Cracks did appear in the piers, spandrel, spandrel-pier connection, and wing. The first crack appeared at 0,3% drift ratio (6.45 mm) in the second cycle loading from the right, but the concrete at the bottom of the element started crushing visibly at 0,2% drift ratio (4.3 mm). Failure details are presented in Figure 4.3.

Figure 4-3 – Failure details of PRCWP 16-L1-E1-T

PRCWP 17-L3-T displayed diagonal cracks in both left and right piers, as well as in the spandrel and parapet. This element had very little concrete crushing, the only parts were there was visible concrete crushing was in the bottom part at the wings. The first crack appeared in the parapet at 0.2% (4.3 mm) drift ratio in the first cycle with the load from the left, while the first diagonal large crack appeared at 0.3% (6.45 mm) drift ration in the second cycle loaded from the right. Figure 4.4 depicts the failure details.

Figure 4-4 – Failure details of PRCWP 17-L3-T

PRCWP 18-L3-E3-T displayed diagonal cracks in both left and right piers, as well as in the spandrel-pier connection and spandrel. This element had concrete crushing at the top corners of the opening, and in the bottom part at the wings. The first crack appeared at the spandrel-pier connection at 0.5% (10.75 mm) drift ratio in the first cycle with the load from the right, while the first diagonal large crack appeared at 0.8% (17.20 mm) drift ration in the first cycle loaded from the right. In Figure 4.5 the failure details are presented.

Figure 4-5 – Failure details of PRCWP 18-L3-E3-T

4.2. Failure details and behaviour of the FRP strengthened specimens

In general, the behaviour aspects, of the wall specimens that were tested, were as expected and similar to the unstrengthen reference specimens. The characteristics observed during the tests, consists of reopening of the existing cracks, from previous tests, FRP laminates debonding, anchorages failure, new cracks appearing, and concrete crushing. However, during these tests no FRP laminates has failed.

PRCWP 13-S-E3-RT revealed very few cracks and signs of failure, specific cracking and fracture noises were heard during the test from the resin and FRP NSM elements. Several cracks appeared in both piers and in the spandrel with the first crack appearing in the right pier at 0.6% (12.9 mm) drift ratio, in the second cycle with the load from the left. Gentle taping of the FRP confinement strips in the left corner of the opening uncovered that it had lost the bond with concrete element at 0.7% (15.05 mm) drift ratio in the first cycle loaded from the left. Crushed concrete was observed at the bottom compressed edges of the element. Figure 4.6 presents the failure details observed for the specimen.

Figure 4-6 – Failure details of PRCWP 13-S-E3-RT

For the PRCWP 16-L1-E1-TR, in the first cycles the cracks from the previous experimental test of the unstrengthen specimen started to reopen, and several new cracks appeared. The failure was characterized by hard snapping sounds of the FRP system, large cracks at the spandrel-left pier connection and spandrel right pear connection. Crushing of concrete was seen at the top corners of the opening. Debonding of the FRP system started at 0.8% (17.2 mm) drift ratio in the spandrel, the anchorage system did was not ripped during the testing.

Figure 4-7 – Failure details of PRCWP 16-L1-E1-TR

PRCWP 17-L3-TR was characterized by reopening of the previous cracks in the first cycles, alongside with specific snapping sounds of the FRP system. At 0.3% (6.45 mm) drift ratio the stitching with the FRP strips started to debond and the epoxy resin to come off the specimen, by the time we reached 0.5% (10.75 mm) drift ratio all the stitching from the right pier hast lost grip from the concrete. Several new cracks appeared in the parapet and left pier. The reinforcement yielded and even bent in both piers, at the bottom edges of the opening were the diagonal cracks intersected. The distinctive behaviour pattern, of this specific element, is that the cracks, which lead to failure, appeared in the opposite pier compared to the previous unstrengthen element test.





Figure 4-8 – Failure details of PRCWP 17-L3-TR

PRCWP 18-L3-E3-TR in the first cycles the cracks from the unstrengthen specimen test, reopened now. Several new cracks appeared in the spandrel, spandrel left and right pier connection. Concrete crushing was observed at the top corners of the opening. Reinforcement yielded and even bent at the spandrel pier connection were the cracked was at its peak.

Figure 4-9 – Failure details of PRCWP 18-L3-E3-TR

4.3. Force-drift ratio data analysis

In order to observe the performance of the tested specimens, several types of analysis on the force and drift ratio responses were necessary. The general seismic performance of the lateral load bearing members is best observed by the following types of analysis: hysteresis loops, envelope curves (cyclic envelope M2 and monotonic envelope M1), backbone envelopes T1 and T2.

4.3.1. Hysteresis loops

The data processing lead off with the hysteresis loops specific constituents being specified. In Figure 4.10 the hysteresis loop loading points and its subsections are presented, at a general x displacement level of a general two reversed cycles load-displacement response. Each cycle is made of four subsections: two opposite loading sections and two opposite unloading sections. Each of these sections are bounded by two points: peak loading point (corresponding to the target displacement) and the reloading point (corresponding to the curve-to-axis intersection). Note that point 8 coincide with point 0 for the next loop. In Figure 4.11 the hysteresis loops for the unstrengthen reference specimens are presented, in figure 4.12 the hysteresis loops for the strengthen retrofitted specimens are presented and in Figure 4.13 a comparison between the reference and strengthen elements is made.

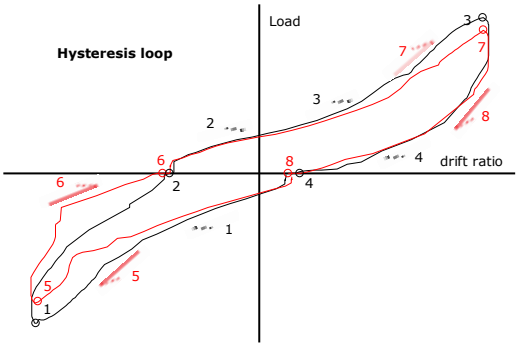

Figure 4-10 – Cycles' loading points and subsections

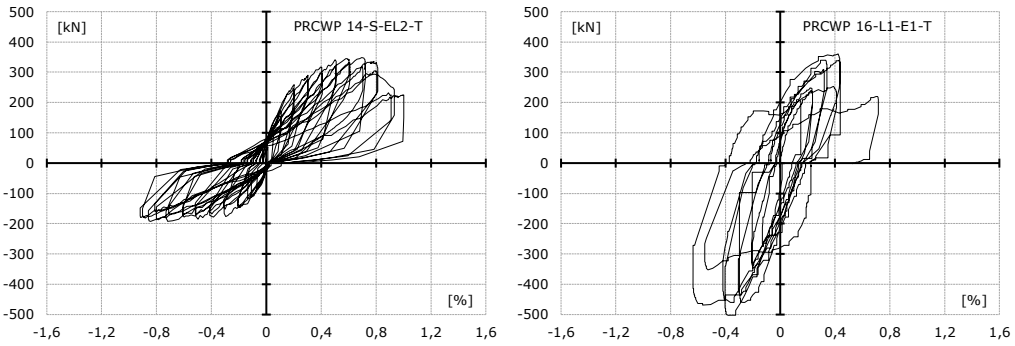

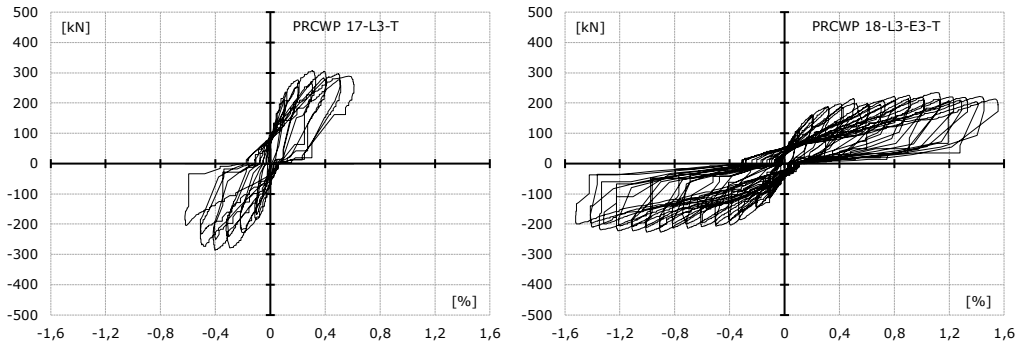

Figure 4-11 – Hysteresis loops for the reference specimens

The PRCWP 16 L1-E1-T specimen had the maximum lateral resisting force due to the fact that it had the largest vertical constant vertical forces. That was caused by an error of the experimental stand, in which one of the pressure transducers was indicating a wrong pressure due to its connection cable head having software issues. From the other hysteresis loops of the specimens it can be reported that the lateral resisting load decreased as the opening dimension increased, so the PRCWP 18-L3-E3-T had the lowest lateral resisting force. For the PRCWP 17-L3-T and PRCWP 18-L3-E3-T specimens, in which the opening and the reinforcement system was symmetrical in regards with the loading system, it can be observed that the maximum lateral load bearing capacity and maximum drift ratio is similar, both in positive and negative direction. While for the PRCWP-S-EL2-T and PRCWP 16-L1-E1-T the maximum lateral resisting force and drift ratio is different in the negative direction compared to the one in the positive direction.

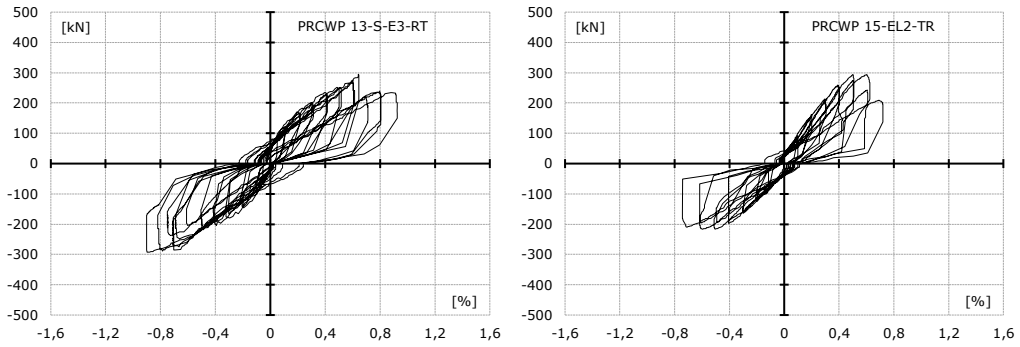

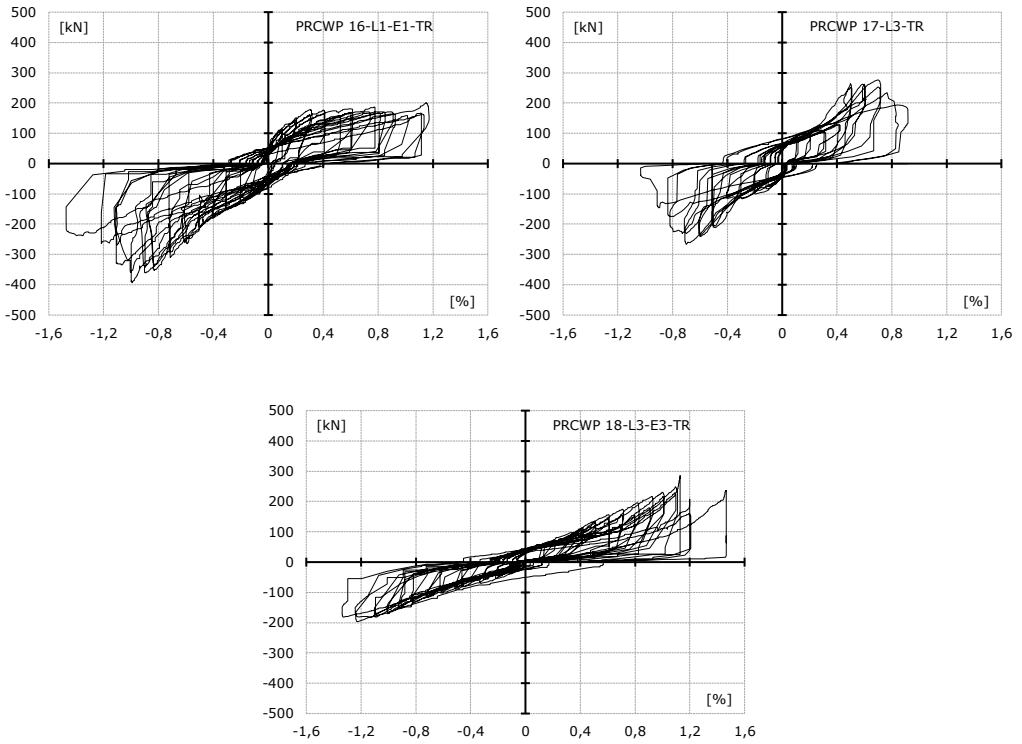

Figure 4-12 – Hysteresis loops for the retrofitted specimens

For the retrofitted specimens, similar conclusions can be drawn, the specimens with large opening to element dimension ratio, had smaller lateral resisting force. The specimens with symmetrical opening and reinforcement in regards to the loading system (PRCWP 13-S-E3-RT, 17-L3-TR, 18 L3-E3-TR) had similar maximum lateral resisting force and drift ration, in both directions, while the ones that were not symmetrical (PRCWP 16-L1-E1-TR, 15-EL2-TR) had different maximum lateral resisting forces and drift ration in positive and negative directions.

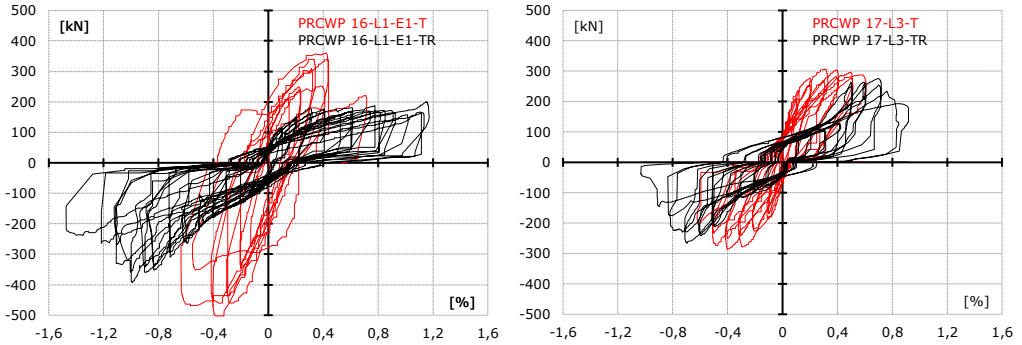

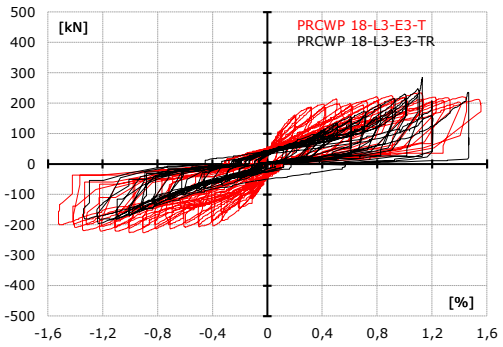

Figure 4-13 – Comparison between hysteresis loops

When comparing the hysteresis loops of the reference specimens and the retrofitted ones presented in Figure 4.13, one can see that the drift ratio was increased for the retrofitted elements and the lateral load resistance was completely restored in case of PRCWP 18-L3-E3, and in case of 17-L3 it was restored to 93% compared to the reference one. In case of 16-L1-E1-TR, the lateral load of the reference specimen was not reached in case of the retrofitted one, this is due to the difference in behaviour caused by the malfunction of the pressure gauge. Hysteresis loops comparison between similar specimens are presented in Appendix A.

4.3.2. Cyclic envelops

The cyclic envelopes can be constructed for any type of cyclic response diagrams. Given the fact that the experimental test presented in this thesis are displacement (drift) controlled, the cyclic envelopes were obtained for the load drift response.

For the construction of the cyclic envelope the peak loading points for each cycle, namely 1 and 3 for the first cycle and 5 and 7 for the second one, were interconnected through the increasing displacement points, thus obtaining one envelope for each cycle, Envelope C1 for the first cycle and envelope C2 for the second one, as shown in Figure 4.14. In order to obtain the average cyclic envelope referred to as Envelope M2, the arrhythmic mean between the peak loading points from C1 and C2 was computed, then by connecting these average loading points the Envelope M2 was constructed, as shown in Figure 4.15.

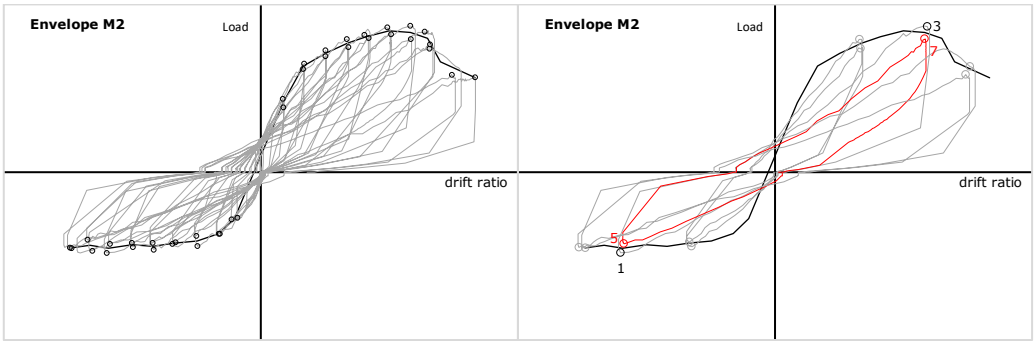

Figure 4-14 – Construction of cyclic envelopes M2

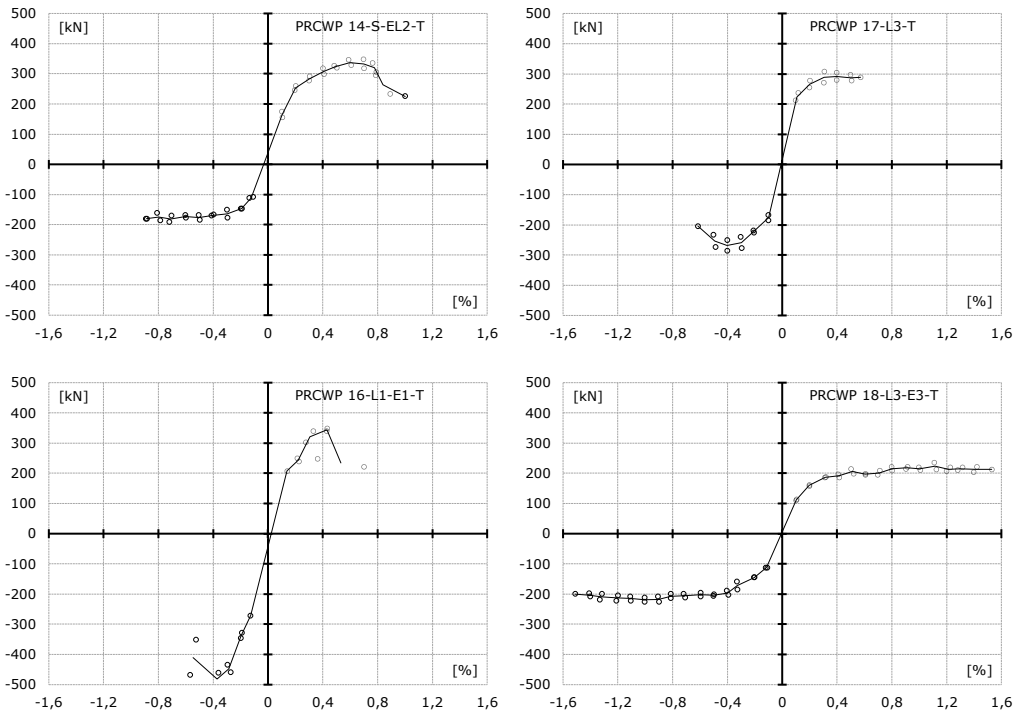

Figure 4-15 – Cyclic envelopes M2 for the reference specimens

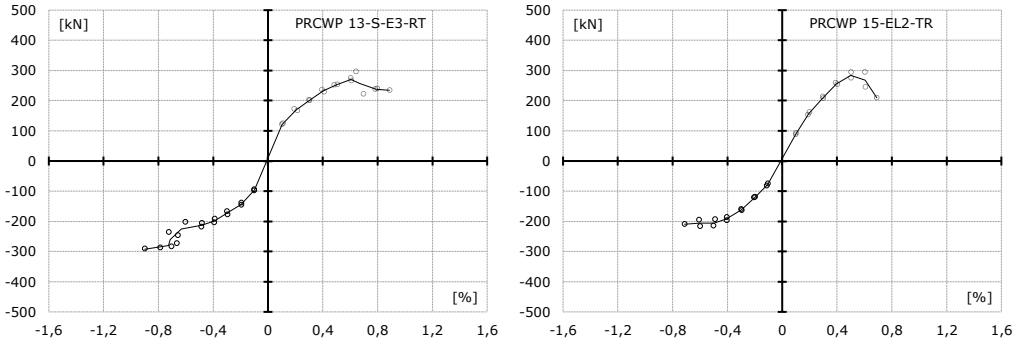

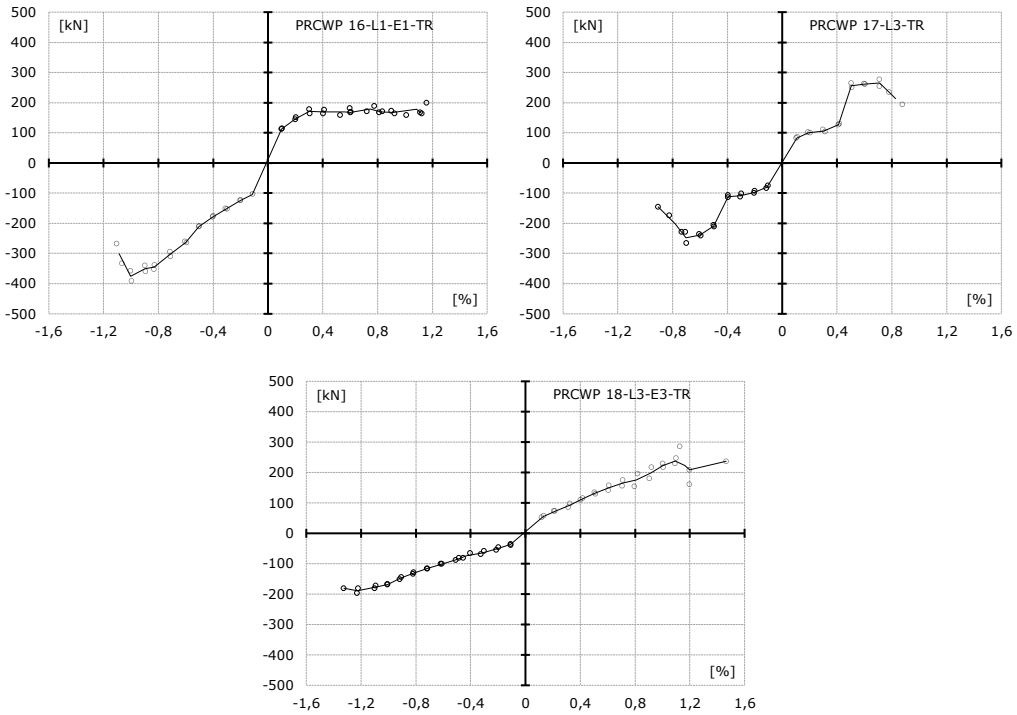

Figure 4-16 – Cyclic envelopes M2 for the strengthen specimens

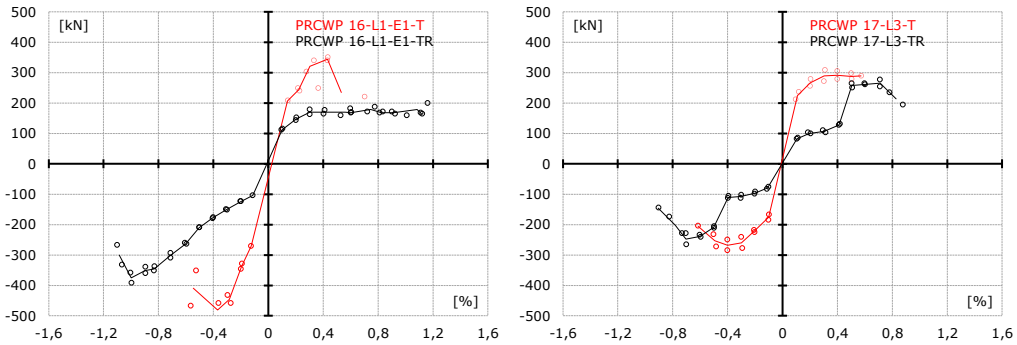

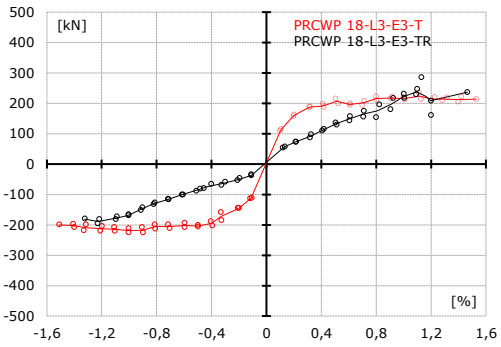

Figure 4-17 – Cyclic envelopes M2 comparison

4.3.3. Monotonic Envelopes

For the construction of the monotonic envelope the arrhythmic mean of the absolute values for the peak loading points at each cycle, namely 1, 3, 5 and 7 was computed, then by connecting these average loading points the Envelope M1 was constructed, as shown in Figure 4.18.

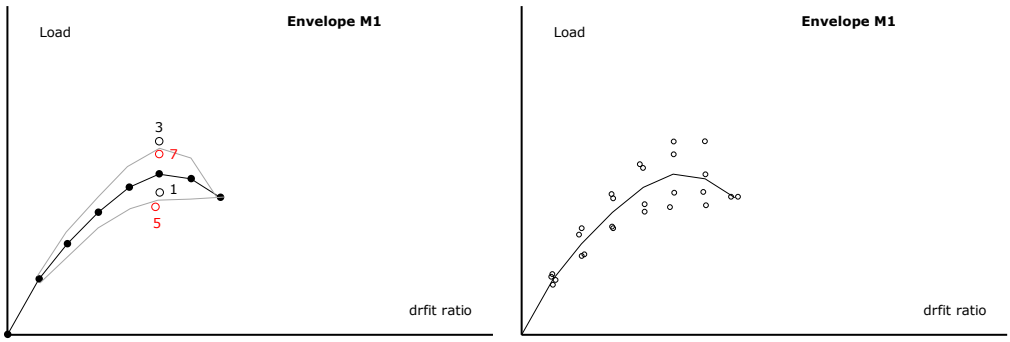

Figure 4-18 – Construction of monotonic envelopes M1

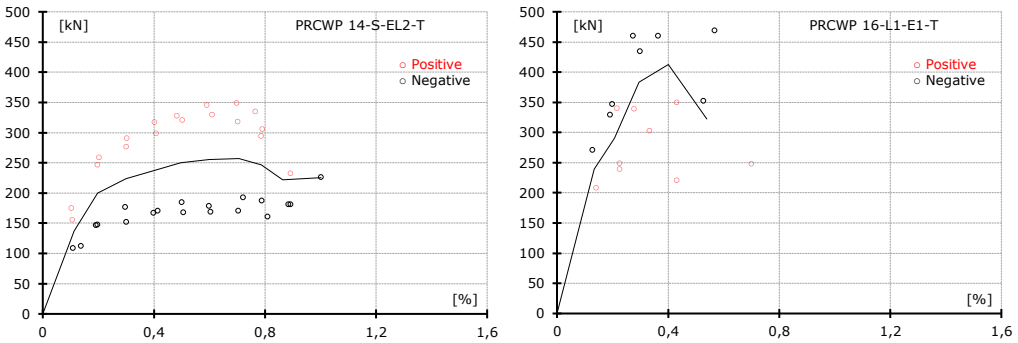

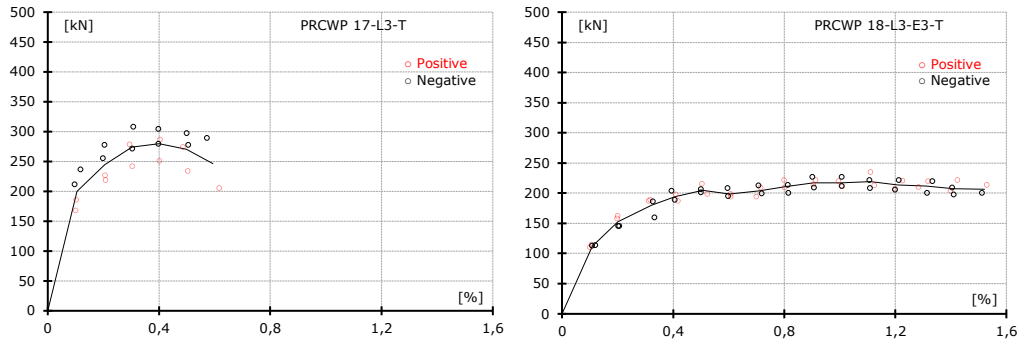

Figure 4-19 – Monotonic envelopes M1 for the reference specimens

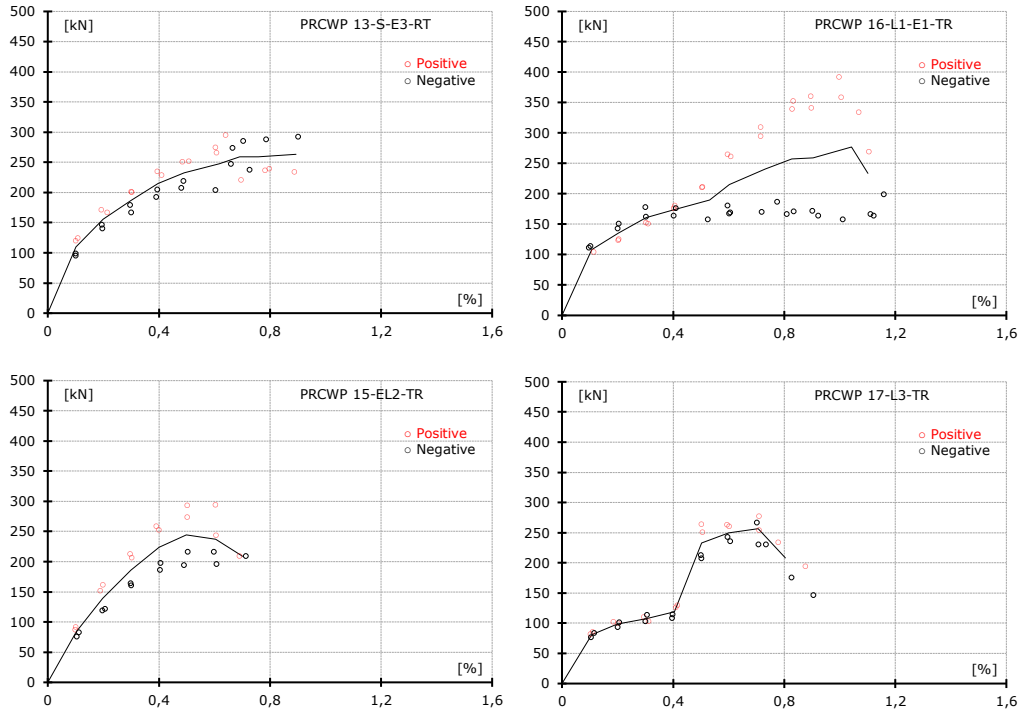

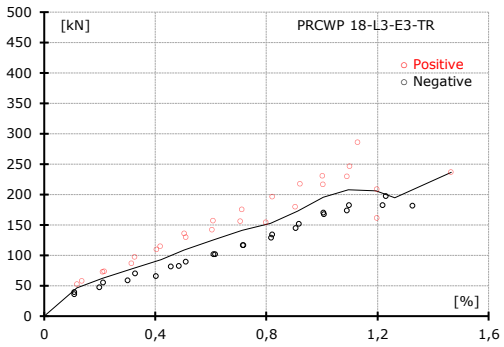

Figure 4-20 – Monotonic envelopes M1 for the strengthen specimens

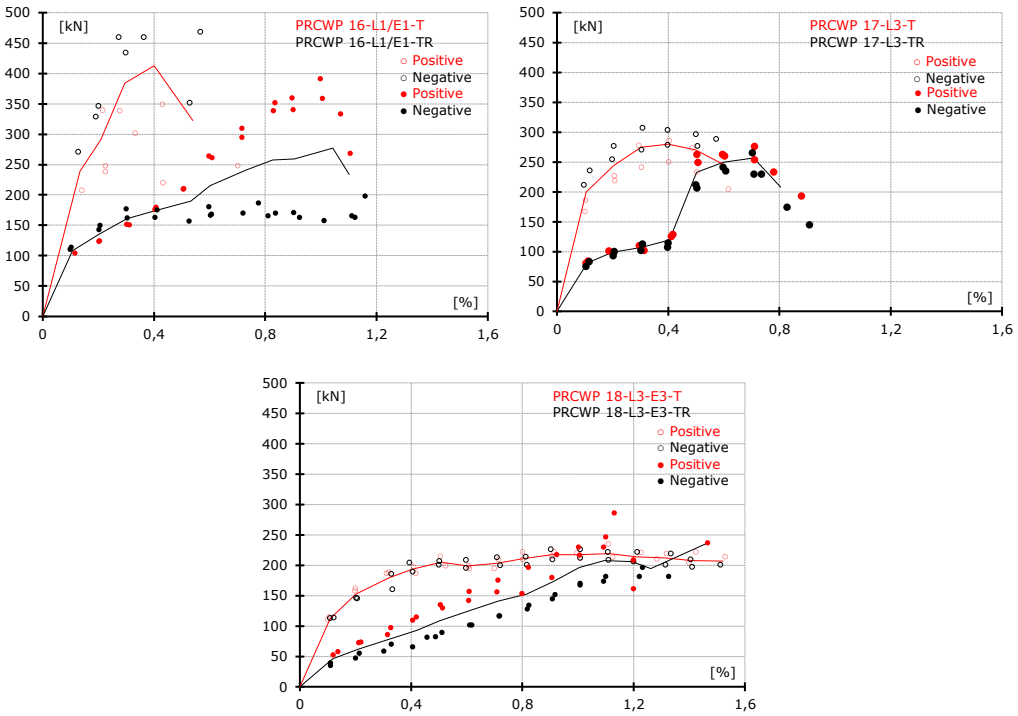

Figure 4-21 – Cyclic envelopes M1 comparison

4.3.4. Backbone envelopes

The author of this thesis adopted the tri-linear backbone envelopes model, due to the fact that it is the closest one to the real response, for each specimen two types of backbones envelopes are presented. Several other different backbone envelopes exist: bi-linear [168, 169] or tetra-linear [170]. The construction of the tri-linear envelope involves the definition of three displacement point.

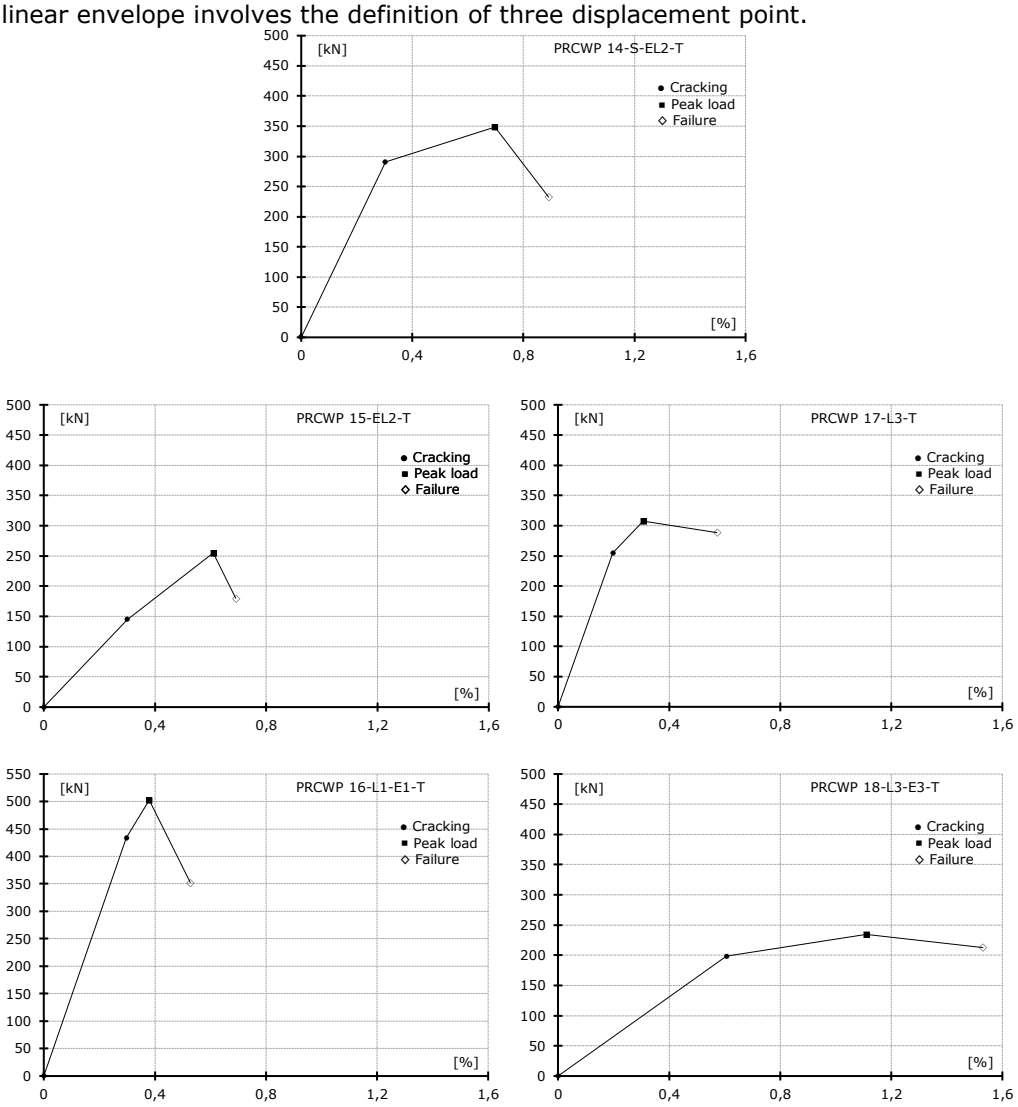

Figure 4-22 – Backbone Envelope (Type 1) for the reference specimens

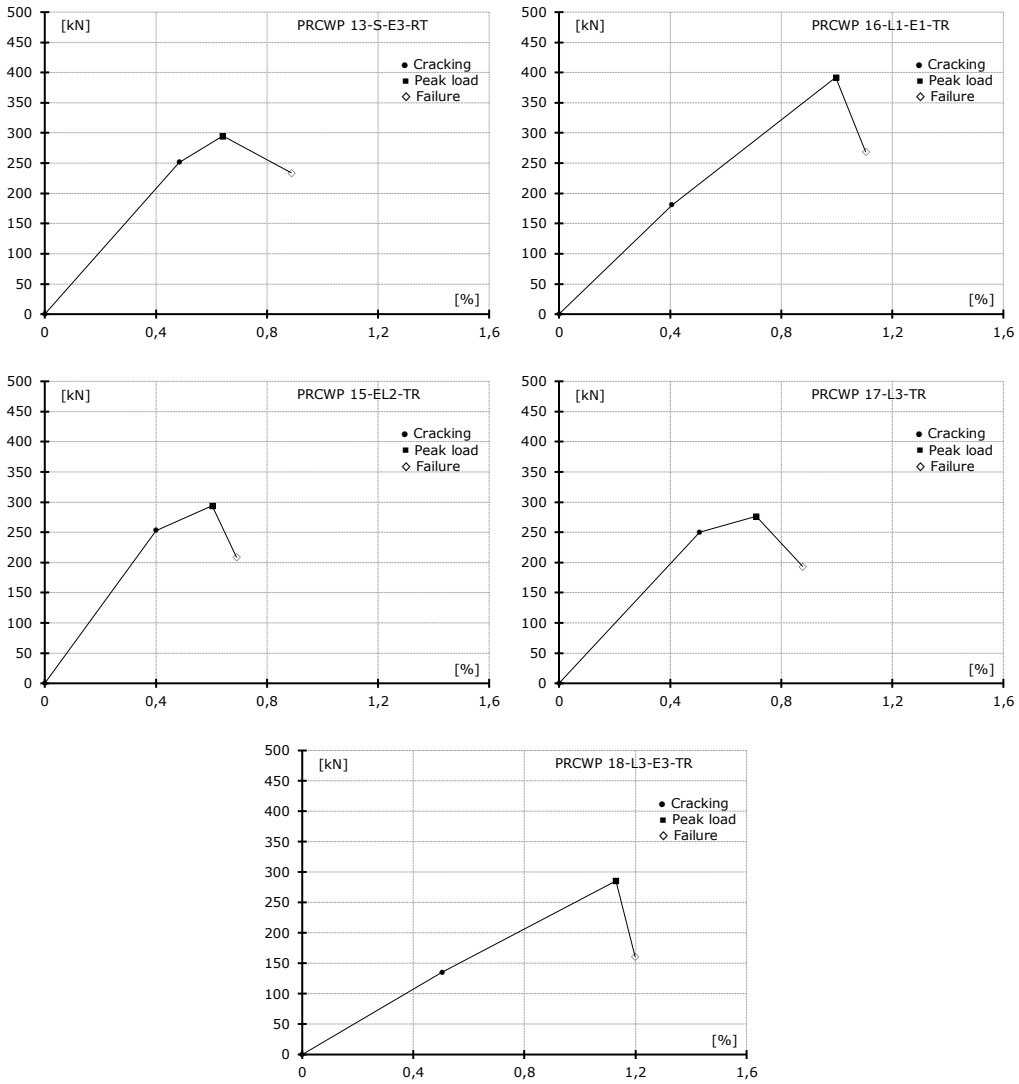

Figure 4-23 – Backbone Envelope (Type 1) for the strengthen specimens

For the first type of backbone envelope presented (Type 1) the three defining points are as follows:
(1) the cracking point - which is the point when the diagonal crack appeared,
(2) the peak loading point – is the point where the lateral force was highest
(3) the failure point – where the specimen lost at least 20% of its load bearing capacity

This method of constructing the backbone envelope has its limitations, due to the fact that the first point is chosen based on the observations made by the authors during the testing. In the case of PRCWP 16 we did not observe a definitive diagonal cracking, however the first point was chosen when significate cracking developed.

For the second type of backbone envelope presented (Type 2) the three defining points are as follows:
(1) the yield point - which is the point when later force is at 0.85 of the peak loading point,
(2) the peak loading point – is the point where the lateral force was highest
(3) the failure point – where the specimen lost at least 20% of its load bearing capacity

In many cases the cracking point is similar to the yield point, making the two envelopes almost identical.

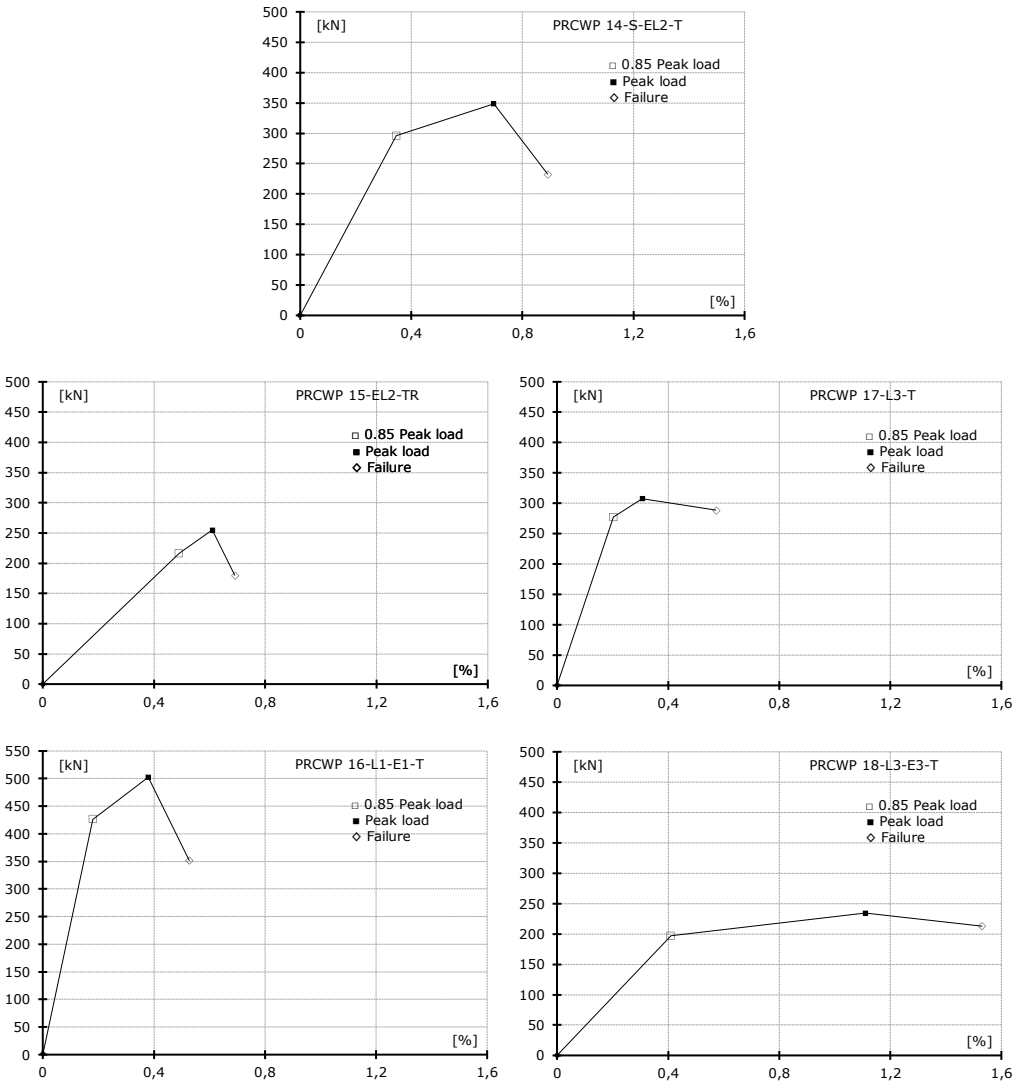

Figure 4-24 – Backbone Envelope (Type 2) for the reference specimens

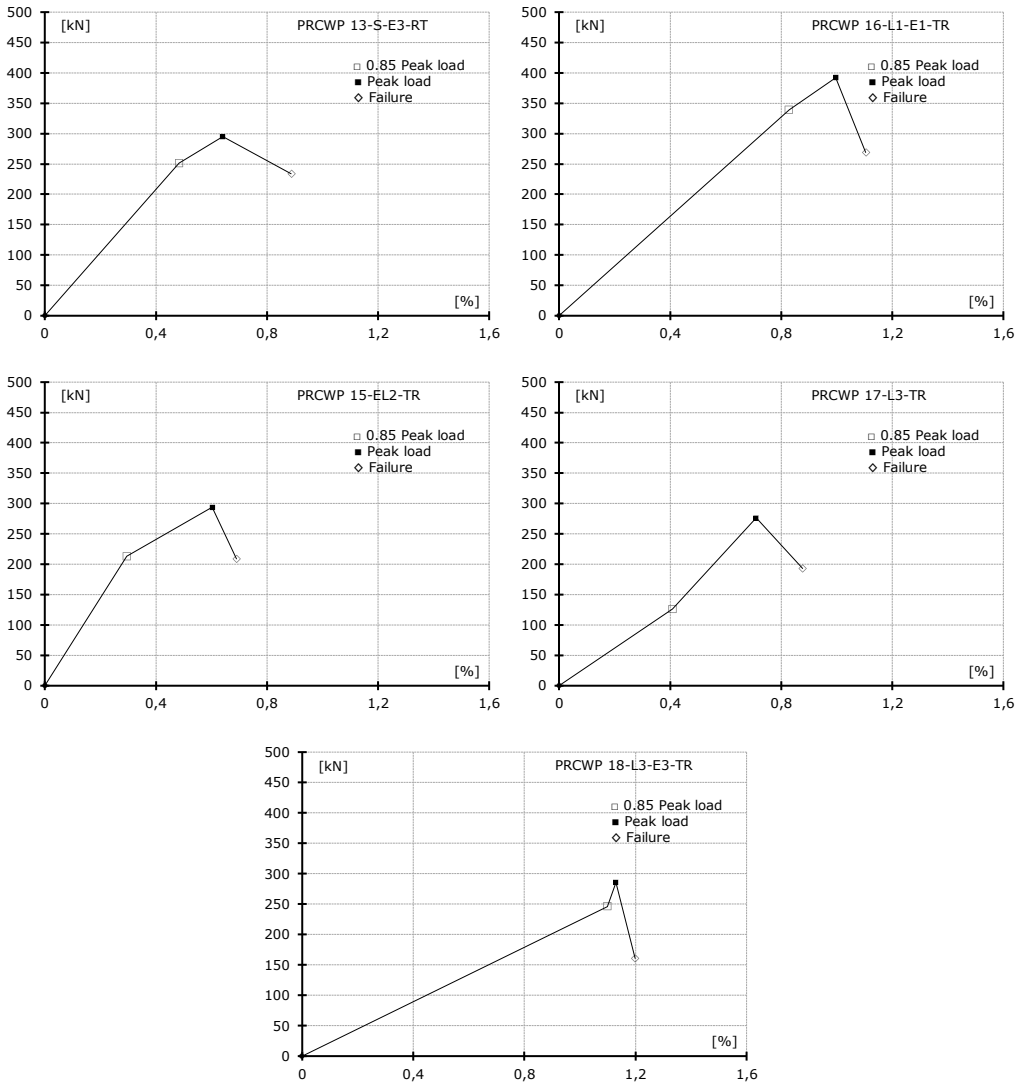

Figure 4-25 – Backbone Envelope (Type 2) for the strengthen specimens

In Figure 4.22 and Figure 4.23 are given the type 1 backbone envelopes for the reference specimens and the strengthen ones, respectively. In Figure 4.24 and 4.25 the type 2 backbone envelopes are presented for the tested specimens. In Figure 4.26 a comparison between references and strengthen specimens backbone envelopes is presented for both types.

In case of the PRCWP 15-EL2 and PRCWP 16-L1-E1 both types of envelopes are similar for the reference and strengthen specimens, although the first point in case of the strengthen element is significantly different.

For the 17-PRCWP-L3 and 18-PRCWP-L3-E3 the two types of backbone envelopes are similar for the reference specimens, but for the strengthen ones they different.

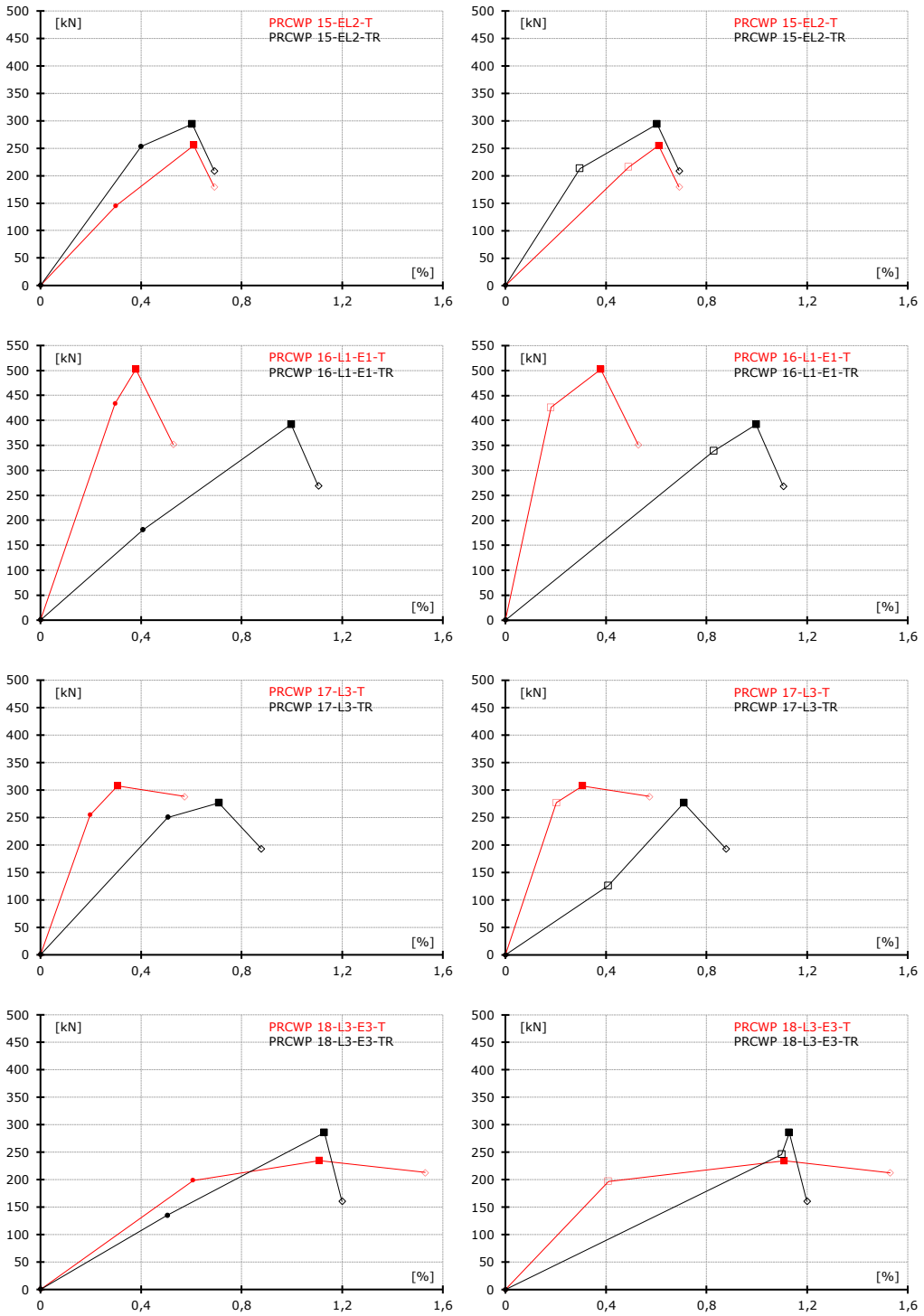

Figure 4-26 – Backbone Envelope comparison: (left) Type 1; (right) Type 2

4.4. Energy dissipation analysis

Of particular significance to the behaviour of precast reinforced large panel buildings is the energy dissipation capacity. In the case of PRCWP, the energy dissipated is calculated by using the area under the force-displacement hysteresis loops as presented in Figure 4.27 and in [171, 172, 59]. In this thesis, the amount of Energy Dissipated is noted with ED and the Cumulative Energy Dissipated is noted with CED. At each cycle, the ED and CED in both positive and negative direction were computed given us the results per half cycle. In order to calculate the Cumulative Energy Dissipated (CED) the following incremental equation for the integration of the load displacement hysteresis loop was used:

$$CED_j = CED_{j-1} + (\delta_j - \delta_{j-1}) \times \left(\frac{V_j}{2} + \frac{V_{j-1}}{2}\right) \tag{4.1}$$

CED is the Cumulative Energy Dissipated
j is a point on the load displacement curve=a data line in the data file
δ_j is the drift level
V_j is the corresponding lateral load value

Two types of representation for the dissipated energy were chosen, as presented in Figure 4.27 and in [Istvan], the Cumulative Energy Dissipated against the drift ratio and Cumulative energy dissipated against the Cumulative Drift ratio (CR). For the computation of the Cumulative Drift (CD) an incrementally equation was used:

$$CD_j = CD_{j-1} + \left|(\delta_j - \delta_{j-1})\right| \tag{4.2}$$

CD is the Cumulative Drift
j is a point on the load displacement curve=a data line in the data file
δ_j is the drift level

$$CR_j = \left(\frac{CD_j}{2150}\right) \times 100 \tag{4.3}$$

CR is the Cumulative Drift ratio
CD is the Cumulative Drift
j is a point on the load displacement curve=a data line in the data file
2150 distance between top and bottom displacement transducers

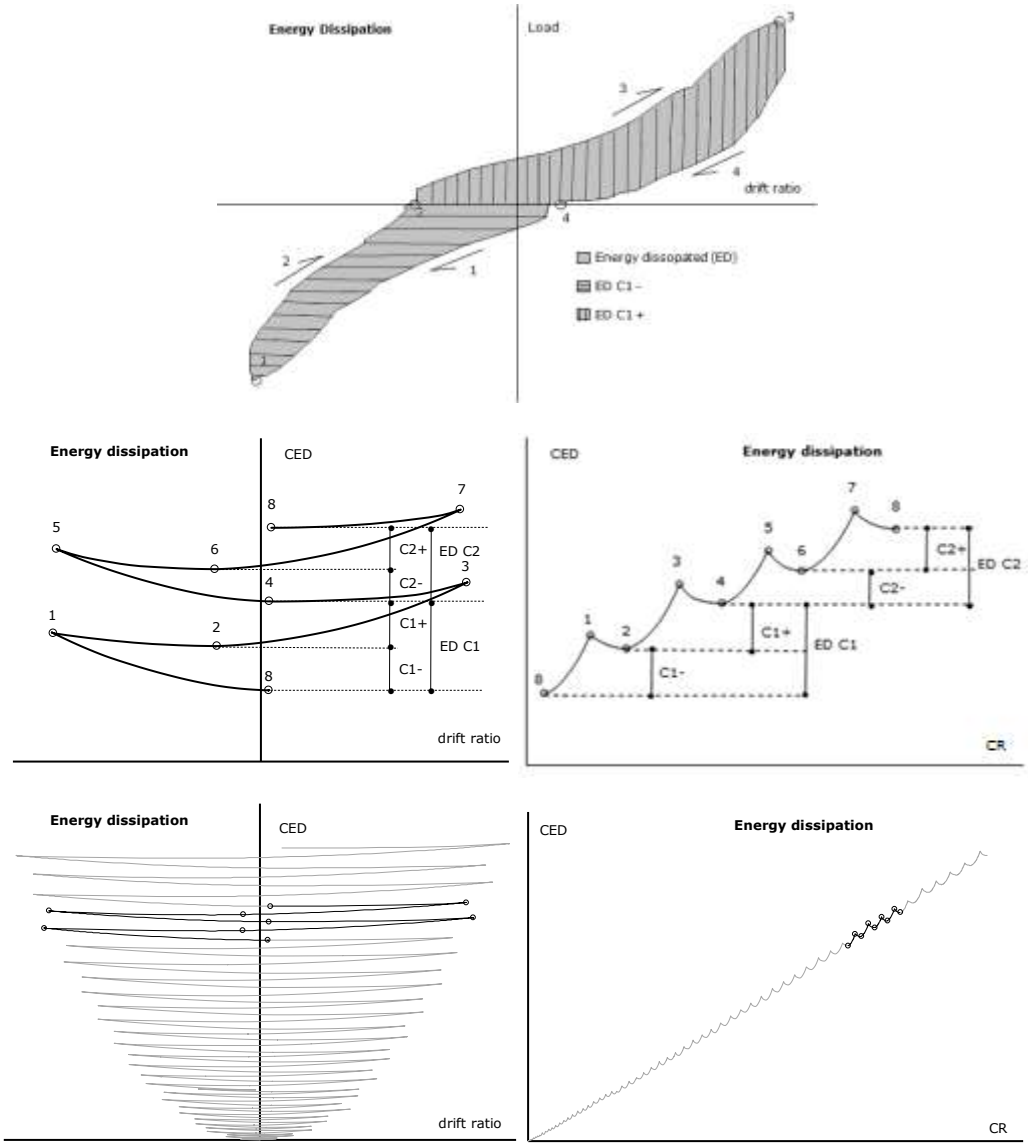

Figure 4-27 – Construction of energy dissipation curves

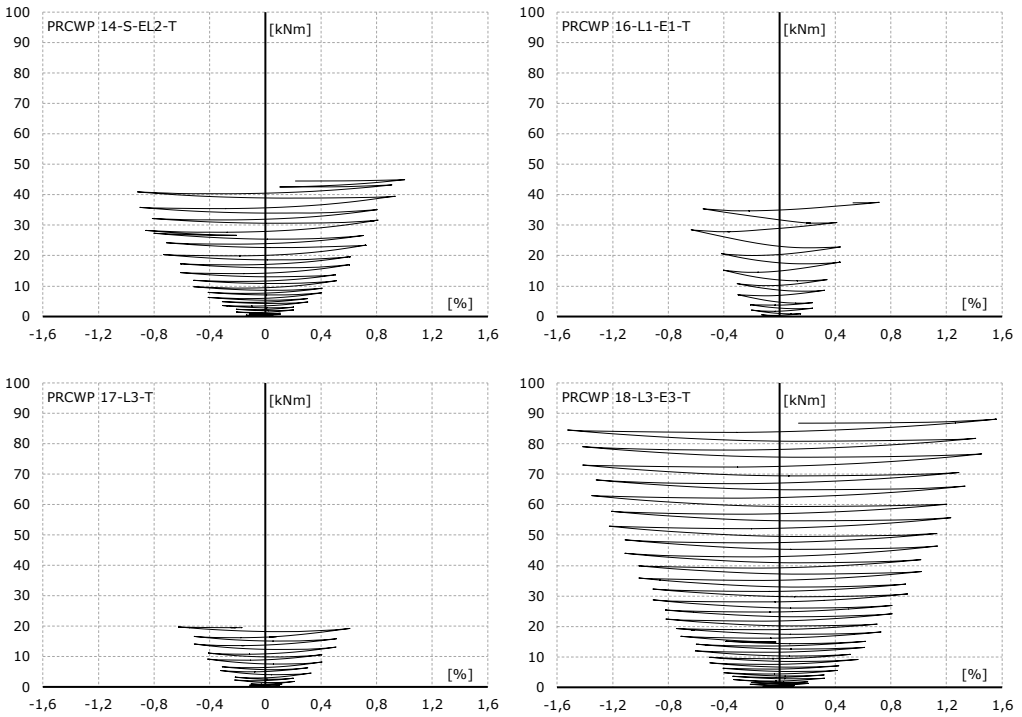

Figure 4-28 – Cumulative energy dissipated vs drift ratio for the reference specimens

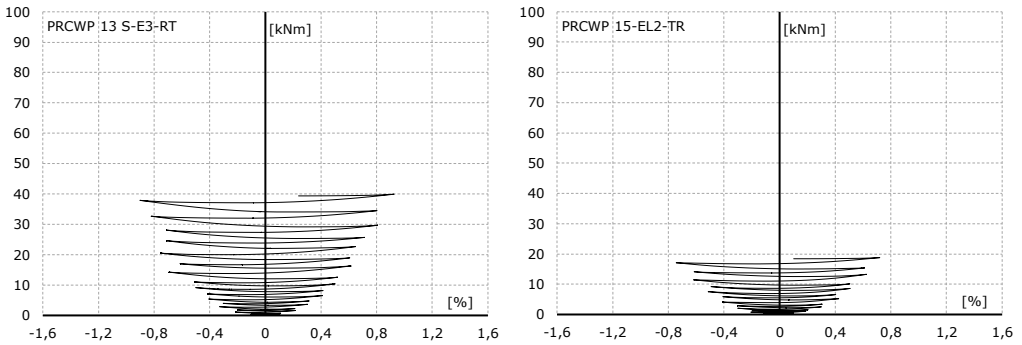

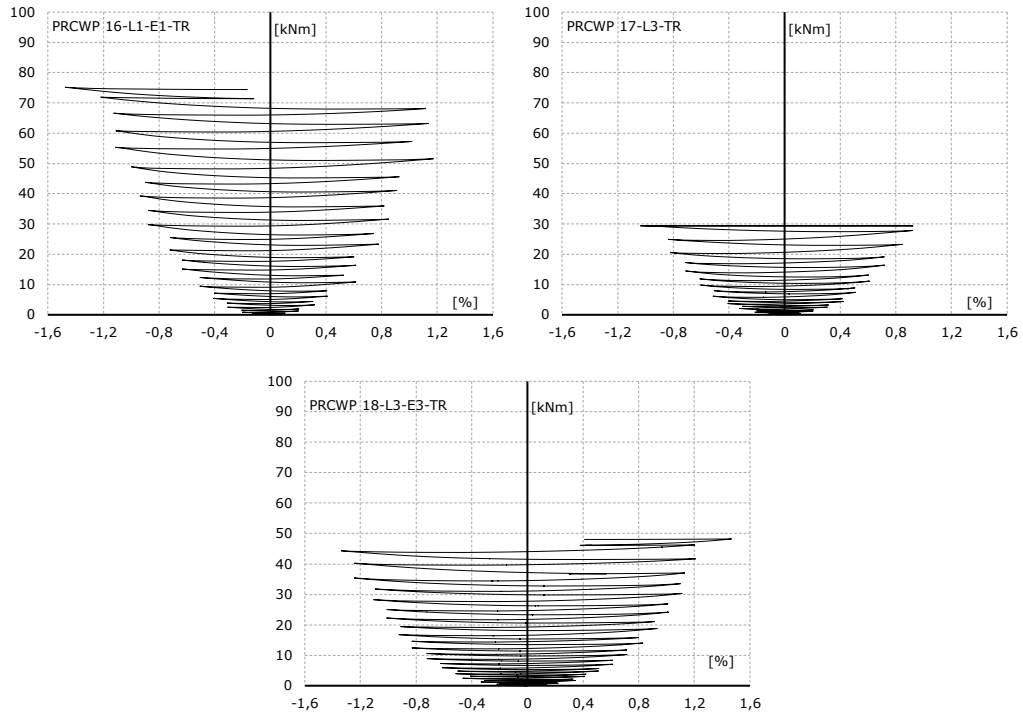

Figure 4-29 – Cumulative energy dissipated vs drift ratio for the strengthen specimens

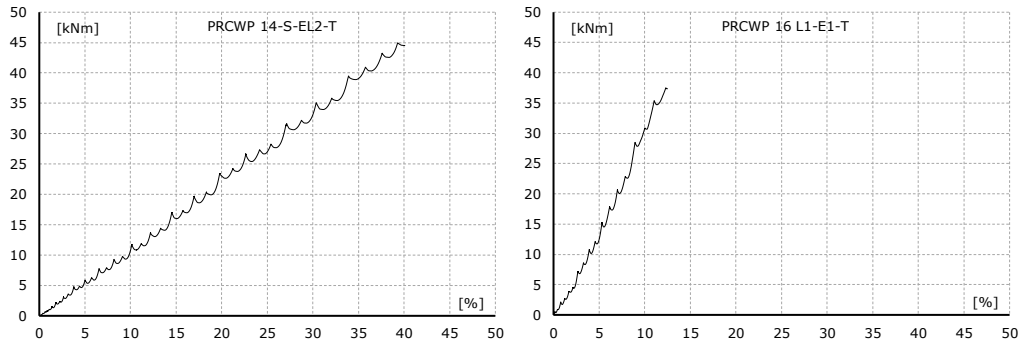

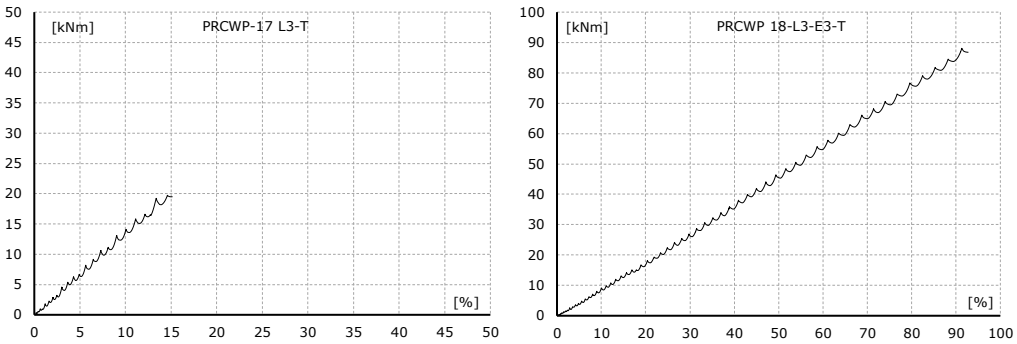

Figure 4-30 – Cumulative energy dissipated vs cumulative drift for the reference specimens

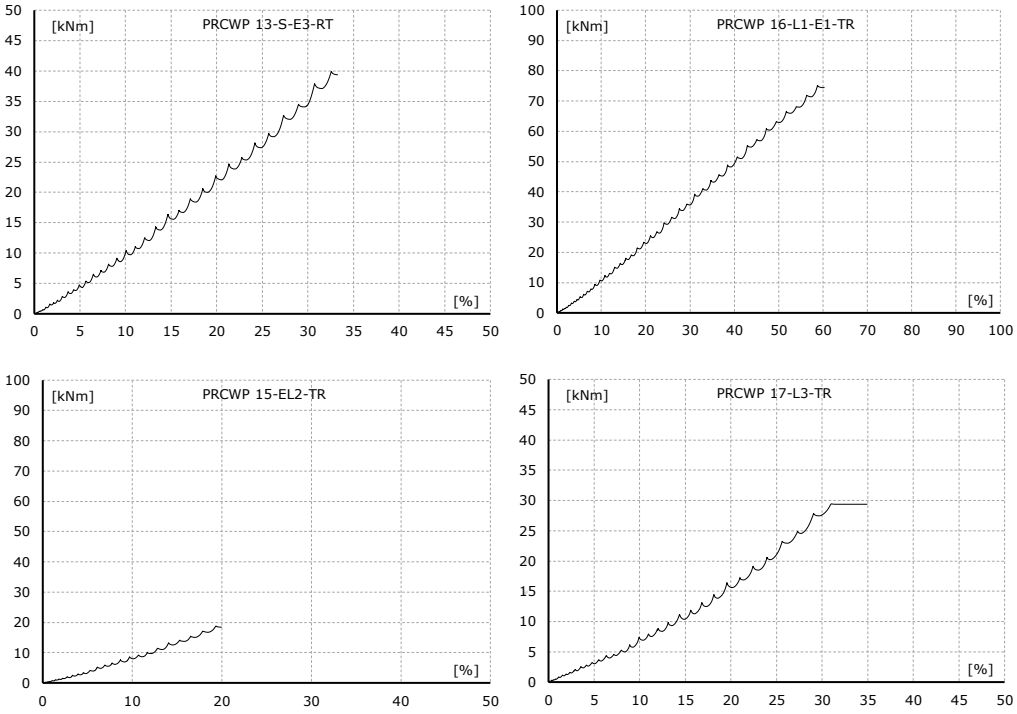

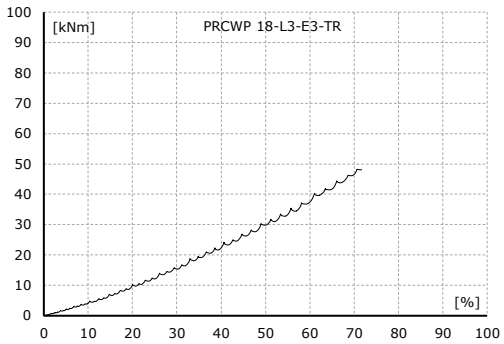

Figure 4-31 – Cumulative energy dissipated vs cumulative drift for the reference specimens

In Figure 4.28 the Cumulative Energy Dissipation vs the drift ratio for the reference specimens is presented, while in Figure 4.29 is presented the Cumulative Energy Dissipations vs drift ratio for the strengthen ones. Figure 4.30 depicts the Cumulative Energy Dissipations vs the Cumulative Drift for the reference specimens and Figure 4.31 depicts the Cumulative Energy Dissipations vs the Cumulative Drift for the strengthen ones.

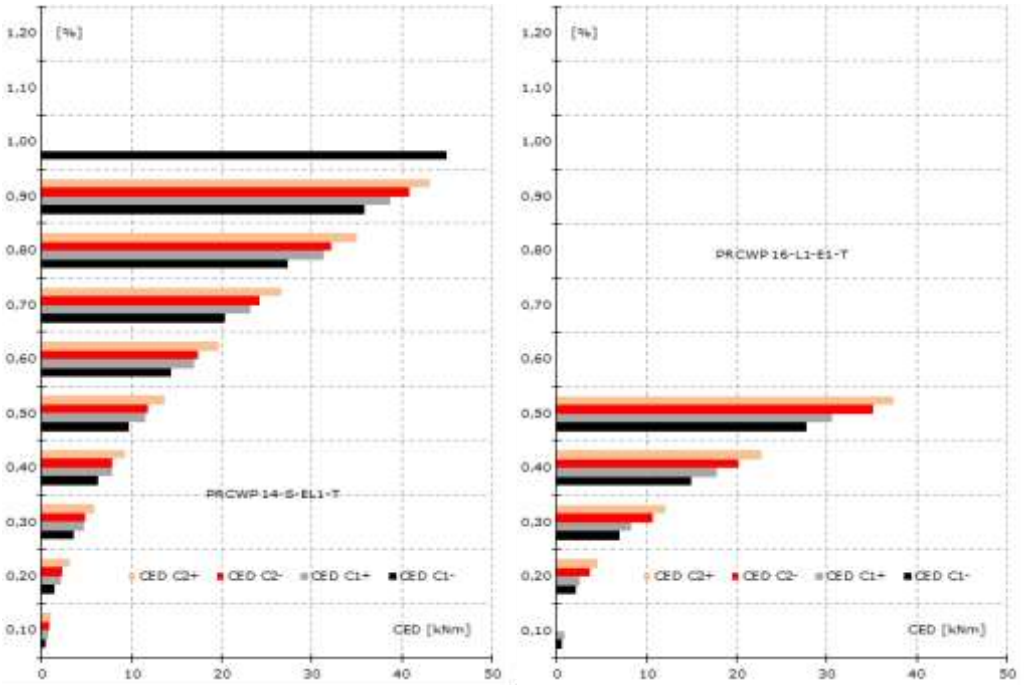

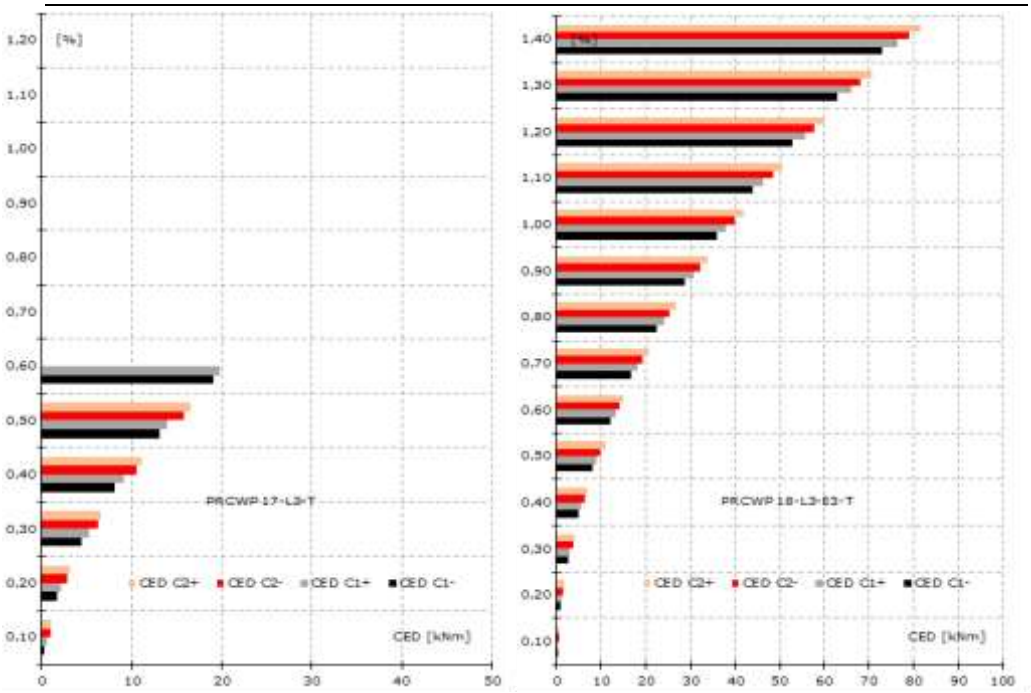

Figure 4-32 – Cumulative energy dissipated per half cycle for the reference specimens

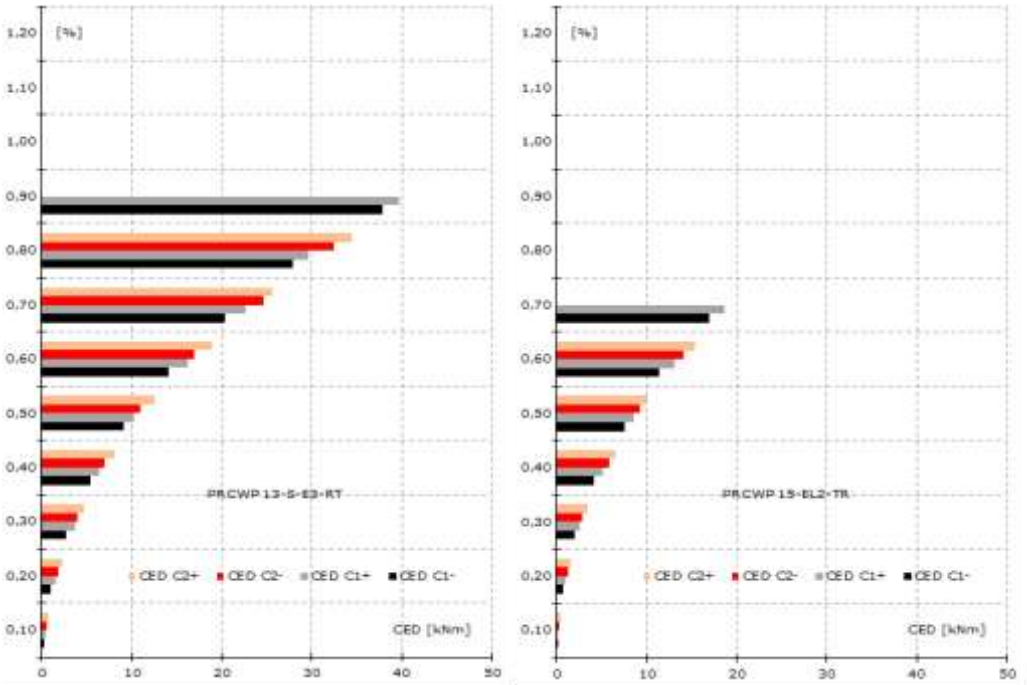

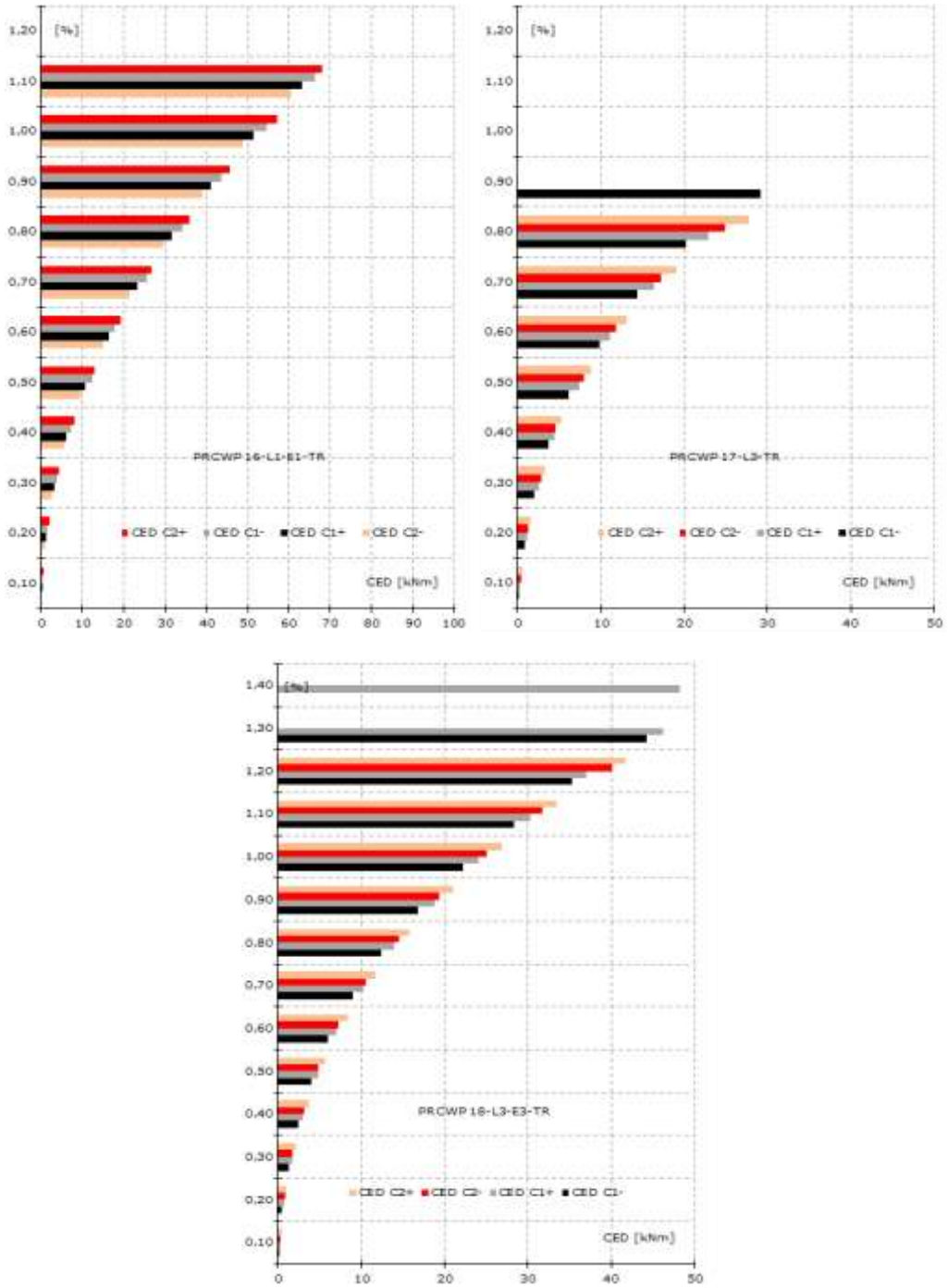

Figure 4-33 – Cumulative energy dissipated per half cycle for the strengthen specimens

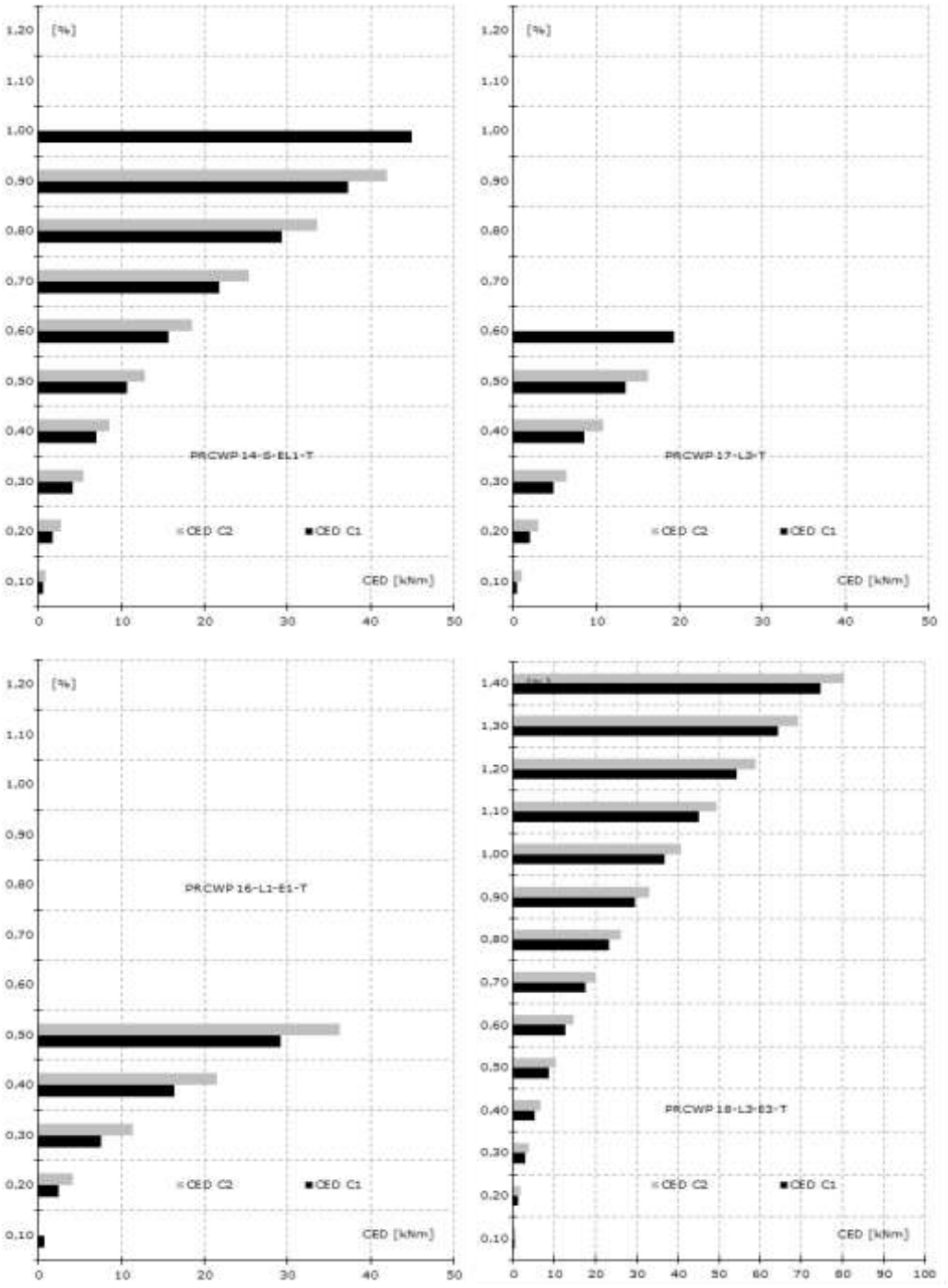

Figure 4-34 – Cumulative energy dissipated per cycle for the reference specimens

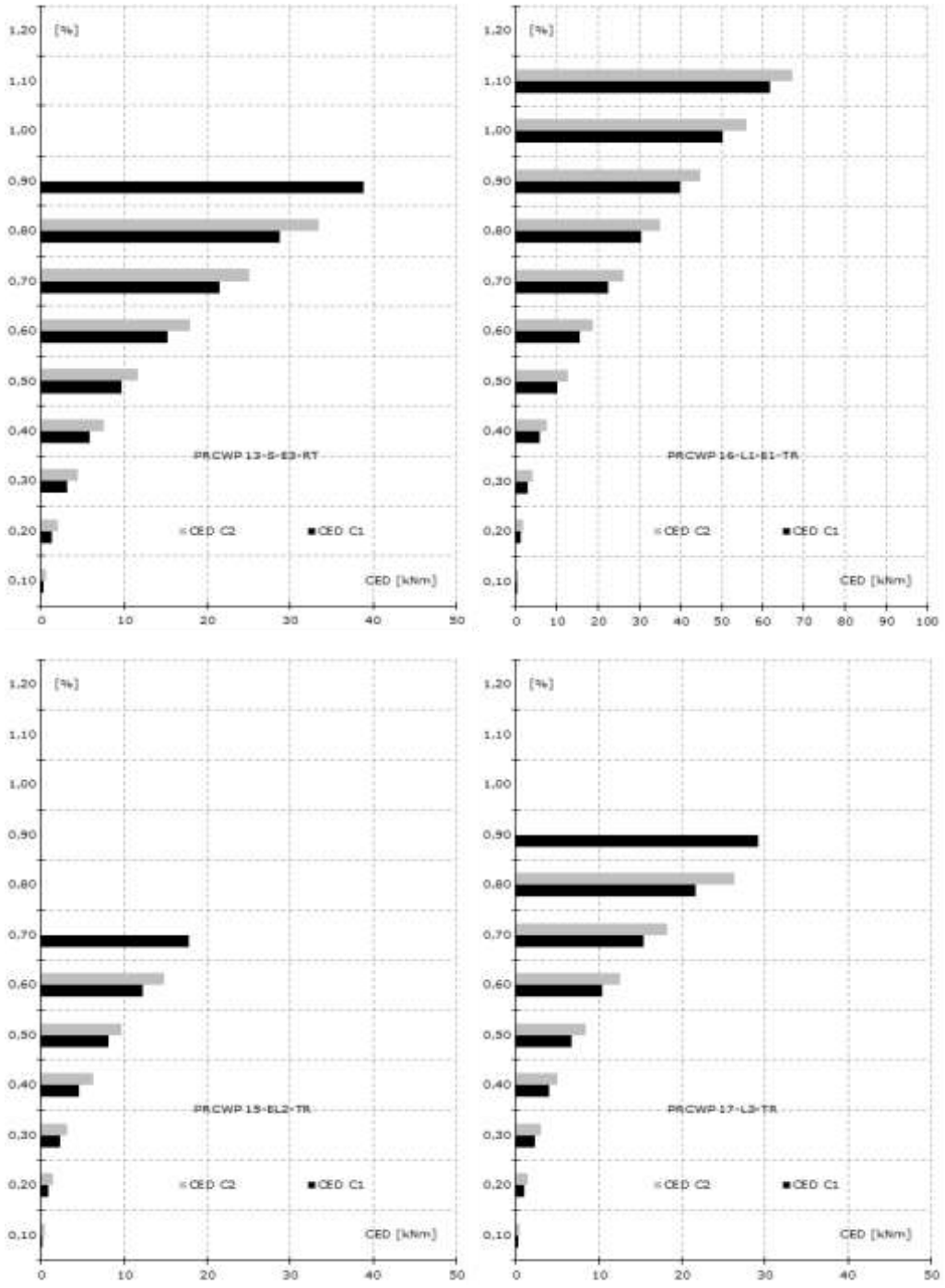
[%]
PRCWP13-S-E3-RT
CED C2
CED C1
CED [kNm]
PRCWP16-L1-E1-TR
PRCWP15-EL2-TR
PRCWP17-L3-TR

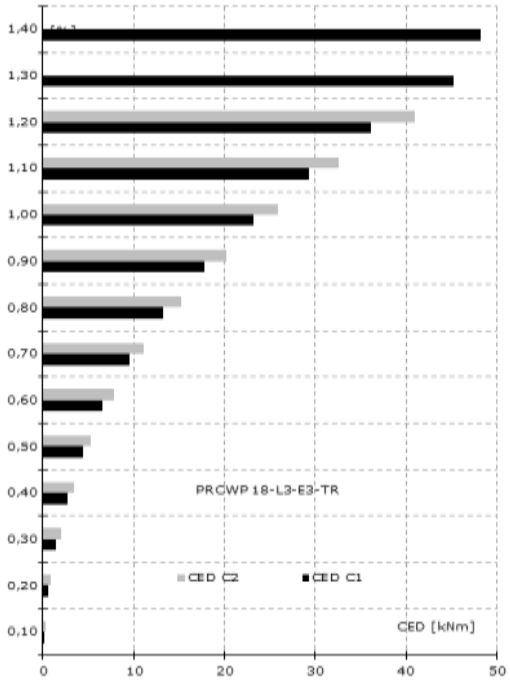

Figure 4-35 – Cumulative energy dissipated per cycle for the strengthen specimens

In Figure 4.32 and Figure 4.34 are presented the Cumulative Energy Dissipation CED at each drift level for the reference elements per each half cycle and complete cycle, respectively. For the strengthen elements the Cumulative Energy Dissipation for each drift level per half cycle and complete cycle are depicted in Figure 4.33 and 4.35, respectively.

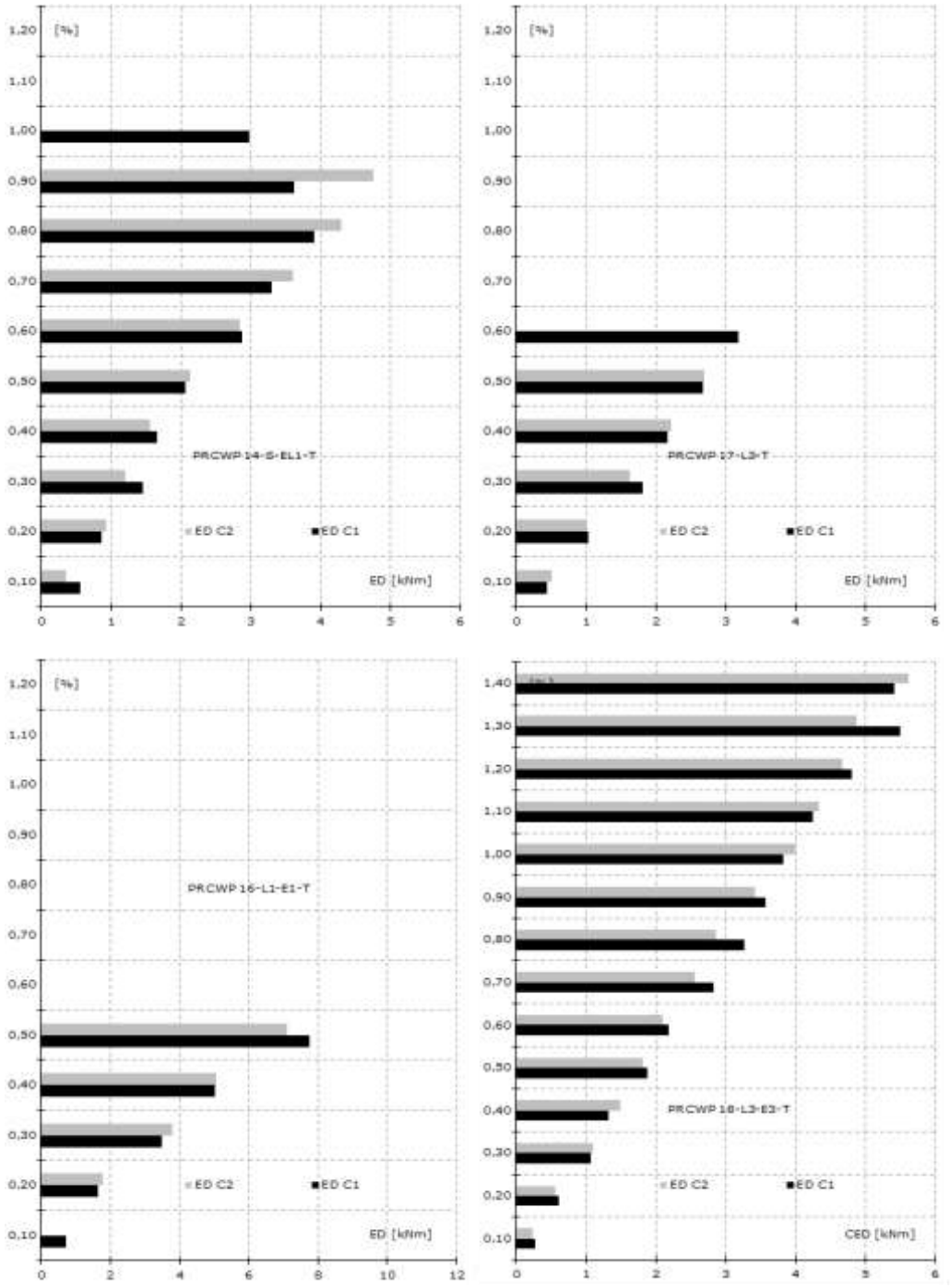

Figure 4-36 – Energy dissipated per cycle for the reference specimens

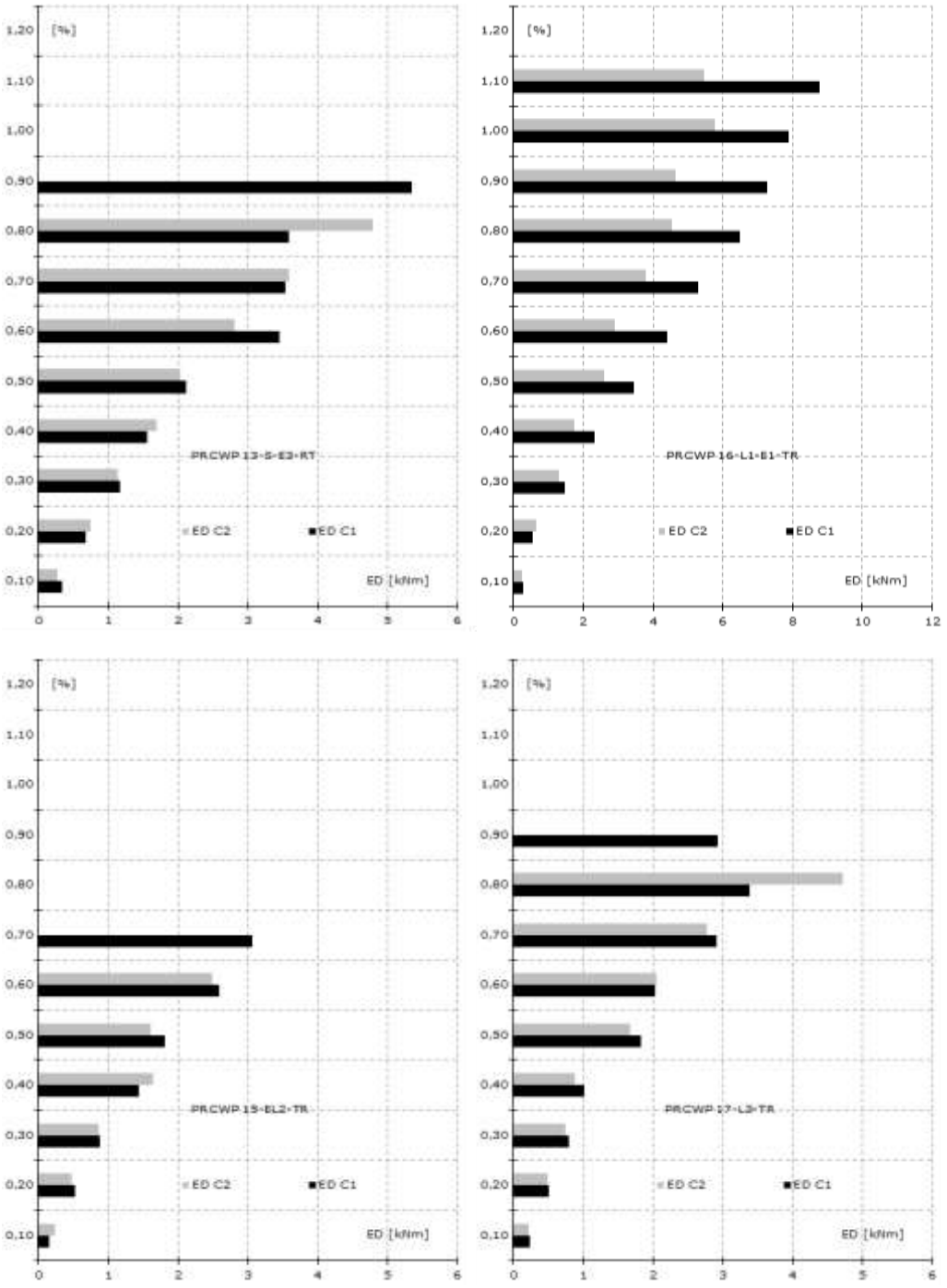
[%]
PRCWP 13-S-E3-RT
ED C2
ED C1
ED [kNm]
[%]
PRCWP 16-L1-E1-TR
ED C2
ED C1
ED [kNm]
[%]
PRCWP 15-EL2-TR
ED C2
ED C1
ED [kNm]
[%]
PRCWP 17-L3-TR
ED C2
ED C1
ED [kNm]

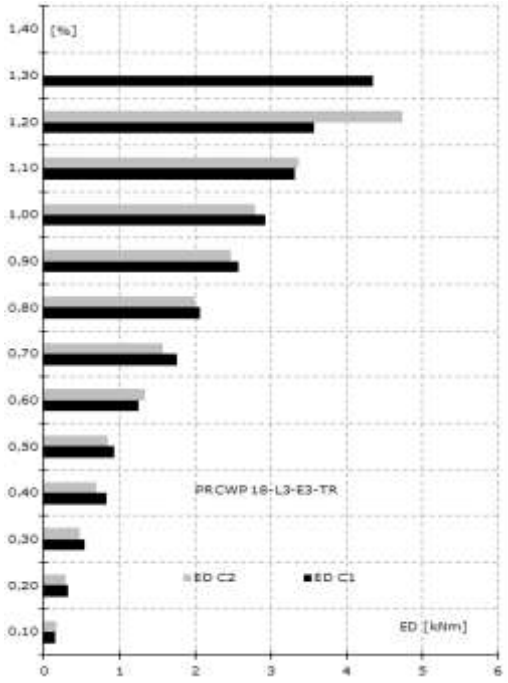

Figure 4-37 – Energy dissipated per cycle for the reference specimens

The Energy Dissipated by the elements for each drift ratio for both the reference and strengthen elements are presented in Figure 4.36 and 4.37. In all cases the elements dissipated more energy in the first cycle than in the second one as reported by [50].

The retrofitted specimens dissipated more energy compare to the reference ones, except PRCWP 18-L3-E3, which had a more simplistic retrofitting procedure which was designed to just restore its maxim load bearing capacity (refer to Chapter 3.4). The Cumulative Energy Dissipated by the reference specimens ranges between 19,37÷86,20, while the retrofitted ones had the range vary between 17,80÷67,3. The high value for CED in case of the reference specimens was obtained by the PRCWP 18-L3-E3-T due to the fact that its failure was more ductile that all the others specimens.

4.5. Strength and ductility analysis

In Figure 4.38 the shear strength of the reference specimens is presented both as absolute value and normalized to the highest recorded value. The shear strength ranges between 234,5 kN and 502,5 kN. For the unstrengthen specimens the highest recorded value was obtained by 16-L1-E1, which had the smallest opening. Following this observation, it can be seen that the strength of the specimens decreases as the opening size increases. Given the fact that the specimens had slightly different classes of concrete, it seems that the presence of the parapet is not so influent in the maximum shear resistance of the walls.

For the strengthen specimens the strength is presented in Figure 4.39 where it can be seen that the strength ranged from 276,5 kN to 392 kN with the maximum shear being obtained by the 16-L1-E1 TR the same specimen as in the unstrengthen tests. These results show that all specimens with similar openings had similar strength. In Figure 4.40 all the strength for all specimens is presented both as absolute value and as normalized one compared to the maximum strength obtained.

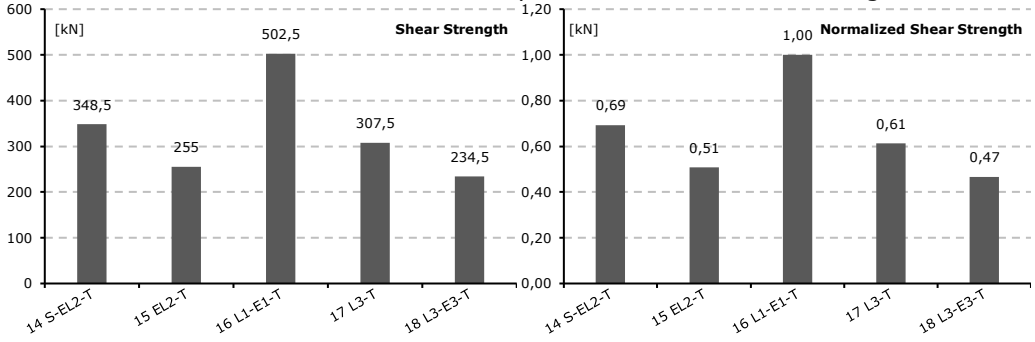

Figure 4-38 – The shear strength for the reference specimens

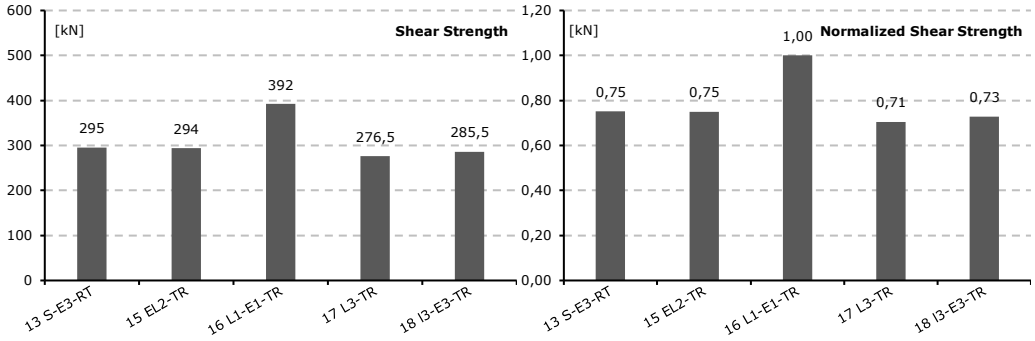

Figure 4-39 – The shear strength for the strengthen specimens

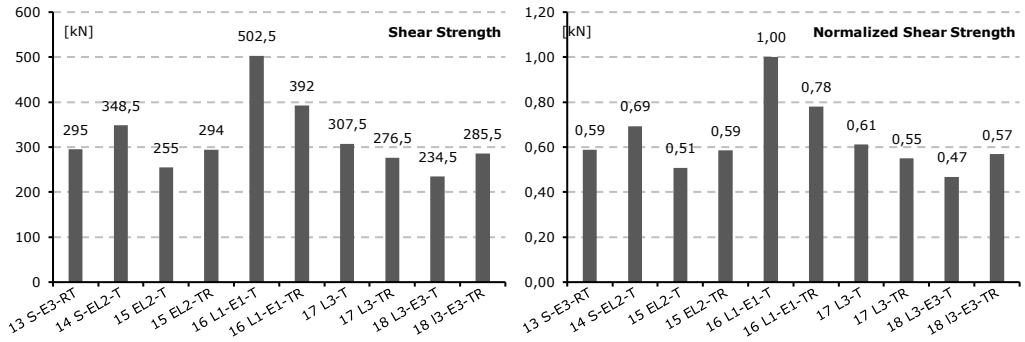

Figure 4-40 – The shear strength for the tested specimens

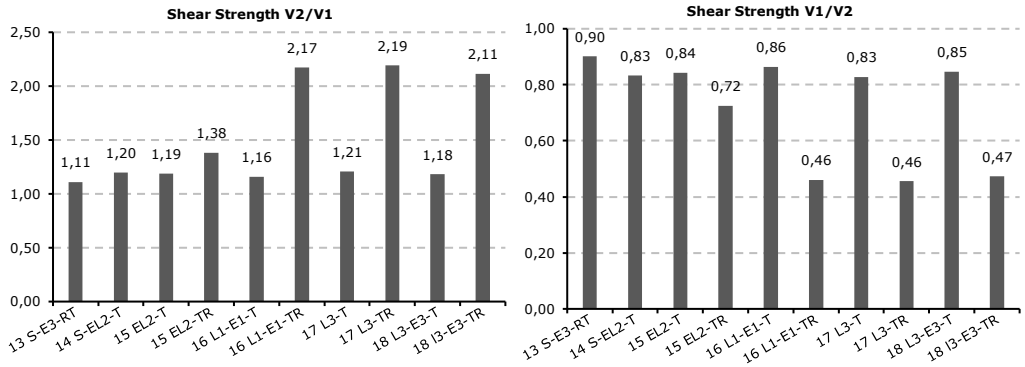

Figure 4-41 – Shear strength ratios

Additionally, to the shear strength (V2), the type 1 backbone envelope presents also the cracking point (V1). The ratio between the two strengths is an important response characteristic and can be given either as cracking-to-shear strength (V1/V2) or shear-to-cracking strength (V2/V1) also known as load sustainability ratio (overstrength). In Figure 4.41 is presented the both ratios and can be seen that the retrofitted specimens presented higher load sustainability (or inversely the lowest cracking point strength ratio) compared to the reference ones.

When calculating ductility ratios, the definition of the yield deformation (displacement, rotation and curvature) often causes difficulty since the strength-deformation relation may not have a well-defined yield point. Different investigators used different definitions, according to Priestley [173] it is defined as the intersection of the initial tangent stiffness with the nominal strength, the intersection of the secant stiffness through first yield with nominal strength, and the displacement at first yield, while Park [174] said it is the yield displacement of the equivalent elastic-perfectly plastic system with reduced stiffness found as secant stiffness at 75% of the peak lateral load of the actual system. In this thesis, the μ0.85 method was used as in [50] which states that the ductility ($\mu=\Delta u/\Delta y$) is the ratio between the ultimate displacement (Δu), corresponding to the loss of 20% of the lateral force resistance of the specimen, and the displacement corresponding to 85% of the maxim lateral load on the ascending curve. In Figure 4.42 the ductility for all specimens is presented, it

can be seen that the ductility ranges from 1.41 to 2.60 for the unstrengthen specimens, Carrillo [175] obtained for walls with shear reinforcement made of deformed bars, the ductility coefficient between 1.63 and 2.92 while Todut [50] obtained for similar walls between 1.45 and 1.87. For the strengthen elements the ductility was lower in almost all cases.

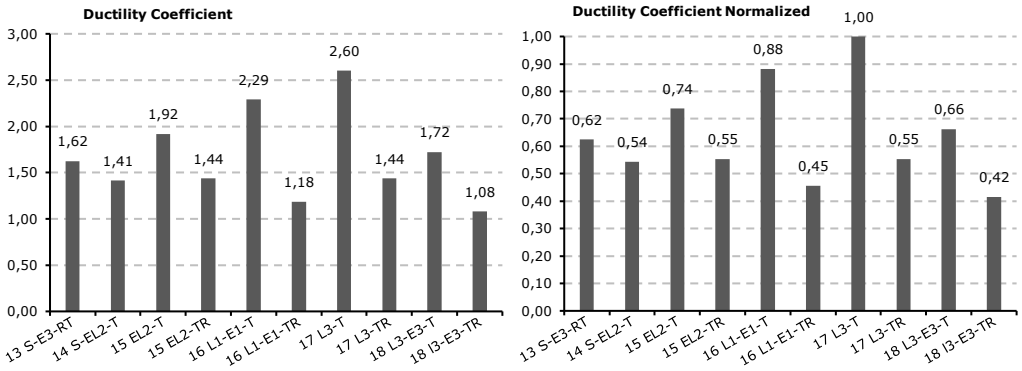

Figure 4-42 – Ductility Coefficient

4.6. Displacement analysis

The main characteristics of the seismic response are defined on the backbone curves as the cracking point, the yield point, the peak loading point and the failure point. As the cracking point is assigned by the author own judgement it seemed unprofessional to use it in the displacement analysis. For the peak loading point a detailed analysis is made in chapter 4.5 where the ductility is analysed. The failure point is presented in figure 4.43 for the reference specimens and in Figure 4.44 for the strengthen ones. From Figure 4.45, where all specimen's failure displacement is presented both as absolute value and as normalized one, one can observe that the strengthen specimens had a much larger ultimate drift point compared to their reference counterparts.

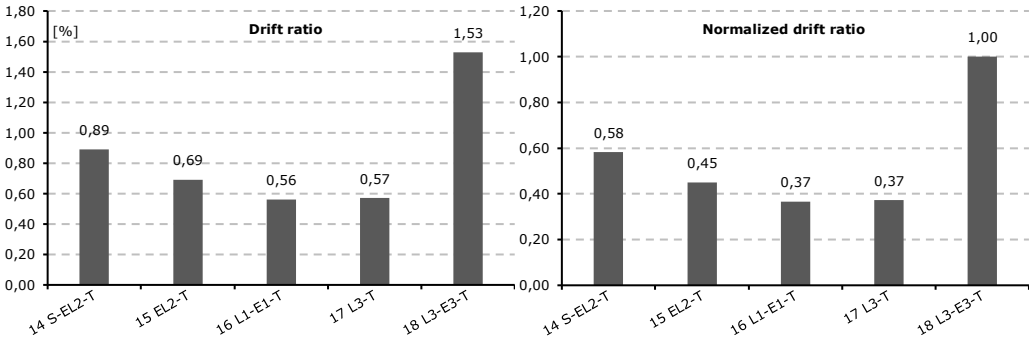

Figure 4-43 –Drift ratio for the reference specimens

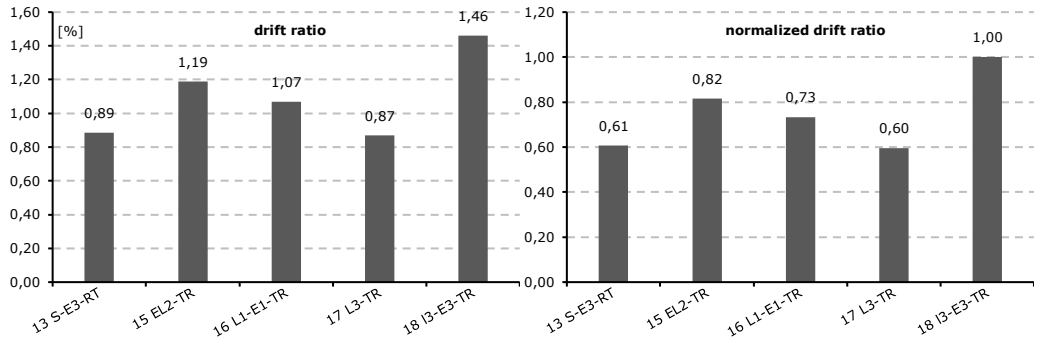

Figure 4-44 – Drift ratio for the strengthen specimens

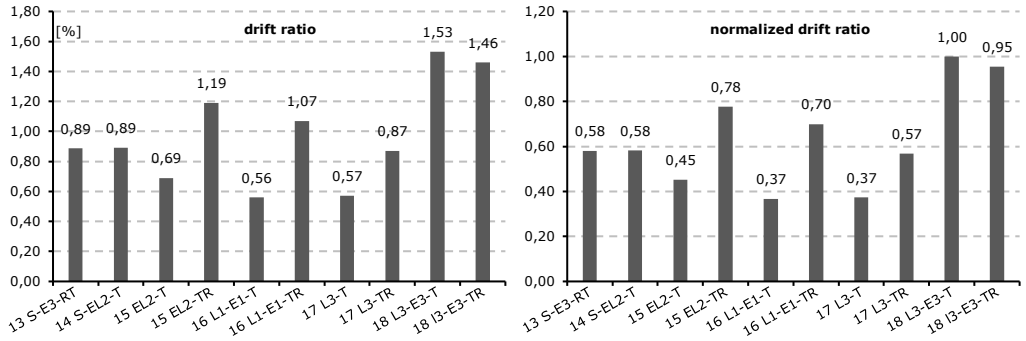

Figure 4-45 – Drift ratio for all tested specimens

4.7. Stiffness analysis

The stiffness of a structural member is defined as its rigidity and is the ratio between the applied load and the resulting deflection. In order to plot the stiffness degradation, the monotonic envelope M1 was used, on the envelope the secant stiffness is the slope of a line connecting the origin point to a point on the curve as defined in [49]. The first point on the graph corresponds to 2,15 mm (0,1%) drift ratio and is called the initial stiffness. In Figure 4.46 the stiffness degradation is plotted for the reference specimens while Figure 4.47 depicts the stiffness degradation for the strengthen ones and in Figure 4.48 presents the comparison between stiffness degradation for all specimens. It can be seen that in all cases the stiffness degradation in case of the reference specimens was higher. In Figure 4.49 the initial stiffness is presented corresponding to 2,15 mm (0,1%) drift ratio, and one can conclude that the retrofitting strategy adopted in this thesis does not restore the initial stiffness of the specimen. However, comparing specimen 13-S-E3-RT and 18-L3-E3-TR it can be seen that the first specimen has more than double the initial stiffness of the latter one, this can be attributed to the difference in the retrofitting strategy, concrete class and shear reinforcement quantity. Analysing the results, it can be observed that the initial stiffness decreases with the increase of the opening.

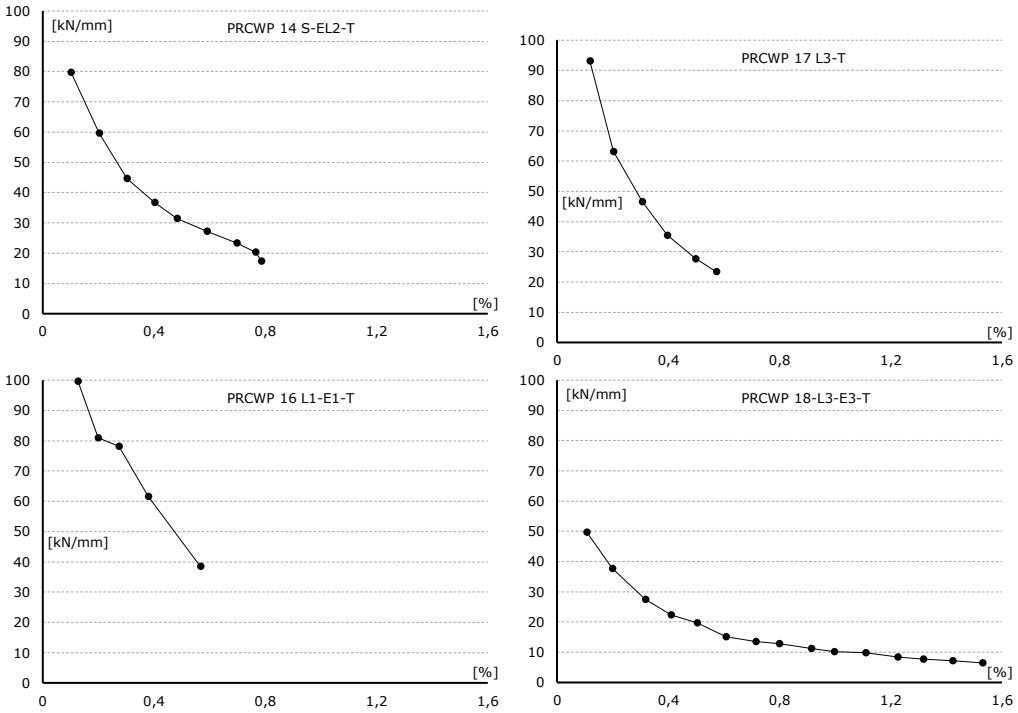

Figure 4-46 – Stiffness degradation for reference specimens

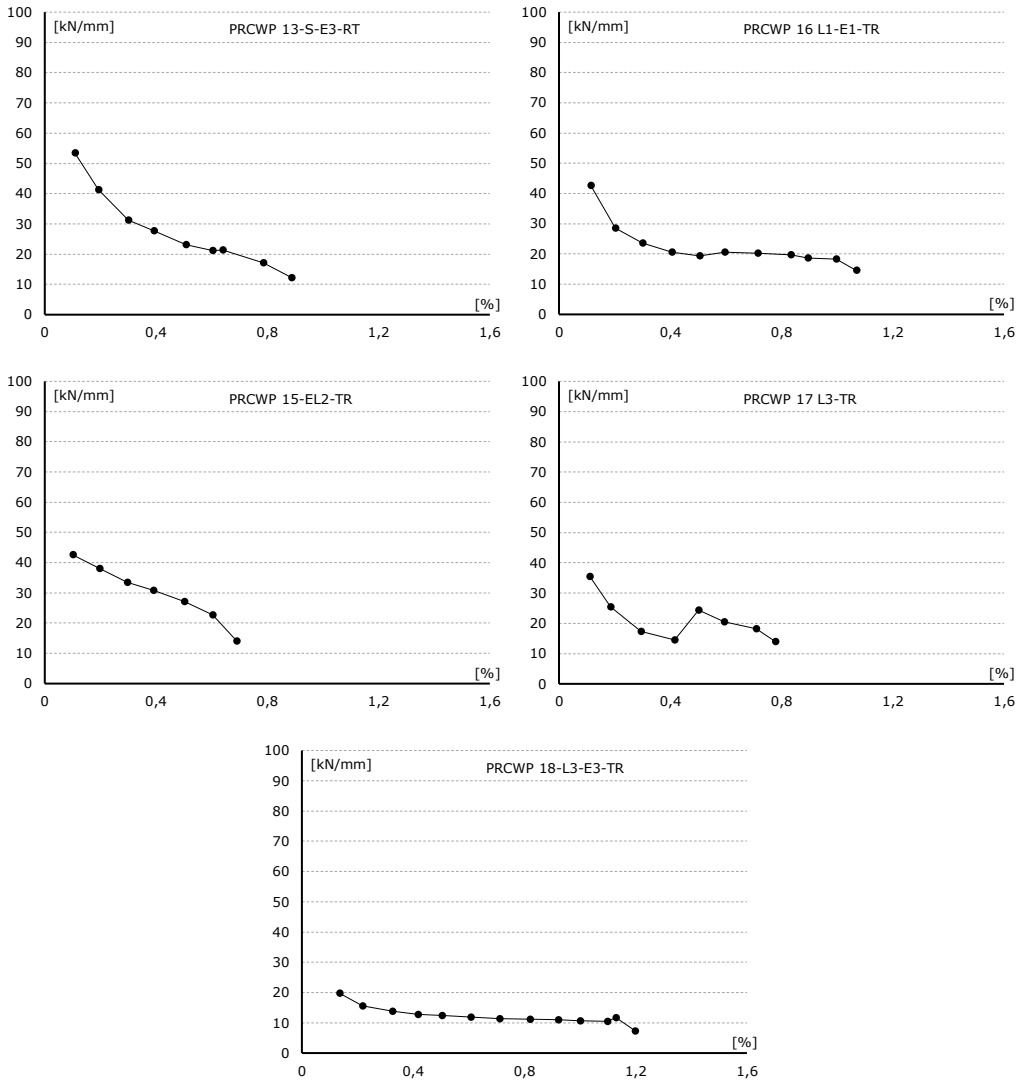

Figure 4-47 – Stiffness degradation for strengthen specimens

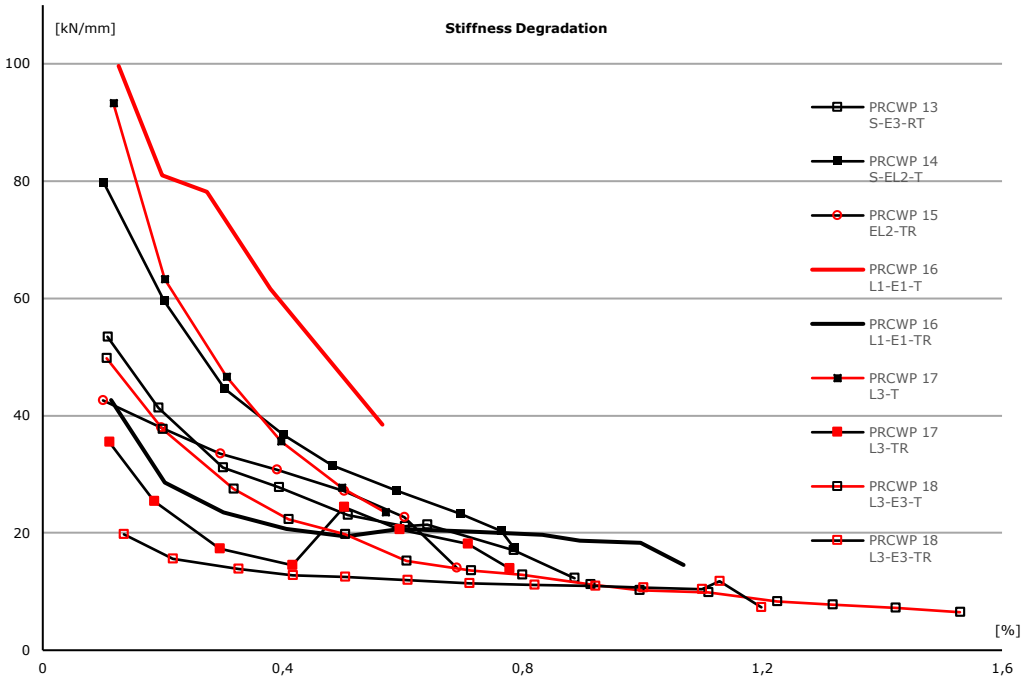

Figure 4-48 – Stiffness degradation comparison

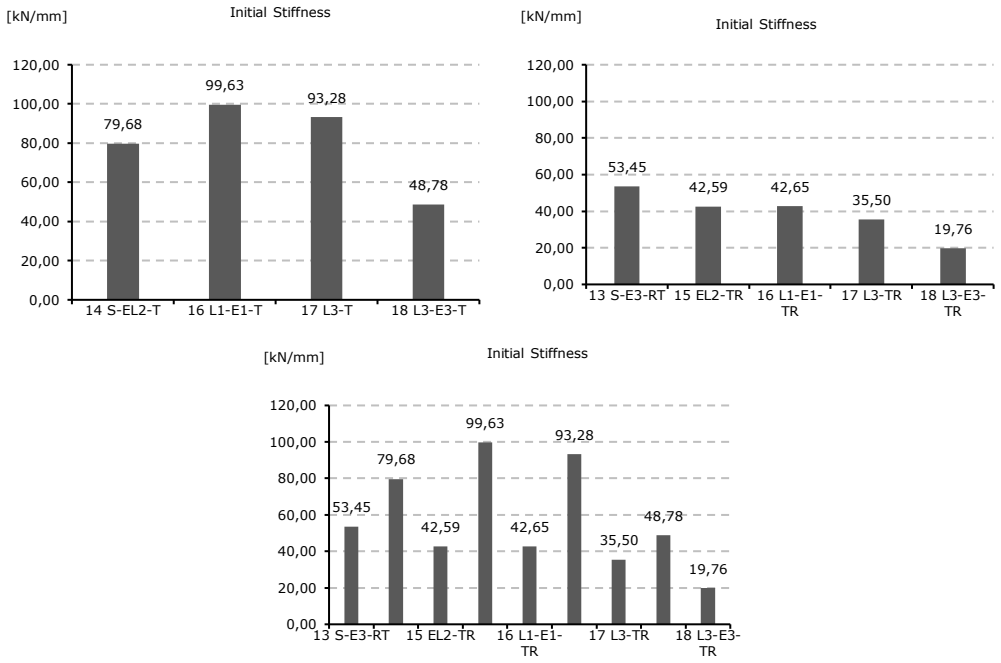

Figure 4-49 Initial Stiffness of the tested specimens

4.8. Theoretical study using Eurocode and CNR provisions

For the reference specimens the provisions in Eurocode 2 [158] section 6 were used to determine the shear resistance. The shear resistance is defined in terms of $V_{Rd,c}$, $V_{Rd,s}$, $V_{Rd,\ max}$

$$V_{Rd,c} = \left[C_{Rd,c} \times k \times (100\rho_1 \times f_{ck})^{1/3} + k_1 \times \sigma_{cp}\right] \times b_w \times d \geq \left(u_{min} + k_1 \times \sigma_{cp}\right) \times b_w \times d$$

Where:

$V_{Rd,c}$ is the design shear resistance of the member without shear reinforcement
Other terms as in [158]

$$V_{Rd,s} = \frac{A_{sw}}{s} \times z \times f_{ywd} \times cot\ \theta$$

Where:

$V_{Rd,s}$ is design shear resistance of the yielding of shear reinforcement
s spacing of the stirrups
f_{ywd} is the design yield strength of the shear reinforcement
z is the inner lever arm, for a member with constant depth, corresponding to the maximum bending moment in the element under consideration. In the shear analysis, the approximate value z = 0,9d may normally be used.
θ is the angle between concrete compression struts and the main tension chord

$$V_{Rd,max} = \frac{\alpha_{cw} \times b_w \times z \times v_1 \times f_{cd}}{cot\ \theta + tan\ \theta}$$

Where:

$V_{Rd,max}$ is design value of the maximum shear force, which can be sustained by the member, limited by crushing of the compression struts
b_w thickness
z is the inner lever arm, for a member with constant depth, corresponding to the maximum bending moment in the element under consideration. In the shear analysis, the approximate value z = 0,8d may normally be used.
f_{cd} is the design value of the concrete compression force in the direction of the longitudinal member axis
θ is the angle between concrete compression struts and the main tension chord
v_1 Compressive strength of concrete

$$v_1 = v = 0.6 \times \left[1 - \frac{f_{ck}}{250}\right]$$
$$z = 0.8 \times l_w$$

Where:

f_{ck} is the design value of the concrete compression force in the direction of the longitudinal member axis
l_w is the wall length

For the retrofitted specimens the provisions in CNR-DT 200 R1/2013 [176] were used to determine the shear resistance taking into account the retrofitting system. According to the code the shear capacity shall be evaluated as follows:

$$V_{Rd} = min\{V_{Rd,s} + V_{Rd,f}, V_{Rd,max}\}$$

Where:

$V_{Rd,S}$ is design shear resistance of the yielding of shear reinforcement
$V_{Rd,f}$ is the shear contribution of the FRP
$V_{Rd,max}$ is design value of the maximum shear force, which can be sustained by the member, limited by crushing of the compression struts

For RC member with a rectangular cross-section and FRP side bonding configuration, the FRP contribution to the shear capacity, shall be calculated as follows:

$$V_{Rd,f} = \frac{1}{\gamma_{Rd}} \times 0.9 \times d \times f_{fed} \times 2 \times t_f \times (cot\theta + cot\beta) \times \frac{b_f}{p_f}$$

Where:

γ_{Rd} is partial factor for resistance model
d is the distance from the extreme compression fibre to the centroid of tension
f_{fed} is the effective design strength of the FRP shear reinforcement
t_f is the thickness of FRP shear reinforcement
θ is the angle of the compressed struts with respect to the member longitudinal axis
β is the angle between fibres and the longitudinal axis of the member
b_f, p_f are the width and the spacing of FRP strips, measured orthogonal to the direction of fibres

For FRP side bonding to a rectangular cross section, the effective FRP design strength, f_{fed}, can be calculated as follows:

$$f_{fed} = f_{fdd} \times \left[1 - \frac{1}{3} \times \frac{l_{ed} \times sin\beta}{min\{0.9 \times d, h_w\}}\right]$$

Where:

f_{fdd} is the design debonding strength of FRP
l_{ed} is the design bond length
β is the angle between fibres and the longitudinal axis of the member
d is effective depth
h_w is the web depth completely impregnated with U-wrap

For laminate/sheet end debonding, the provided bond length is equal to or larger than the optimal bond length. The ultimate design strength, f_{fdd}, is defined as the maximum allowed strength before debonding of the ends and can be calculated as follows:

$$f_{fdd} = \frac{1}{\gamma_{f,d}} \times \sqrt{\frac{2 \times E_f \times \Gamma_{Fd}}{t_f}}$$

Where:

$\gamma_{f,d}$ is the partial factor
E_f modulus of elasticity in the direction of force
Γ_{Fd} is the fracture energy
t_f is the thickness of FRP shear reinforcement

$$l_{ed} = min\left\{\frac{1}{\gamma_{Rd} \times f_{bd}} \times \sqrt{\frac{\pi^2 \times E_f \times t_f \times \Gamma_{FD}}{2}}, 200\ mm\right\}$$

Where:

γ_{Rd} corrective factor
f_{bd} is the design bond strength between FRP and concrete
E_f is the modulus of elasticity in the direction of force
t_f is the thickness of FRP shear reinforcement
Γ_{Fd} is the fracture energy

$$f_{bd} = \frac{2 \times \Gamma_{Fd}}{s_u}$$

Where:

Γ_{Fd} is the fracture energy
s_u interface slip at full debonding

The design fracture energy is computed as follow:

$$\Gamma_{Fd} = \frac{k_b \times k_g}{FC} \times \sqrt{f_{cm} \times f_{ctm}}$$

Where:

k_b is the geometrical corrective factor
k_g is an additional corrective factor calibrated from experimental results and equal to 0.023 mm
FC is the confidence factor
f_{cm} is the mean values of the concrete compressive strengths evaluated on-site
f_{ctm} is the mean values of the concrete tensile strengths evaluated on-site

The geometrical corrective factor is defined with the following equation:

$$k_b = \sqrt{\frac{2 - \frac{b_f}{b}}{1 + \frac{b_f}{b}}} \geq 1$$

Where:

b_f is the FRP width
b is the concrete width

Table 4-1 – Shear resistance evaluated using Eurocode provisions

ELEMENT	PRCWP 14-S-EL2-T		PRCWP 15-EL2-T		PRCWP 16-L1-E1-T		PRCWP 17-L3-T		PRCWP 18-L3-E3-T	
	Pier 1	Pier 2	Pier 1	Pier 2	Pier 1	Pier 2	Pier 1	Pier 2	Pier 1	Pier 2
Reinforcement	Ø10	Ø10	Ø10; Ø6	Ø10; Ø3	Ø10; Ø3	Ø10; Ø3	Ø10; Ø3	Ø10; Ø3	Ø10; Ø3	Ø10; Ø3
A_{sw} [mm^2]	78,5	78,5	78,5; 28,26	78,5; 7	78,5; 7	78,5; 7	78,5; 7	78,5; 7	78,5; 7	78,5; 7
s [mm]	265	265	530; 265	530; 100	530; 100	530; 100	530; 100	530; 100	530; 100	530; 100
z [mm]	560	560	560	560	560	1360	560	560	560	560
f_y [N/mm^2]	300	300	300/390	300/390	300/390	300/390	300/390	300/390	300/390	300/390
θ [°]	28	40	25	30	45	28	25	30	22	20
θ [°]	45	45	45	45	45	45	45	45	45	45
α_{cw}	1	1	1	1	1	1	1	1	1	1
b_w [mm]	100	100	100	100	100	100	100	100	100	100
ν_1	0,56	0,56	0,56	0,56	0,56	0,56	0,55	0,55	0,56	0,56
f_{cm} [N/mm^2]	30	30	28	28	29	29	34	34	30	30
f_{ck} [N/mm^2]	18,69	18,69	16,91	16,91	17,95	17,95	21,08	21,08	18,69	18,69
$V_{R,s}$ [kN]	93,60	59,31	48,17	107,95	40,17	107,95	32,01	51,36	62,72	66,89
$V_{R,s}$ (Pier 1+2) [kN]	153		156		148		83		130	
$V_{R,max}$ [kN]	386,60	459,24	335,97	379,82	452,22	910,49	400,67	452,96	323,93	299,75
$V_{R,max}$ (Pier 1+2) [kN]	846		716		1363		854		624	
$0,4 \cdot V_{R,max}$ (Pier 1+2) [kN]	338		286		545		341		249	
$V_{exp,max}$ [kN]	349		255		503		308		235	
$V_{Rd,f}$ [kN]	0,00	0,00	1061,50	857,34	422,38	2133,88	875,87	707,41	299,35	332,29
$V_{Rd,f}$ (Pier 1+2) [kN]	0		1918,84		2556,26		1583,29		631,65	
$V_{R,max,\ \theta=45°}$ [kN]	466,32	466,32	438,58	438,58	452,22	1098,25	523,04	523,04	466,32	466,32
$V_{R,max}$ (Pier 1+2) θ =45° [kN]	933		877		1550		1046		933	
$0,4 \cdot V_{R,max}$ θ =45° (Pier 1+2) [kN]	373		351		620		418		373	
$V_{exp,max}$ TR [kN]	0		294		392		377		286	

In Eurocode 8 it is assumed that $V_{Rd,max} > V_{Rd,s}$ so the maximum shear resistance is limited by the yielding of the shear reinforcement. The results presented in Table 4.1 are made according to the above equations and the design values were replaced with the experimental measured ones.
It can be observed that the predictions based on the shear resistance of the yielding of the shear reinforcement are highly conservative for the tested elements. For the case were the shear resistance is limited by the crushing of the compression strut it is observed that the results using the Eurocode provisions are overestimated.

$$\alpha_s = \frac{h_w}{l_w}$$

Although for walls with aspect ratio ($\alpha_s \leq 1{,}5$), referred to as large lightly reinforced walls, designed according to DCM (medium ductility), no reduction factor is specified. However, using the reduction factor for high ductility class, 0.4 of the of the value determined in other regions than the critical base one, it can be seen from Figure 4.50 that this reduction factor seems to be very close to the reality as reported also by Postelnicu et al. [177] and Todut [50].

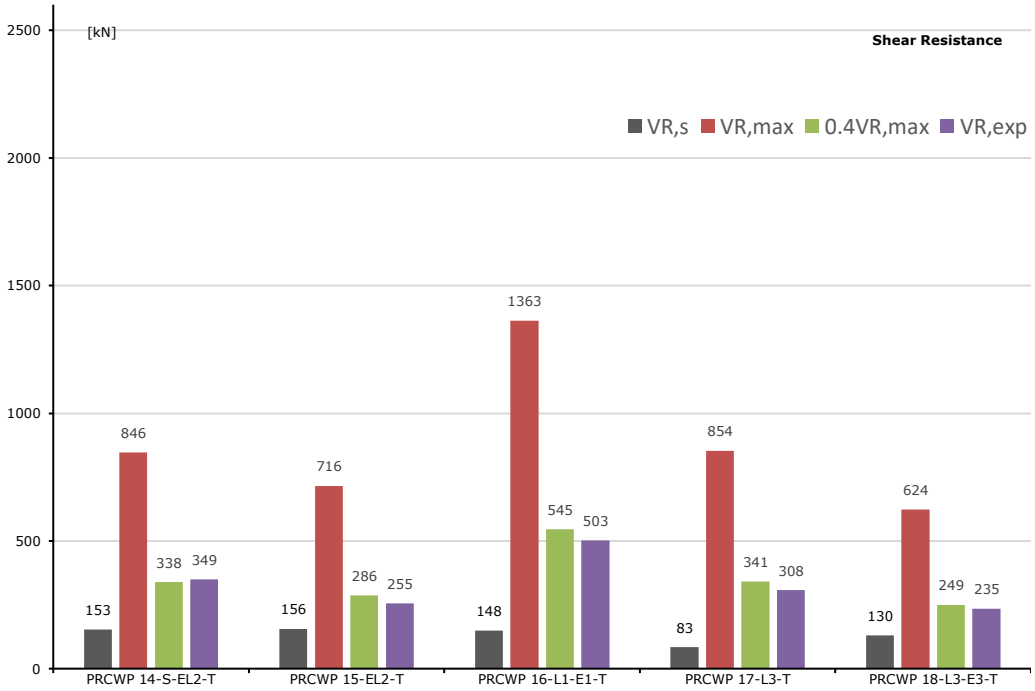

Figure 4-50 – Shear resistance of reference specimens comparison

In Figure 4.51 the shear capacity of the element is computed based on CNR provisions. It can be seen that the shear capacity of the specimens with FRP is larger than that of the specimens resistance limited by the crushing of the compressive struts. However, the experimental test show that the element does not reach the computed shear force, the failure force being similar to initial test.

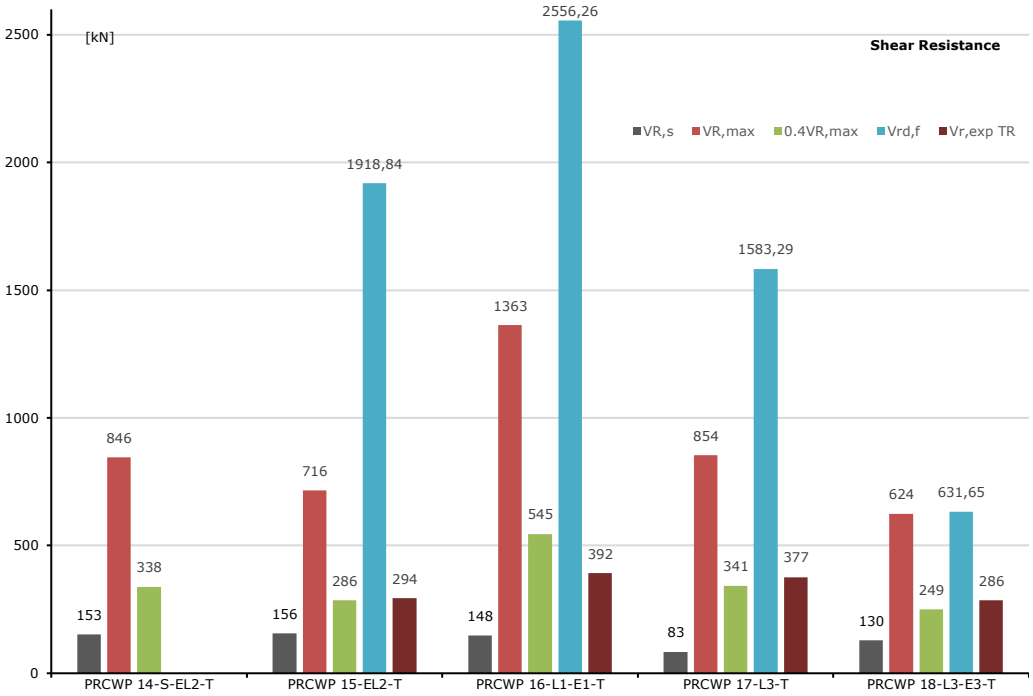

Figure 4-51 – Shear resistance retrofitted specimens comparison

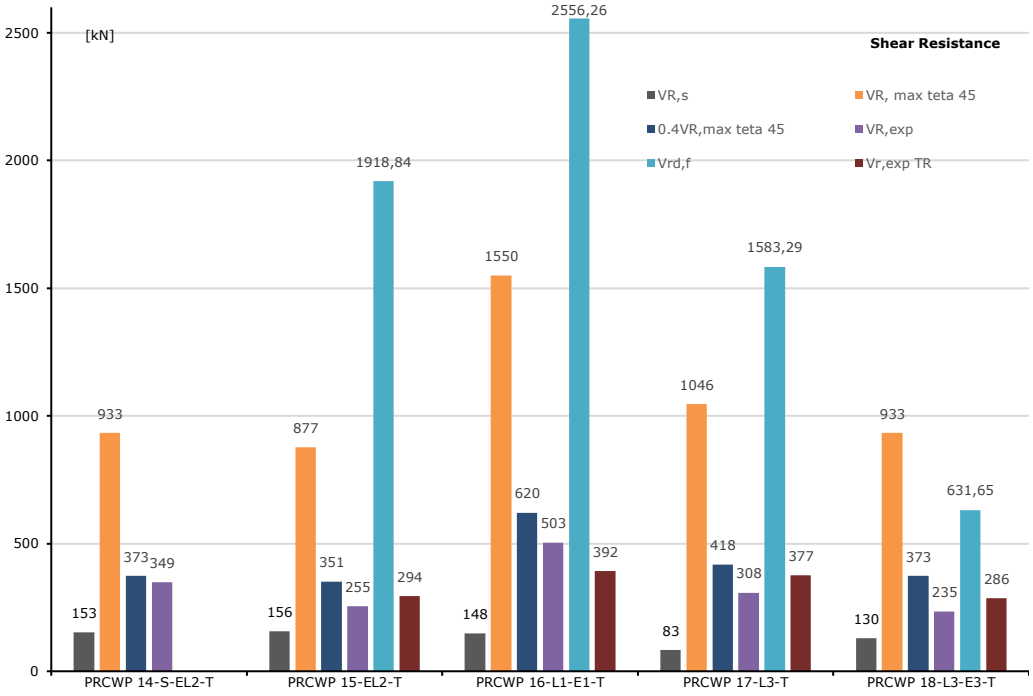

Figure 4-52 – Shear resistance with angle θ=45° comparison

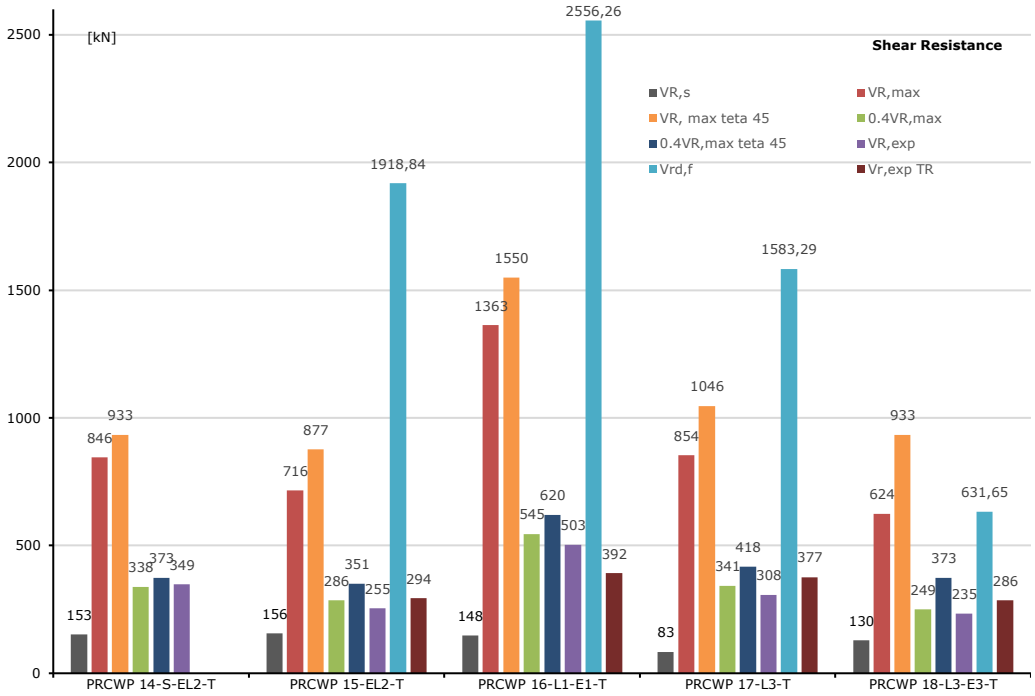

Figure 4-53 – Shear resistance comparison between computed elements

By computing the shear capacity of the specimens with the angle of the compressed struts with respect to the member longitudinal axis of 45°, as assumed in the codes, we can see that the overestimation of the shear capacity of the element limited by the crushing of the compressive struts is higher. Applying the factor of 0.4 we are close to the experimental results.

4.9. Cracking Pattern

A very important behavioural aspect of the reinforced concrete elements, besides the measured response is the cracking patter. In concrete elements cracks appear very early if the element is subjected to increasing load/deflection. In this thesis, the author monitored only one face of the specimen, namely the front face, because the back face was occupied with monitoring equipment so it was not possible to have access to that face. It should be mentioned that the cracking pattern was inspected also on the back face, after the testing was completed and the equipment was removed, and it was observed that the cracking pattern was very similar on both faces, most of the cracks from the front face being visible on the back face as well.

The expected behaviour of reinforced concrete walls subjected to in-plane lateral loading is either flexural or shear. Each behaviour is characterized by different cracking patterns, for the flexural behaviour one can expect horizontal cracks to appear, while the shear behaviour is characterized by inclined cracks. Still in some cases it is not unusual to observe cracks that start horizontally, typical for flexural behaviour, then changing their direction becoming inclined, typical for shear. This case is known as flexural-shear behaviour

In Figure 4.51 the cracking pattern for all tested specimen is presented, in order to compute the pattern, detailed photos of each section were taken and put together to create the photo-map of the cracks. It can be observed that both flexural and shear cracks appeared. The flexural cracks are alongside the pier base and at the pier-to-beam connection. Actually, the flexural cracks appeared in the cast in place mortar that connected the wall and the base beam, and not in the wall itself. However, there was one execution in case of PRCWP 16-L1-E1 specimen which developed flexural cracks alongside the bottom part. The shear cracks appeared mainly in the piers and all specimens developed them.

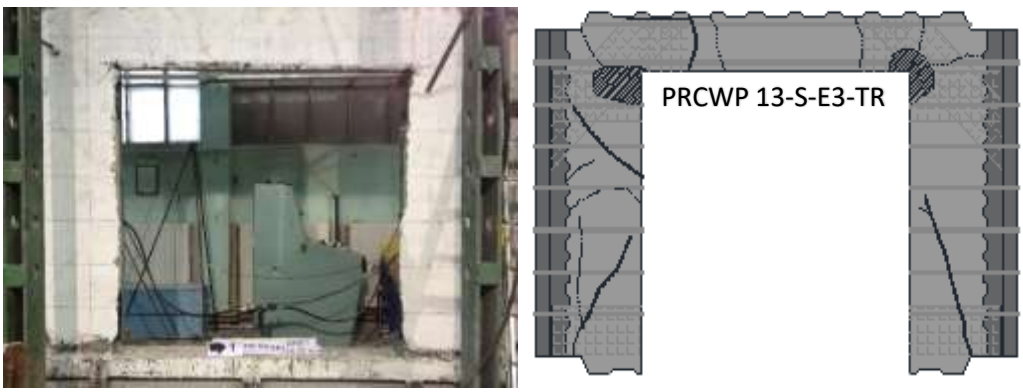

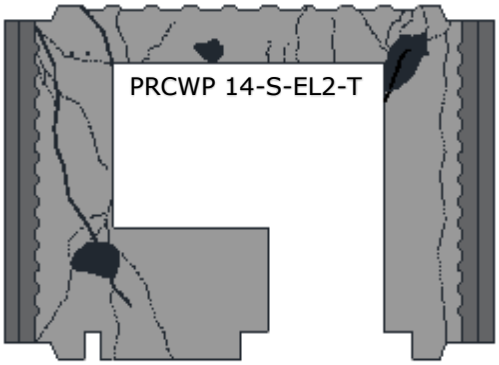
PRCWP 14-S-EL2-T

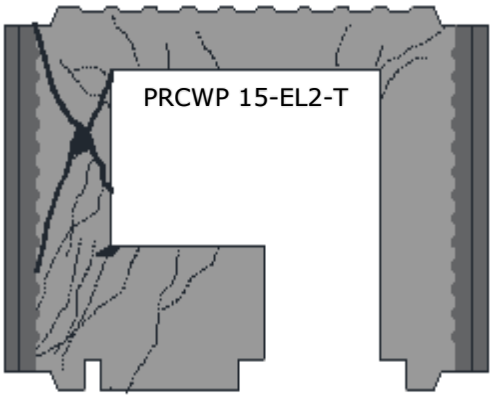
PRCWP 15-EL2-T

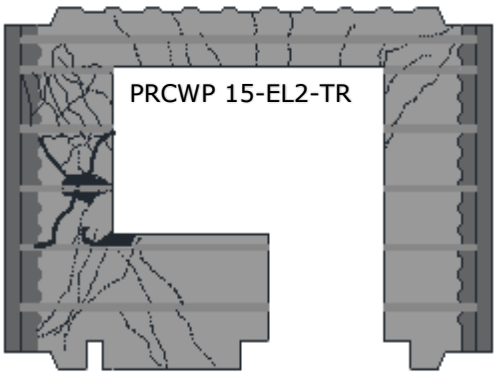
PRCWP 15-EL2-TR

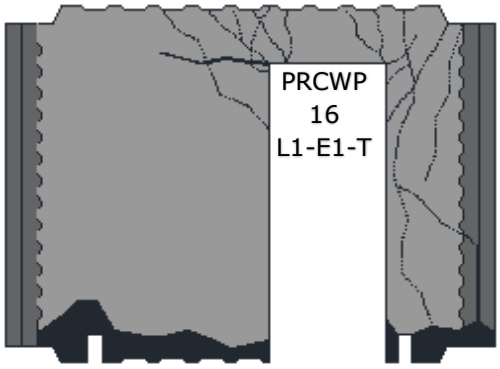

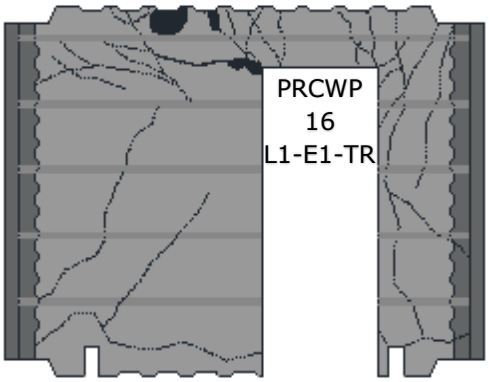

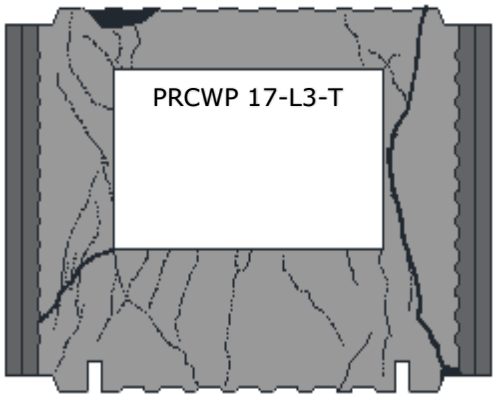

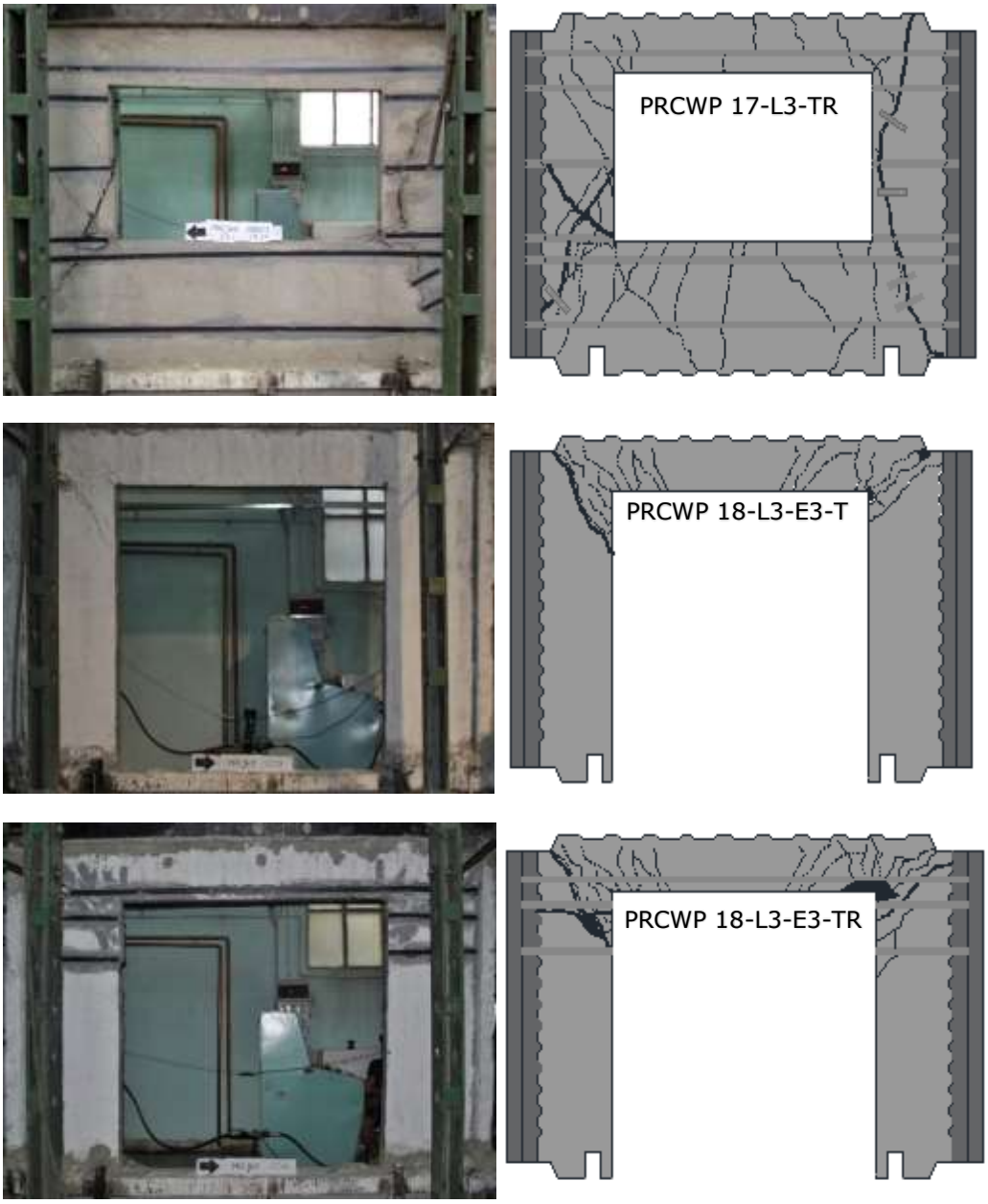

Figure 4-54 The cracking pattern of the tested elements

5. CONCLUSIONS AND PERSONAL CONTRIBUTIONS

5.1. Conclusions

This thesis addresses the subject of retrofitting PRCWP subjected to seismic loads using CFRP materials. Within this chapter are reported the main conclusions that derived from this research, that was performed on six close to full scale precast reinforced concrete wall panels. The results obtained are equivalent to the real behaviour since the specimens are 1:1.2 real scaled elements.

-regarding the load bearing capacity of the specimens, it can be said that the retrofitting solutions adopted in this thesis were successful managing to restore the load bearing capacity of most of the specimens and in several cases to increase it. The load variation between the reference specimen and the retrofitted one was 115,3 % for PRCWP 15-EL2, 78 % for PRCWP 16-L1-E1, 89,9 % for PRCWP 17-L3 and 121,75 for PRCWP 18-L3-E3. In case of the PRCWP 16-L1-E1 we managed to restore only 78 % of its initial load beating capacity due to the fact that the reference specimen had a failure behaviour typical to compression and not shear, thus achieving a larger load bearing capacity.

-comparing the maximum displacements of the refence specimens and the retrofitted ones, one can conclude that the retrofitting procedure increases the displacement of the specimens, the displacement was increased by the retrofitting method in all cases except the PRCWP 18-L3-E3 for which even the reference specimen had a very large displacement that are attributed to the large door opening. The displacements percentages of retrofitted elements compared to refence ones are as follows: 100 % for PRCWP 15-EL2, 207,5 % for PRCWP 16-L1-E1, 152,6 % for PRCWP 17-L3 and 78 % for PRCWP 18-L3-E3. The large displacement difference for the PRCWP 16-L1-E1 is associated with the failure behaviour, that was different for the reference specimen compared to the retrofitted one.

- the failure of the reference specimens was characterized by extensive cracking of all the areas, most common places for the cracks to develop were at the left and right pier and in the spandrel at the opening corners. The main crack that lead to the failure of most of the specimens was a large diagonal crack in the piers. Also common was concrete crushing of the diagonal compressed struts and the corners of the openings.

-in case of the retrofitted specimens the main failure criteria was the debonding of the FRP system. In case of the EBR-CFRP combined with NSM-CFRP system the CFRP used for confinement debonded, whilst the NSM-CFRP did not show signs of weakness. For the EBR-CFRP laminates system debonding of the laminates and failure of the anchorage was observed, however, in most cases the CFRP debonded with the crushed concrete, so the adhesion between the retrofitting system and the concrete surface was good. Again, for the retrofitted specimens concrete crushing was observed in the same regions as for the reference specimens, and in

several extreme cases reinforcement buckling occurred. There was no CFRP rupture in any of the tests.

-in regards to the energy dissipation capacity of the specimen, a clear and definitive conclusion cannot be drawn from these tests only, more tests are required for a clearer observation of the results, with this in mind, the author observed that the retrofitted elements dissipated more energy, with the exception of PRCWP 18-L3-E3, results that are similar with other research developed on the subject. About the influence of the opening type and dimensions on the energy dissipation capacity, the author cannot make a definitive assumption based on these tests due to the difference in concrete quality of the specimens. An interesting remark can be made here, based on the results obtained, comparing the energy dissipated between the two loading cycles with the same displacement ratio, virtually all specimens exhibited the same performance. In the first loading cycle the capacity to dissipate energy was higher than in the second cycle, and was increasing as the displacement increases.

-concerning the stiffness reduction, by comparing specimens with similar concrete quality, it was observed that the stiffness is influenced by the opening, namely, the bigger the opening the smaller the stiffness. For the retrofitted specimens, the initial stiffness was not achieved using the EBR-CFRP laminates method, however, by using the EBR-CFRP combined with NSM-CFRP method we obtained one of the highest stiffness for a large door opening specimen and one of the highest overall, meaning that in this case this method increases the stiffness of the specimens, this affirmation must be further investigated and the author is aware of its limitations due to the small number of tested specimens.

-Using EC2 expressions for the shear strength evaluation denoted that the shear bearing capacity that can be sustained by the yielding reinforcement is conservative compared to the experimental test, whilst the maximum shear resistance of the member limited by the crushing of the compression strut is highly overestimated. Taking all this in consideration the proposed coefficient by Biskinis et al. [177] of "0.4", is very close to reality and seems very suited for the prediction of the real behaviour of PRCWP subjected to shear forces, the same results were obtained also by Todut et al. [50].

Further studies are recommended to be made in regards to the effects of different retrofitting procedure before the most favourable solution is found for the seismic response. In addition to the retrofitting procedure, the behaviour of different specimens with different wall opening needs to be investigated to further observe the effects of the cut-outs.

5.2. Personal contributions

1. Improving the existing experimental program by:

- organizing the cut-outs for the solid elements and casting of 4 new test specimens with specific reinforcement placements and concrete quality;
- testing six near-full scale specimens all with different openings, conducting 10 tests, adding to more than 38 hours of testing time;
- testing and designing strategies for the used retrofitting systems of EBR-CFRP combined with NSM-CFRP and EBR-CFRP laminates;
- different materials used for the retrofitting of the specimens;
- adding four stabilisers to the test set-up in order to avoid the out of plane movement of the specimens.

2. Processing and analysing the recorded data from the instrumentation:

- more than 100 000 raw data rows and over 39 000 "clean" data rows processed;
- more than 250 diagrams generated;
- production of load vs displacement hysteresis loops;
- production of load vs displacement envelops (cyclic envelops, monotonic envelops, two types of backbone envelops);
- energy dissipation analysis (cumulative energy dissipation, cumulative energy dissipation per half cycle, cumulative energy dissipation per cycle, energy dissipation per cycle);
- strength, ductility and displacement analysis;
- stiffness analysis (initial stiffness and stiffness degradation);
- failure details observations and behaviour mode examination;
- shear strength evaluation using design code provisions;
- computation of cracking pattern.

3. investigation of current similar research such as: precast shear elements, reinforced concrete structures, reinforced concrete walls subjected to seismic loads, retrofitting of concrete elements using FRPs, deign code analysis. The database contains 178 refences.

4. synthesis of the results and further directions of research.
5. listing of personal contributions.

5.3. Published papers and acknowledgements

1. **M. Fofiu**, V. Stoian "Using EBR CFRP strips only on failure cracks to retrofit a reinforced concrete wall panel subjected to seismic actions", 16th National Technical-Scientific Conference on Modern Technologies for the 3rd Millennium, pp. 163-168, 2017
2. I.A. Bindean, **M. Fofiu**, V. Stoian "Energy Dissipation of retrofitted Precast Reinforced Concrete Walls subjected to seismic loading", 16th National Technical-Scientific Conference on Modern Technologies for the 3rd Millennium, pp. 123-126, 2017
3. C. Todut, D. Dan V. Stoian, **M. Fofiu**, "Cut-out Weakening Investigation on Precast Reinforced Concrete Wall Panels" 16th National Technical-Scientific Conference on Modern Technologies for the 3rd Millennium, pp. 279-284, 2017
4. **M. Fofiu**, I.A. Bindean, E. Partene, V. Stoian, "Retrofitting of Precast Reinforced Concrete Wall Panel using Carbon Fiber Strips", Advances in Engineering Mechanics and Materials, Santorini Island, Greece, pp. 93-97, July 2014
5. **M. Fofiu**, V. Stoian, I. Demeter, "Retrofitting of precast reinforced concrete walls with cut-out opening using mixed NSM-EBR FRP techniques", International Conference on Earthquake Engineering, pp.852-858, May 2013
6. **M. Fofiu**, V Stoian, C. Todut, "Influence on the bearing capacity of a large door and window cut-out opening in precast reinforced concrete wall panel" 4th European Conference of Civil Engineering, pp. 111-115, 2013
7. **M. Fofiu**, I.A. Bindean and V. Stoian, "Seismic performance of a Precast Reinforced Concrete Wall with cut-out opening retrofitted using carbon fibre strips" Journal of Applied Engineering Sciences, vol. 5(18), pp. 15-22, 2015
8. **M. Fofiu**, V. Stoian, "Analysis of carbon fiber strips retrofitting system for one precast reinforced concrete wall panel"
9. C. Todut, V. Stoian, I. Demeter, **M. Fofiu**, "Seismic Strengthening of a Precast Reinforced Concrete Wall Panel using Textile Reinforced Mortar", 4th European Conference of Civil Engineering, pp. 1056-1062, 2013
10. V. Stoian, T. Nicolae, **M. Fofiu**, "Romanian research activity in the field of FRP rehabilitation of structures affected by the earthquake", Earthquake Engineering and Engineering Seismology, pp. 15-34, May 2014
11. E. Partene, I.A. Bindean, **M. Fofiu**, V. Stoian, L. Fekete-Nagy "Cyclic in-plane testing for evaluation of shear capacity for ceramic block walls" Advances in Engineering Mechanics and Materials, pp. 247-251, July 2014
12. I. A. Bindean, E. Partene, **M. Fofiu**, V. Stoian, „Determination of remaining bearing capacity for damaged masonry arch ceilings of historical buildings using 3d scanning and fem analysis software", 2nd International Conference on Protection of Historical Constructions, 2013
13. **M. Fofiu**, A. Bindean and V. Stoian, "Carbon fiber strips retrofiting sistem for Precast Reinforced Concrete Wall Panel" Innovative Materials and Engineering Research Periodical Key Engineering Materials vl. 660, pp.208-212, May 2015
14. A. Bindean, **M. Fofiu**, E. Partene, V Stoian "Structural health monitoring system, development and testing" Innovative Materials and Engineering Research Periodical Key Engineering Materials vl. 660, pp.340-345, May 2015
15. C. Tanasa, **M. Fofiu**, D. Stoian, "Air Tightness Measurements for an Energy Efficient Residential House Using the Blower Door Procedure", 15th National Technical-Scientific Conference on Modern Technologies for the 3rd Millennium, pp. 169-174, 2016

Contribution to research projects:

1. Strategic grant POSDRU/159/1.5/S/134378 (2014) of the Ministry of National Education, Romania, co-financed by the European Social Fund – Investing in People, within the Sectoral Operational Programme Human Resources Development 2007-2013.

Acknowledgements

1. This paper is partially supported by the Sectoral Operational Programme Human Resources Development (SOP HRD), ID134378 financed from the European Social Fund and by the Romanian Government.

2. Strategic grant POSDRU/159/1.5/S/134378 (2014) of the Ministry of National Education, Romania, co-financed by the European Social Fund – Investing in People, within the Sectoral Operational Programme Human Resources Development 2007-2013.

3. SC MIROCOM SRL company by representative Mr. Mihai Fofiu

4. MAPEI company by representative Mr. Cristi Cartas.

6. FURTHER RESEARCH RECOMMENDATIONS

The current research is based on an ongoing investigation of the behaviour of the PRCWPs and the strengthening and retrofitting procedures for these elements. Given the fact that in this research a limited number of experimental specimens were tested it is obvious the need for further investigation on experimental specimens.

This experimental investigation was conducted on nearly full-scale precast reinforced concrete walls subjected to shear, the walls had initial and/or cut-out openings. This test series contains both door and window openings, further experimental research is necessary to explore the following areas:

- influence of different retrofitting strategies on the shear capacity of the walls;
- strengthening procedures and their effect;
- influence of the opening dimensions and type of opening on the seismic behaviour;
- investigating other types of openings in walls;
- make further investigations on the walls capacity to dissipate energy;
- evaluate further the ductility of the specimens;
- create numerical analysis in terms of strengthening modelling for these experimental tests;
- further evaluate the calibration factor for the shear strength using design codes provisions, by conducting extend experimental test on shear walls.

A large number of experimental test have to be conducted in order to obtain all the answerers in the current research and to solidify the concluded observations.

Bibliography

[1] "Romanian national Statistics Institutee," Governmental, [Online]. Available: http://www.insse.ro/cms/. [Accessed 01 February 2015].

[2] "United Sates Geological Survey," Governmental, [Online]. Available: https://www2.usgs.gov/faq/categories/9831/3342. [Accessed 02 February 2015].

[3] D. Giardini, J. Woessner and L. Danciu, "SHARE," Seismc Hazard Harmonization in Europe, [Online]. Available: http://www.share-eu.org/node/90. [Accessed 15 3 2014].

[4] V. I. Khalturin and T. G. Rautian, "The spectral content of Pamir Hindu Kush intermediate depth earthquakes: Evidence for a high-Q zone in the upper mantle," *Journal of Geophysical,* vol. 82, pp. 2931-2943, 1977.

[5] R. J. Mellors, Two studies in central Asian seismology: A teleseismic study of the Pamir/Hindu Kush seismic zone and analysis of data from the Kyrgyzstan broadband seismic network, Indiana: ProQuest Dissertations Publishing, 1995.

[6] C. Wan-Jou, Investigation of the mechanism of intermediate-depth earthquakes in the Pamir-Hindu kush region, Saint Loiuis: ProQuest Dissertations Publishing, 2012.

[7] Z. Zarifi, J. Havskov and A. Hanyga, "An insight into the Bucaramanga nest," *Tectonophysics,* vol. 443, no. 1-2, pp. 93-105, 2007.

[8] Z. Jian, Precision-seismology studies of inner core rotation and seismotectonics using correlated earthquake signals, Columbia: ProQuest Dissertations Publishing, 2007.

[9] F. M. Richter, "Focal mechanisms and seismic energy release of deep and intermediate earthquakes in the Tonga-Kermadec Region and their bearing on the depth extent of mantle flow," *Journal of Geophysical Reserach,* vol. 84, no. B12, pp. 6783-6795, 1979.

[10] M. Wyss, R. E. Habermann and J. -C. Griesser, "Seismic quiescence and asperities in the Tonga-Kermadec Arc," *Journal of Geophysical Research,* vol. 89, no. B11, pp. 9293-9304, 1984.

[11] M. Radulian, M. N. Mândrescu, G. F. Panza, E. Popescu and A. Utale, "Characterization of seismogenic zones of Romania," *Pure Appl. Geophys.,* vol. 157, pp. 57-77, 2000.

[12] Cod de proiectare antiseismică - PARTEA I - indicative P100-1, 2013, pp. 44.

[13] A. Ismail-Zadeh, L. Matenco, M. Radulian, S. Cloetingh and G. Panza, "Geodynamics and intermediate-depth seismicity in Vrancea (the south-eastern Carpathians): Current state-of-the art," *Tectonophysics,* Vols. 530-531, pp. 50-79, 2012.

[14] G. Marmureanu, C. O. Cioflan and A. Marmureanu, "Intensity seismic hazard map of Romania by probabilistic and (neo) deterministic approaches, linear and nonlinear analyses," *Romanian Reports in Physics,* vol. 63, no. 1, pp. 226-239, 27 September 2011.

[15] M. Kouteva-Guentcheva, "Estimates of some ground motion parameters, related to the damage potential of strong intermediate-depth Vrancea

earthquakes," *Acta Geodaetica et Geophysica Hungarica,* vol. 45, no. 3, pp. 356-371, 2010.

[16] I. Paskaleva, M. Kouteva, F. Vaccari and G. F. Panza, "Characterization of the elastic displacement demand: case study Sofia city," in *Proceedings of the 50th International Conference on Recent Advances in Geotechnical Earthquake Engineering and Soil Dynamics.*, San Diego, California, 2010.

[17] G. F. Panza, M. Kouteva, F. Vaccari, A. Peresan, C. O. Cioflan, F. Romanelli, I. Paskaleva, M. Radulian, K. Gribovszke, M. Herak, A. Zaichenco, G. Marmureanu, P. Varga and M. Zivcic, "Recent Achievements of the Neo-Deterministic Seismic Hazard Assessment in the CEI Region," in *Seismic Engineering Conference Commemorating the 1908 Messina and Reggio Calabria Earthquake: American Institute of Physics.*, 1020, pp. 402–409, 2008.

[18] D. Solakov, S. Simeonova, L. Christoskov, P. Trifonova and I. Aleksandrova, "Probabilistic Seismic Hazard Assesment for Bulgaria as a Basis for a new National Building Code," in *GU General Assembly*, Vienna, Austria., p.4600, 2012.

[19] E. Delavaud, F. Cotton, S. Akkar, F. Scherbaum, L. Danciu, C. Beauval, S. Drouet, J. Douglas, R. Basili, M. A. Sandikkaya and e. al., "Toward a Ground-Motion Logic Tree for Probabilistic Seismic Hazard Assessment in Europe," *Journal of Seismology,* vol. 16, no. 3, pp. 451-473, 2012.

[20] L. Ardeleanu, G. Leydecker, K. -P. Bonjer, H. Busche, D. Kaiser and T. Schmitt, "Probabilistic seismic hazard map for Romania as a basis for a new building code," *Natural Hazards and Earth System Sciences,* vol. 5, pp. 679-684, 2005.

[21] A. Oth, S. Parolai, D. Bindi and F. Wenzel, "Source Spectra and Site Response from S Waves of Intermediate-Depth Vrancea, Romania, Earthquakes," *Bulletin of the Seismological Society of Americ,* vol. 99, no. 1, pp. 235-254, 2009.

[22] F. Pavel, R. Vacareanu, J. Douglas, M. Radulian, C. Cioflan and A. Barbat, "An Updated Probabilistic Seismic Hazard Assessment for Romania and Comparison with the Approach and Outcomes of the SHARE Project," *Pure and Applied Geophysics,* vol. 173, no. 6, pp. 1181-1905, 2016.

[23] "BIGEES," National Institute for Earth Physics, [Online]. Available: http://infp.infp.ro/bigsees/default.htm. [Accessed 04 03 2014].

[24] M. B. Sørensen, D. Stromeyer and G. Grünthal, "A macroseismic intensity prediction equation for intermediate depth earthquakes in the Vrancea region, Romania," *Soli Dynamics and Earthquake Engineering,* vol. 30, no. 11, pp. 1268-1278, 2010.

[25] M. B. Sørensen, D. Stromeyer and G. Grünthal, "Intensity attenuation in the Campania region, Southern Italy," *Journal of Seismology,* vol. 14, no. 2, pp. 209-223, 2010.

[26] A. Craiu, M. Diaconescu, M. Craiu, A. Marmureanu and C. Ionesc, "Analysis of the Seismic Activity in the Vrancea Intermediate-Depth Source Region During the Period 2010–2015," *Springer Natural Hazards, The 1940 Vrancea Earthquake. Issues, Insights and Lessons Learnt,* pp. 189-203, 03 March 2016.

[27] G. Mărmureanu, A. Mărmureanu, E. F. Manea, D. Toma-Danila and V. Mihnea, "Can we still use classic seismic hazard analysis for strong and deep Vrancea earthquakes?," *ROMANIAN JOURNAL OF PHYSICS,* vol. 61, no. 3-4, pp. 728-738, 2016.

[28] O. V. Novikova, I. A. Vorobieva, D. Enescu, M. Radulian, I. Kuznetzov and G. F. Panza, "Prediction of the Strong Earthquakes in Vrancea, Romania, Using the CN Algorithm," *Pure and Applied Geophysics,* vol. 147, no. 1, pp. 99-118, 1996.

[29] V. I. Keilis-Borok and I. M. Rotwain, "Diagnosis of time of increased probability of strong earthquakes in different regions of the world: algorithm CN," *Physics of The Earth and Planetary Interiors,* vol. 61, no. 1-2, pp. 57-72, 1990.

[30] C. L. Moldoveanu, O. V. Novikova, G. F. Panza and M. Radulian, "Monitoring of the future strong Vrancea events by using the CN formal earthquake prediction algorithm," *No. IC--2003/36. Abdus Salam International Centre for Theoretical Physics,* 2003.

[31] V. I. Keilis-Borok and V. G. Kossobokov, "Premonitory activation of earthquake flow: algorithm M8," *Physics of the Earth and Planetary Interiors,* vol. 61, no. 1-2, pp. 73-83, 1990.

[32] L. L. Romashkova and V. G. Kossobokov, "Analysis of the seismic catalogues for the Vrancea Region, Romania," *No. IC/IR--2005/018. Abdus Salam International Centre for Theoretical Physics,* 2005.

[33] M. Popa, N. Cadichian, L. L. Romashkova, M. Radulian, D. Stanica and V. G. Kossobokov, "Seismic monitoring aimed at intermediate-term prediction of strong earthquakes in the Vrancea region," *Geophys Res Abstr,* vol. 9, 2007.

[34] V. G. Kossobokov, "Times of increased probabilities for occurrence of catastrophic earthquakes: 25 years of hypothesis testing in real time," *Wyss (ed.) Earthquake Hazard, Risk and Disasters, Hazards and Disasters Series, Academic Press,* 478-504 2014.

[35] V. G. Kossobokov, "Earthquake prediction: 20 years of global experiment," *Natural Hazards,* vol. 69, no. 2, pp. 1155-1177, 2013.

[36] M. Böse, C. Ionescu and F. Wenzel, "Earthquake early warning for Bucharest, Romania: Novel and revised scaling relations," *Geophys Res Lett. 34, L07302,* vol. 34, no. 7, 2007.

[37] F. Wenzel, M. Oncescu, M. Baur and F. Fierdich, "An Early Warning System for Bucharest," *Seismol. Res. Lett.,* vol. 70, no. 2, pp. 161-169, 1999.

[38] P. Rydelek and S. Horiuchi, "Is the earthquake rupture deterministic?," *nature Brief Communications Arising from E. L. Olson and R. M. Allen,* vol. 441, pp. E5-E6, 2006.

[39] H. Kanamori, "Real-time seismology and earthquake damage mitigation," *Annu. Rev. Earth Planet. Sci.,* vol. 33, pp. 195-214, 2005.

[40] E. S. Georgescu and A. Pomonis, "Emergency management in Vrancea (Romania) earthquakes of 1940 and 1977: casualty patterns vs. search and rescue needs.," in *Proceedings of TIEMS–The International Emergency Management Society, 18th Annual Conference.*, 2011.

[41] I. Armas, "Earthquake risk perception in Bucharest, Romania.," *Risk Analysis,* vol. 26, no. 5, pp. 1223-1234, 2006.

[42] F. Pavel and R. Vacareanu, "Scenario-based earthquake risk assessment for Bucharest, Romania.," *International Journal of Disaster Risk Reduction,* vol. 20, pp. 138-144, 2016.

[43] G. Pásztor and P. László, "Romanian Housing Problems: Past and Present," *Studia Universitatis Babes-Bolyai-Sociologia,* vol. 1, pp. 79-100, 2009.

[44] National Institute of Statistics, "Census of Population and Dwellings 2011," vol IV, Buildings, Dwellings, Households, 2011.

[45] I. Demeter, "Short history of large panel structures in Romania," *Scientific Bulletin of Politehnica University of Timisoara,* vol. 51, no. 65, pp. 87-94, 2005.

[46] National Institute of Statistics, "Census of Population and Dwellings 2011," Vol. I: stable population (rezidents) - demographic structure, 2011.

[47] "eurostat.eu," European Uninion, [Online]. Available: https://europa.eu/european-union/about-eu/figures/living_en#tab-1-3. [Accessed 03 04 2016].

[48] "cia.gov," Central Inteligence Agency, [Online]. Available: https://www.cia.gov/library/publications/the-world-factbook/rankorder/2119rank.html. [Accessed 02 03 2016].

[49] I. Demeter, Seismic Retrofit of precast RC walls by externally bonded CFRP composites, Phd. Thesis: Politehnica University of Timisoara, 2011.

[50] C. Todut, Seismic strenghtening of precast RC wall panels using FRP composites, Phd. Thesis: Politehnica University of Timisoara, 2015.

[51] Inforisx, "Evolutia codurilor pentru proiectarea antiseismica in Romania (1941-2006)," Urban INCD Incerc , [Online]. Available: http://inforisx.incd.ro/cod.htm. [Accessed 05 08 2015].

[52] Z. F. Gobesz and C. Kegyes, "Brief history and evolution of seismic design codes in Hungary and Romania," in *C60 International Conference, "Tradition and Innovation - 60 Years of Civil Engineering Higher Education in Transilvania"*, CLuj-Napoca, Romania, 2013.

[53] "Google Earth 7.1.8.3036," Berceni neighborhood in Bucharest, 44° 22' 57.9515'' N, 26° 6' 9.7153'' E, 3D Buildings data layer,, 2008. [Online]. Available: http://www.google.com/earth/index.html. [Accessed 2017 February 17].

[54] "Google Earth 7.1.8.3036," Manaștur neighborhood in Cluj Napoca, 46° 44' 34.0076'' N, 23° 34' 26.9994'' E, 3D Buildings data layer,, 2008. [Online]. Available: http://www.google.com/earth/index.html. [Accessed 17 February 2017].

[55] "Google Earth 7.1.8.3036," Astra neighborhood in Brașov, 45° 37' 33.6072'' N, 25° 37' 19.2742'' E, 3D Buildings data layer,, 2008. [Online]. Available: http://www.google.com/earth/index.html. [Accessed 2017 February 2017].

[56] "Google Earth 7.1.8.3036," Țiglina neighborhood in Galați, 45° 25' 3.1879'' N, 28° 0' 44.1868'' E, 3D Buildings data layer,, 2008. [Online]. Available: http://www.google.com/earth/index.html. [Accessed 17 February 2017].

[57] "Google Earth 7.1.8.3036," Circumvalațiunii neighborhood in Timișoara, 45° 44' 54.7735'' N, 21° 13' 12.7254'' E, 3D Buildings data layer,, 2008. [Online]. Available: http://www.google.com/earth/index.html. [Accessed 17 February 2017].

[58] R. Taleb, H. Bechtoula, M. Sakashita, N. Bourahla and S. Kono, "Investigation of the shear behaviour of multi-story reinforced concrete walls with eccentric openings," *Computers and Concrete,* vol. 10, no. 4, pp. 361-377, 2012.

[59] T. Holden, J. Restrepo and J. B. Mander, "Seismic Performance of Precast Reinforced and Prestressed," *Journal of Structural Engineering,* vol. 129, no. 3, pp. 286-296, 2003.

[60] K. Beyer, A. Dazio and M. J. N. Priestely, "Shear Deformations of Slender Reinforced Concrete Walls," *ACI Structural Journal, Title no. 108-S17,* pp. 167-177, 2011.

[61] K. Pilakoutas and A. S. Elnashai, "Cyclic behavior of reinforced concrete cantilever walls. I: Experimental results," *ACI Structural Journal-American Concrete Institute,* vol. 92, no. 3, pp. 271-281, 1995.

[62] K. Pilakoutas and A. S. Elnashai, "Cyclic behavior of reinforced concrete cantilever walls, Part II: discussions and theoretical comparisons," *ACI Structural Journal-American Concrete Institute,* vol. 92, no. 4, pp. 425-434, 1995.

[63] D. Dan, A. Fabian and V. Stoian, "Theoretical and experimental study on composite steel–concrete shear walls with vertical steel encased profiles.," *Journal of Constructional Steel Research,* vol. 67, no. 5, pp. 800-813, 2011.

[64] T. A. Tran, Experimental and Analytical Studies of Moderate Aspect Ratio Reinforced Concrete Structural Walls, Phd Thesis: University of California, ProQuest LLC, 2012.

[65] A. Athanasopoulou, Shear strength and drift capacity of reinforced concrete and high-performance fiber reinforced concrete low-rise walls subjected to displacement reversals, Phd Thesis: University of Michigan ProQuest LLC , 2010.

[66] S. J. Bristowe, Seismic response of precast concrete wall panels, Msc Thesis: McGill University of Montreal, 1994.

[67] L. H., Effect of concrete strength on the response of ductile shear walls, Phd. Thesis: McG ill University, Montreal, Canada, 2004.

[68] M. V. V. Edgardo, Experimental cyclic behavior of reinforced concrete wall houses loaded in their weak direction, Phd Thesis: UMI Microform, University of Puerto Rico Mayagüez Campus, 2007.

[69] D. Palermo, Behaviour and analysis of reinforced concrete walls subjected to reversed cyclic loading, Phd Thesis: University of Toronto, National Library of Canada, 2002.

[70] J. F. Rocks, Large scale testing of low aspect ratio reinforced concrete walls, Msc. Thesis: UMI dissertation Publishing, ProQuest LLC., 2012.

[71] C. Greifenhagen and P. Lestuzzi, "Static cyclic tests on lightly reinforced concrete shear walls," *Engineering Structures,* vol. 27, no. 11, pp. 1703-1712, 2005.

[72] A. M. Nasr, Seismic performance of RC shear walls with openings strengthened with advanced composites, PhD Theis: University of California, Irvine, ProQuest LLC, 2011.

[73] M. A. Masuelli, Introduction of Fibre-Reinforced Polymers – Polymers and Composites: Concepts, Properties and Processes, INTECH Open Access Publisher, 2013.

[74] P. Soroushian, S. Ravanbakhsh and M. A. Nagi, "Laboratory Evaluation and Field Application of Concrete Reinforcement with Aramid Fiber-Reinforced Polymer Bars," *Materials Journal ,* vol. 99, no. 6, pp. 584-590, 2002.

[75] R. Okelo and R. L. Yuan, "Bond strength of fiber reinforced polymer rebars in normal strength concrete," *Journal of composites for construction,* vol. 9, no. 3, pp. 203-213, 2005.

[76] P. Zhang, J. S., Y. Xiong and W. Fei, "Experimental study on bond behavior of AFRP rebars in concrete," *Sichuan Building Science 3,* p. 027, 2007.

[77] A. Rolland, S. Chataigner, K. Benzarti, M. Quiertant, P. Argoul and P. J., *Mechanical behaviour of aramid fiber reinforced polymer (AFRP) rebar/concrete interfaces,* TRA, 2014.

[78] M. Saafi and H. Toutanji, "Flexural capacity of prestressed concrete beams reinforced with aramid fiber reinforced polymer (AFRP) rectangular tendons," *Construction and Building Materials,* vol. 12, no. 5, pp. 245-249, 1998.

[79] H. Toutanji and M. Saafi, "Performance of concrete beams prestressed with aramid fiber-reinforced polymer tendons," *Composite Structures,* vol. 44, no. 1, pp. 63-70, 1999.

[80] M. S. Kim, Y. H. Lee, H. Kim, A. Scanlon and J. Lee, "Flexural behavior of concrete beams reinforced with aramid fiber reinforced polymer (AFRP) bars," *Structural Engineering and Mechanics,* vol. 38, no. 4, pp. 459-477, 2011.

[81] "www.sireggeotech.it," SIREG GEOTECH S.R.L., [Online]. Available: https://www.sireggeotech.it/en/products/arapree%C2%AE-rods-permanent-structural-reinforcement. [Accessed 12 06 2016].

[82] N. Subramanian, "www.sefindia.org," 25 09 2014. [Online]. Available: http://www.sefindia.org/forum/viewtopic.php?p=66821. [Accessed 12 08 2016].

[83] H. L. Wu and Y. F. Wang, "Experimental study on reinforced high-strength concrete short columns confined with AFRP sheets," *Steel and Composite Structures,* vol. 10, no. 6, pp. 501-516, 2010.

[84] H. Toutanji and D. Y., "Strength and durability performance of concrete axially loaded members confined with AFRP composite sheets," *Composites Part B: Engineering,* vol. 33, no. 4, pp. 255-261, 2002.

[85] J. Park, S. N. Hong, T. W. Kim and S. Park, "Evaluation of Behavior and Ductility of Reinforced Concrete Beams Strengthened with AFRP," in *International conference of International Institute for FRP in construction for Asia-pacific region*, 2009.

[86] Z. Deng and R. Xiao, "Flexural Performance of RC Beams Strengthened with Prestressed AFRP Sheets: Part I. Experiments," in *CICE 2010 - The 5th International Conference on FRP Composites in Civil Engineering*, Beijing, China, 2010.

[87] "ascsales.com," ACP composites, [Online]. Available: http://www.acpsales.com/OnlineStore.php?cat=252. [Accessed 19 08 2016].

[88] B. Islam, R. Ahsan and M. G. Rashed, "Retrofit Techniques of Structures Associated with Soft Story," in *1st International Conference on Advances in Civil Engineering*, 2012.

[89] V. Fiore, T. Scalici, G. Di Bella and A. Valenza, "A review on basalt fibre and its composites," *Composites Part B: Engineering,* vol. 74, pp. 74-94, 2015.

[90] F. M. Kogan and O. V. Nikitina, "Kogan, F. M., & Nikitina, O. V. (1994). Solubility of chrysotile asbestos and basalt fibers in relation to their fibrogenic and carcinogenic action.," *Environmental health perspectives,* vol. 102, no. 5, p. 205, 1994.

[91] E. E. McConnell, O. Kamstrup, R. Musselman, T. W. Hesterberg, J. Chevalier, W. C. Miiller and P. Thevenaz, "Chronic inhalation study of size-separated rock and slag wool insulation fibers in Fischer 344/N rats," *Inhalation toxicology,* vol. 6, no. 6, pp. 571-614, 1994.

[92] V. Fiore, G. Di Bella and A. Valenza, "Glass–basalt/epoxy hybrid composites for marine applications," *Materials & Design,* vol. 32, no. 4, pp. 2091-2099, 2011.

[93] "Hangzhou Chiheng Technology Co.,Ltd," [Online]. Available: http://www.chtechint.en.ecplaza.net. [Accessed 15 11 2016].

[94] "Basalt Fabric," Smarter Building Systems, [Online]. Available: http://basalt-fabric.com/. [Accessed 16 11 2016].

[95] P. Banibayat and A. Patnaik, "Banibayat, P., & Patnaik, A. (2014). Variability of mechanical properties of basalt fiber reinforced polymer bars manufactured by wet-layup method," *Materials & Design,* vol. 56, pp. 898-906, 2014.

[96] M. Urbanski, A. Lapko and A. Garbacz, "Investigation on concrete beams reinforced with basalt rebars as an effective alternative of conventional R/C structures," *Procedia Engineering,* vol. 57, pp. 1183-1191, 2013.

[97] J. Sim and C. Park, "Characteristics of basalt fiber as a strengthening material for concrete structures," *Composites Part B: Engineering,* vol. 36, no. 6, pp. 504-512, 2005.

[98] O. Y. W. P. Z. Yunchao, "Calculation and analysis of flexural and shear capacity of RC beams strengthened with BFRP sheets [J]," *Industrial Construction,* vol. 6, p. 006, 2007.

[99] L. J. Ouyang, D. B. and Z. D. Lu, "BFRP and its application review in structural strengthening," *Fiber Reinforced Plastics,* vol. 3, p. 023, 2010.

[100] A. Ashour, "Flexural and shear capacities of concrete beams reinforced with GFRP bars," *Construction and Building Materials,* vol. 20, no. 10, pp. 1005-1015, 2006.

[101] J. R. Yost, S. P. Gross and D. w. Dinehart, "Shear strength of normal strength concrete beams reinforced with deformed GFRP bars," *Journal of Composite Construction,* vol. 5, no. 4, pp. 268-275, 2001.

[102] B. Benmokrane, O. Chaallal and R. Masmoudi, "Glass fibre reinforced plastic (GFRP) rebars for concrete structures," *Construction and Building Materials,* vol. 9, no. 6, pp. 353-364, 1995.

[103] D. T. C. Johnson, Investigation of glass fibre reinforced polymer reinforcing bars as internal reinforcement for concrete structures, Diss. : University of Toronto, 2009.

[104] N. A. A. R. Mohamed, Strength and drift capacity of gfrp reinforced concrete shear walls, PhD Theisi: Library and Archives Canada, Universite de Sherbrooke , 2013.

[105] A. Karlovic, "Linkedin," 27 03 2016. [Online]. Available: https://www.linkedin.com/pulse/glass-fiber-reinforced-polymer-gfrp-rebar-alen-karlovic. [Accessed 16 08 2016].

[106] "Exportersindia," Safety Tonny Trade, 2014. [Online]. Available: http://www.exportersindia.com/safety-tonny-trade/gfrp-bars-canada-1010630.htm. [Accessed 23 08 2016].

[107] C. A. Daescu, Reabilitarea elementelor de constructie utilizand materiale compozite polimerice, PhD Thesis: "Politehnica" University of Timisoara, 2011.

[108] S. M. Muhamed, Seismic Behaviour of square concrete columns retrofitted with glass fibre reinforced polymers (GFRPs), University of Toronto, 2002.

[109] N. Aravind, A. K. Samanta, J. V. Thanikal and D. K. S. Roy, "An experimental study on the effectiveness of externally bonded corrugated GFRP laminates for flexural cracks of RC beams," *Construction and Building Materials,* vol. 136, pp. 348-360, 2017.

[110] D. Lee, Flexural Rehabilitation of Concrete Structures Using NSM FRP Composites, Phd Thesis: ProQuest LLC, University of California, 2012.

[111] M. Derias, Durability of concrete beams strengthened in flexure using Near-Surface-Mounted Fibre-Reinforced-Polymers, Library and Archives Canada , 2008.

[112] P. Kankeri and S. Prakash S., "Experimental evaluation of bonded overlay and NSM GFRP bar strengthening on flexural behavior of precast prestressed hollow core slabs," *Engineering Structures,* vol. 120, pp. 49-57, 2016.

[113] R. M. Reda, I. A. Sharaky, M. Ghanem, M. H. Seleem and H. E. M. Sallam, "Flexural behavior of RC beams strengthened by NSM GFRP Bars having different end conditions," *Composite Structures,* vol. 147, pp. 131-142, 2016.

[114] N. Gattesco, C. Amadio and C. Bedon, "Experimental and numerical study on the shear behavior of stone masonry walls strengthened with GFRP reinforced mortar coating and steel-cord reinforced repointing," *Engineering Structures,* vol. 90, pp. 143-157, 2015.

[115] M. Corradi, A. Borri, G. Castori and R. Sisti, "Shear strengthening of wall panels through jacketing with cement mortar reinforced by GFRP grids," *Composites Part B: Engineering,* vol. 64, pp. 33-42, 2014.

[116] "www.mapei.com," MAPEI, [Online]. Available: http://www.mapei.com/RO-RO/Consolidari-Structurale/Consolidarea-structurilor-din-beton-si-otel. [Accessed 03 09 2016].

[117] S. A. M. Gazi, Durability performance of gfrp bars under aggressive local exposure conditions, Msc. theisi: ProQuest LLC, 2005.

[118] P. Yeonho, Long-term performance of GFRP reinforced concrete beams and bars subjected to aggressive environments, Phd Thesis: ProQuest LLC., 2012.

[119] "zoltek.com," Zoltek commercial carbon fiber, [Online]. Available: http://zoltek.com/pre-cured-carbon-fiber-laminates-promise-lower-manufacturing-time-costs/. [Accessed 02 09 2016].

[120] "zacarbon.com," Zhongao carbon, [Online]. Available: http://www.zacarbon.com/carbon-fiber-fabrics. [Accessed 02 09 2016].

[121] T. Kubat, R. Al-Mahaidi and A. Shayan, "Strain development in CFRP-wrapped circular concrete columns affected by alkali-aggregate reaction," *Construction and Building Materials,* vol. 113, pp. 603-612, 2016.

[122] D. Wang, Z. Wang, S. T. Shith and T. Yu, "Seismic performance of CFRP-confined circular high-strength concrete columns with high axial compression ratio," *Construction and Building Materials,* vol. 134, pp. 91-103, 2017.

[123] R. Z. Al-Rousan, Experimental and Theoretical Behavior of Reinforced Concrete Beams and Columns Strengthened with CFRP, Phd Thesis Chicago, Illinois : ProQuest LLC , 2008.

[124] A. W. Al Zand, W. H. .. Badaruzzaman, A. A. Mutalib and S. J. Hilo, "Rehabilitation and strengthening of high-strength rectangular CFST beams using a partial wrapping scheme of CFRP sheets: Experimental and numerical study," *Thin-Walled Structures,* vol. 114, pp. 80-91, 2017.

[125] N. Akroush, T. Almahallawi, M. Seif and E. Y. Sayed-Ahmed, "CFRP shear strengthening of reinforced concrete beams in zones of combined shear and normal stresses," *Composite Structures,* vol. 162, pp. 47-53, 2017.

[126] Q. Abdulrahman, Z. Wu and L. S. Cunningham, "Experimental and numerical investigation into strengthening flat slabs at corner columns with externally bonded CFRP," *Construction and Building Materials,* vol. 139, pp. 132-147, 2017.

[127] G. El-Saikaly and O. Chaallal, "Fatigue behavior of RC T-beams strengthened in shear with EB CFRP L-shaped laminates," *Composites Part B: Engineering,* vol. 68, pp. 100-112, 2015.

[128] S. C. Florut, G. Sas, C. Popescu and V. Stoian, "Tests on reinforced concrete slabs with cut-out openings strengthened with fibre-reinforced polymers," *Composites Part B: Engineering,* vol. 66, pp. 484-493, 2014.

[129] J. A. O. Barros and S. J. E. Dias, "Near surface mounted CFRP laminates for shear strengthening of concrete beams," *Cement and Concrete Composites,* vol. 28, no. 3, pp. 176-292, 2006.

[130] J. A. O. Barros and A. S. Fortes, "Flexural strengthening of concrete beams with CFRP laminates bonded into slits," *Cement and Concrete Composites,* vol. 27, no. 4, pp. 471-480, 2005.

[131] A. Bilotta, F. Ceroni, E. Nigro and M. Pecce, "Efficiency of CFRP NSM strips and EBR plates for flexural strengthening of RC beams and loading pattern influence," *Composite Structures,* vol. 124, pp. 163-175, 2015.

[132] R. Capozucca, S. Bossoletti and S. Montecchiani, "Assessment of RC beams with NSM CFRP rectangular rods damaged by notches," *Composite Structures,* vol. 128, pp. 322-341, 2015.

[133] Ç. Mertog˘lu, Ö. Anil and C. Durucan, "Bond slip behavior of anchored CFRP strips on concrete surfaces," *Construction and Building Materials,* vol. 123, pp. 553-564, 2016.

[134] M. I. Kabir, R. Shrestha and B. Samali, "Effects of applied environmental conditions on the pull-out strengths of CFRP-concrete bond," *Effects of applied environmental conditions on the pull-out strengths of CFRP-concrete bond,* vol. 114, pp. 817-830, 2016.

[135] R. Al-Safy, R. Al-Mahaidi and P. Simon. G., "A study of the use of high functionality-based resin for bonding between CFRP and concrete under harsh environmental conditions," *Composite Structures,* vol. 95, pp. 295-306, 2013.

[136] J. C. P. H. Gamage, R. AL-Mahaidi, B. Wong and M. R. E. F. Ariyachandra, "Bond characteristics of CFRP-strengthened concrete members subjected to

cyclic temperature and mechanical stress at low humidity," *Composite Structures,* vol. 160, pp. 1051-1059, 2017.

[137] T. Alkhrdaji, "Strengthening of Concrete Structures Using FRP Composites," *Building Blocks,* Jun 2015.

[138] "Radyab.co," Radyab Engineered Solutions, [Online]. Available: http://www.radyab.co/en/projects. [Accessed 08 9 2016].

[139] "gelijmde-wapening.be," TD Gelijmde Wapening, [Online]. Available: http://www.gelijmde-wapening.be/index.cfm?n01=new_technics&n02=nsm. [Accessed 12 08 2016].

[140] M. M. E. Elnady, Seismic Rehabilitation of RC Structural Walls, PhD Thesis: Library and Archives Canada, 2008.

[141] J. Lombard, D. T. Lau, J. L. Humar, S. Foo and M. S. Cheung, "Seismic strengthening and repair of reinforced concrete shear walls," in *12th World Conf. on Earthquake Engineering*, Auckland, 2000.

[142] D. Dan, "Experimental tests on seismically damaged composite steel concrete walls retrofitted with CFRP composites," *Engineering Structures,* vol. 45, pp. 338-348, 2012.

[143] D. Dan, T. Nagy-György, V. Stoian, A. Fabian and I. Demeter, "FRP Composites for Seismic Retrofitting of Steel-Concrete Shear Walls with Steel Encased Profiles," *Behaviour of Steel Structures in Seismic Areas (STESSA 2012),* pp. 1071-1076, 2012.

[144] S. Qazi, L. Michel and E. Ferrier, "Impact of CFRP partial bonding on the behaviour of short reinforced concrete wall under monotonic lateral loading," *Composite Structures,* vol. 128, pp. 251-259, 2015.

[145] H. Y. Zhou, T. L. Attard, B. Zhao, J. T. Yu, W. S. Lu and L. W. Tong, "Experimental study of retrofitted reinforced concrete shear wall and concrete-encased steel girders using a new CarbonFlex composite for damage stabilization," *Engineering Failure Analysis,* vol. 35, no. SI, pp. 219-233, 2013.

[146] K. Dhiradhamvit, T. L. Attard and H. Zhou, "Development of a new lightweight ''Rubberized-Carbon'' composite for wood home protection," in *ATINER construction conference*, Athens, Greece, 2011.

[147] B. Li and C. L. Lim, "Tests on seismically damaged reinforced concrete structural walls repaired using fiber-reinforced polymers," *Journal of composites for construction,* vol. 14, no. 5, pp. 597-608, 2010.

[148] J. E. Woods, D. T. Lau and C. A. Cruz-Noguez, "In-Plane Seismic Strengthening of Nonductile Reinforced Concrete Shear Walls Using Externally Bonded CFRP Sheets," *Journal of Composites for Construction,* vol. 20, no. 6, p. 04016052, 2016.

[149] K. Kobayashi, "Innovative application of FRPs for seismic strengthening of RC shear wall," in *Proceeding, Fiber-Reinforced Polymer (FRP) Reinforcement for Concrete Structures*, Kansas City, Missouri, 2005.

[150] A. A. Khalil, Rehabilitation of reinforced concrete structural walls using fibre composites, Hamilton: ProQuest Dissertations Publishing,, 2005.

[151] D. Shen, Q. Yang, Y. Jiao, Z. Cui and J. Zhang, "Shen, Dejian, et al. "Experimental investigations on reinforced concrete shear walls strengthened with basalt fiber-reinforced polymers under cyclic load," *Construction and Building Materials,* vol. 136, pp. 217-229, 2017.

[152] A. S. Mosallam and A. Nasr, "Structural performance of RC shear walls with post-construction openings strengthened with FRP composite laminates," *Composites Part B: Engineering,* pp. In Press, Corrected Proof,, 2016.

[153] S. J. Hwang, Y. S. Tu, Y. H. Yeh and T. C. Chiou, "Reinforced concrete partition walls retrofitted with carbon fiber reinforced polymer," ANCER annual meeting: networking of young earthquake engineering researchers and professionals., Honolulu, Hawaii, 2004.

[154] B. S. Mohammed, L. W. Ean and M. A. Malek, "One way RC wall panels with openings strengthened with CFRP," *Construction and Building Materials,* vol. 40, pp. 575-583, 2013.

[155] CEN, "Part 3: Compressive strength of tested specimens," in *EN 12390-3:2001 Testing of hardened concrete*, Brusseles, Belgium, European Comittee for Standardization (CEN), 2001.

[156] CEN, "EN ISO 15630-1:2002 Steel for the reinforcement and prestressing of concrete," in *Test methods - Part 1: Reinforcing bars, wire rod and wire*, Brusseles, Belgium, European Comittee for Standardization (CEN), 2002.

[157] CEN, "EN 10002-1:2001 Tensile Testing Metallic Materials," in *Tensile Testing Metallic Materials*, Brusseles, Belgium, European Comittee for Standardization (CEN), 2001.

[158] CEN/TC250, "EN 1992-1-1:2004:E Eurocode 2: Design of concrete structures," in *Part 1-1: General rules and rules for buildings*, Brusseles, Belgium, European Committee for Standardization (CEN), 2004.

[159] N. Zabihi and E. Ö., "Compressive strength conversion factors of concrete as affected by specimen shape and size," *Research journal of applied sciences, engineering and technology,* vol. 7, no. 20, pp. 4251-4257, 2014.

[160] C. Sittipunt, S. L. Wood, P. Lukkunaprasit and P. Pattararattanakul, "Cyclic behavior of reinforced concrete structural walls with diagonal web reinforcement," *Structural Journal,* vol. 98, no. 4, pp. 554-562, 2001.

[161] "www.mapei.com," MAPEI, [Online]. Available: http://www.mapei.com/public/RO/products/Mapegrout-Rapido-Flyer-148,5x210mm.pdf. [Accessed 28 10 2016].

[162] "www.mapei.com," MAPEI, [Online]. Available: http://www.mapei.com/public/COM/products/1066_mapegrout%20easy%20flow%20gf_gb.pdf. [Accessed 28 10 2016].

[163] M. Fofiu, A. Bindean and V. Stoian, "Carbon fiber strips retrofitting system for precast reinforced concrete wall panel," *Key Engineering Materials,* vol. 660, pp. 208-212, 2015.

[164] M. Fofiu, A. Bindean and V. Stoian, "Seismic Performance Of A Precast Reinforced Concrete Wall With Cut-Out Opening Retrofitted Using Carbon Fibre Strips," *Journal of Applied Engineering Sciences,* vol. 5, no. 1, pp. 15-22, 2015.

[165] M. Fofiu, I. Bindean, E. Partene and V. Stoian, "Retrofitting of Precast Reinforced Concrete Wall Panel using Carbon Fiber Strips," in *International Conference on Civil Engineering*, Santorini, Greece, 2014.

[166] I. Demeter, T. Nagy-György, V. Stoian and D. Dan, "Quasi-static loading strategy for earthquake simulation on precast RC shear walls," in *Demeter, István, et al. "Quasi-static loading strategy for earthquake simulation on*

precast RC shear walls." WSEAS International Conference. Proceedings. Mathematics and Computers in Science and Engineering, 2008.

[167] I. Demeter, T. Nagy-György and V. Stoian, "Axial loading strtegy for experimental tests on precast RC walls subjected to in-plane seismic actions," *Scientific Bulletin of the "Politehnica" University of Timisoara,* vol. 52, no. 66, pp. 11-16, 2007.

[168] M. Mansour, J. Y. Lee and T. T. Hsu, "Cyclic stress-strain curves of concrete and steel bars in membrane elements," *Journal of Structural Engineering,* vol. 127, no. 12, pp. 1402-1411, 2001.

[169] A. S. Elnashai and R. Pinho, "Repair and retrofitting of RC walls using selective techniques," *Journal of Earthquake Engineering,* vol. 2, no. 04, pp. 525-568, 1998.

[170] M. Warashina, S. Kono, M. Sakashita and H. Tanaka, "Shear behavior of multi-story RC structural walls with eccentric openings," in *The 14th World Conference on Earthquake Engineering*, Beijing, China, 2008.

[171] P. A. Hidalgo, C. A. Ledezma and R. M. Jordan, "Seismic behavior of squat reinforced concrete shear walls," *Earthquake Spectra,* vol. 18, no. 2, pp. 287-308, 2002.

[172] K. K. Antoniades, T. N. Salonikios and A. J. Kappos, "Evaluation of hysteretic response and strength of repaired R/C walls strengthened with FRPs," *Engineering structures,* vol. 29, no. 9, pp. 2158-2171, 2007.

[173] M. J. N. Priestley, "Performance based seismic design," *Bulletin of the New Zealand society for earthquake engineering,* vol. 33, no. 3, pp. 325-346, 2000.

[174] R. Park, "Ductility evaluation from laboratory and analytical testing," in *Proceedings of the 9th world conference on earthquake engineering*, Tokyo-Kyoto, Japan, 1988.

[175] J. Carrillo, G. González and A. Rubiano, "Displacement ductility for seismic design of RC walls for low-rise housing," *Latin American Journal of Solids and Structures,* vol. 11, no. 4, pp. 725-737, 2014.

[176] CNR, DT 200 R1/2013 Guide for the Design and Construction of Externally Bonded FRP Systems for Strengthening Existing Structures, Rome: Italian National Research Council, 2014.

[177] I. Damian, E. Morariu, B. Buzaianu, T. Postelnicu and D. Zamfirescu, in Postelnicu T, editor.; Proiectarea structurilor de beton armat in zone seismice (Design of reinforced concrete structures placed in semismic areas - in Romanian), Bucharest: MarLink, 2012.

[178] D. E. Biskinis, G. K. Roupakias and M. N. Fardis, "Degradation of shear strength of reinforced concrete members with inelastic cyclic displacement," *ACI Structural Journal,* vol. 101, no. 6, pp. 773-783, 2004.

APPENDIX A - Force-drift ratio analysis comparison between similar specimens

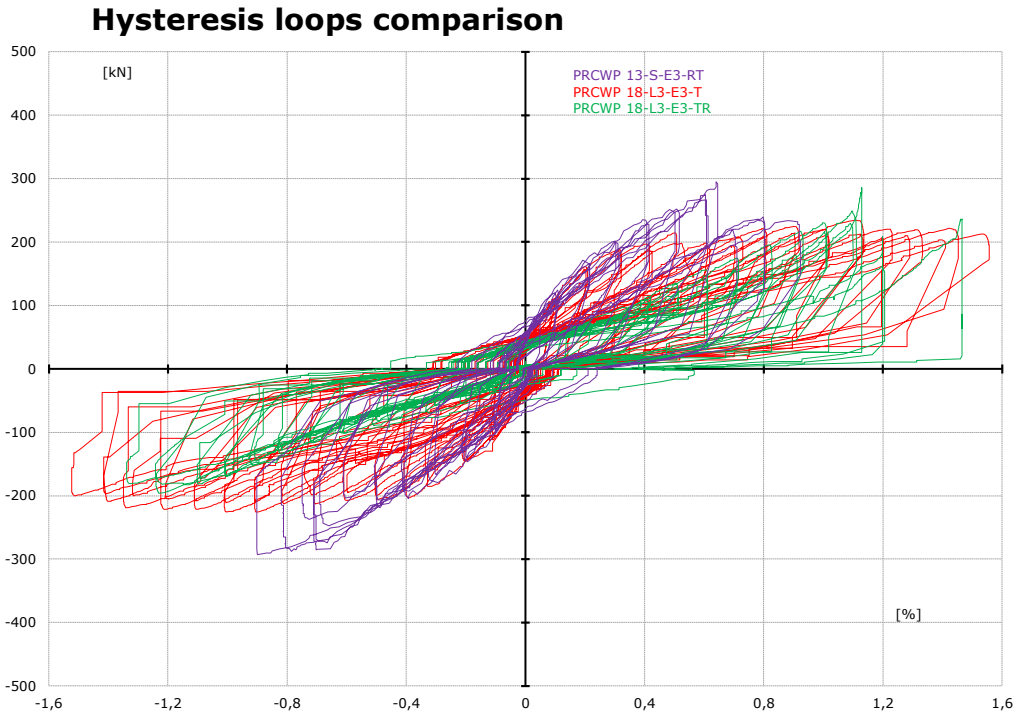

Figure A - 1 – PRCWP 13-S-E3-RT, 18-L3-E3-T and 18-L3-E3-RT hysteresis comparison

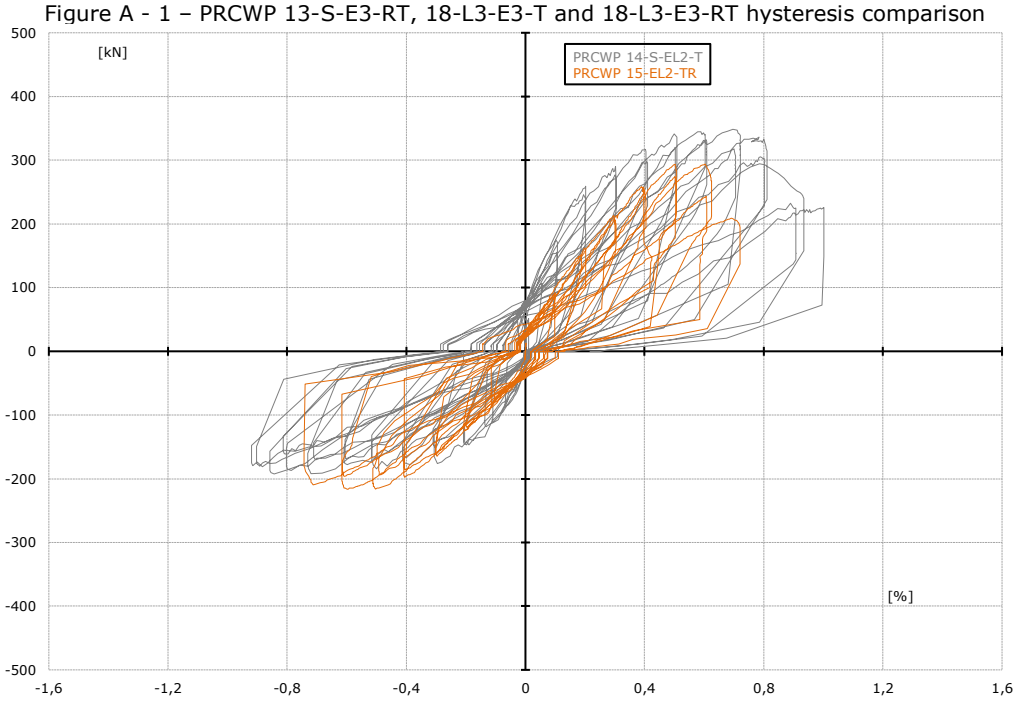

Figure A- 1 – PRCWP 14-S-EL2-T, 17-EL2-T hysteresis comparison

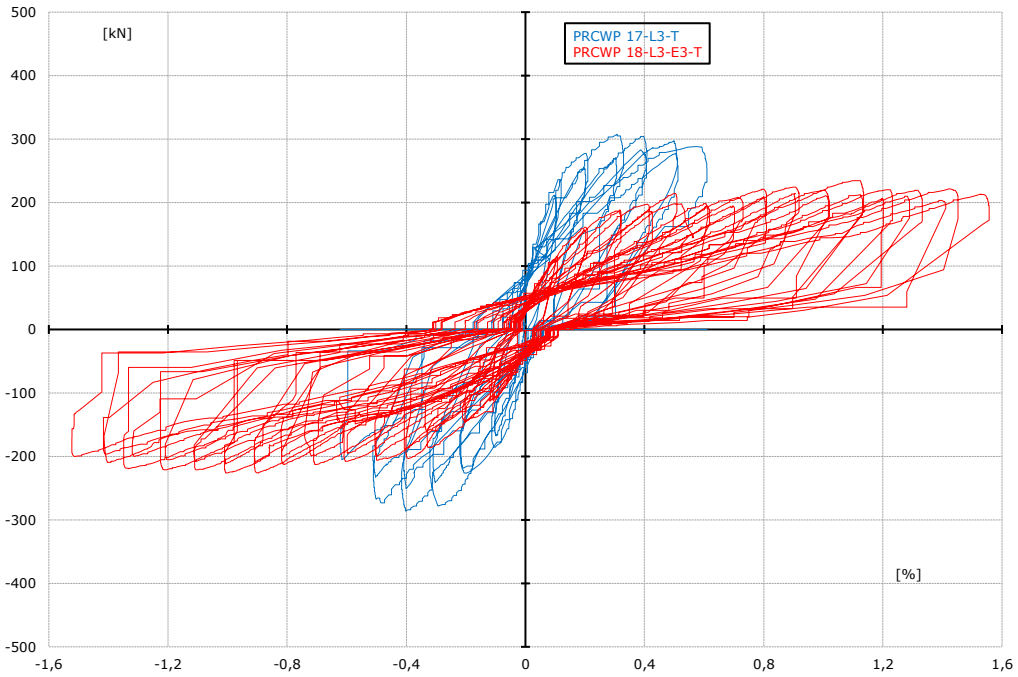

Figure A- 2 – PRCWP 17-S-L3-T, 18-L3-E3-T hysteresis comparison

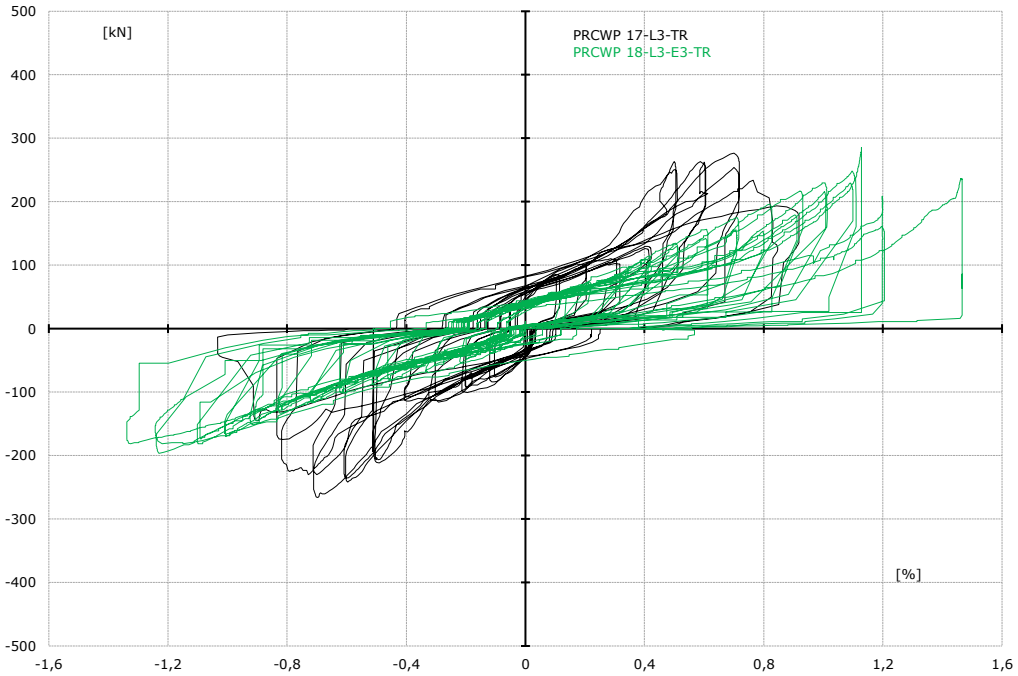

Figure A- 3 – PRCWP 17-S-L3-TR, 18-L3-E3-TR hysteresis comparison

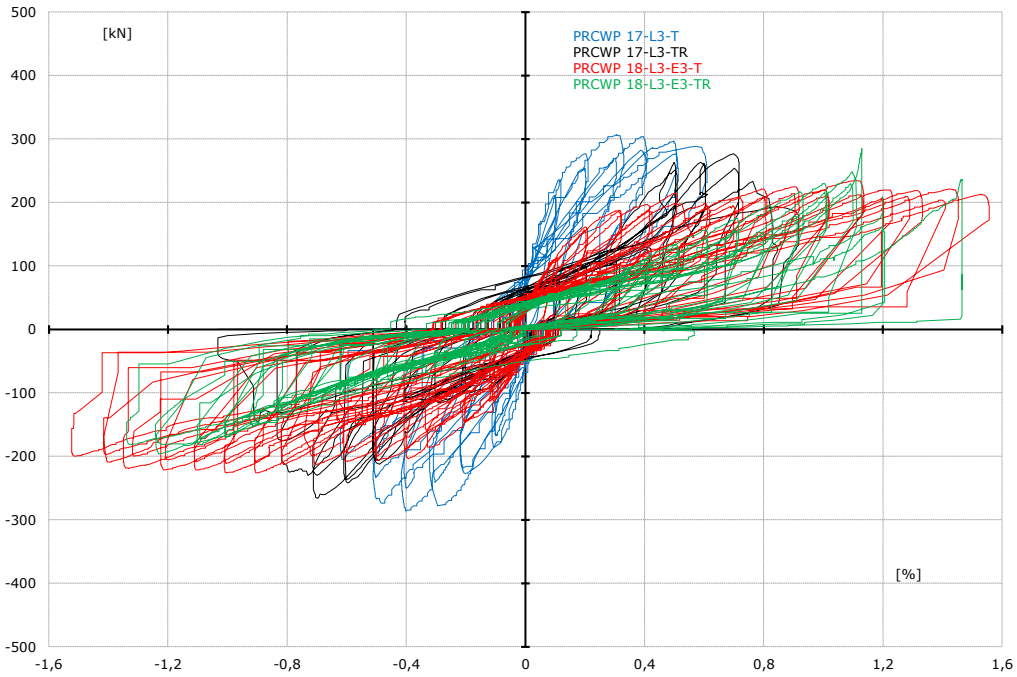

Figure A- 4 – PRCWP 17-S-L3-T, 18-L3-E3-T, 17-S-L3-TR, 18-L3-E3-TR hysteresis comparison

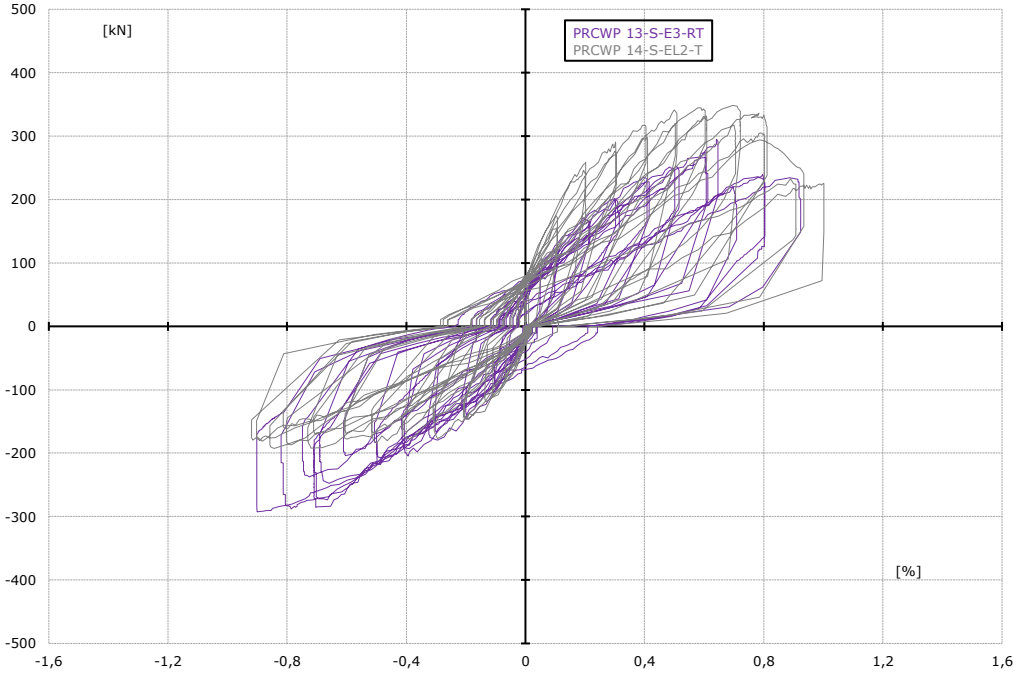

Figure A- 5 – PRCWP 13-S-E3-RT, 14-S-EL2-T hysteresis comparison

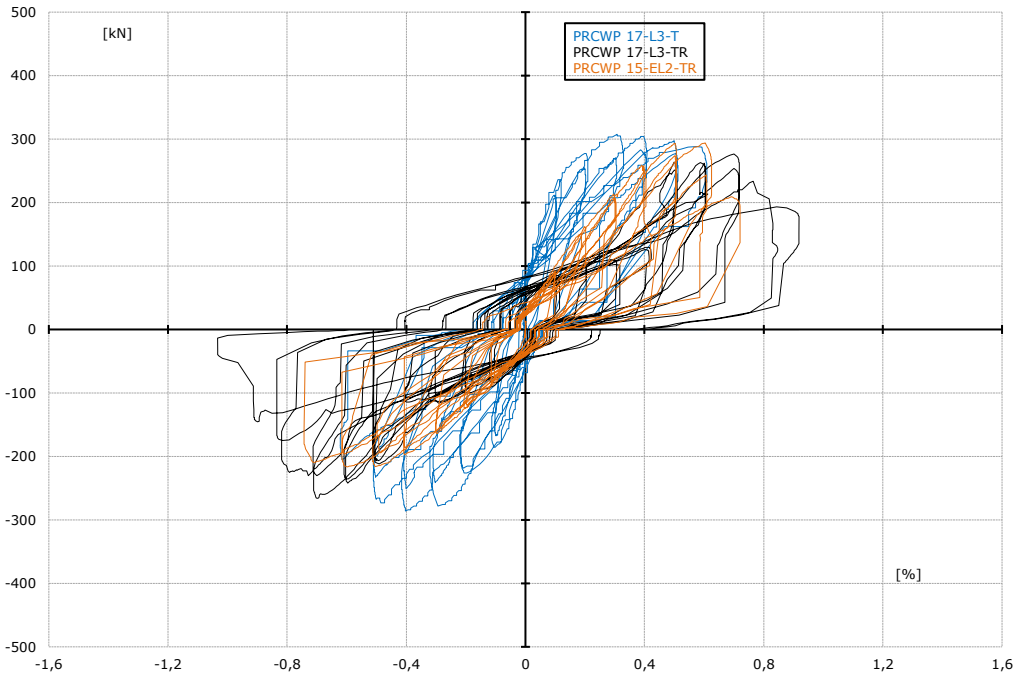

Figure A- 6 – PRCWP 17-S-L3-T, 17-S-L3-TR, 15-EL2-TR hysteresis comparison

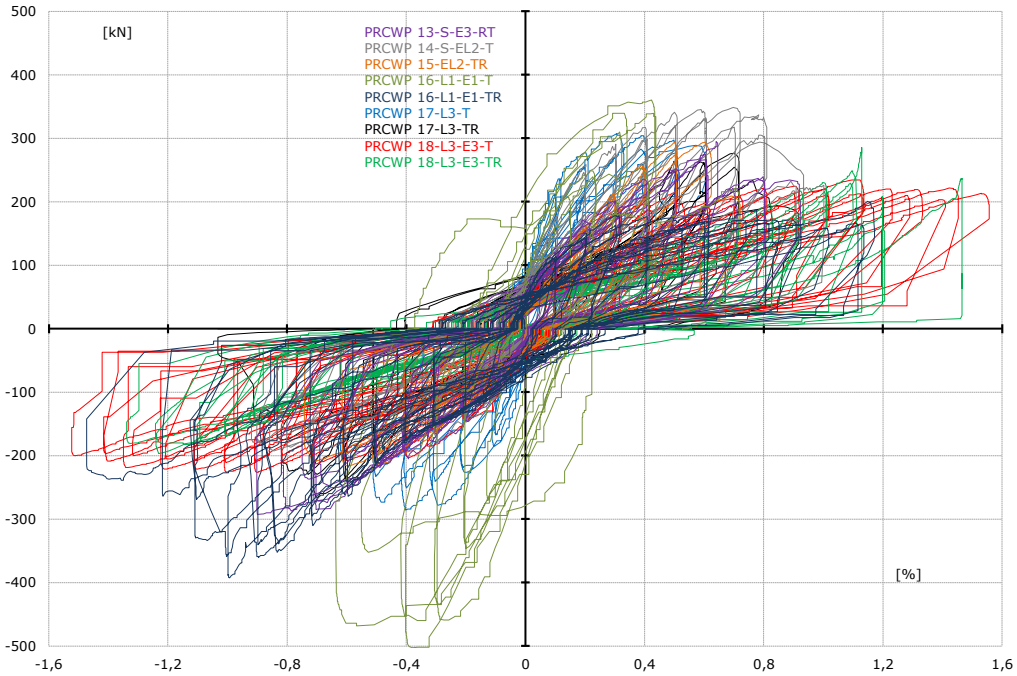

Figure A- 7 – All specimens hysteresis comparison

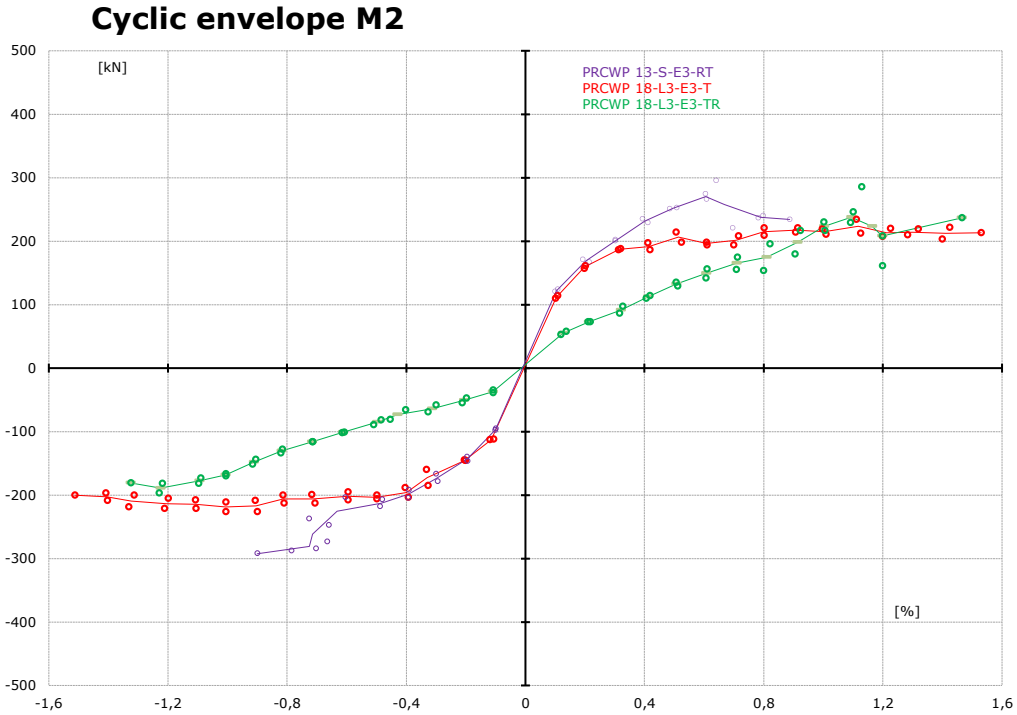

Figure A- 8 – PRCWP 13-S-E3-RT, 18-L3-E3-T and 18-L3-E3-RT M2 Envelope comparison

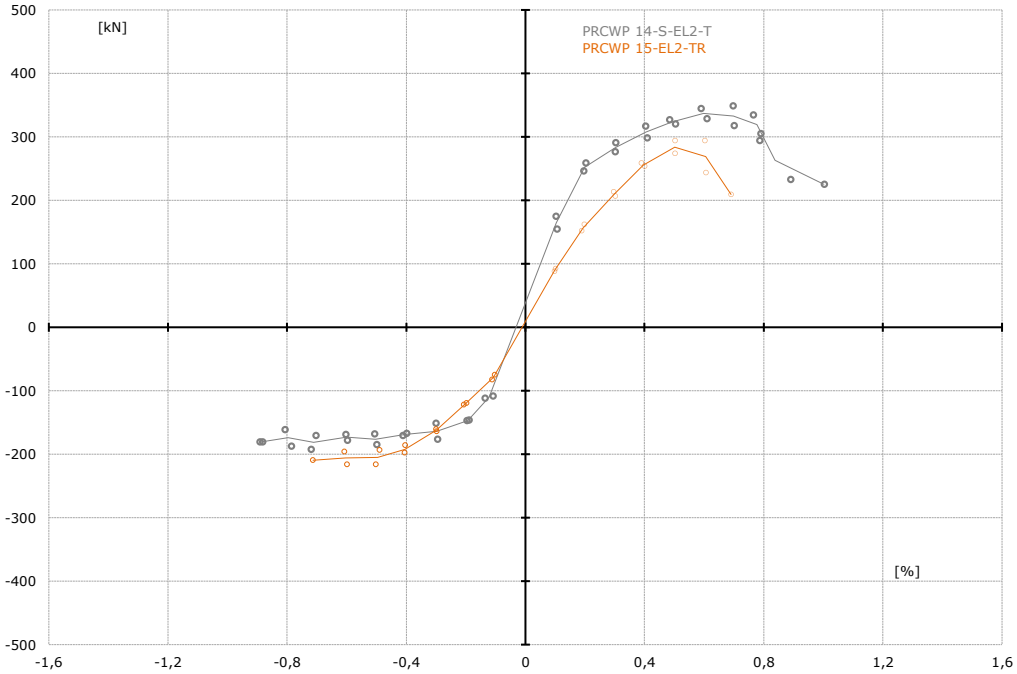

Figure A- 9 – PRCWP 14-S-EL2-T, 17-EL2-T M2 envelope comparison

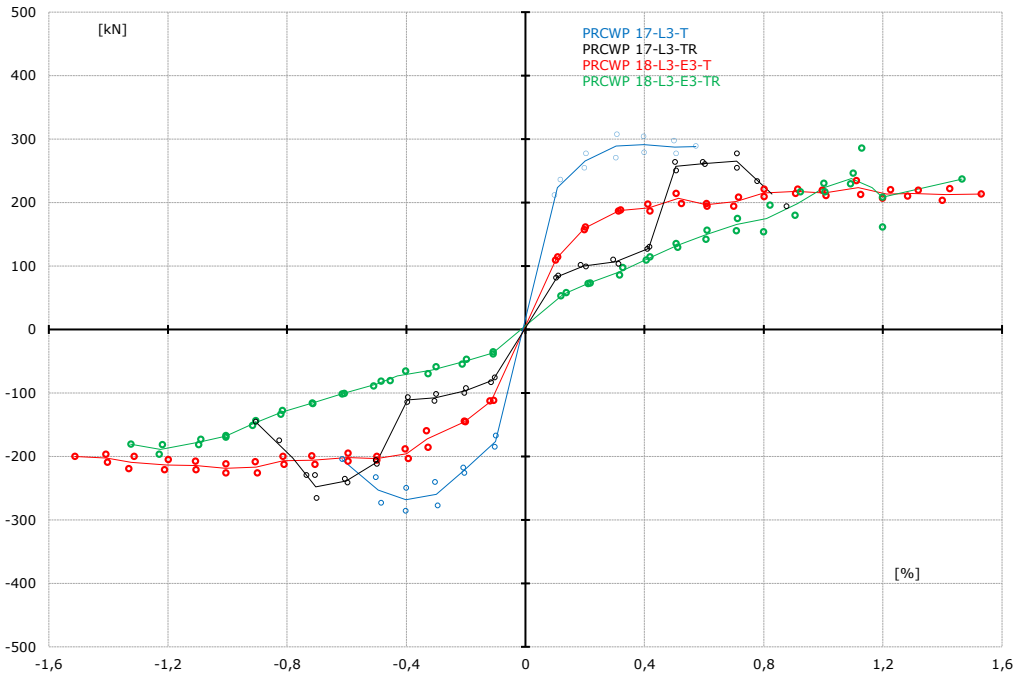

Figure A- 10 – PRCWP 17-S-L3-T, 18-L3-E3-T, 17-S-L3-TR, 18-L3-E3-TR M2 envelope comparison

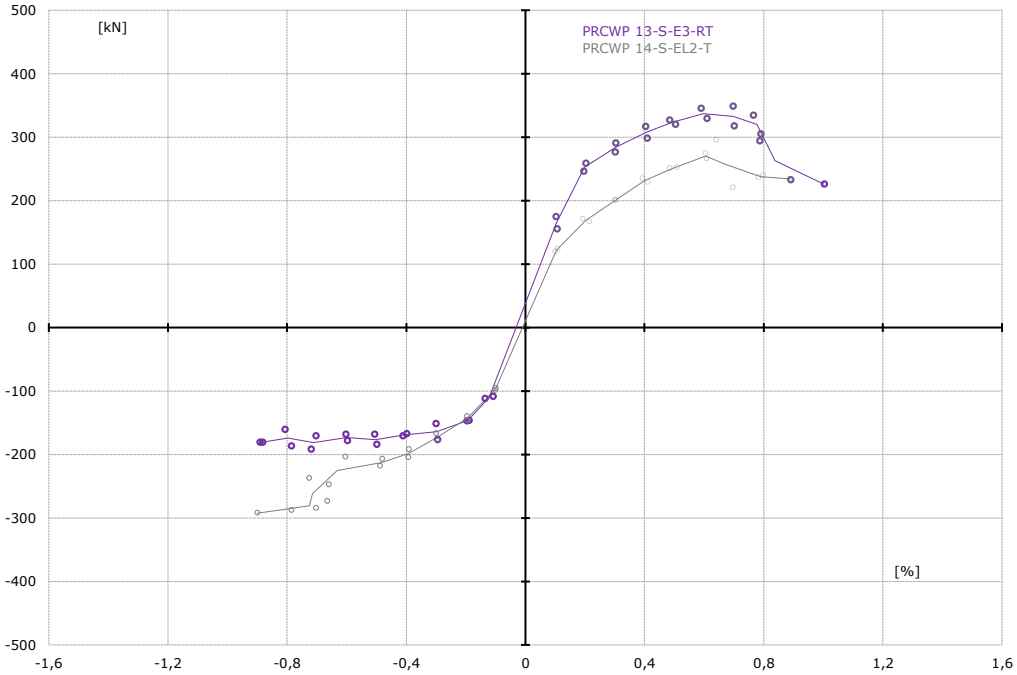

Figure A- 11 – PRCWP 13-S-E3-RT, 14-S-EL2-T M2 envelope comparison

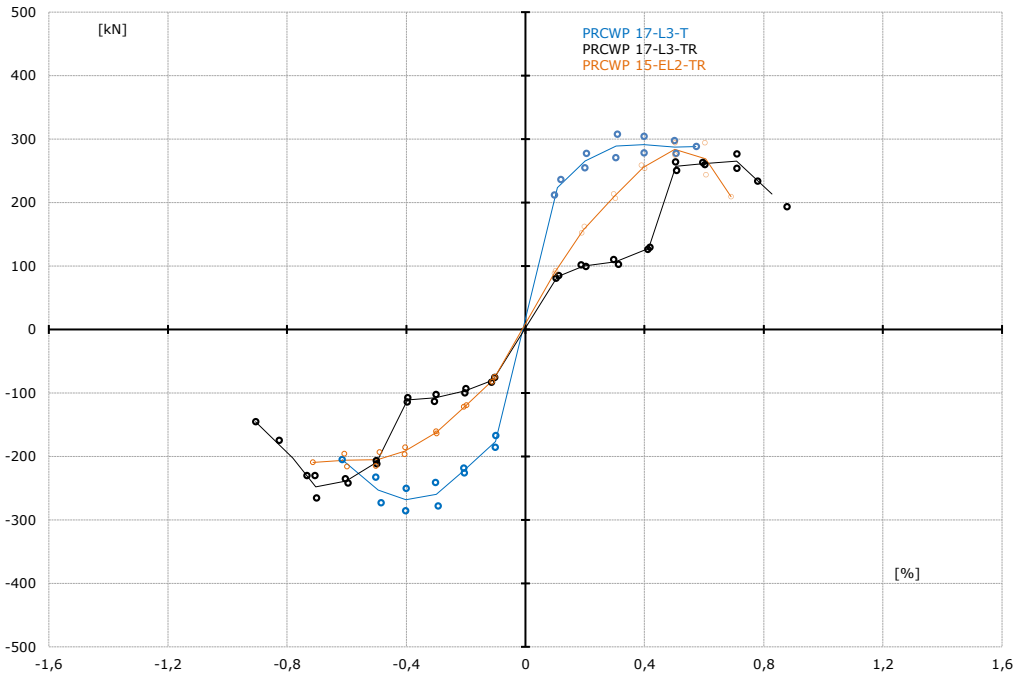

Figure A- 12 – PRCWP 17-S-L3-T, 17-S-L3-TR, 15-EL2-TR M2 envelope comparison

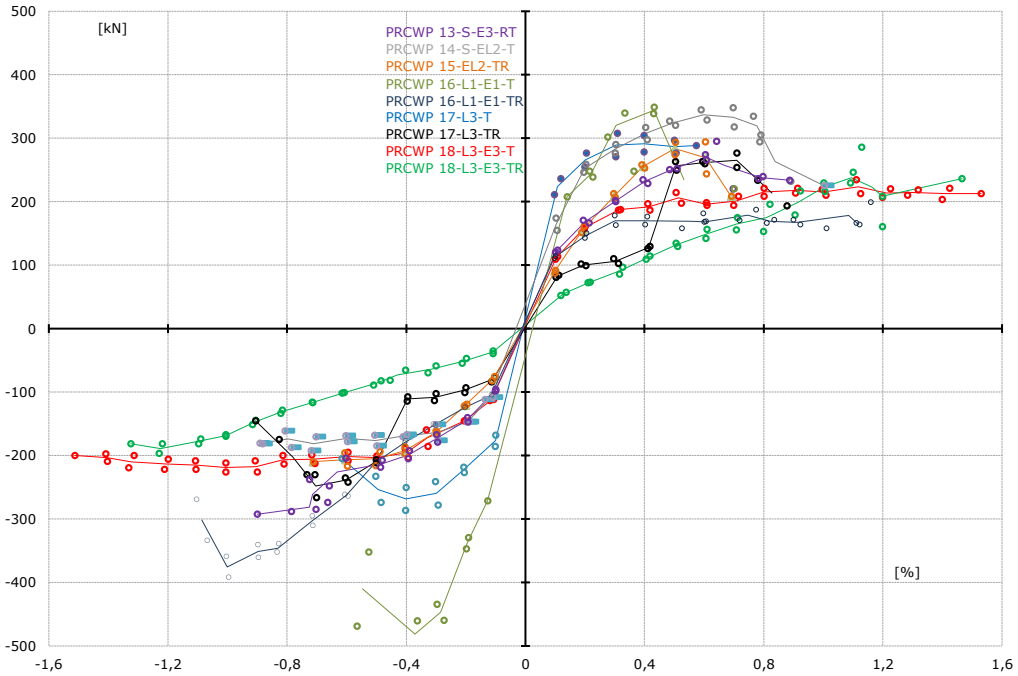

Figure A- 13 – All specimens M2 envelope comparison

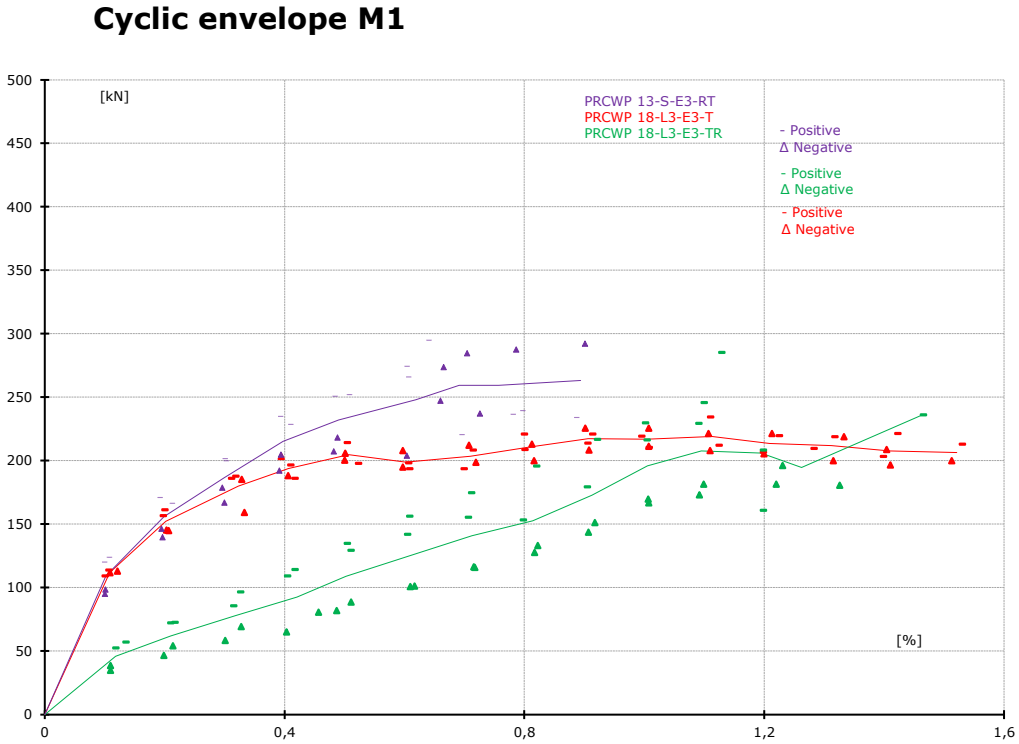

Figure A- 14 – PRCWP 13-S-E3-RT, 18-L3-E3-T and 18-L3-E3-RT M1 Envelope comparison

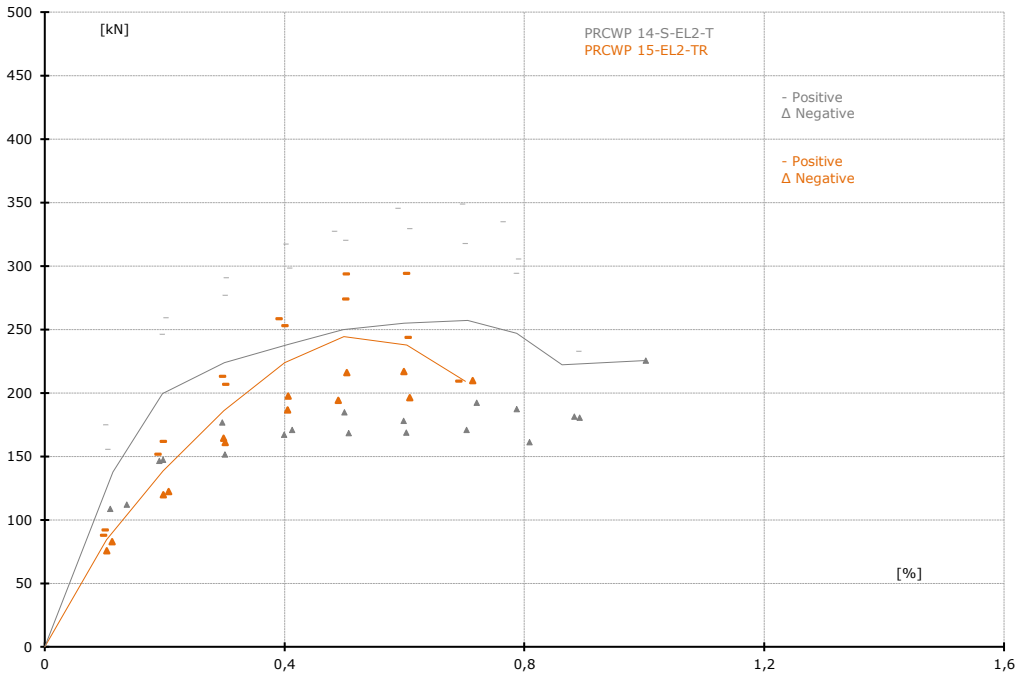

Figure A- 15 – PRCWP 14-S-EL2-T, 17-EL2-T M1 envelope comparison

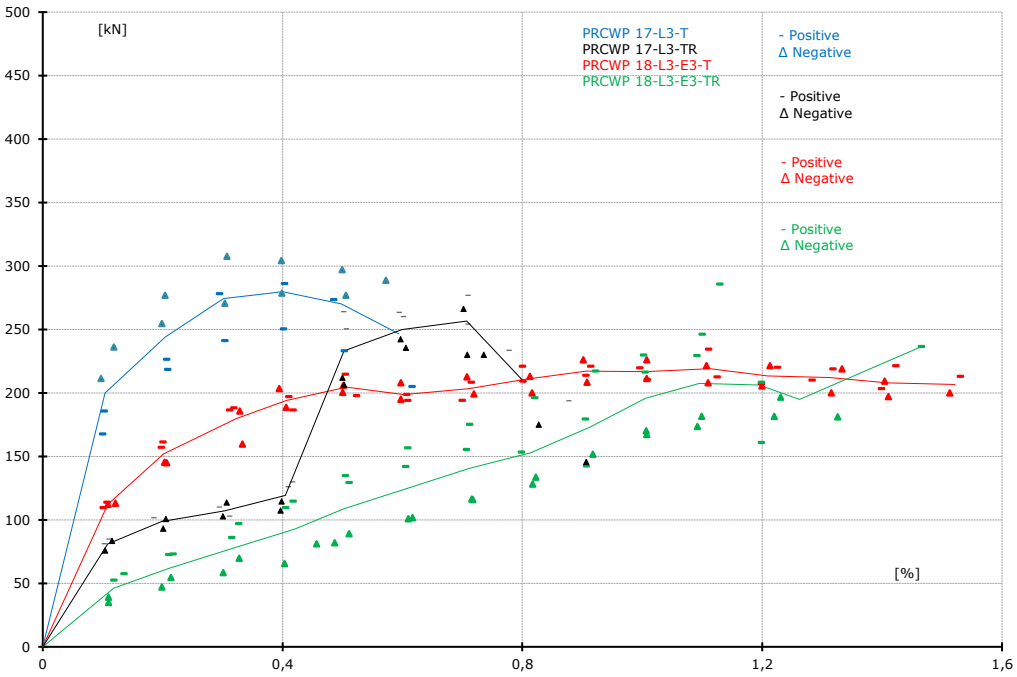

Figure A- 16 – PRCWP 17-S-L3-T, 18-L3-E3-T, 17-S-L3-TR, 18-L3-E3-TR M1 envelope comparison

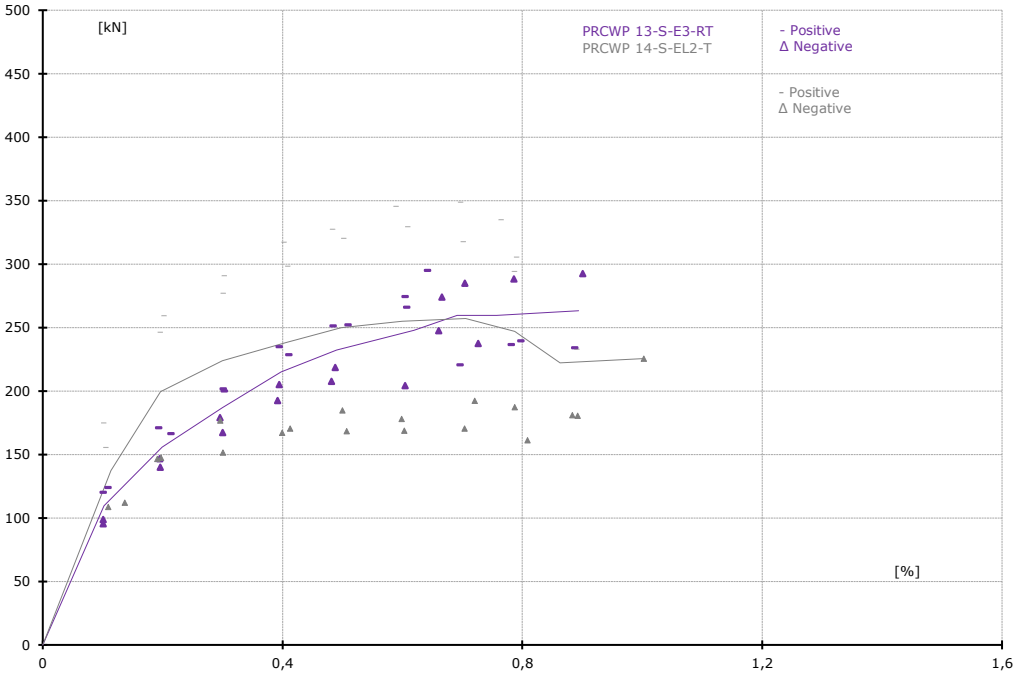

Figure A- 17 – PRCWP 13-S-E3-RT, 14-S-EL2-T M1 envelope comparison

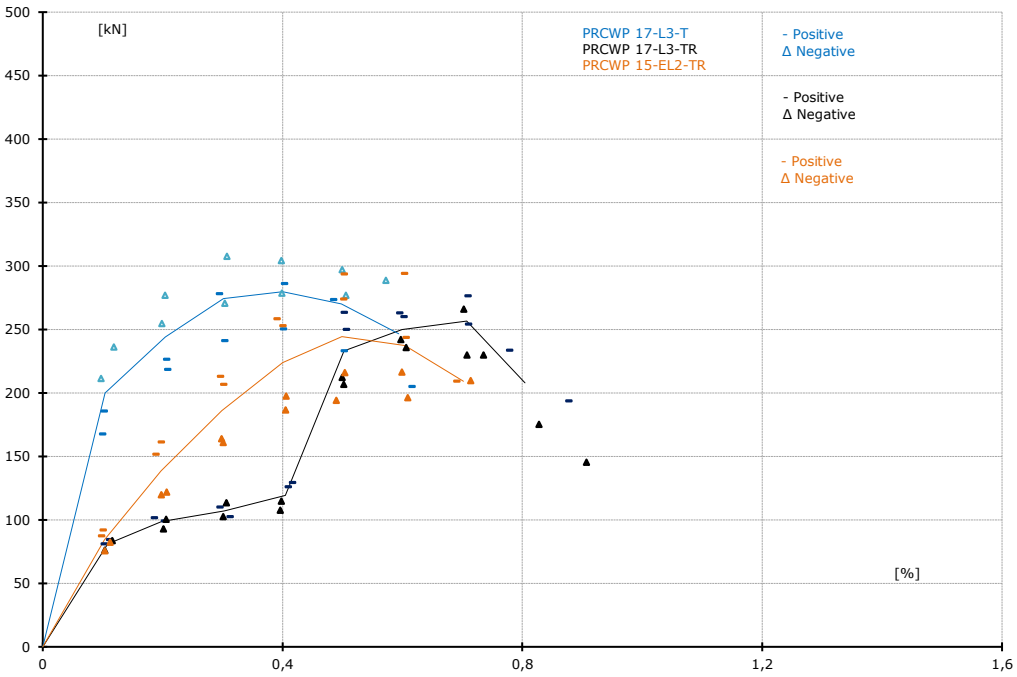

Figure A- 18 – PRCWP 17-S-L3-T, 17-S-L3-TR, 15-EL2-TR M1 envelope comparison

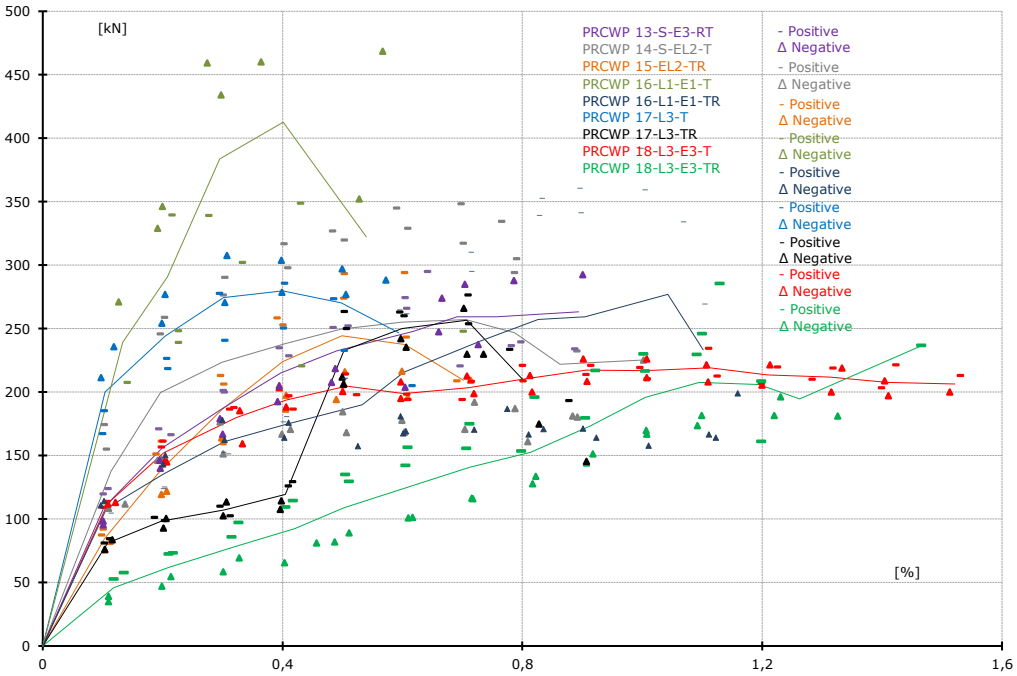

Figure A- 19 – All specimens M1 envelope comparison

Backbone envelopes

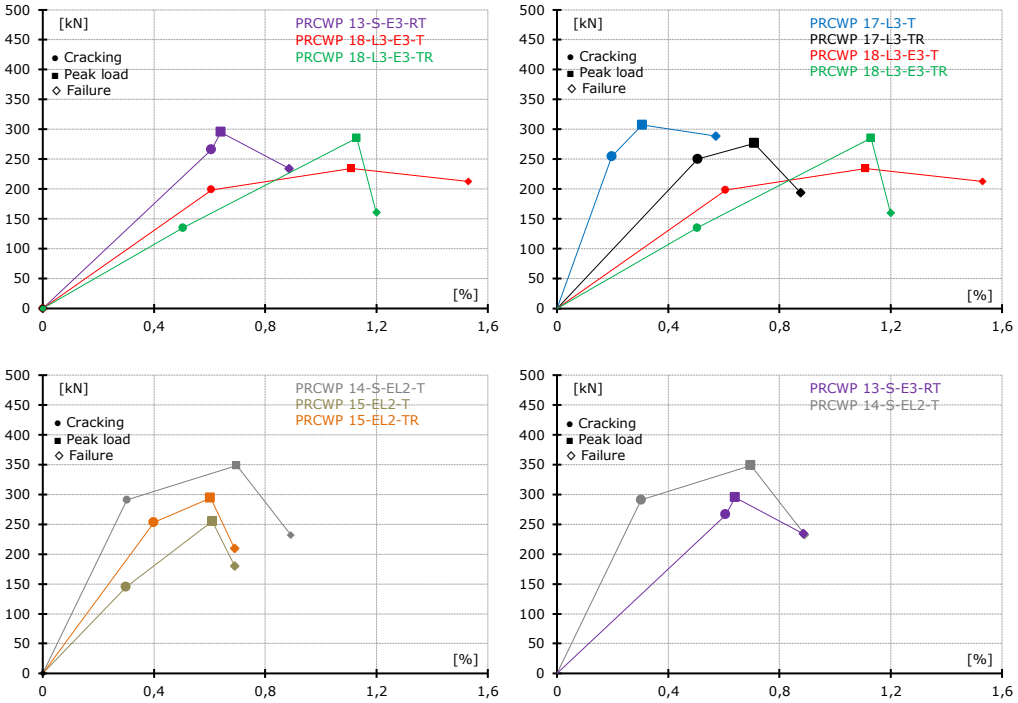

Figure A- 20 – Backbone Type 1 envelope comparisons

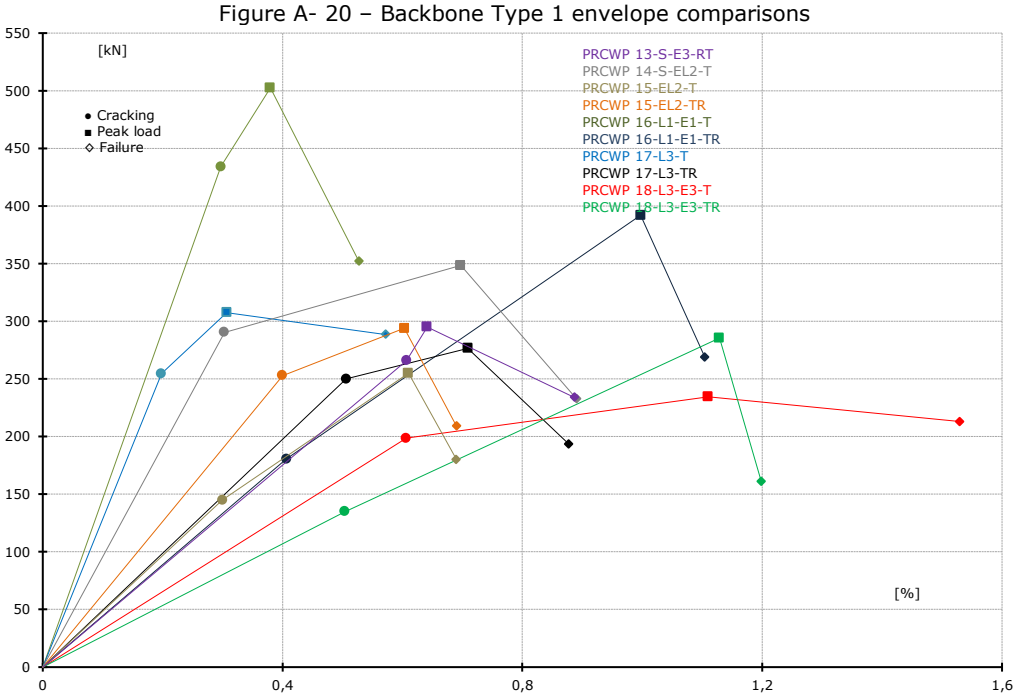

Figure A- 21 – All specimens Backbone Type 1 comparison

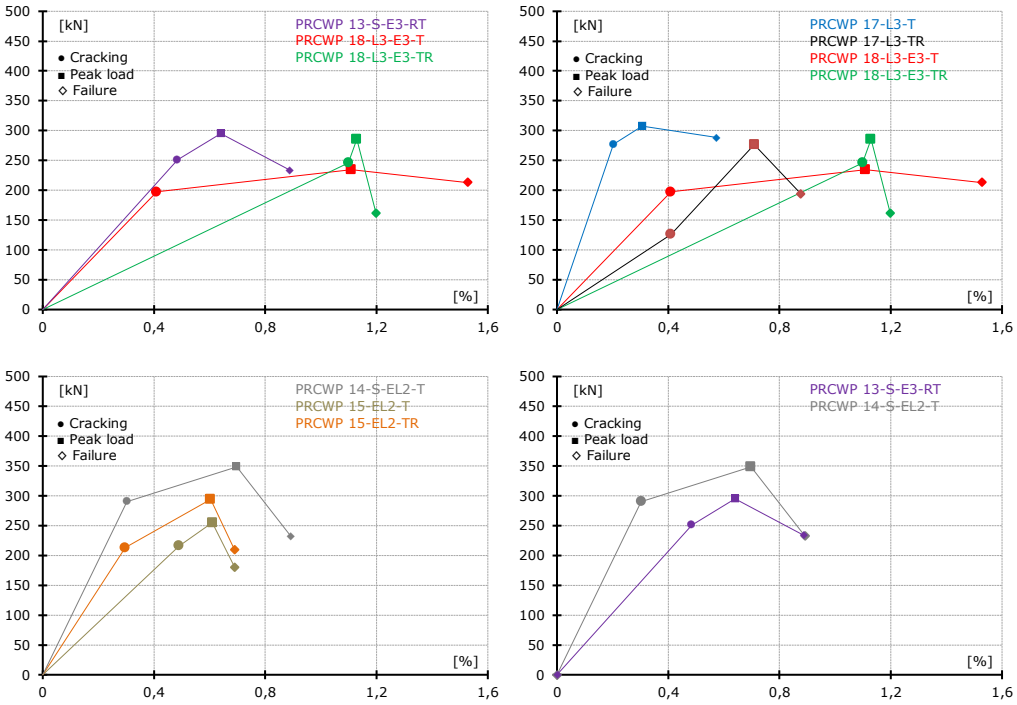

Figure A- 22 – Backbone Type 2 envelope comparisons

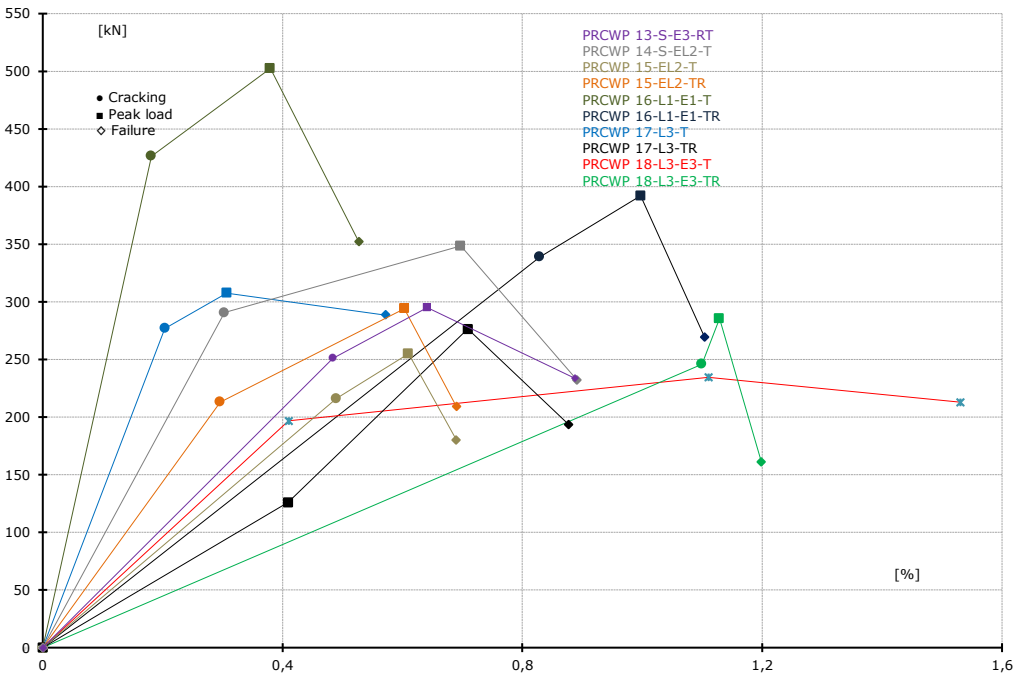

Figure A- 23 – All specimens Backbone Type 2 comparison

APPENDIX B – Test logs

Specimen 13 S-E3-RT

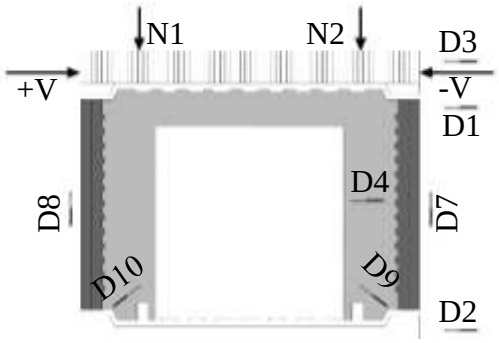

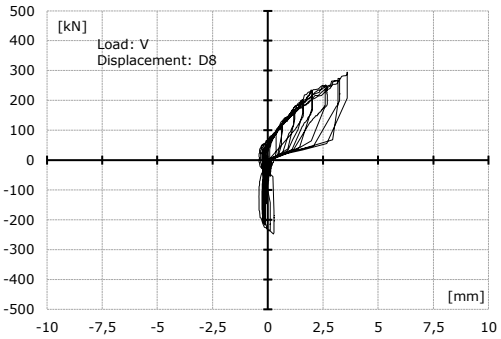

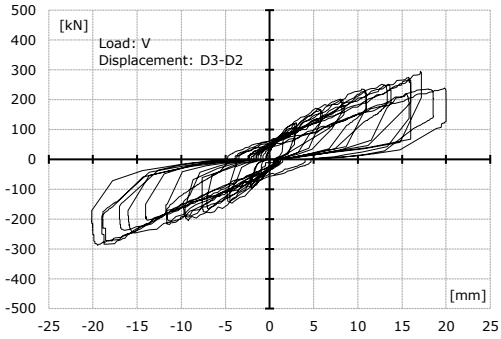

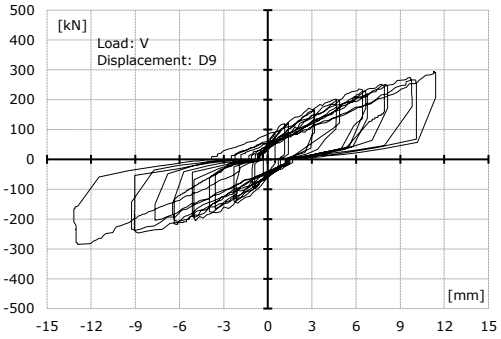

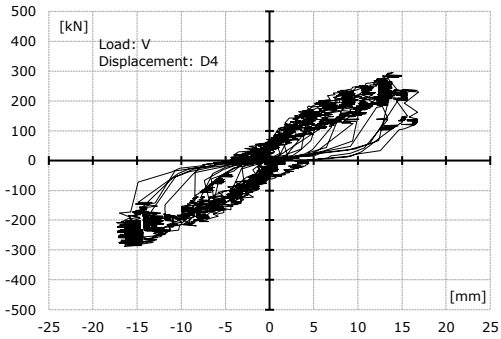

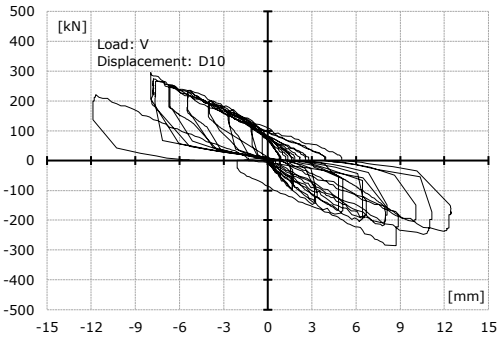

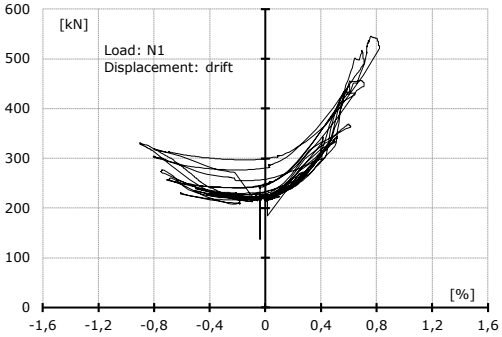
[kN]
Load: N1
Displacement: drift
[%]

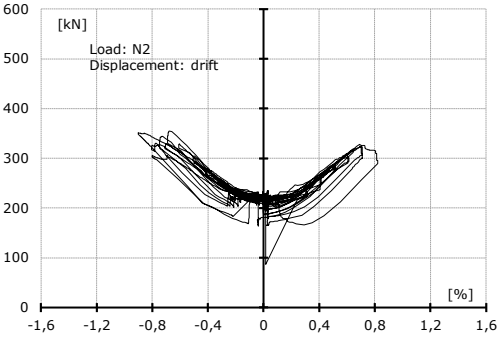
[kN]
Load: N2
Displacement: drift
[%]

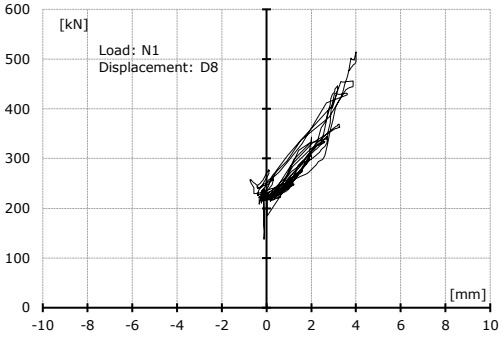
[kN]
Load: N1
Displacement: D8
[mm]

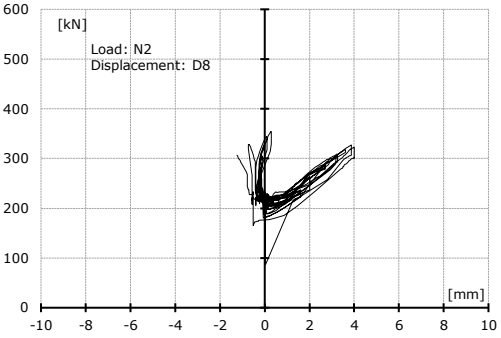
[kN]
Load: N2
Displacement: D8
[mm]

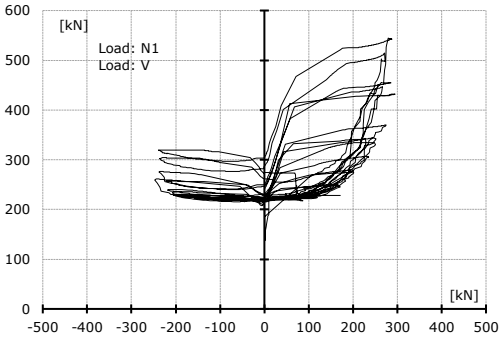
[kN]
Load: N1
Load: V
[kN]

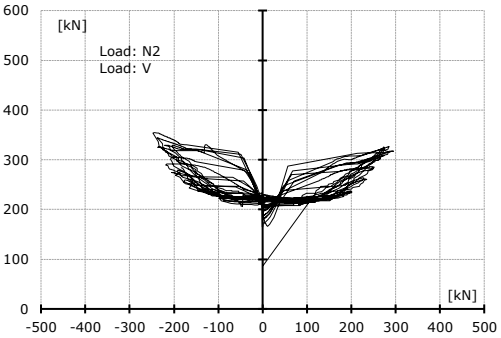
[kN]
Load: N2
Load: V
[kN]

Specimen 14 S-EL2-T

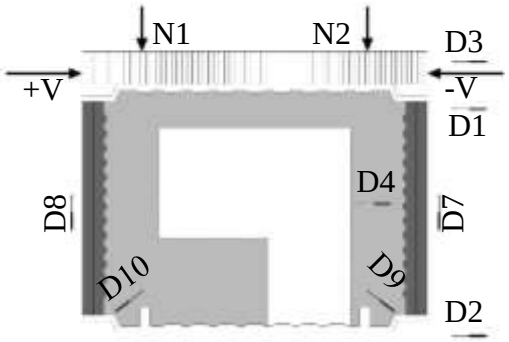

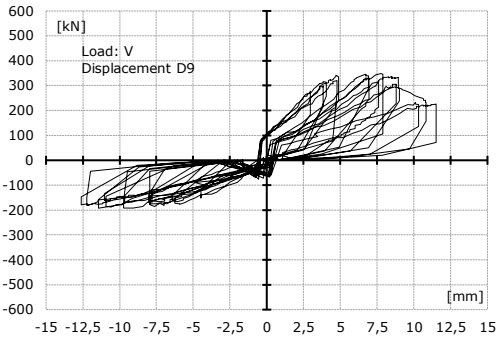

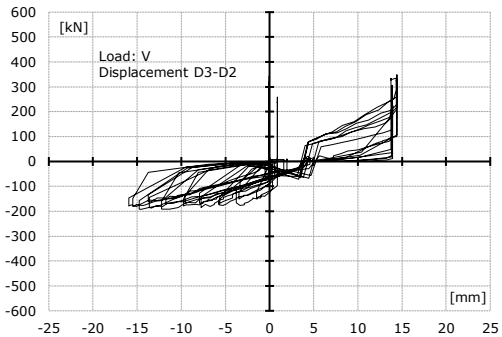

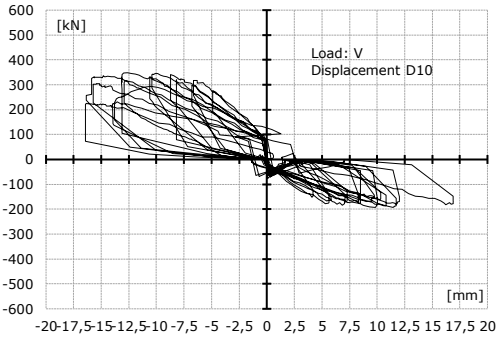

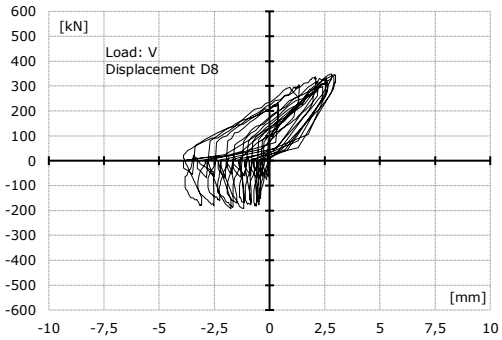

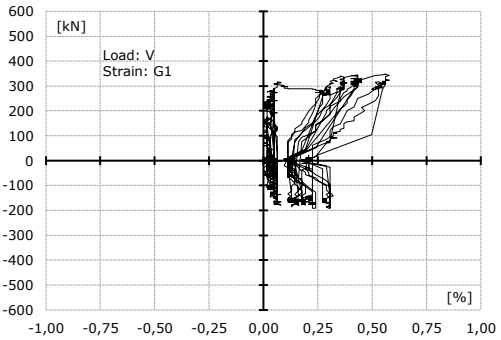

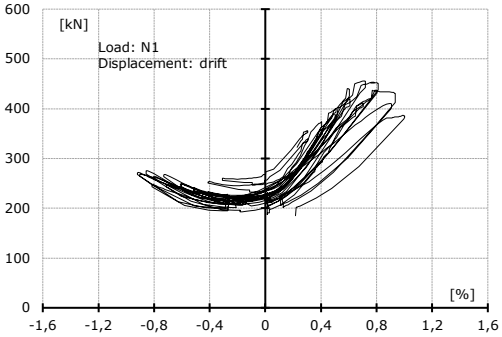
[kN]
Load: N1
Displacement: drift
[%]
600
500
400
300
200
100
0
-1,6 -1,2 -0,8 -0,4 0 0,4 0,8 1,2 1,6

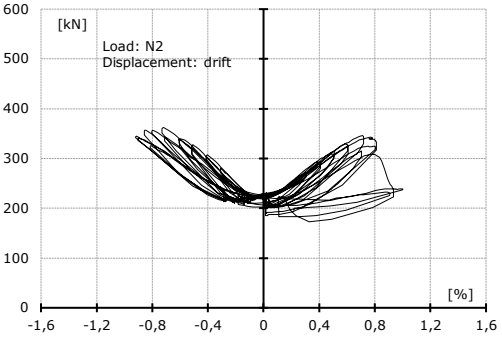
[kN]
Load: N2
Displacement: drift
[%]
600
500
400
300
200
100
0
-1,6 -1,2 -0,8 -0,4 0 0,4 0,8 1,2 1,6

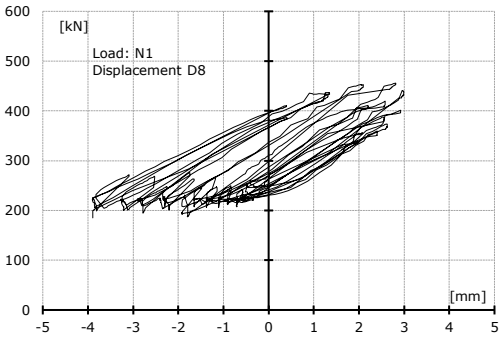
[kN]
Load: N1
Displacement D8
[mm]
600
500
400
300
200
100
0
-5 -4 -3 -2 -1 0 1 2 3 4 5

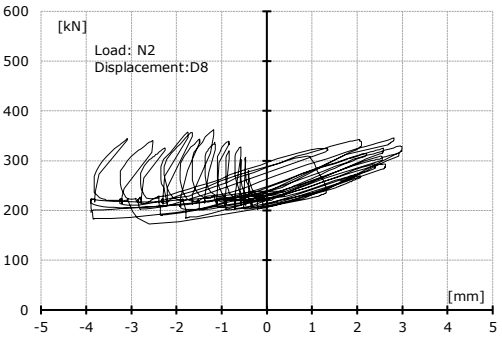
[kN]
Load: N2
Displacement:D8
[mm]
600
500
400
300
200
100
0
-5 -4 -3 -2 -1 0 1 2 3 4 5

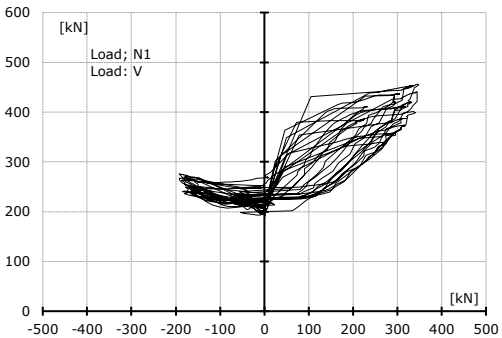
[kN]
Load; N1
Load: V
[kN]
600
500
400
300
200
100
0
-500 -400 -300 -200 -100 0 100 200 300 400 500

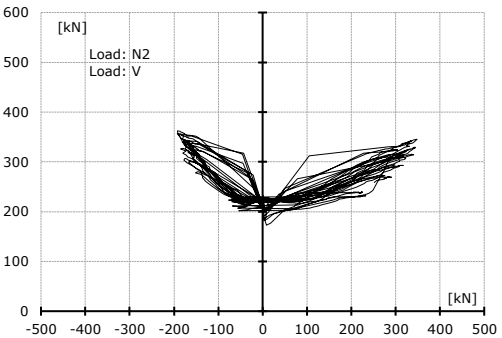
[kN]
Load: N2
Load: V
[kN]
600
500
400
300
200
100
0
-500 -400 -300 -200 -100 0 100 200 300 400 500

Specimen 15 EL2-TR

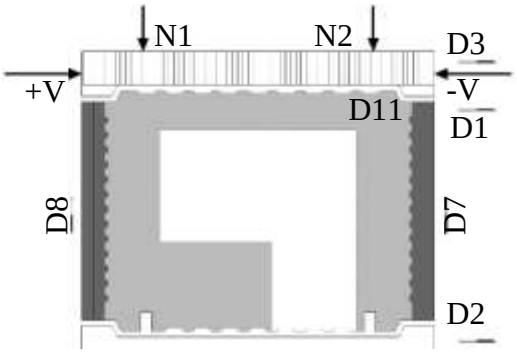

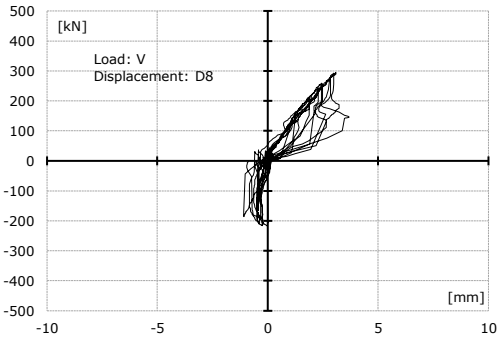

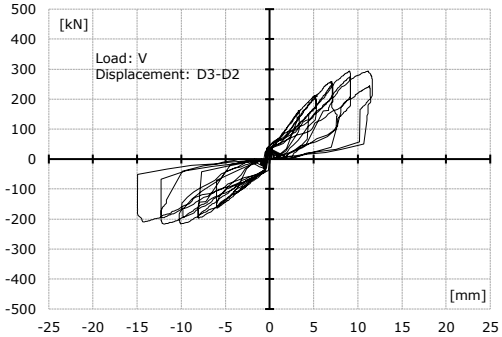

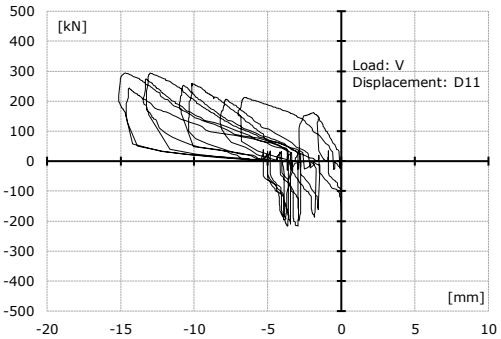

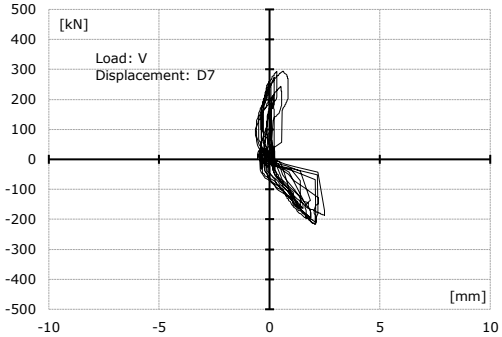

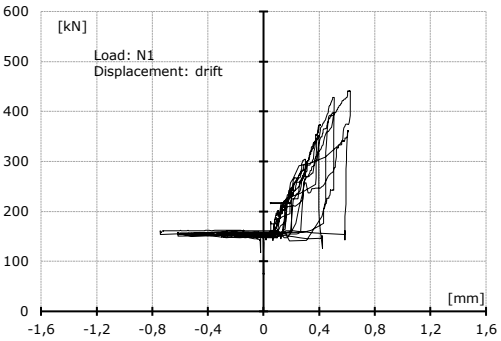

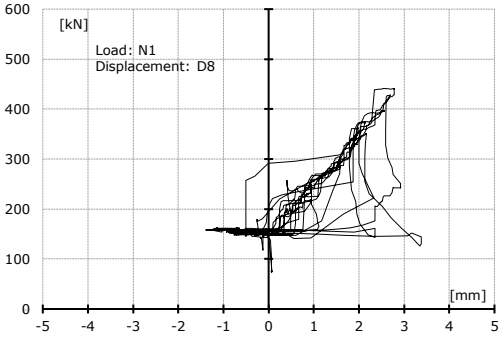

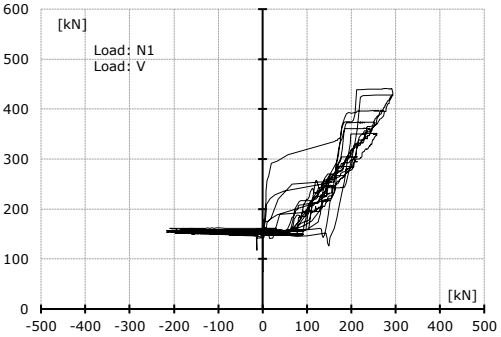

Specimen 16 L1-E1-T

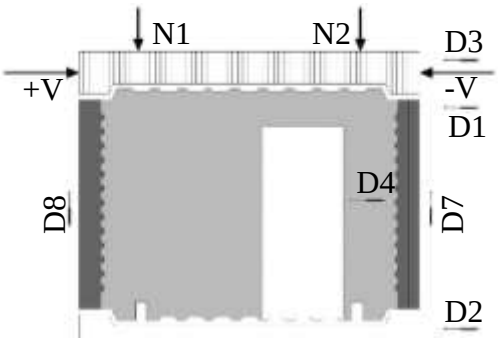

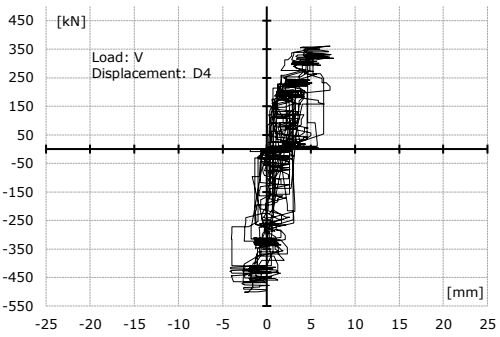

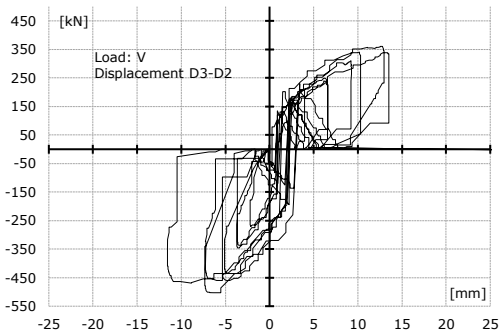

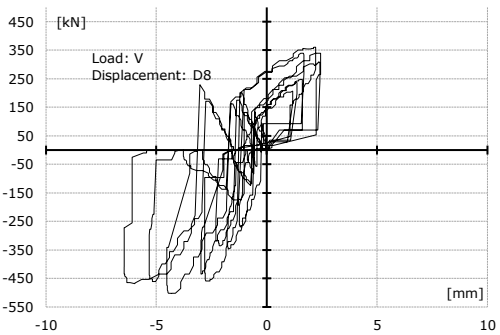

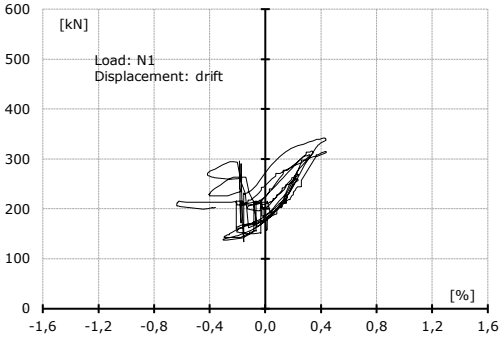
[kN]
Load: N1
Displacement: drift
[%]

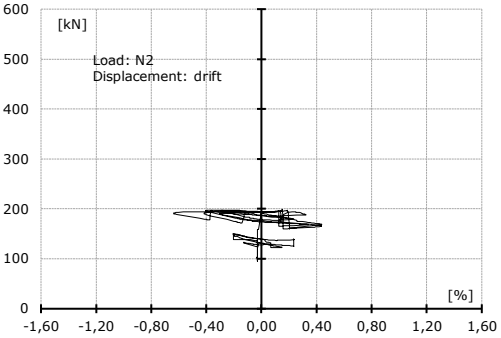
[kN]
Load: N2
Displacement: drift
[%]

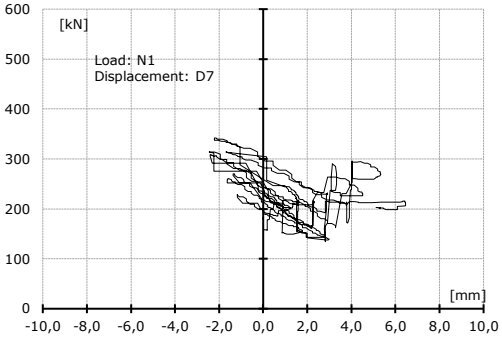
[kN]
Load: N1
Displacement: D7
[mm]

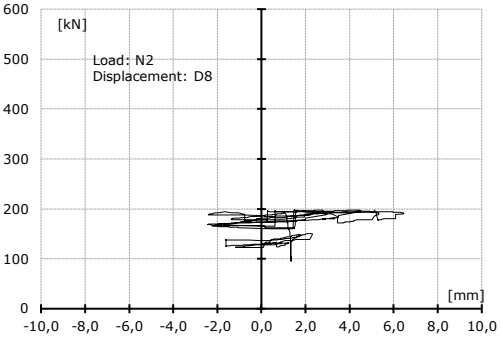
[kN]
Load: N2
Displacement: D8
[mm]

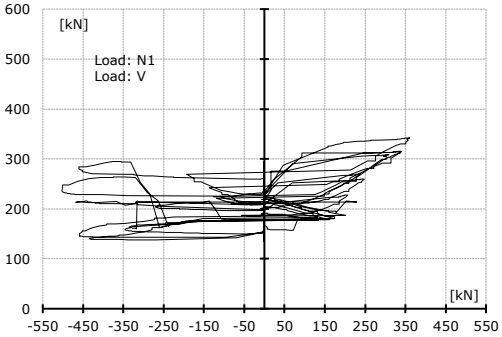
[kN]
Load: N1
Load: V
[kN]

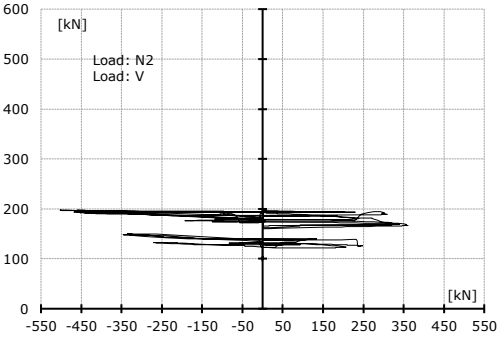
[kN]
Load: N2
Load: V
[kN]

Specimen 16 L1-E1-TR

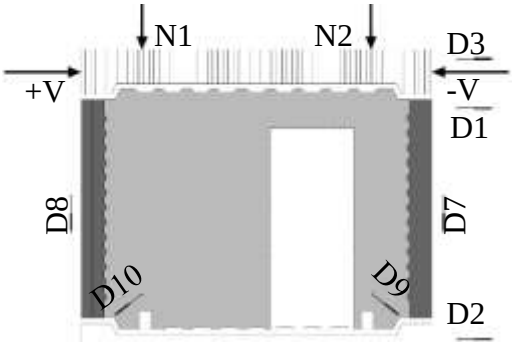

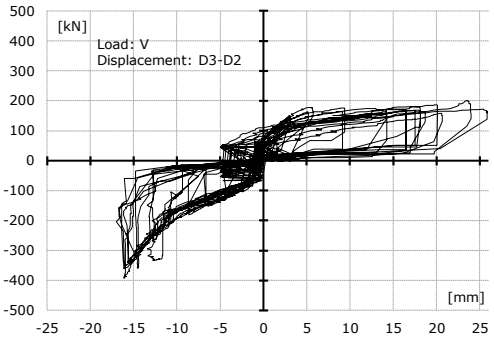

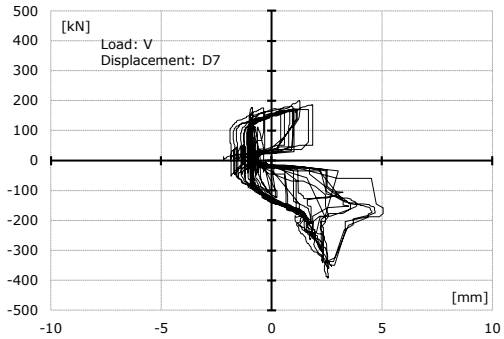

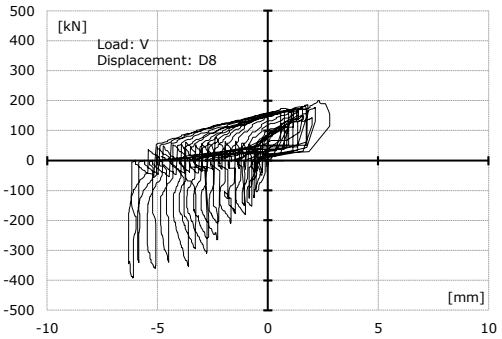

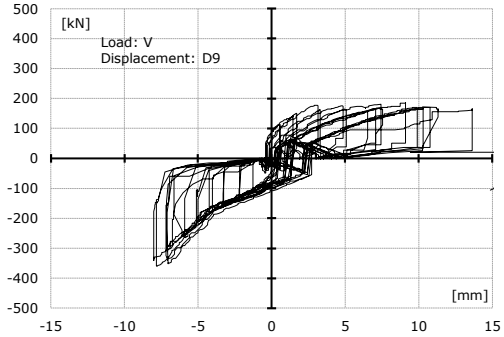

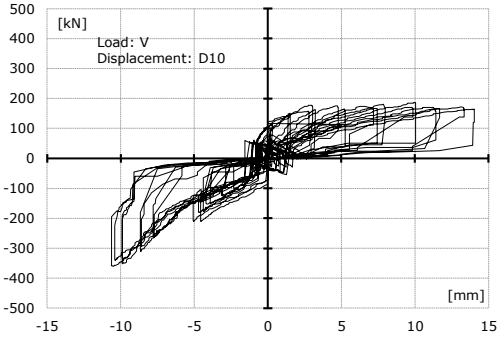

Specimen 17 L3-T

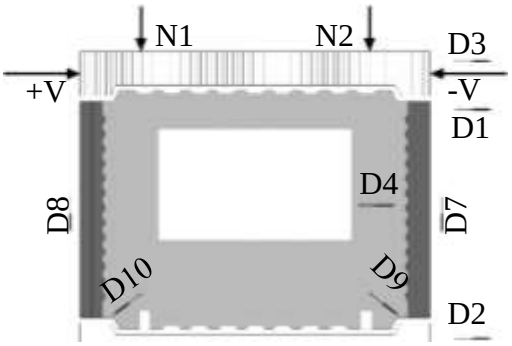

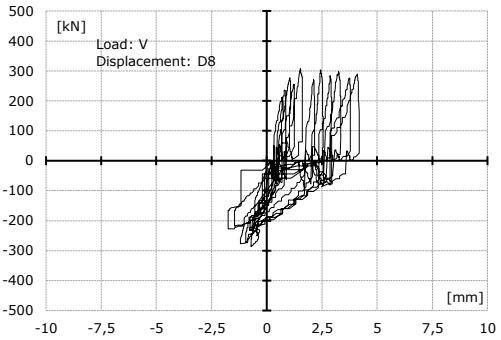

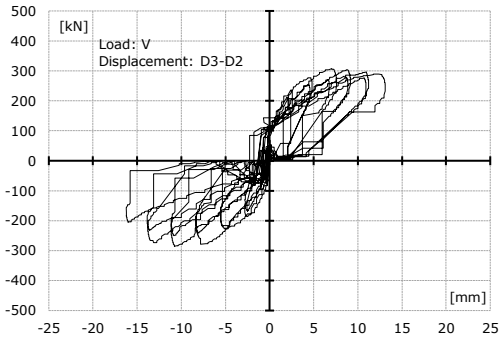

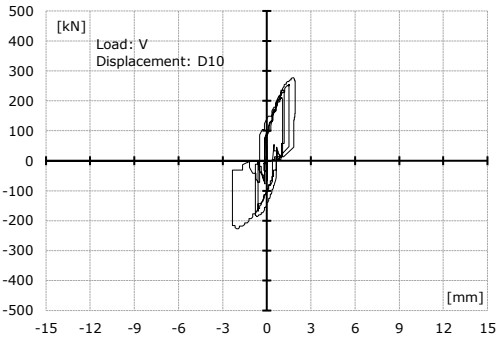

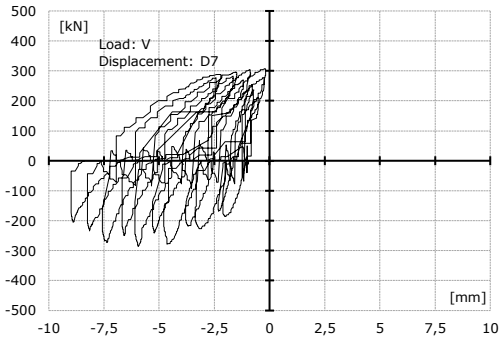

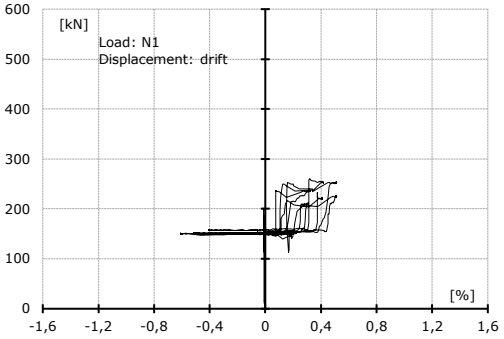
[kN]
Load: N1
Displacement: drift
[%]
600
500
400
300
200
100
0
-1,6 -1,2 -0,8 -0,4 0 0,4 0,8 1,2 1,6

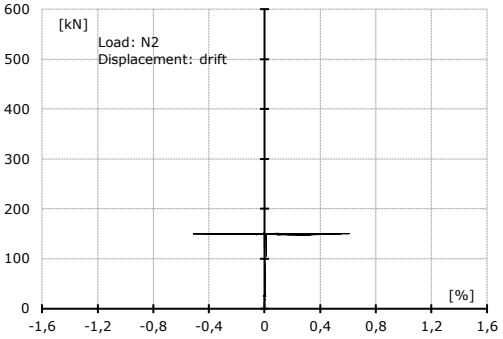
[kN]
Load: N2
Displacement: drift
[%]
600
500
400
300
200
100
0
-1,6 -1,2 -0,8 -0,4 0 0,4 0,8 1,2 1,6

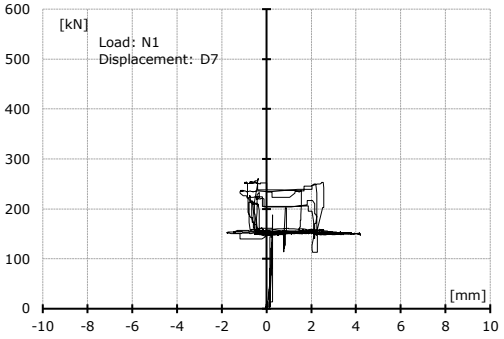
[kN]
Load: N1
Displacement: D7
[mm]
600
500
400
300
200
100
0
-10 -8 -6 -4 -2 0 2 4 6 8 10

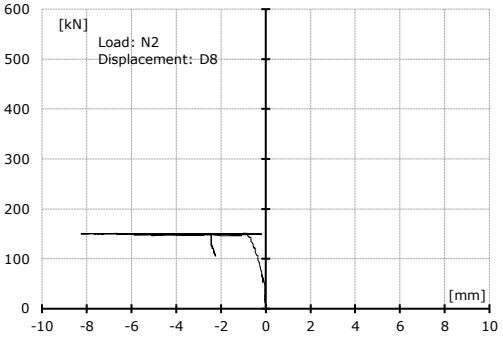
[kN]
Load: N2
Displacement: D8
[mm]
600
500
400
300
200
100
0
-10 -8 -6 -4 -2 0 2 4 6 8 10

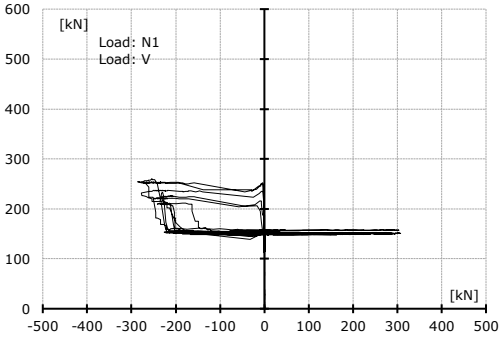
[kN]
Load: N1
Load: V
[kN]
600
500
400
300
200
100
0
-500 -400 -300 -200 -100 0 100 200 300 400 500

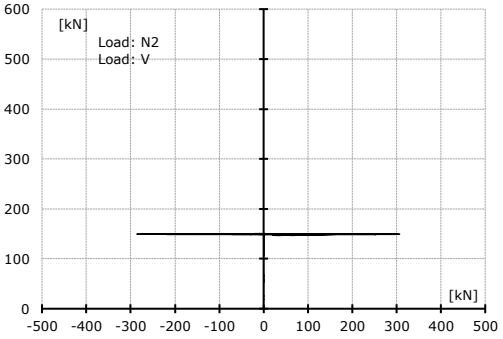
[kN]
Load: N2
Load: V
[kN]
600
500
400
300
200
100
0
-500 -400 -300 -200 -100 0 100 200 300 400 500

Specimen 17 L3-TR

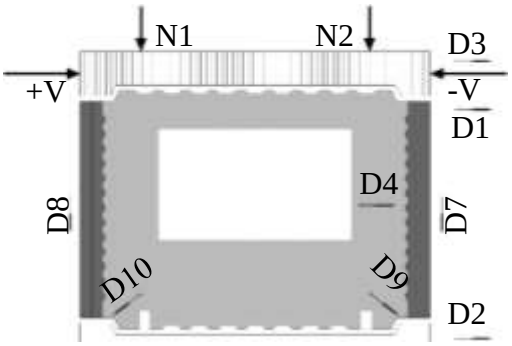

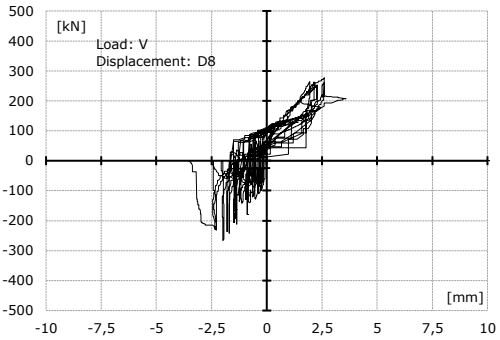

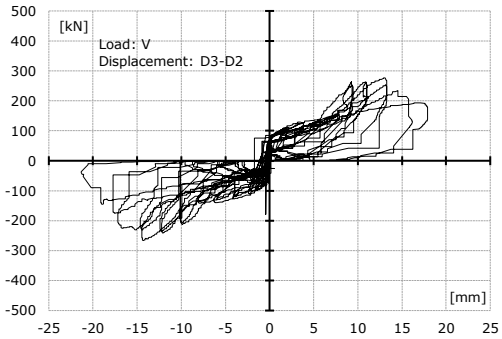

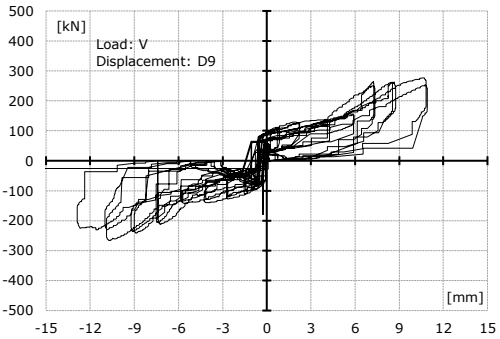

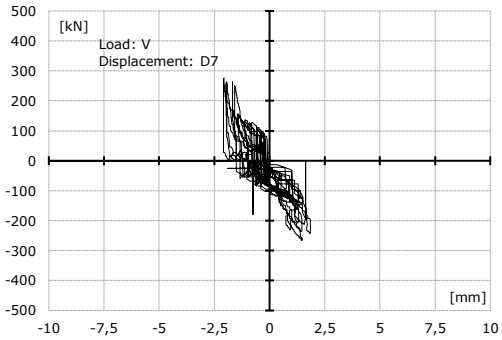

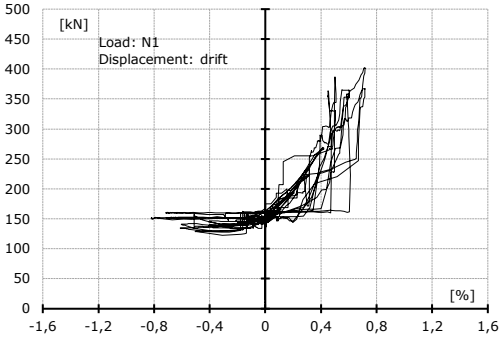
[kN]
Load: N1
Displacement: drift
[%]

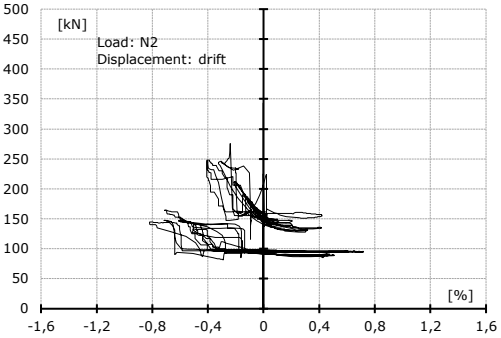
[kN]
Load: N2
Displacement: drift
[%]

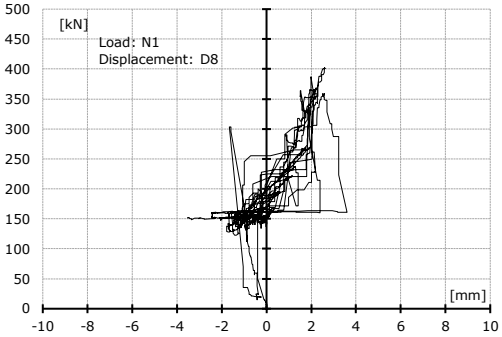
[kN]
Load: N1
Displacement: D8
[mm]

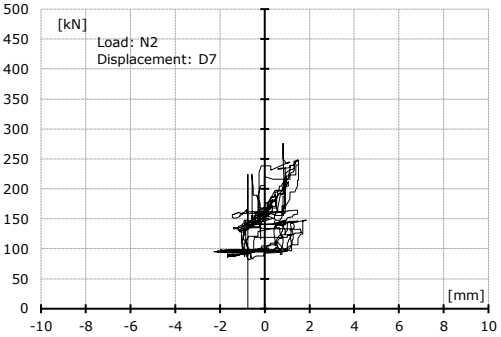
[kN]
Load: N2
Displacement: D7
[mm]

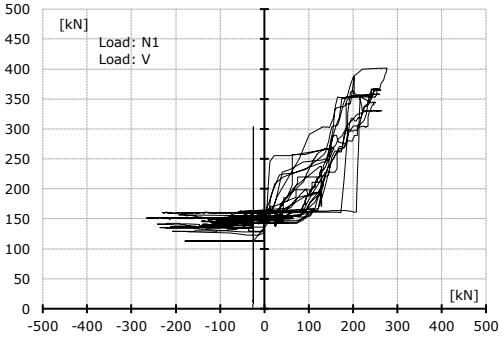
[kN]
Load: N1
Load: V
[kN]

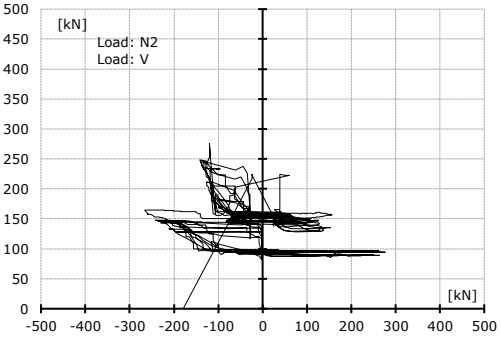
[kN]
Load: N2
Load: V
[kN]

Specimen 18 -L3-E3-T

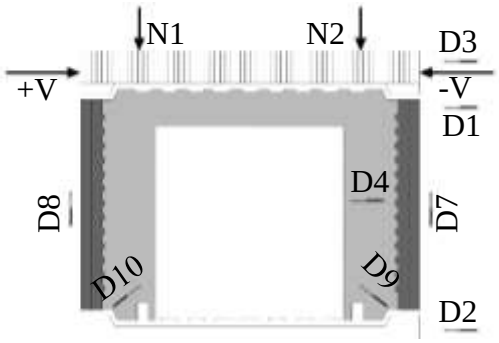

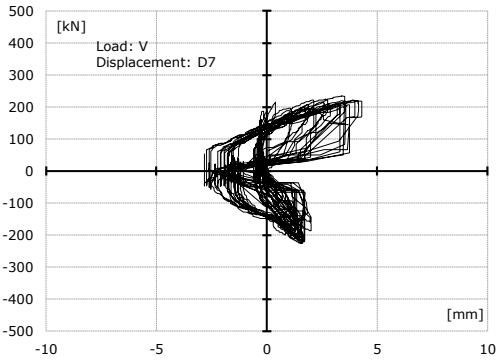

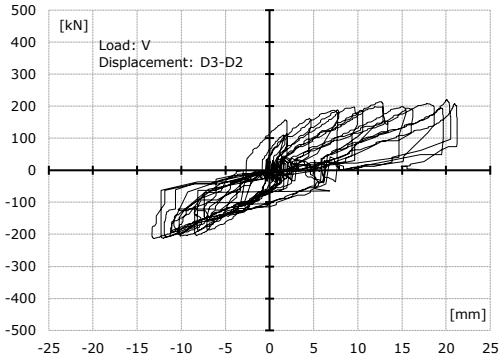

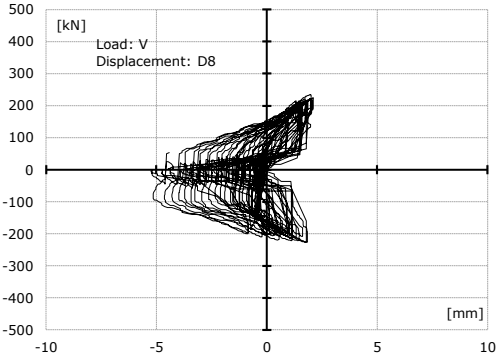

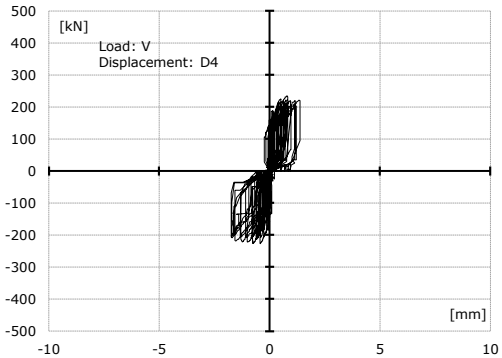

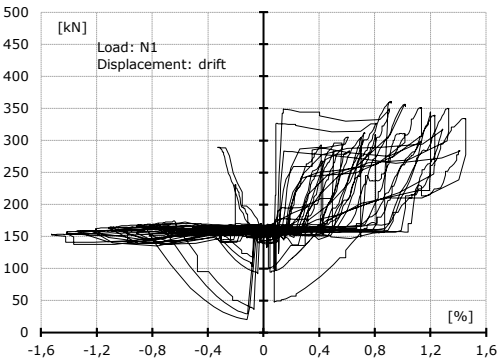

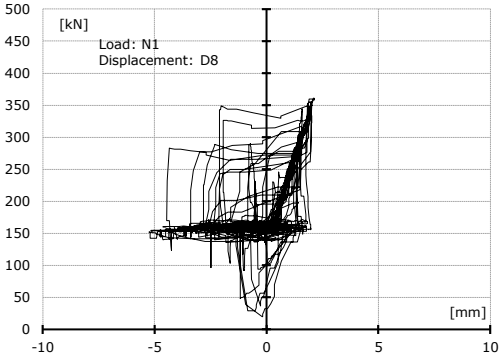

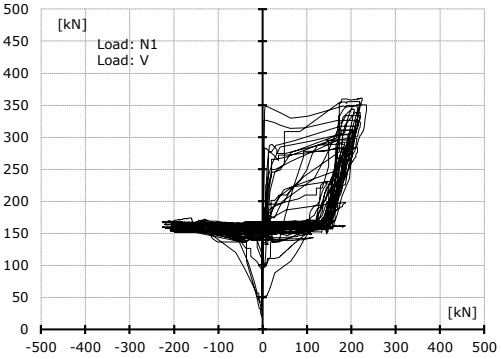

Specimen 18 -L3-E3-TR

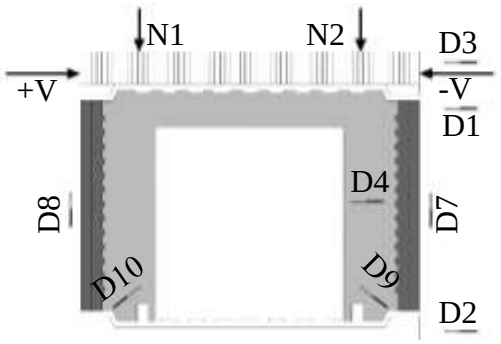

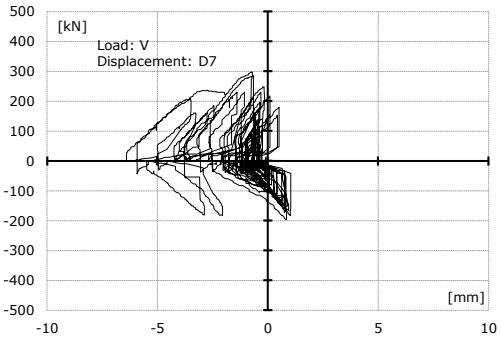

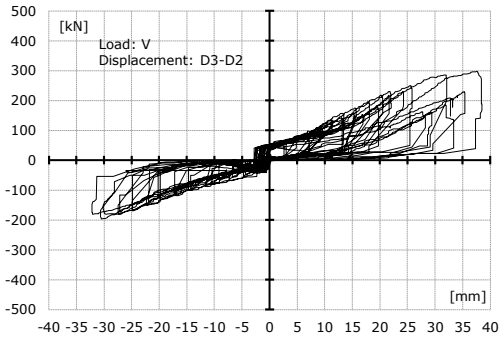

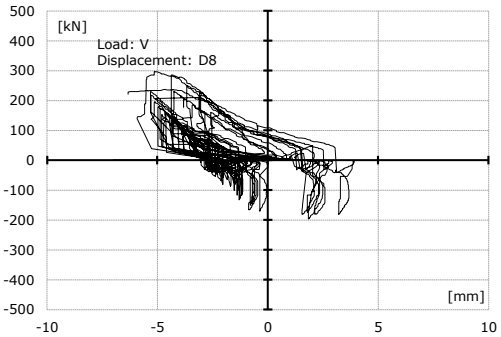

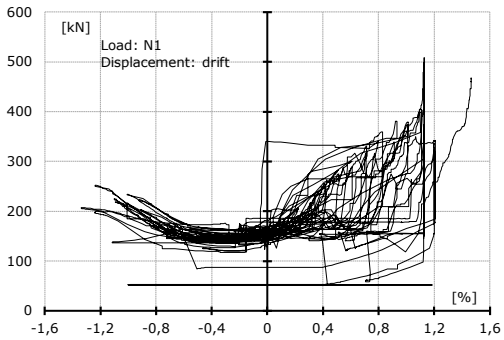
[kN]
Load: N1
Displacement: drift
[%]
600
500
400
300
200
100
0
-1,6 -1,2 -0,8 -0,4 0 0,4 0,8 1,2 1,6

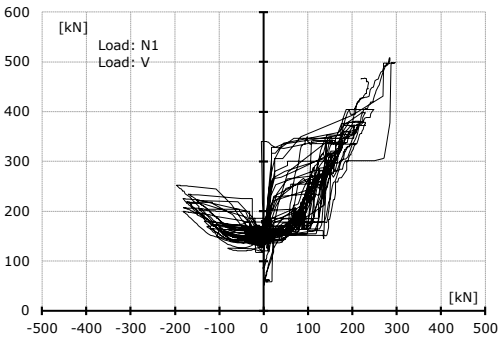
[kN]
Load: N1
Load: V
[kN]
600
500
400
300
200
100
0
-500 -400 -300 -200 -100 0 100 200 300 400 500

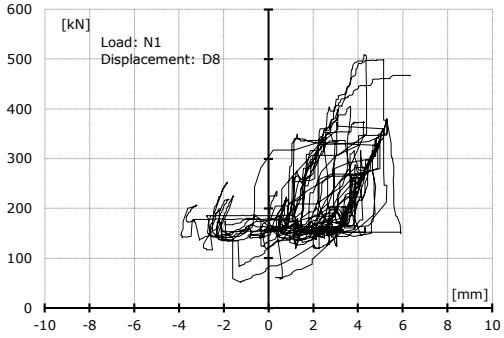
[kN]
Load: N1
Displacement: D8
[mm]
600
500
400
300
200
100
0
-10 -8 -6 -4 -2 0 2 4 6 8 10

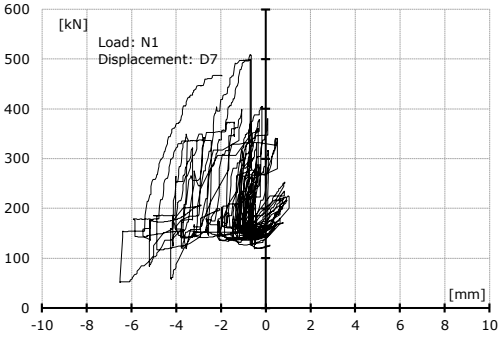
[kN]
Load: N1
Displacement: D7
[mm]
600
500
400
300
200
100
0
-10 -8 -6 -4 -2 0 2 4 6 8 10